Geochemical Investigations of Calcite Fracture Fills and Mesa-Top Water Dynamics on the Pajarito Plateau, New Mexico

By

Brent D. Newman

Dissertation

Submitted in Partial Fulfillment of the Requirement for the Degree of

Doctor of Philosophy in Geoscience with a Specialization in

Geochemistry

New Mexico Institute of Mining and Technology

Socorro, New Mexico

ABSTRACT

Semiarid regions are economically and socially important environments on which anthropogenic effects, such as contamination and rising demand for water, are increasingly having an impact. Semiarid environments, like arid ones, are complex systems in which many of the biological, geochemical, and hydrologic processes must function under water-limited conditions. At the same time, because they are less water-limited than arid environments, semiarid environments also share some characteristics with humid environments. This transitional and heterogeneous nature complicates efforts to understand the geochemistry and hydrology of semiarid environments. However, recent developments in analytical techniques, such as quadrupole mass-spectrometric analysis of fluid inclusion gases and the creation of models describing the behavior of meteoric stable isotopes and chloride in the vadose zone, are providing new ways of investigating these environments. This dissertation describes how these new approaches, and others, were used to examine aspects of the geochemistry and hydrology of the Pajarito Plateau in north-central New Mexico. Moreover, because the Los Alamos National Laboratory is located on this plateau, there is concern about contamination resulting from past research activities. The studies described here were intended not only to improve

our general understanding of semiarid processes, but also to help identify some of the hydrogeologic factors that affect contaminant transport at the Laboratory.

An investigation of the origins of calcite fracture fillings in Bandelier Tuff showed that their formation was controlled by a combination of inorganic and biological processes and, unexpectedly, that at least some of the calcite precipitated under anaerobic conditions. The origin of the calcite is important both because it may explain how other pedogenic calcites form, and because the unusual fracture chemistry is likely to affect the mobility of contaminants that enter the fracture system.

Another area that was investigated is that of interflow processes on the plateau. Natural stable isotope and chloride tracers were used to track water movement; the results show that interflow is dominated by preferential flow and that its chemistry varies depending upon soil moisture content. Further, the variability in interflow chemistry can be much larger than that reported for humid systems. Like the processes of calcite formation, interflow on the plateau is important because it potentially affects the distribution of contaminants on the mesa tops.

Finally, vertical flow in the near-surface soils and tuff of the mesas was investigated using stable isotopes, chloride, and bromide. Chloride-based fluxes were generally low, between about 1.2 and 0.02 cm/yr;

interestingly, they were typically higher in the pinyon-juniper zone than in the ponderosa pine zone, even though the latter receives more precipitation. These differences are probably a result of different soil textural properties. An order of magnitude difference was observed for chloride- and bromide-based flux estimates in the ponderosa pine zone. The difference is probably related to either an artificial perturbation of the hydrologic system caused by the death of the grass cover during bromide application, and/or differences between the net advective and diffusive fluxes that controlled the distributions of the two tracers. In terms of the overall hydrogeologic system, the low chloride-based fluxes indicate that matrix recharge through the mesas is probably insignificant. However, the results of these studies of fracture calcites, interflow, and vertical fluxes demonstrate the presence of a dynamic hydrogeologic system in the mesa tops of the plateau that will control contaminant distributions in the soils and near-surface Bandelier Tuff.

ACKNOWLEDGMENTS

I would like to thank my advisor, Dr. Andrew Campbell, for his support and guidance. It has been a pleasure to interact with someone who has always maintained an interest in my resarch and been enjoyable to work with. Dr. Bradford Wilcox also deserves special thanks for his input, support, and enthusiasm. Important contributions from my other committee members, Dr. Peter Mozley, Dr. David Norman, and Dr. Fred Phillips, were made, and I appreciate their efforts and interest as well.

I am grateful for the support and encouragement of the members of the Environmental Science Group at Los Alamos National Laboratory, nearly all of whom have contributed to this research in some way. In particular, I would like to thank Dr. Thomas Hakonson, Dr. Wayne Hansen and Dr. Everett Springer for supporting and encouraging me to pursue a Ph.D. Also, Bridget Bergquist, Dr. David Davenport, Tina Degaw, Marvin Gard, Vivi Hriscu, Darlene Linzey, and Donna Sharp were of tremendous help in various ways.

James Corboy, Greg Hill, and Jeff Klein performed a substantial part of the isotope work and I appreciate their efforts. Madhukar Gundimeda was invaluable when the quadrupole analyses were being conducted. Drs. Thomas Kieft and David Ringelberg were very helpful in helping me understand aspects of microbiology and were very gracious

in providing the lipid analyses. Dr. Robert Raymond was very helpful during the scanning electron microscope sessions, and Steve Chipera kindly performed the x-ray diffraction analysis. Dr. Michaele Kashgarian was instrumental in getting the ^{14}C analyses performed. Finally, funding for this work was provided by the Los Alamos Environmental Resoration Program, and I am very appreciative of the ER program's support.

TABLE OF CONTENTS

LIST OF TABLES

LIST OF FIGURES

PREFACE

This dissertation is composed of four chapters, each of which is presented as a separate manuscript. The first three chapters describe different aspects of the geochemistry and hydrology of the Pajarito Plateau in north-central New Mexico. Chapter 1 presents the results of a study of the origin of calcite fracture fillings in Bandelier Tuff. These calcites precipitated in a peculiar and interesting way, and one that may explain the formation of other vadose zone calcites. Chapter 2 describes a study of subsurface lateral flow (interflow) processes at a ponderosa pine hillslope site on the plateau. The relationship between preferential and matrix flow is examined by means of natural chloride and stable isotope tracers. Chapter 3 discusses the process of vertical soil water movement in mesa tops on the plateau and examines the effect of soils on water movement in ponderosa pine and pinyon-juniper zones. Chapter 4 discusses the findings of the first three chapters and how these new results help refine our understanding of the overall plateau hydrogeologic system. In addition, the implications of these results on the potential for contaminant transport are described.

CHAPTER 1: A MODEL FOR MICROBIALLY INDUCED PRECIPITATION OF VADOSE-ZONE CALCITES IN FRACTURES AT LOS ALAMOS, NEW MEXICO.

ABSTRACT

Calcite fracture fillings are present in the near surface in the Bandelier Tuff Formation at Los Alamos, New Mexico and provide a record of the geochemical and hydrologic processes that have occurred in fractures. Understanding processes involved in fracture filling is necessary to predict the potential for contaminant movement from contaminated sites at Los Alamos National Laboratory. Samples of calcite fillings were collected from vertical and horizontal fractures exposed in a shallow waste-burial pit. Scanning electron microscopy showed morphologies suggesting that plants, fungi, and bacteria were important in the calcite precipitation process. Quadrupole mass spectrometric analyses of fluid inclusion gases showed a dominance of methane and little oxygen suggesting precipitation under anaerobic conditions. Ester-linked phospholipid biomarker analysis confirmed the presence of a diverse microbial community in the fractures, and the detection of di-ether lipids indicated that the methane was likely generated by anaerobic bacteria. It is interpreted that the calcite fillings

resulted from multistage biological and chemical processes in which plant roots in the fractures were converted to calcite. Roots grew into the fractures, eventually died, and were decomposed by bacteria and fungi. Excess oxygen consumption by microbes transformed the system from aerobic to anaerobic allowing for the growth of methanogenic bacteria. Calcite precipitation occurred during methanogenesis either as a direct precipitation by bacteria or as a result of a pH change caused by anaerobic microbial respiration. It is likely that the anaerobic calcite formation process that occurred in the Los Alamos fractures may also occur in soils, and may explain the occurrence of other types of pedogenic calcites.

INTRODUCTION

Numerous calcite, smectite clay, and mixed calcite/clay fracture fillings are hosted by the near-surface Bandelier tuff on the Pajarito Plateau at Los Alamos, New Mexico (Figure 1.1). The fillings occur in both horizontal and vertical fractures and extend from the surface to at least 10 m into the tuff (Davenport, 1993). The clay fillings are the result of eluviation from soils above the tuff (Davenport et al., 1995) but, prior to this study, the origin of the calcite fillings had not been investigated. Because it appears that the calcites were precipitated in a

vadose environment, it was assumed that pedogenic processes (as opposed to hydrothermal or groundwater processes) may have controlled calcite precipitation in the fractures. Calcium in pedogenic calcites is thought to be derived mainly from atmospheric sources including dust and rain, but a variety of mechanisms have been proposed for the actual precipitation. Dixon (1994) cited several studies that suggest calcite precipitation is caused either by evaporation, pH increase (which may be caused by a loss of CO_2), temperature increase, the common ion effect, or biological processes. The objective of this study was to determine which of these processes controlled calcite precipitation in the Bandelier tuff fractures, and the results may help explain calcite precipitation in other kinds of vadose environments. Understanding the genesis of the calcite fillings is also important because fractures in the Bandelier tuff are potential pathways for downward contaminant movement at Los Alamos National Laboratory, and these fillings provide insight to the processes which might be involved.

DESCRIPTION OF THE SAMPLE SITE AND FRACTURES

The horizontal and vertical fracture fillings examined in this study are exposed in the north wall of a shallow waste-burial pit dug into a mesa top at Area J, Technical Area 54, of Los Alamos National

Laboratory (see Figures 1.1 and 1.2). The pit is about 6 m at its deepest point and exposes a portion of the Tshirege Member of the Bandelier Tuff. Fractures in the pit include open fractures, dominantly clay-filled fractures (which were examined by Davenport et al., 1995), dominantly calcite-filled fractures, and mixed clay/calcite-filled fractures. This study focuses on the dominantly calcite-filled fractures. These range in width from 0.1-10 cm and are exposed over lengths ranging from less than 1 m to over 50 m.

METHODS

Sampling was accomplished by either chipping samples out of the fractures with a rock hammer or by cutting out an intact block of tuff and fracture filling with a concrete saw (Davenport, 1993). The intact blocks were used for oriented microsampling across fracture fillings.

Scanning electron microscope and powder X-ray diffraction (XRD) analyses were performed at the Los Alamos Geology and Geochemistry Group Laboratory. A Tracor-Northern ADEM was used for the SEM analyses: sample chips were attached to aluminum stubs using colloidal graphite and were then sputtered with gold. The XRD analyses were done on a Siemens D-500 diffractometer with a Kevex Psi Si(Li) solid-state detector, using Cu-Ka radiation.

Fluid inclusion gases were analyzed by quadrupole mass spectrometry at New Mexico Tech. Samples consisted of 3- to 10-mm diameter pieces of calcite hand picked to remove visible clasts of tuff. These were placed in a stainless steel mechanical crusher and baked overnight at 100 °C under high vacuum to reduce the amount of adsorbed and interstitial volatile species. The system was then allowed to return to room temperature. Analyses were conducted using a Balzers model QMG 125 quadrupole mass spectrometer in multiple-ion detection mode. When the quadrupole pressure reached 10^{-7} mbar or lower, background intensities for the various gases were established. The sample was then crushed and a mass spectrum obtained on the released gases. Two to four crushes were made per sample. Mass spectra were reduced by integrating background and peak intensities using Balzers Quadstar® software (Balzers, Inc. 1989). Mole percentages of the volatile gases were calculated according to methods in Norman and Sawkins (1987), and Ruff (1993). Analytical precision for quadrupole measurement of major gaseous species is less than ±10% and for minor species is ±20% (Norman and Sawkins, 1987). H_2 percentages may be overestimates, but the magnitude of the problem has not been quantified. Artificial H_2 production can occur from the

interaction of hydrogen bearing species (e.g., CH_4 and H_2O) and the quadrupole filament.

For stable isotope measurements, 7- to 12-mg of calcite fracture fillings were taken with a dental drill. CO_2 was liberated using the standard phosphoric acid technique (McCrea, 1950). All isotope measurements were made with a Finnegan-Mat Delta-E stable-isotope-ratio mass spectrometer at New Mexico Tech using OZ-Tech gas standards. The $\delta^{18}O$ results were corrected for acid fractionation caused by the extraction process based on analysis of NBS-18 and NBS-20 calcite standards, and $\delta^{18}O$ values are reported relative to the SMOW standard. The $\delta^{13}C$ results are reported relative to the PDB standard. One sample of the in-house standard calcite was extracted and analyzed with every five samples to monitor for extraction and analysis problems. Based on eight replicate extractions of the in-house standard, the analytical precision is 0.05 ‰ (1σ) for $\delta^{13}C$ and 0.07 ‰ (1σ) for $\delta^{18}O$.

For ^{14}C age determinations, 10-mg samples of calcite were extracted by drilling on an oriented block from the vertical fracture in the same way as for the stable-isotope sampling (Figure 1.2). Samples were taken in a line from one edge of the vertical fracture to the other in order to understand the timing of calcite deposition. These were analyzed by accelerator mass spectroscopy at the Lawrence Livermore

Center for Accelerator Mass Spectroscopy. The reported analytical precision on the ^{14}C ages is ±240 years or better. Amundson et al. (1994) have found that sampling pedogenic calcites of more than one age can cause over- or underestimations of the true age. Because a "micro" sampling technique was used in this study, any errors due to sampling calcites of more than one age are minimized.

For ester-linked phospholipid biomarker analysis, a composite sample of about 100-gm of calcite was collected from the 3-m depth of the vertical fracture and from sample site 6 in the horizontal fracture (Figure 1.2). Before sampling, the outer 15-20 cm of material was removed to reduce the potential for surface contamination. All sampling equipment was autoclaved prior to use, and sterile gloves were worn at all times. After being scraped clean of any tuff adhering to them, the samples were placed in sterile whirlpack bags, and immediately packed with ice. Upon delivery to the laboratory, the samples were stored in a freezer until shipment (on dry-ice) to the University of Tennessee Center for Environmental Biotechnology. There, the sample was crushed into a powder using a sterile mortar and pestle. Phospholipids were extracted and analyzed according to Guckert et al. (1985). The ether-lipids, lipopolysaccharide-hydroxy fatty acids (lps-ohfa), and sterols were extracted using the method of Mayberry and Lane (1993) and analyzed

by the gas chromatography method of Parker, et al. (1982). The di-ethers were analyzed using high temperature capillary gas chromatography according to Nichols et al. (1993). Three replicate analyses were done on the sample.

RESULTS

Calcite Morphology

The calcite fillings are white and are typically friable and powdery (Figure 1.3). Small portions of some fillings are indurated, but there are no obvious field characteristics that indicated what controlled the variable induration. Brown decomposed root material is present along some of the tuff-calcite contacts and is occasionally observed along cracks in the fillings. Root material is present in various places from the soil-tuff interface to the bottom of the pit. The decomposed material retained the branching form of roots, and individual rootlets are usually less than one mm in diameter. Individual tuff-derived mineral grains and pieces of tuff are also present and concentrated along the edges of the fillings.

SEM examination reveals two main calcite morphologies: lath-like and amorphous (Figures 1.4a-1.4c). In addition, unusual branched, tubular structures, characterized by crystals less than 0.3 mm wide,

were observed (Figure 1.4d). This morphology is not common, having been observed only twice in our samples. Thin section examination of the calcites using a petrographic microscope revealed calcite laths (Figure 1.5a-b) similar to those observed using SEM, and cross sections of branched tubes (Figure 1.5b) .

A single X-ray diffraction analysis of a mixed sample, collected from the horizontal and vertical fractures, shows that the fracture fillings are dominantly calcite, with minor amounts of minerals such as albite, sanadine, and tridymite. A nonexpanding clay, that has a diffraction pattern similar to sepiolite, is also present. The x-ray results substantiate that the SEM and thin-section morphologies described above are calcite.

Gas Analysis

Results from the quadrupole analyses are reported in mole % and represent 34 individual crushes of 9 samples (Table 1.1). Most crushes have substantial amounts of CH_4, CO_2, and N_2, trace amounts of Ar, and little to no O_2. H_2 was observed in small amounts in 6 analyses in which it was analyzed. Because of the previously mentioned analytical problems, analysis of H_2 was not normally done. Most crushes did not yield quantifiable amounts of H_2O, however, 38% of the crushes did

produce substantial quantities of H_2O. None of the crushes yielded any H_2S.

Isotopes

The fracture filling stable isotope results are fairly uniform, with a range of only 1.1 ‰ (-5.2 to -4.1‰) in $\delta^{13}C$ and a range of 3.1 ‰ (20.4 to 23.5‰) in $\delta^{18}O$ (Table 1.2). Average values were -4.6 (PDB) and 21.8 ‰ (SMOW) for $\delta^{13}C$ and $\delta^{18}O$ respectively. Carbon-14 age dates ranged from 23,280 years to 25,300 years and show a well defined pattern where the middle of the fracture filling is older than the edges (Figure 1.6).

Lipid Biomarkers

Phospholipid analysis has been used to determine the types and environmental responses of microorganisms in rocks and sediments (Hefter et al., 1993; Tunlid and White, 1992; Vestal and White, 1989; and Ward et al., 1985). The types of lipids recovered are diagnostic of the kinds of organisms present. A large number of lipids of different structures were found (Table 1.3). The ester-linked phospholipid fatty acids (PLFA) indicate that a viable microbial community existed in the fractures at the time of sampling (Tunlid and White, 1992). Lipids are

identified in the table using shorthand notation (Vestal and White, 1989). The number before the colon indicates the number of carbons in the fatty acid, and the number after the colon indicates the number of double bonds in the fatty acid chain. The position of the initial unsaturation is indicated by the number of carbon units from the methyl, or ω, end of the molecule. The geometry of the double bond is shown by c for cis and t for trans. Methyl branching is indicated as iso (i; the second carbon from the methyl end), anteiso (a; the third carbon), or br if the position is unknown. When a branch is known but is not in the i or a position, it is indicated by the position from the carboxyl end followed by Me before the carbon chain length (e.g., 10Me18:0). Cyclopropane fatty acids are indicated as cy.

A summary of the types of organisms found to be present in the fractures, through the detection of various lipid moieties, is presented in Table 1.4. The summary shows that archaebacteria, actinomycetes, fungi, gram-positive and gram-negative bacteria, and vascular plants all likely existed in the fractures. Membrane fatty acids averaged 29.3 pmol/gm of calcite for the three replicates, which translates roughly into 7.3×10^5 cells/gm assuming that there are 2.5×10^4 cells of a typical subsurface bacteria in 1 pmole of PLFA (Blackwill et al., 1988).

DISCUSSION

Calcite Morphology

The calcite morphologies observed are very similar to morphologies described in previous studies of calcites in pedogenic environments (e.g., Callot et al., 1985; Folk 1993; Klappa 1979; Monger et al., 1991; Vaniman et al., 1994; and Verrecchia and Verrecchia, 1994). These studies attributed the morphologies to plant- and microbial-growth and decay processes and this explanation appears to be applicable to the Los Alamos calcite fillings. The calcite laths observed during the SEM and thin section analyses (Figures 1.4 and 1.5) are probably remnants of fungal hyphae (see Verrecchia and Verrecchia, 1994). The laths were surrounded by a gelatinous sheath which formed the tubular hyphal structures that housed the fungal cytoplasm. The gelatinous sheath is broken down by bacteria, releasing the laths from their growth position (Verrecchia and Verrecchia, 1994). It is unclear whether the laths originally grew as organic material and were later replaced by calcite or whether they originally grew as calcite. Callot et al. (1985) have demonstrated that some fungi have the ability to grow laths as calcite.

Two types of hyphae-like, tubular structures were observed (Figures 1.4d and 1.5b). The morphology of the crystals in Figure 1.4d is similar to that of calcium oxalate crystals grown on fungal hyphae, as

observed by Graustein et al. (1977), and to calcified fungal filaments observed by Vaniman et al. (1993). Klappa (1979) also described calcified hyphae with the same morphology and attributed the precipitation to microbes. The hyhae-like cross sections shown in Figure 1.5b are probably either from fungi or actinomycetes because they are very similar to the examples in Forster et al. (1983).

The amorphous-looking material in Figure 1.4c, appears to be a calcified gel. This material is very similar to plant mucilage or could be remnant fungal sheaths (see Forster et al., 1983). Associated with the gel material are the hair- and bagel-like structures shown by arrows in Figure 1.4c. These features are similar to those observed in calcites by Folk (1993), and in root-soil interface samples by Forster et al. (1983). Both of these studies interpreted the morphologies as bacterial in origin. The possibility that the calcite lath, hyphae-like, and amorphous morphologies are the product of inorganic precipitation was considered, but no inorganically precipitated examples of these morphologies were found in the literature.

Stable Isotopes

Stable isotope compositions of all of the fracture filling samples fall within or close to the range of $\delta^{13}C$ and $\delta^{18}O$ values of pedogenic calcites

given by Talma and Netterberg (1983) consistent with calcite precipitation under pedogenic conditions (Figure 1.7). They are also consistent with some freshwater limestones and marine calcite concretions, but no signs of a previous saturated or lacustrine environment exists at the site, and marine conditions have not existed in the area since the Bandelier Tuff was deposited. Some of the $\delta^{18}O$ analyses are about one permil lighter than the lightest values reported by Talma and Netterberg. This most likely reflects the light isotopic composition of local precipitation which is controlled by the high elevation and interior-continental position of Los Alamos.

The calcite $\delta^{13}C$ values are in apparent contradiction to the presence of CH_4 which is indicated by the fluid inclusion gas analyses. Marine calcites produced during methanogenesis typically have heavy $\delta^{13}C$ values because of ^{12}C fractionation into the CH_4, which leaves dissolved carbonate (that contributes to calcite precipitation) enriched in ^{13}C (Figure 1.7). One possible explanation for the apparent discrepancy is that methane was generated by the acetate pathway rather than the CO_2 pathway. Whiticar et al. (1986) pointed out that many investigators regard the acetate pathway as being dominant in freshwater environments, while the CO_2 pathway is regarded as dominant in marine environments. However; it should not be assumed that the CO_2 pathway

is inactive in freshwater environments (see Mozley and Wersin 1992, and Whiticar et al., 1986). The general acetate fermentation reaction is given below (Lovley and Klug, 1986):

$$CH_3COO^- + H_2O \leftrightarrow CH_4 + HCO_3^- \quad (1)$$

Methane generation from acetate would not enrich the carbon pool available for calcite precipitation to the same degree as from the CO_2 pathway for two reasons. First, acetate has two carbons, one in a methyl group and the other in a carboxyl group. Methanogens use the methyl carbon (Whiticar et al., 1986) and thus, do not directly fractionate the carboxyl carbon which is more likely to end up in calcite. The result is that while the CO_2 methanogenic pathway can result in a large fractionation of the carbon available for calcite precipitation, the acetate pathway more likely results in little fractionation because the carbon pool is not depleted in ^{12}C as a result of acetate fermentation. Second, if the methanogens mainly utilize the acetate carbon, there are presumably other carbon sources in the system that would be unaffected by methanogenic fractionation (such as existing HCO_3^-) that could contribute to calcite precipitation.

Another explanation for the "light" calcites can be applied with production of CH_4 through the CO_2 pathway. If only a small amount of CH_4 is produced, a correspondingly small shift in the $\delta^{13}C$ values would

occur. Closed-system Rayleigh calculations by Nissenbaum et al. (1972) and Claypool and Kaplan (1974) indicate that 25-50% of the CO_2 (total dissolved carbon) in a system must be converted to methane before there is enough fractionation of the carbon pool to yield the isotopically-heavy $\delta^{13}C$ values observed from marine calcites. Because deep-marine methanogenic environments typically have only a few percent organic carbon (e.g., 2-3%, Hammond, 1974 and Whelan, 1974), methanogenesis can utilize a substantial proportion of the CO_2 generated from the organics. However, in the Bandelier Tuff fracture system there is a very large amount of organic carbon (plant roots) which serves as a tremendous source of CO_2. In this case, it seems unlikely that methanogenesis could deplete the large carbon pool to a degree that would cause observable fractionation. The dominance of CH_4 in the inclusion gas (Table 1.1) does not necessarily indicate that there was a lot of methane generated in the fractures, which would contradict this explanation for the light calcites. The quadrupole data represent only the relative proportions of gases and not their absolute quantity and therefore, no inference can be made regarding the absolute amount of CH_4 production.

From the above discussion it does not appear that methanogenesis has affected the $\delta^{13}C$ of the dissolved carbonate from which calcite

precipitated. Since it appears that calcite has formed in a pedogenic environment, the $\delta^{13}C$ should reflect local plant carbon. Cerling et al. (1989) and Quade and Cerling (1990) have shown that the type of vegetative cover (i.e., the relative percentages of C3 and C4 plants) is what indirectly controls pedogenic calcite $\delta^{13}C$ values (Figure 1.7). The C3 and C4 designation indicates the type of photosynthetic pathway that a species of plant uses and the pathway affects the $\delta^{13}C$ of the plant carbon. C3 plant carbon has an average $\delta^{13}C$ of -24 ‰ and C4 plant carbon has an average $\delta^{13}C$ of -13 ‰ (Quade and Cerling, 1990). Cerling et al. (1989) developed a relationship that permits the estimation of organic matter $\delta^{13}C$ values from pedogenic calcite $\delta^{13}C$ values. The resulting Los Alamos organic carbon $\delta^{13}C$ estimates can be compared to $\delta^{13}C$ values for modern and Pleistocene Los Alamos plant types. If the organic carbon $\delta^{13}C$ estimates are consistent with the $\delta^{13}C$ of modern and Pleistocene plants, then this further supports the lack of a methane control on calcite $\delta^{13}C$ values, and reinforces the importance of pedogenic processes in the fractures. Cerling et al. (1989) found that organic matter (plant carbon) is consistently 14-16 ‰ lighter than the associated calcite. Atmospheric CO_2 input is a potentially complicating factor in the estimation, but Cerling et al. (1989) suggested that if sampling is performed in areas with precipitation over 35 cm/yr and at

depths greater than 30 cm that atmospheric CO_2 effects will be minimized. Both of these conditions apply to the sampling done for this study. Using the average $\delta^{13}C$ of the Los Alamos calcites (-4.6 ‰) in the relationship of Cerling et al. (1989), the fracture organic matter would have had a $\delta^{13}C$ between -18.6 and -20.6 ‰. Based on the average values for C3 and C4 plants above, it appears that the fractures had a mixture of C3 and C4 organic matter. The result is consistent with the modern plant cover which is made up of Pinyon Pine, Juniper (both C3 plants) and some C4 grasses. Leavitt and Long (1986) measured the $\delta^{13}C$ of pinyon and juniper cellulose and found values between -19 and -23 ‰. The similarity of the estimated organic carbon $\delta^{13}C$ range from the Los Alamos calcites compared to the Leavitt and Long values suggests that pinyon pine and juniper trees may have provided the main control on the Los Alamos $\delta^{13}C$ values. The estimated organic carbon values are also consistent with Pleistocene paleoecological studies of New Mexico that indicate that the vegetative cover around Los Alamos was mainly C3, either Pinyon-Juniper or mixed-conifer forest (Betancourt et al., 1993).

Gas Analyses

The calcite fluid inclusion gas compositions from (Table 1.1) show a suite of gases similar to what one would expect under anaerobic decay conditions. Characteristics of anaerobic decay include the production of CH_4, H_2, and N_2, combined with very low amounts of O_2.

Additional interpretations of the gas compositions can be made by comparison with gas data from other low-temperature, near-surface calcite deposits. Newman et al. (1995) have analyzed gases from inclusions in travertines which are formed on the surface from upwelling water. N_2/Ar ratios in the fracture-fill calcites vary much more than those from the travertines, which are relatively constant and lie between the values for air and air-saturated water on a N_2-Ar-CO_2 ternary plot (Figure 1.8). This difference suggests that N_2 was probably produced *in situ* because most of the Los Alamos samples fall above the value for air. Likely sources of N_2 production are microbial reactions such as NO_3^- reduction.

$$2NO_3^- + 12H^+ + 10e^- \leftrightarrow N_2 + 6H_2O \qquad (2)$$

Analysis of NH_3 would have been useful in understanding the details of the nitrogen cycle in the fractures. However, QMS sensitivity for NH_3 is

poor because NH_3 peaks are obscured by the mass spectra of CH_4, CO_2, and H_2O hence, NH_3 analyses were not performed.

In addition to indicating N_2 production, the large variation in N_2/Ar ratios (Table 1.1, Figure 1.8) also shows that the calcites did not precipitate from rising groundwaters. Travertines and hydrothermal vein calcites have well constrained N_2/Ar ratios and plot between the boundaries defined by air and air-saturated water (Newman et al., 1995). The Los Alamos calcites do not consistently plot within these boundaries indicating that they were precipitated under different conditions than the groundwater-derived travertines. The fluid inclusion gas compositions of the Los Alamos calcites show that they were precipitated in a vadose or unsaturated environment because they do not contain much water (Table 1.1). Gundimeda (1995), and Newman et al. (1995) showed that calcites with gas dominant inclusions have a vadose origin, while those with inclusions that contain over 98 mole% water form under saturated conditions.

One potential problem with the interpretation of the gas analyses is that the gases may have resulted from migration from the surrounding tuff. However, the tuffs contain H_2S, and no sulfur-containing gases were observed in any of the calcite crushes. It also does not appear that the gases resulted from microbial decomposition of encapsulated organic

matter after calcite precipitation had occurred, although this possibility can not be totally ruled out. Newman et al. (1995) analyzed travertines from different springs using the same procedure used here, and found much less methane and no evidence of excess nitrogen production as was the case in the Los Alamos fracture fillings. Yet, the travertines have a much higher organic content than do the Los Alamos fracture fillings. If the post-precipitation encapsulation process was contributing significant amounts of anaerobic gas it should occur in the travertines, but this was not observed. In addition, if gas is produced by the decay of encapsulated organic material, there would be an increase in pressure that would likely crack the seal and allow movement of atmospheric gases in and the decay products out. In fact, it seems unlikely that significant quantities of organic matter could be sealed so well that gaseous diffusion in and out of the encapsulated area would not occur. A final argument against the encapsulation idea is that if the anaerobic gases were produced after calcite precipitation, the quadrupole results would show mixtures of both anaerobic and aerobic gases. This is because there would likely be aerobic inclusions that would be opened along with the anaerobic interstitial or nonprimary inclusion sources. Occasional crushes did produce mixtures, but the majority of crushes did not show any significant aerobic input, and many crushes showed

no quantifiable O_2 at all. It is likely that the few mixtures that were observed were samples with interstitially trapped atmospheric volatiles.

Age Determinations

Carbon-14 age determinations show that the calcite in the middle of the fracture is older than that on the edges (Figure 1.6). This trend in ages is not consistent with the typical paragenesis of inorganic vein deposits where precipitation begins at the fracture edges and fills inward. Precipitation on an organic substrate could result in the observed trend in ages. If plant roots run down the center of the fracture, calcite can precipitate there first and subsequent roots that grow along the edges could become the substrate for a younger generation of calcite creating the observed trend in ages.

Amundson et al. (1994) found that microbial gas input can cause ^{14}C ages to vary from the true age of precipitation. Unfortunately, because some required parameters are unknown, the Los Alamos calcite ages can not be corrected for microbial gas contribution using the approach in Amundson et al. However, even though the absolute ages will include some unquantifiable error due to microbial gas input, the relative age differences should be significant because levels of microbial gas input to the fracture were probably similar across the transect.

Lipid Biomarker Analysis

Fatty acid results from the fracture fillings (Table 1.3) were summarized as to organism presence (Table 1.4), in order to obtain an estimate of the microbial community composition in the fracture fillings. The profile of the PLFA recovered showed that the viable microbial community was composed primarily of gram negative bacteria as indicated by the detection of a high mole percentage (42.2%) of monounsaturates. Also detected at a high mole percentage was the mid-chain branched saturate, 10me18:0 or tuberculosteric acid at 17.7%. This PLFA has been found in the cell membranes of a number of Actonomycetes. Apha-hydroxy fatty acids (2-OHFAME) comprised 25.5% of the total lipids assayed for and are indicative of gram negative bacteria such as the *Sphingomonas* genus as well as the higher plants (Parker et al., 1982). Sterols were found to comprise 36.7% of the total lipids assayed for with the types found in the fracture fillings being indicative of higher plants (sitosterol and stigmasterol) and certain mycorrhizal fungi (campesterol, stigmasterol) (Vestal and White, 1989). Di-ethers are indicative of the archaebacteria and have been detected in halophiles and methanogens (from Hedrick et al., 1991; Nichols et al., 1993). There was no evidence of a high salt concentration in the fractures making it unlikely that the di-ethers were derived from halophiles. The relatively

high percentage of di-ethers (37.9%) of the total lipids assayed for suggests that the methanogens were an important part of the microbiota.

Precipitation Model

The progression from organic (plant material) to inorganic (calcite) carbon in the vertical fracture is depicted in Figure 1.9. At the initial stage, the fractures were filled with live roots and other organic material, indicated by the presence of occasional root casts and dead root material in the fractures, the hydroxy fatty acids and sterols in the phospholipid analysis, and the fact that "recent" fractures are often filled with plant roots. Water movement in the fractures must have been sufficient to support plant growth.

Stage two is death of the plant roots. The cause of death is not known, but it could be related to erosion of an older soil on the mesa top (as evidenced by the presence of nearby clay-filled fractures) or from natural root turnover. Once dead, the roots were attacked by aerobic fungi and bacteria. (Fungal growth also occurs in stage one, as part of the mycorrhizal association of fungi and plant roots.) Fungi are important because they are generally the primary decomposers of organic matter (Paul and Clark, 1989), and constitute a large fraction of

the microbial biomass in soil (Atlas and Bartha, 1993). Calcite precipitation of fungal fibers may occur at this stage if the types of fungi present have a direct precipitation capability. However, if fungal calcite precipitation occurs at this stage, the laths must contain little or no inclusion gas, because only small percentages of O_2 were observed in most of the quadrupole analyses. In addition, if the lath calcite is precipitated by fungi, based on a very qualitative assessment of the SEM and thin section results, roughly half of the calcite in the fillings may be fungal in origin.

Even if the fungi do not directly precipitate the calcite, they still play an important role in the calcium cycle because they are extremely effective in concentrating calcium in the form of calcium oxalate. Calcium oxalate, is a major metabolic product of fungi, and forms on the outside of the fungal hyphae (Cromack et al., 1977; Graustein et al., 1977; Verrecchia, 1990). The oxalate is typically in the form of whewellite ($CaC_2O_4 \cdot H_2O$) or weddellite ($CaC_2O_4 \cdot nH_2O$).

Certain bacteria and actinomycetes that inhabit soils and the guts of soil organisms are known to decompose calcium oxalate, which promotes the precipitation of calcite by releasing calcium and increasing the system pH (Cromack et al., 1977; Verrecchia, 1990). The general decomposition reaction is:

$$CaC_2O_4 + O_2 + 2H^+ \leftrightarrow Ca^{++} + 2HCO_3^- \quad (3)$$

Because oxygen is used in the breakdown of calcium oxalate, this reaction may help create anaerobic conditions. No oxalate minerals were found by x-ray diffraction of the Los Alamos fracture fillings, which indicates that all of it must have been converted to calcite.

At some point, fungal growth ceases, either because the organic substrate is exhausted or because of the development of anaerobic conditions. Once fungal growth ends, bacteria can attack the gelatinous sheath of the fungal hyphae, causing breakdown of the hyphal structure. With the breakdown of the sheath, the network of laths is destroyed. If the laths were initially organic, the breakdown of the fungal sheath would be a likely time for the replacement process to begin because fracture solutions and bacteria would have direct access to the laths.

Stage 3 of the model is the onset of anaerobic conditions which can develop in one of two ways: first, the fracture may become physically sealed. This does not appear to be the case at our site, because no evidence of material sealing the edges of the fracture is visible. In addition, if the system were closed, the amount of Ca needed to create

the relatively extensive calcite mineralization observed could not be supplied.

The second way in which an aerobic system becomes anaerobic is analogous to the anaerobic microsite process observed in soils (Atlas and Bartha, 1993; Engel and Macko, 1993): aerobic microbes in a packet of organic matter use up oxygen faster than it can be transported into the system. Ultimately, the system ends up with an outer aerobic zone in which oxygen entering the system is used up; an inner zone in which microaerobes use any remaining oxygen; and an anaerobic core. An example of the development of an anaerobic soil ped is shown in Figure 1.10. It is likely that this type of excess oxygen respiration process produced the anaerobic conditions in the Los Alamos calcites. It is at this stage that trapping of the inclusion gases apparently began, based on the anaerobic suite of gases within the inclusions.

Stage 4 of the model is that of anaerobic conditions. A host of microbial reactions involving nitrogen could occur at this stage–some of which could change the pH of the system (e.g., equation 2). Because of the complexity of the nitrogen cycle, it is difficult to specify which particular set of reactions may have resulted in the production of N_2 gas, although the N_2/Ar data (Figure 1.8) strongly suggests that N_2 production took place.

Any reactions involving nitrogen are eventually followed by methanogenesis because methanogenesis is the terminal stage of anaerobic microbial decay. Certain methanogenesis reactions can bring about conditions favorable for precipitation of calcite. One of these, in which both H_2 and CO_2 are used as reactants, produces methane and increases system pH:

$$CO_2 + 4H_2 \leftrightarrow CH_4 + 2H_2O. \quad (4)$$

There is some evidence that this reaction may have occurred in the fractures. When the relationships between the mole percentages of the gas species were examined, a significant inverse correlation between CO_2 and CH_4 was found (Figure 1.11). The correlation between H_2 and CH_4 was not significant, possibly because of the small number of H_2 analyses. The linearity of the CO_2 and CH_4 data in Figure 1.11 is striking considering the natural variability in the samples: a linear regression yielded an R^2 of -0.70 at a 95% confidence level. Three of the worst outliers came from crushes of sample 4706 which contained anomalous amounts of air. If these three crushes are not included in the regression the R^2 increases to -0.90. The inverse correlation

suggests that CH_4 is produced at the expense of CO_2, which is consistent with equation 4.

Although the acetate pathway was suggested earlier as a possible explanation for the lack of a methanogenic fractionation of the calcite $\delta^{13}C$ values, the CH_4 and CO_2 inverse correlation does not support acetate as the methane source. If a significant amount of CH_4 was produced from acetate, a positive correlation would be expected because CH_4 and CO_2 are both produced during acetate fermentation. However, the correlation does not prove that the CO_2 pathway was dominant. The correlation could represent instead, methane production through acetate fermentation simultaneous with another process which lowers the amount of CO_2 such as calcite precipitation.

Ultimately, there is conflicting evidence on which of the methanogenic pathways were used. The strong inverse correlation of CH_4 and CO_2 suggests methanogenesis via CO_2 reduction, while the lack of heavy calcite $\delta^{13}C$ values and freshwater conditions support production via acetate fermentation. Future research will involve investigating ways to collect inclusion-hosted methane so that the isotopic composition can be measured. These results could then be compared to the $\delta^{13}C$ and dD relationships in Whiticar et al. (1986) allowing a determination of the methanogenic pathway.

The above description of the CO_2-reduction pathway shows that because of a pH increase, methanogenesis can cause inorganic calcite precipitation. But, another possibility exists: the direct precipitation of calcite by anaerobes. Direct precipitation of calcite by aerobic bacteria has been demonstrated (Boquet et al., 1973; Monger et al., 1991). It is possible that anaerobes have this same capability, however, no research demonstrating direct precipitation by anaerobes was found.

The model described here may have applications beyond that of the fracture fillings at Los Alamos. For example, it may explain the occurrence of other pedogenic calcites. Gundimeda (1995) and Newman et al. (1995) have conducted quadrupole gas analyses of soil-hosted pedogenic calcites from various sites in New Mexico and have obtained results similar to those reported here, which suggests that microbial processes are important in controlling calcite precipitation in soils as well as fractures.

It seems unlikely, given the presence of anaerobic zones in oxidizing soils and sediments, that pedogenic carbonates are precipitated solely under aerobic conditions. Unpublished work by Chin and Zinder (1982), cited by Zinder (1993), suggests that development of anaerobic zones may be common. They found viable counts of methanogens greater than 10^3 per gram dry weight in "presumably aerobic soil under

grass." Further research may reveal more examples of anaerobic calcite precipitation similar to those described here.

SUMMARY & CONCLUSIONS

The present study focused on a determination of the processes that led to the precipitation of calcite fracture fillings at Los Alamos, New Mexico. Precipitation was due to both aerobic and anaerobic microbial activity. Fluid inclusion gas analyses showed a unique and consistent suite of gases that included Ar, CH_4, CO_2, H_2, N_2, and little or no O_2. Except for Ar and CO_2, these gases could have been created only through anaerobic microbial decay. Scanning electron microscopy images of the calcites confirmed the importance of fungi and bacteria in the fracture system. Lipid analysis confirmed that a diverse microbial community, including gram positive- and negative-bacteria, fungi, actinomycetes, and methanogens, existed in the fractures.

A model was developed to describe the transition from a root-filled fracture to a calcite-filled fracture. It considers fungal decay of the roots, the importance of fungally produced calcium oxalate, and the transition from an aerobic to an anaerobic state as oxygen, because of excessive microbial respiration, becomes a limiting nutrient. It also suggests that anaerobic reactions involving the production of nitrogen and methane

may have led to the precipitation of a substantial portion of the calcite. Finally, the model may explain the development of some soil calcites such as calcite nodules, coatings on peds, and fillings in macropores. Based on these results, it is possible that anaerobic calcite formation in soils and in the vadose zone may be a common phenomenon and is most likely to occur in zones of high organic content.

REFERENCES

Amundson, R., Y. Wang, O. Chadwick, S. Trumbore, L. McFadden, E. McDonald, S. Wells, M. DeNiro. 1994. Factors and Processes Governing the ^{14}C Content of Carbonate in Desert Soils. Earth Planet. Sci. Lett., V. 125. pp. 385-405.

Arthur, M. A., T. F. Anderson, I. R. Kaplan, J. Veizer, and L. S. Land. 1983. Stable Isotopes in Sedimentary Geology, SEPM Short Course No. 10. SEPM, Tulsa.

Atlas, R. M. and R. Bartha. 1993. Microbial Ecology. 3rd ed. Benjamin/Cummings Publishing Co. New York. pp. 274-276.

Balzers Corporation. 1989. QUADSTAR®-gas analysis software, Version 2.33. Balzers Corporation, Liechtenstein.

Betancourt, J. L., E. A. Pierson, K. Aasen-Rylander, J. A. Fairchild-Parks, and J. S. Dean. 1993. Influence of History and Climate on New Mexico Piñyon-Juniper Woodlands. In Managing Piñyon-Juniper Ecosystems for Sustainability and Social Needs, Proceedings of the 1993 Sante Fe Conference. USDA Forest Serv. Gen. Tech. Report, RM-236. 169 pp.

Blackwill, D. L., F. R. Leach, J. T. Wilson, J. F. McNabb, and D. C. White. 1988. Equivalence of Microbial Biomass Measures Based on Membrane Lipid and Cell Wall Components, Adenosine Triphosphate, and Direct Counts in Subsurface Aquifer Sediments. Microb. Ecol. V. 16. pp. 73-84.

Boquet, E., A. Boronat, and A. Ramos-Cormenzana. 1973. Production of Calcite (Calcium Carbonate) Crystals by Soil Bacteria is a General Phenomenon. Nature, V. 246. pp. 527-529.

Callot, G., A. Guyon, and D. Mousain. 1985. Inter-Relations Entre Aiguilles de Calcite et Hyphes Mycéliens. Agronomie, V. 5, No. 3. pp. 209-216.

Cerling, T. E., J. Quade, Y. Wang, and J. R. Bowman. 1989. Carbon Isotopes in Soils and Paleosols as Ecology and Palaeoecology Indicators. Nature, V. 341. pp. 138-139.

Chin, S. and S. H. Zinder. 1982. Unpublished results.

Claypool, G. E. and I. R. Kaplan. 1974. The Origin and Distribution of Methane in Marine Sediments. In Marine Science, V. 3, Natural Gases in Marine Sediments. I. R. Kaplan, ed. Plenum Press, NY. pp. 99-139.

Cromack, K., Jr., P. Sollins, R. L. Todd, R. Fogel, A. W. Todd, W. M. Fender, M. E. Crossley, and D. A. Crossley, Jr. 1977. The Role of Oxalic Acid and Bicarbonate in Calcium Cycling by Fungi and Bacteria: Some Possible Implications for Soil Animals. Ecol. Bull. (Stockh.) V. 25. pp. 246-252.

Davenport, D. W. 1993. Micromorphology, Mineralogy, and Genesis of Soils and Fracture Fills on the Pajarito Plateau, New Mexico. Ph.D. dissertation, Texas Tech. Univ., Lubbock, TX. 109 pp.

Davenport, D. W., B. P. Wilcox, and B. L. Allen. 1995. Micromorphology of Pedogenically Derived Fracture Fills in Bandelier Tuff, New Mexico. Soil Sci. Soc. Am. J. V. 59. pp. 1672-1683.

Dixon, J. C. 1994. Duricrusts. In Geomorphology of Desert Environments A. D. Abrahams and A. J. Parsons (eds.). Chapman and Hall, New York. pp. 82-105.

Engel, M. H. and S. A. Macko. 1993. Organic Geochemistry. Plenum Press, New York. pp. 136-137.

Folk, R. L. 1993. SEM Imaging of Bacteria and Nannobacteria in Carbonate Sediments and Rocks. J. Sed. Pet. V. 63, No. 5. pp. 990-999.

Forster, R. C., A. D. Rovira, and T. W. Cook. 1983. Ultrastructure of the Root-Soil Interface. American Phytopathological Society, St. Paul. 157 pp.

Graustein, W. C., K. Cromack Jr., and P. Sollins. 1977. Calcium Oxalate: Occurrence in Soils and Effects on Nutrient and Geochemical Cycles. Science, V. 198. pp. 1252-1254.

Guckert, J. B., C. P. Antworth, P. D. Nichols, and D. C. White. 1985. Phospholipid, Ester-Linked Fatty Acid Profiles as Reproducible Assays for Changes in Prokaryotic Community Structure of Estuarine Sediments. FEMS Micobiol. Ecol. V. 31. pp. 147-158.

Gundimeda, M. 1995. Environmental Gas Analysis of Fluid Inclusions In Calcium Carbonates From New Mexico, Including Vein Calcites From Los Alamos National Laboratory, Using Quadrupole Mass Spectrometry. MS Thesis, New Mexico Tech., Socorro, NM. 141 pp.

Hammond, D. E. 1974. Dissolved Gases in Cariaco Sediments: Anaerobic Diagenesis. In Marine Science, V. 3, Natural Gases in Marine Sediments. I. R. Kaplan, ed. Plenum Press, NY. pp. 71-97.

Hefter, J., V. Thiel, A. Jenisch, U. Galling, S. Kempe, and W. Michaelis. 1993. Biomarker Indications for Microbial Contribution to Recent and Late Jurassic Carbonate Deposits. Facies, V. 29. pp. 93-106.

Hedrick, D. B., J. B. Guckert, and D. C. White. 1991. Archaebacterial Ether Lipid Diversity Analyzed by Supercritical Fluid Chromatography: Integration With a Bacterial Lipid Protocol. J. of Lipid Res., V. 32.

Jayasuriya, G. C. N. 1955. The Isolation and Characteristics of an Oxalate-Decomposing Bacterium. J. Gen. Microbiol, V. 12 pp. 419-428.

Klappa, C. F. 1979. Calcified Filaments in Quaternary Calcretes: Organo-Mineral Interactions in the Subaerial Vadose Environment. J. of Sed. Pet., V. 49, No. 3. pp. 955-968.

Leavitt, S. W., and A. Long. 1986. Stable-Carbon Isotope Variability in Tree Foliage and Wood. Ecology, V. 64, No. 4. pp. 1002-1010.

Lovley, D. R., and M. J. Klug. 1986. Model for the Distribution of Sulfate Reduction and Methanogenesis in Freshwater Sediments. Geochim Cosmochim. Acta, V. 50. pp. 11-18.

Mayberry, W. R. and J. R. Lane. 1993. Sequential Alkaline Saponification/Acid Hydrolysis/Esterification: a One Tube Method with Enhanced Recovery of Both Cyclopropane and Hydroxylated Fatty Acids. J. Microb. Meth. V. 18. pp. 21-32.

McCrea, J. M. 1950. The Isotopic Chemistry of Carbonates and a Paleotemperature Scale. J. Chem. Phys. V.18. pp. 849-857.

Monger, H. C., L. A. Daugherty, W. C. Lindemann, and C. M. Liddell. 1991. Microbial Precipitation of Pedogenic Calcite. Geology, V. 19. pp. 997-1000.

Mozley, P. S. and P. Wersin. 1992. Isotopic Composition of Siderite as an Indicator of Depositional Environment. Geology, V. 20. pp. 817-820.

Mozley, P. S. and S. J. Burns. 1993. Oxygen and Carbon Isotopic Composition of Marine Carbonate Concretions: An Overview. J. of Sed. Pet., V. 63, No. 1. pp. 73-83.

Newman, B. D., D. I. Norman, and M. Gundimeda. 1995. Understanding the Genesis of Nonmarine Calcite Deposits Through Quadrupole Mass Spectrometric Analysis of Fluid Inclusion Gases. Chem. Geology. In Press.

Nichols, P. D., P. M. Shaw, C. A. Mancuso, and P. D. Franzmann. 1993. Analysis of Archaeal Phospholipid-Derived Di- and Tetraether Lipids by High Temperature Capillary Gas Chromatography. J. Micorb. Meth. V. 18. pp. 1-9.

Nissenbaum, A., B. J. Presley, and I. R. Kaplan. 1972. Geochim. Cosmochim. Acta, V. 36. pp. 1007-1027.

Norman, D. I. and F. J. Sawkins. 1987. Analysis of Volatiles in Fluid Inclusions by Mass Spectroscopy. Chem. Geol. v. 61. pp 1-10.

Parker, J. H., G. A. Smith, H. L. Fredrickson, J. R. Vestal, and D. C. White. 1982. Sensitive Assay, Based on Hydroxy Fatty Acids from Lipopolysaccharide Lipid A, for Gram-Negative Bacteria in Sediments. Applied and Environ. Microbiology. V. 44, No. 5. pp 1170-1177.

Paul, E. A., F. E. Clark. 1989. Soil Microbiology and Biochemistry. Academic Press, NY. 273 pp.

Phillips, S. E. and P. G. Self. 1987. Morphology, Crystallography and Origin of Needle-fibre Calcite in Quaternary Pedogenic Calcretes of South Australia. Aust. J. Soil Res., V. 25. pp. 429-444.

Quade, J. and T. E. Cerling. 1990. Stable Isotopic Evidence for a Pedogenic Origin of Carbonates in Trench 14 near Yucca Mountain, Nevada. Science, V. 250. pp. 1549-1552.

Reneau, S. L. and D. T. Vaniman. 1994. Fracture Characteristics in a Disposal Pit on Mesita del Buey, Los Alamos National Laboratory. Unpublished Los Alamos National Laboratory Report, Los Alamos, NM. 17 pp.

Ruff, R. K. 1993. Gas Analysis of Fluid Inclusions: Application Towards Precious Metal Exploration, Steeple Rock Mining District, Grant County, New Mexico. MS Thesis, New Mexico Tech., Socorro, NM. 95 pp.

Talma, A. S., and F. Netterberg. 1983. Stable Isotope Abundances in Calcretes. In Residual Deposits: Surface Related Weathering Processes and Materials, R. C. Wilson, ed. Blackwell Scientific Publications, London. 258 pp.

Tunlid, A., and D. C. White. 1992. Biochemical Analysis of Biomass, Community Structure, Nutritional Status, and Metabolic Activity of Microbial Communities in Soil. In Soil Biochemistry, V. 7, G. Stotzky and J.-M. Bollag, eds. Marcel Dekker, NY. pp. 229-262.

Vaniman, D. T., S. J. Chipera, and D. L. Bish. 1994. Pedogenesis of Siliceous Calcretes at Yucca Mountain, Nevada. Geoderma, V. 63. pp. 1-7.

Verrecchia, E. P. 1990. Litho-Diagenetic Implications of the Calcium-Oxalate-Carbonate Biogeochemical Cycle in Semiarid Calcretes, Nazareth, Israel. Geomicrobiology Journal, V. 8. pp 87-99

Verrecchia, E. P., and K. E. Verrecchia. 1994. Needle-Fiber Calcite: A Critical Review and A Proposed Classification. J. of Sed. Research, V. A64, No. 3. pp. 650-654.

Vestal, J. R. and D. C. White. 1989. Lipid Analysis in Microbial Ecology. Bioscience, V. 39, No. 8. pp. 535-541.

Ward, D. M., S. C. Brassell and G. Eglinton. 1985. Archaebacterial Lipids in Hot-Spring Microbial Mats. Nature, V. 318 pp. 656-659.

Whelan, T. 1974. Methane and Carbon Dioxide in Marsh Sediments. In Marine Science, V. 3, Natural Gases in Marine Sediments. I. R. Kaplan, ed. Plenum Press, NY. pp. 47-61.

White, D. C. 1988. Validation of Quantitative Analysis for Microbial Biomass, Community Structure, and Metabolic Activity. Archive für Hydrobiology Beihefte, V. 31. pp. 1-18.

Whiticar, M. J., E. Faber, and M. Schoell. 1986. Biogenic Methane Formation in Marine and Freshwater Environments: CO_2 Reduction *vs.* Acetate Fermentation-Isotope Evidence. Geochim. Cosmochim. Acta, V. 50. pp. 693-709.

Wright, V. P. 1986. The Role of Fungal Biomineralization in the Formation of Early Carboniferous Soil Fabrics. Sedimentology, V. 33. pp. 831-838.

Zinder, S. H. 1993. Physiological Ecology of Methanogens. In Methanogenesis. J. G. Ferry ed. Chapman and Hall, New York. pg. 136.

Table 1.1. Quadrupole Results for Individual Calcite Crushes
All analyses in mole%.

Sample No.	H_2	CH_4	N_2	O_2	Ar	CO_2	H2O	N/Ar
4510A	2.30	43.26	22.77	0.00	0.10	31.57	0.00	223.98
4510B1	7.32	39.72	26.39	0.00	0.11	26.46	0.00	229.67
4510B2	0.64	7.11	0.73	0.00	0.01	3.01	88.50	72.38
4510C	4.48	16.32	6.05	0.00	0.03	73.12	0.00	201.48
4510D	8.75	59.49	15.02	0.00	0.02	16.72	0.00	746.64
4418A	NA	31.75	10.22	0.00	0.01	58.01	0.00	706.15
4418B	NA	49.33	15.52	0.00	0.07	35.09	0.00	219.60
4418C	7.43	68.55	18.03	0.12	0.13	5.75	0.00	141.61
4675A	NA	66.61	13.35	0.00	0.00	20.02	0.00	-
4675B	NA	38.56	9.51	0.00	0.00	7.05	44.88	-
4675C	NA	76.09	15.44	0.00	0.02	8.43	0.00	696.51
4675D	NA	56.03	11.50	0.00	0.06	32.41	0.00	182.60
4676A	NA	11.19	2.50	0.00	0.02	3.59	82.70	130.63
4676B	NA	27.41	6.83	0.29	0.06	7.48	57.92	123.71
4676C	NA	69.81	12.63	0.00	0.06	17.49	0.00	197.13
4677A	NA	31.63	12.52	1.56	0.02	54.21	0.00	634.35
4677B	NA	24.52	6.43	0.00	0.03	69.01	0.00	217.76
4677C	NA	5.73	2.29	0.02	0.03	13.19	78.72	65.56
4699A	NA	52.74	0.83	0.00	0.11	46.32	0.00	7.55
4699B	NA	5.85	0.60	0.00	0.00	7.61	85.94	-
4699C	NA	49.42	10.92	0.00	0.00	39.65	0.00	-
4699D	NA	53.71	13.92	0.00	0.03	32.32	0.00	464.00
4700A	NA	2.29	0.04	0.00	0.01	9.60	88.05	4.00
4700B	NA	26.86	4.88	0.00	0.04	25.24	42.97	122.00
4700C	NA	52.64	5.06	0.00	0.14	42.16	0.00	36.14
4700D	NA	37.12	7.41	0.00	0.06	19.42	35.97	123.50
4701A	NA	7.80	0.06	0.00	0.02	16.97	75.14	3.00
4701B	NA	3.38	0.59	0.00	0.01	10.10	85.92	59.00
4701C	NA	8.27	2.46	0.03	0.01	11.40	77.60	246.00
4701D	NA	74.13	18.66	6.38	0.12	0.72	0.00	155.50
4706A	NA	26.91	33.95	1.50	0.31	37.32	0.00	109.52

Table 1.1 (cont.). Quadrupole Results for Individual Calcite Crushes
All analyses in mole%.

Sample No.	H_2	CH_4	N_2	O_2	Ar	CO_2	H2O	N/Ar
4706B	NA	15.10	4.09	0.46	0.00	0.00	80.35	-
4706C	NA	49.68	41.77	4.03	0.26	4.10	0.00	160.65
4706D	NA	43.96	38.04	17.27	0.73	0.00	0.00	52.11

NA - Not Analyzed

Sample identifications with the same number, but different alphabetic suffixes, represent multiple crushes of the same sample.

Table 1.2. Stable-Isotope Data for Calcite Fracture Fillings

Samples from Vertical Fracture

Sample No.	$\delta^{13}C$	1σ	$\delta^{18}O$	1σ
LA1-8898-1	-4.25	0.05	22.06	0.08
LA1-8898-2	-4.68	0.04	22.01	0.12
LA1-8898-3	-4.38	0.04	22.03	0.09
LA1-8898-4	-4.59	0.08	21.79	0.14
LA1-8898-5	-4.69	0.02	21.59	0.15
LA1-8898-6	-4.48	0.07	21.93	0.15
LA1-8898-7	-4.11	0.04	22.47	0.17
LA1A-8898-1	-4.47	0.08	22.05	0.09
LA1A-8898-2	-4.61	0.18	21.68	0.26
LA1A-8898-3	-4.62	0.04	21.39	0.04
LA1A-8898-4	-4.61	0.08	21.58	0.14
LA1A-8898-5	-4.84	0.03	21.50	0.03
LA1A-8898-6	-4.64	0.02	22.30	0.09
LA1-300	-4.20	0.04	23.06	0.19

Samples from Horizontal Fracture

Sample No.	$\delta^{13}C$	1σ	$\delta^{18}O$	1σ
LAH-2-1	-5.19	0.02	21.60	0.08
LAH-2-2	-5.22	0.06	20.57	0.03
LAH-2-3	-4.23	0.03	21.62	0.06
LAH-2-4	-4.38	0.07	22.71	0.07
LAH-4-1	-4.93	0.05	21.16	0.12
LAH-4-2	-4.81	0.09	20.96	0.14
LAH-4-3	-4.43	0.06	20.36	0.08
LAH-4-4	-5.07	0.03	19.99	0.10
LAH-4.5-1	-4.21	0.05	23.14	0.03
LAH-4.5-2	-5.12	0.04	21.03	0.06
LAH-4.5-3	-5.07	0.06	20.90	0.09
LAH-4.5-4	-4.53	0.04	21.33	0.10
LAH-5-1	-4.69	0.07	23.52	0.12
LAH-5-2	-4.77	0.09	22.74	0.07
LAH-5-3	-4.64	0.11	21.83	0.11
Average	-4.64	0.06	21.75	0.10

All results are given in permil. $\delta^{13}C$ results are reported with respect to PDB, and $\delta^{18}O$ results are reported with respect to SMOW.

Sampling locations are shown in Figure 2. The last digits in the sample numbers represent different sample locations across the widths of the fractures.

Table 1.3. Lipids in Los Alamos Calcites.

PLFA[1]	pmol/g[2]		mole%[2]	
	average	std. dev.	average	std. dev.
15:0	0.01	0.02	0.1	0.2
16:0	0.49	0.03	2.6	1.3
17:0	0.04	0.02	0.1	0.0
18:0	1.06	0.34	4.9	1.7
20:0	0.21	0.22	0.5	0.2
24:0	0.01	0.01	0.1	0.1
tot. normal saturates	1.82	0.58	8.4	2.9
i15:0	0.03	0.03	0.2	0.3
a15:0	0.03	0.04	0.2	0.3
i16:0	0.20	0.05	1.1	0.6
i17 :0	0.26	0.12	1.1	0.3
a17:0	0.26	0.12	1.1	0.3
i19:0	0.03	0.04	0.0	0.1
a19:0/19:1	0.02	0.02	0.1	0.1
tot. terminally branched saturates	0.83	0.29	3.8	1.4
16:1w7c	0.01	0.01	0.0	0.1
cy17:0	0.36	0.17	1.6	0.9
18:1w9c	1.53	0.55	6.9	2.5
18:1w7c	0.93	0.35	4.1	1.3
18:1w7t	0.07	0.09	0.1	0.1
19:1w6c	0.87	0.52	3.3	0.9
cy19:0	11.33	14.1	23.9	19.7
20:1w9c	0.45	0.26	1.7	0.4
20:1w7c	0.14	0.09	0.5	0.3
tot. monounsaturates	15.69	15.94	42.2	15.2
9me16:0	0.11	0.05	0.5	0.2
10me16:0	1.01	0.37	4.6	2.0
10me18:0	4.04	1.58	17.7	5.4
12me18:0	0.06	0.09	0.5	0.8
br16:0a	0.21	0.05	1.0	0.4
br16:0b	0.05	0.02	0.2	0.1
br17:0a	1.69	0.54	7.8	2.7
br17:0b	0.11	0.06	0.4	0.1
br17:0c	0.39	0.25	1.4	0.4

Table 1.3 Continued. Lipids in Los Alamos Calcites.

PLFA[1]	pmol/g[2]		mole%[2]	
	average	std. dev.	average	std. dev.
br18:0	0.06	0.05	0.2	0.1
br19:0a	0.27	0.13	1.1	0.3
br20:0a	0.10	0.08	0.7	0.5
br20:0b	0.05	0.06	0.1	0.1
dimeth21:0	2.03	1.9	6.8	5.3
dimeth22:0	0.38	0.31	1.3	0.1
tot. mid-chain branched saturates	10.58	4.92	44.4	11.2
i17:1w7c	0.03	0.02	0.1	0.1
br19:1	0.10	0.08	0.3	0.1
tot. branched monounsaturates	0.12	0.11	0.4	0.2
2-oxo-20:0	0.26	0.23	0.8	0.1
total PLFA	29.32	22.07	100.0	-

Total Lipid			relative %[6]
2-OHFAME[3]	55.7	16.7	25.5
sterols[4]	80.1	68.4	36.7
di-ether16:0[5]	82.8	100.2	37.9
Total	218.5	185.2	100.0

[1]ester-linked phospholipid fatty acid; [2]n=3; [3]alpha-hydroxy fatty acid methyl esters, sum of 8 compounds; [4]sterol trimethyl silyl ether, sum of 5 compounds; [5]16 carbon di-ethers, sum of 4 compounds; [6]percent of total lipid.

Table 1.4. Lipid biomarkers of various cell types.

Archaebacteria di-ethers, tetra-ethers
Eubacteria common markers: 15:0, i15:0, a15:0, 16:1ω7c, i17:0, a17:0, 17:0 gram (+): i15:0, a15:0, i17:0, a17:0 gram (-): 16:1ω7c, cy17:0, 18:1ω7c, cy19:0 sulfate-reducing bacteria: i17:1ω7c, 10Me16:0
Actinomycetes 10Me18:0
Fungi 18:1ω9c, 18:2ω6, 18:3ω3, sterols
Plants 2-hydroxy fatty acids, 18:1ω9c, 18:3ω3, sterols

Modified from Vestal and White (1989), archeabacterial lipids are from Hedrick et al. (1991).

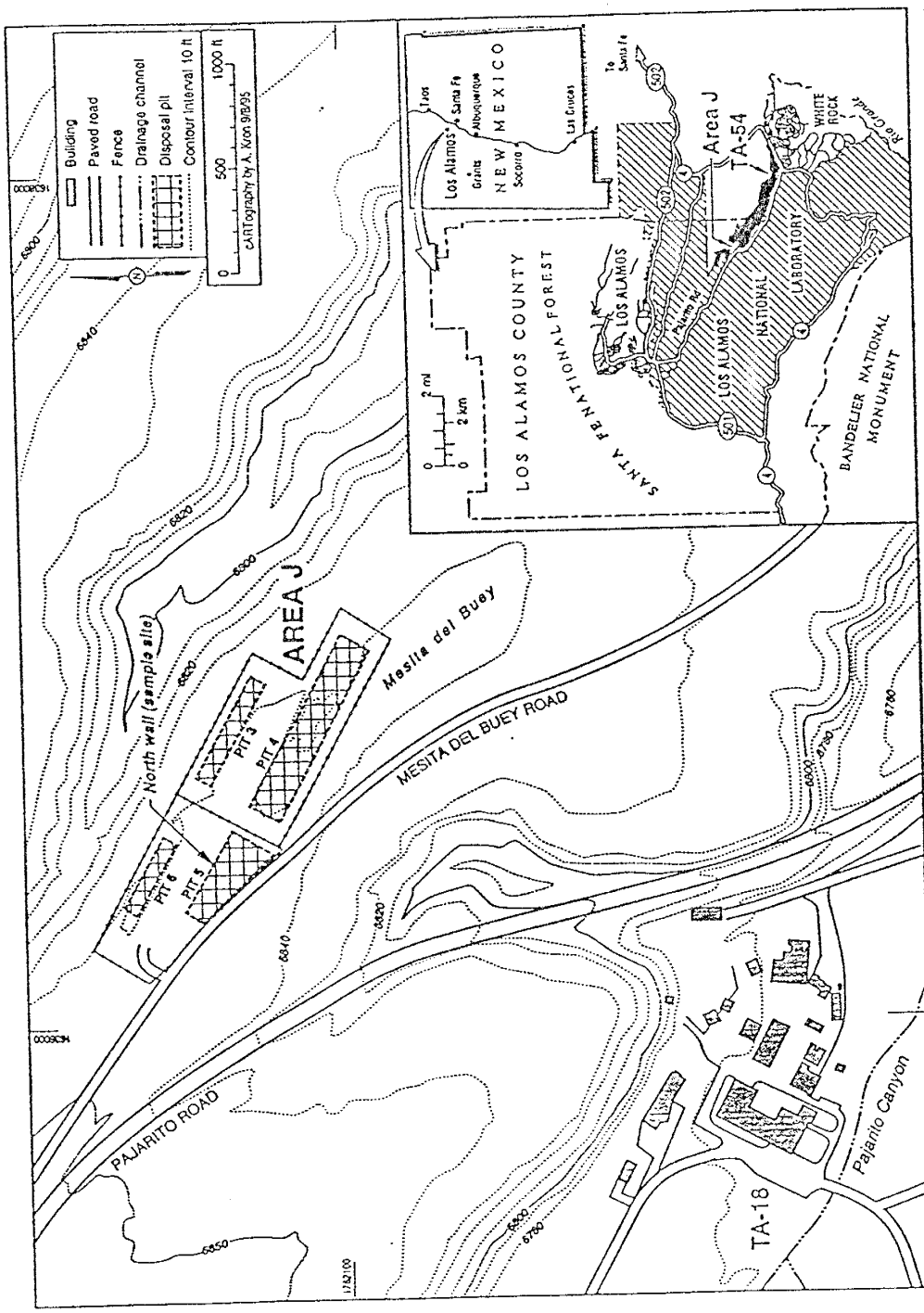

Figure 1.1. Location map of Los Alamos and study area.

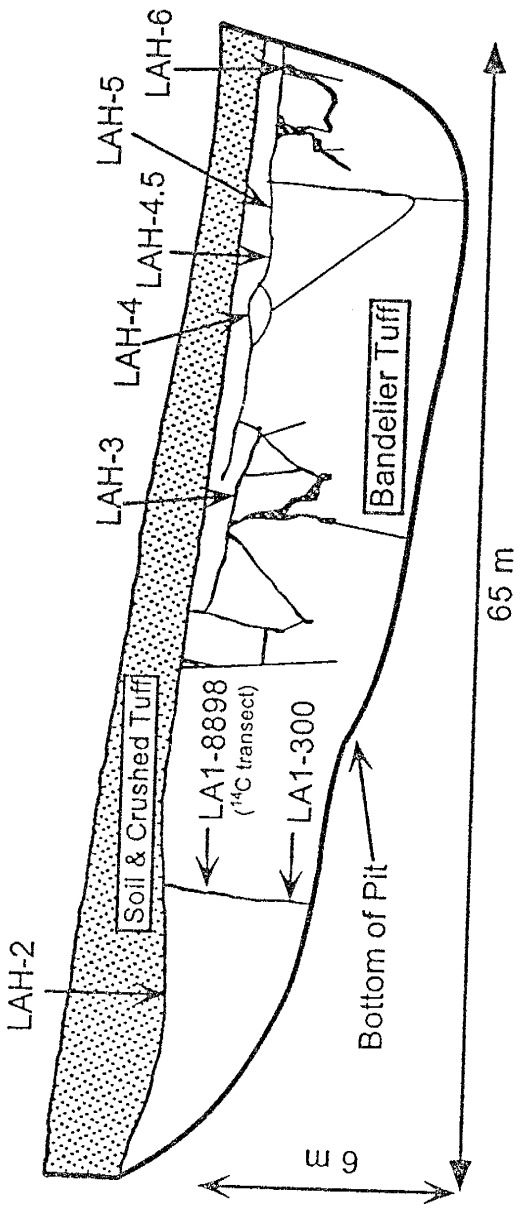

Figure 1.2. Drawing of the north wall of Pit 5, Area J, TA-54. Major fractures are shown along with sampling locations. Many minor fractures are not shown and fracture widths (apertures) are not to scale. Drawing is vertically exaggerated.

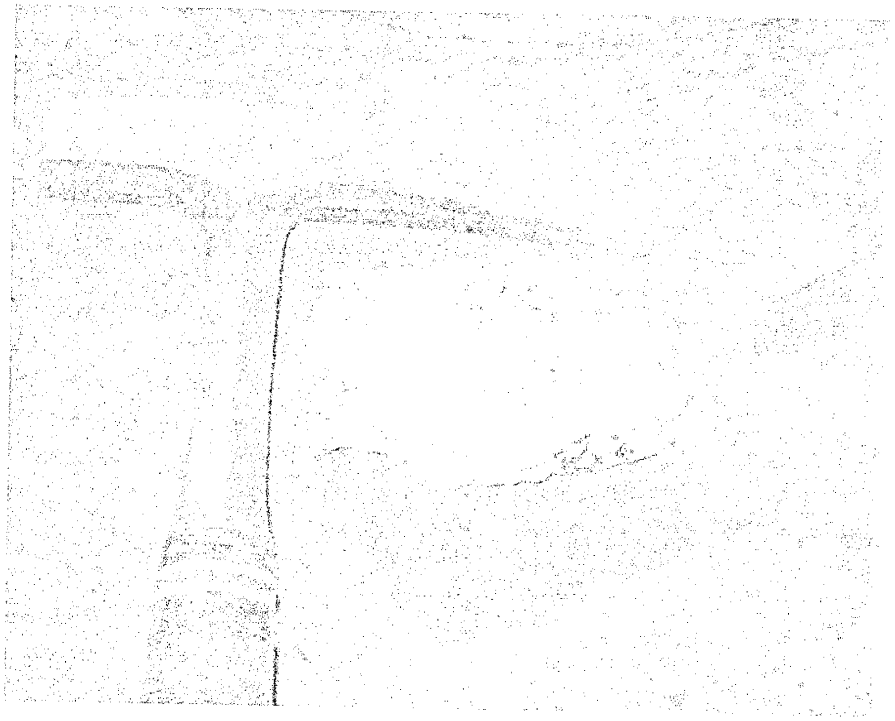

Figure 1.3. Photograph of calcite from Bandelier Tuff fractures.

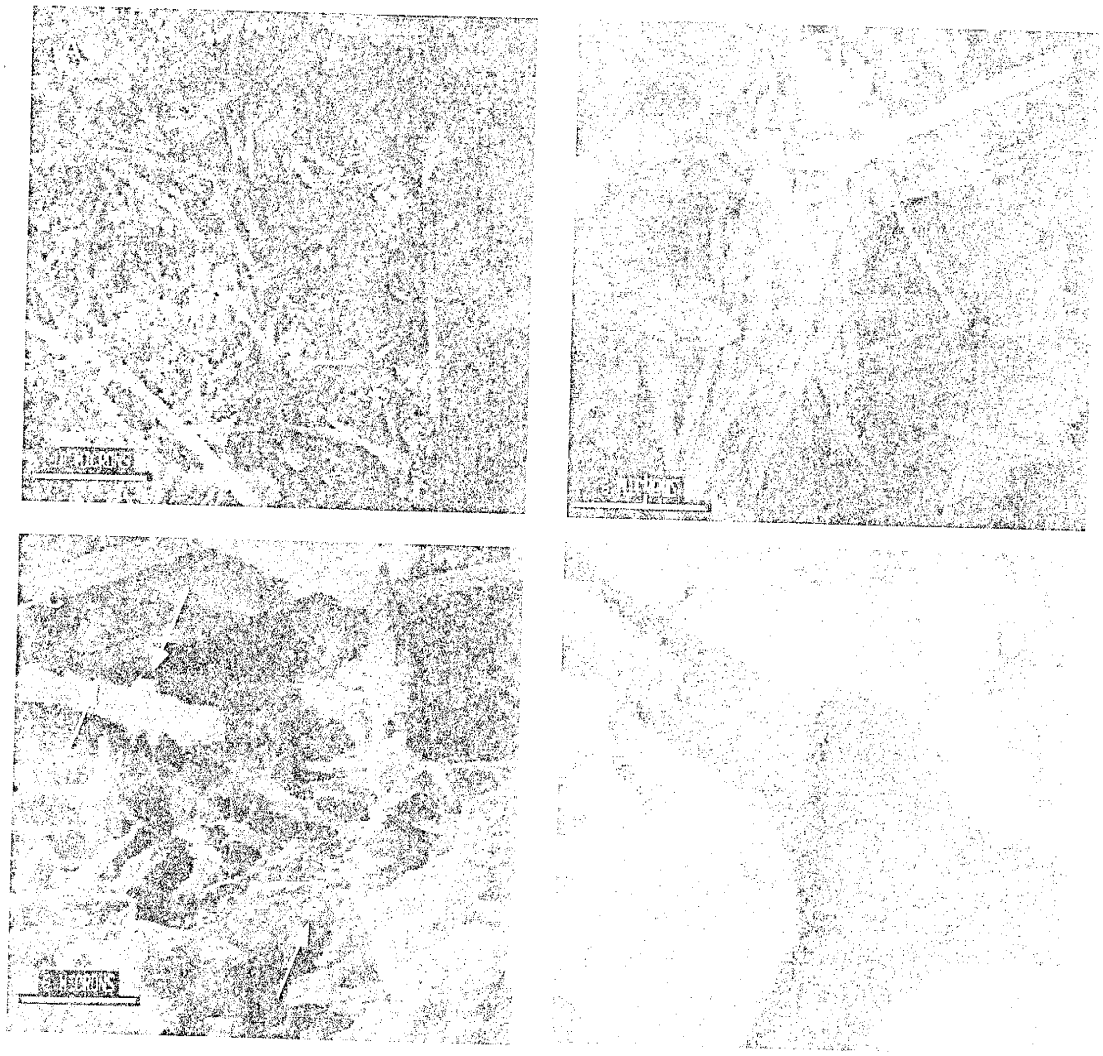

Figure 1.4. Scanning electron photomicrographs of calcite fracture fillings. (A) image showing fungal fibers and amorphous calcite. (B) image showing bundles of fungal fibers. (C) image of amorphous calcite shown in (A); Fungal fibers can be seen along with gel-like calcite and bacterial forms (latter denoted by arrows). (D) image of hypha composed of submicron crystals.

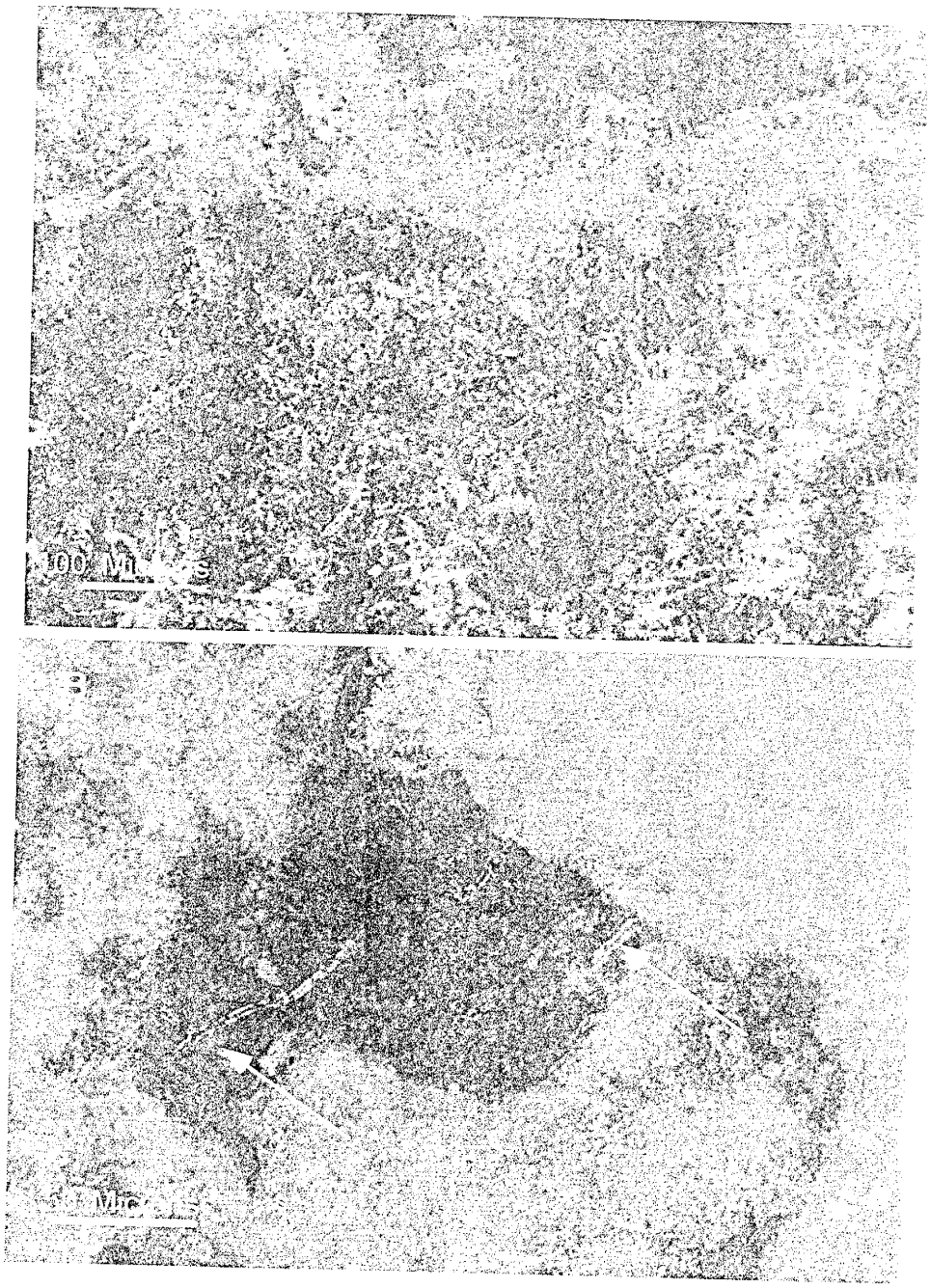

Figure 1.5. Photomicrographs of fracture-filling thin sections. (A) image showing fungal fibers. (B) image showing branched hyphae.

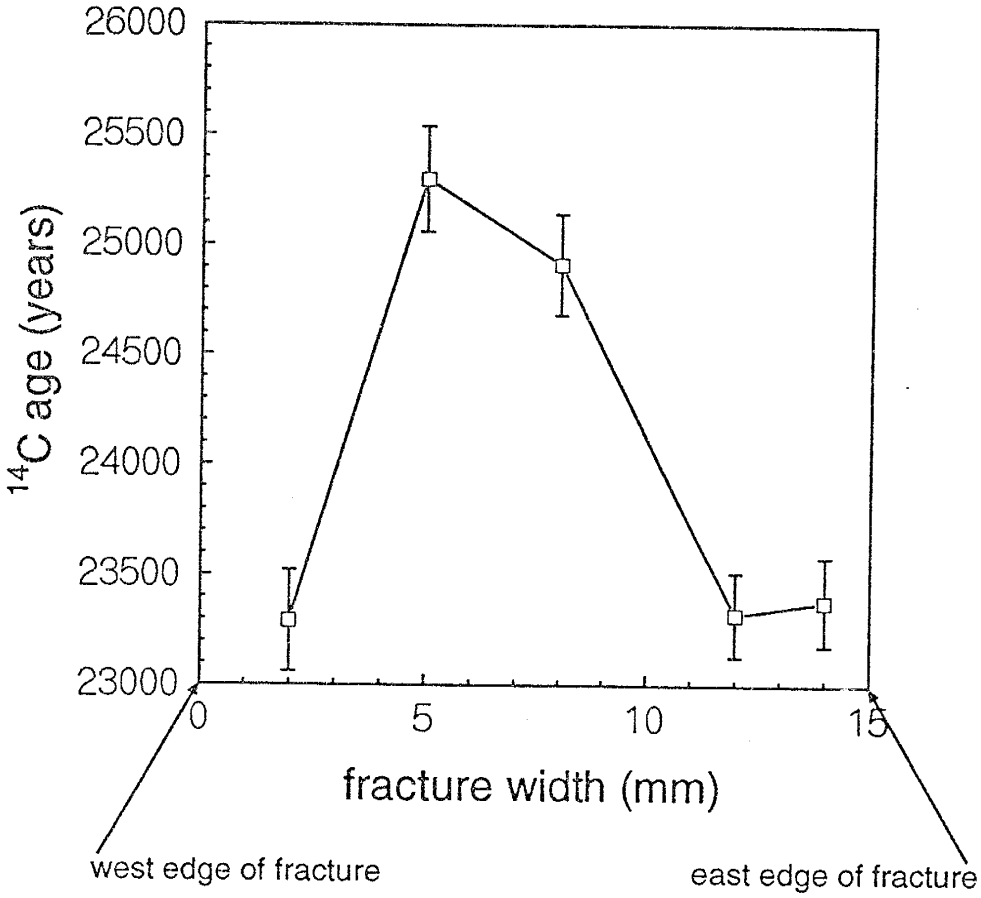

Figure 1.6. Carbon-14 age transect across the vertical fracture at 90 cm depth. Error bars represent the analytical error only.

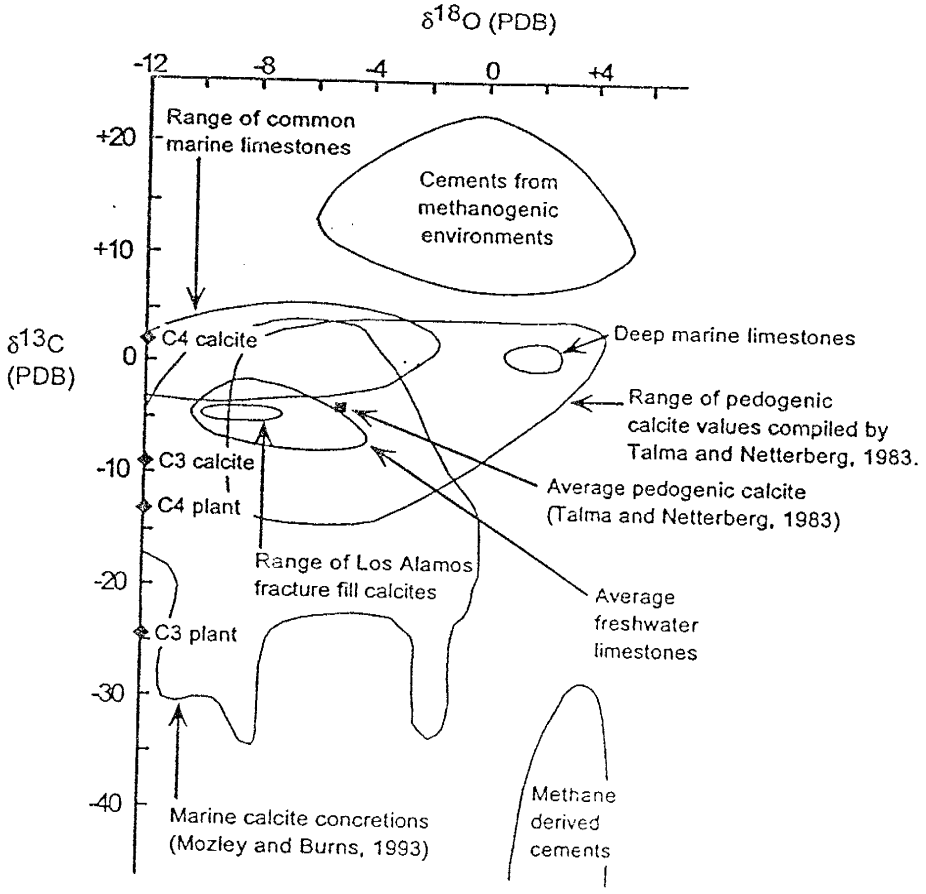

Figure 1.7. $\delta^{18}O$-$\delta^{13}C$ plot of calcites precipitated in different environments. The average and range of pedogenic calcites are from Talma and Netterberg (1983). The field represented by the marine calcite concretions is from Mozley and Burns (1993). Other fields are from Arthur et al. (1983). The diamonds represent the average $\delta^{13}C$ of C3 and C4 plants and C3- and C4-derived calcites. The figure was modified from Arthur et al. (1983).

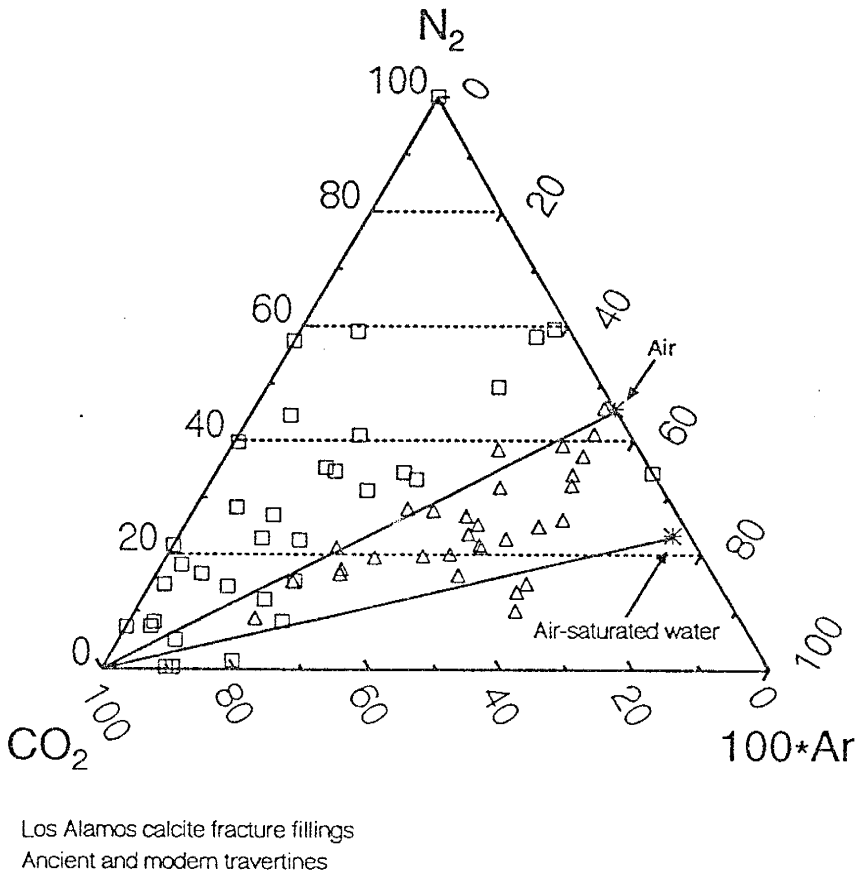

Figure 1.8. 100*Ar-CO_2-N_2 ternary plot of fluid inclusion gases from Los Alamos calcite fracture fillings and travertines (from Newman et al., 1995). Boundaries shown are for air and air-saturated water.

Stage 1: Root growth into fracture

- Aerobic conditions

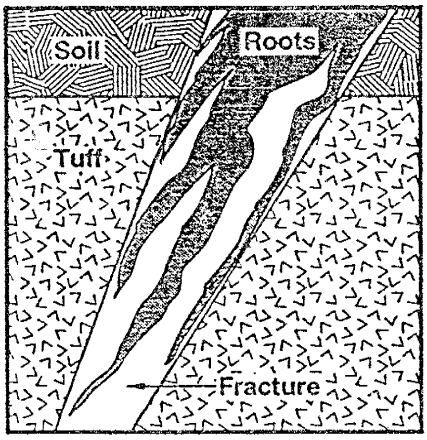

Stage 2: Death of roots

- Aerobic conditions
- Death from an erosional event or natural root turnover
- Fungal decay

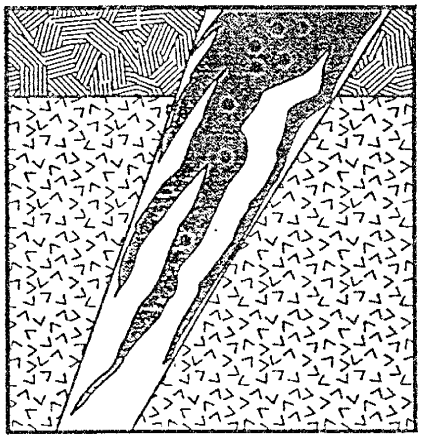

Stage 3: Development of anaerobic conditions

- Microbial respiration exceeds O_2 input
- Outer aerobic zone
- Inner micro-aerobic zone
- Anaerobic core

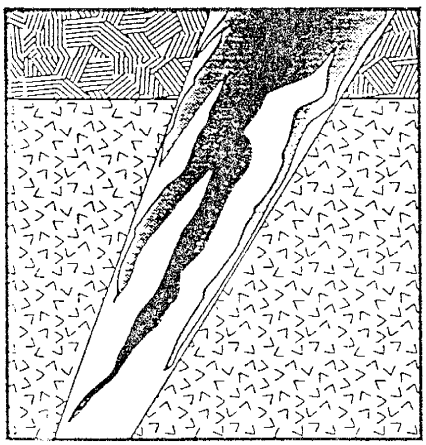

Stage 4: Anaerobic conditions

- Nitrogen production
- Methanogenesis
- Gradual filling of fracture by precipitation of calcite

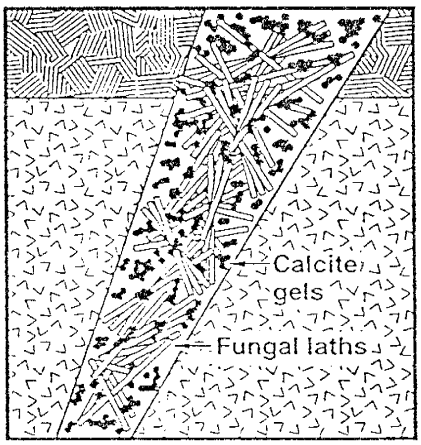

Figure 1.9. Model for the development of an anaerobic state and calcite precipitation in the Los Alamos fractures.

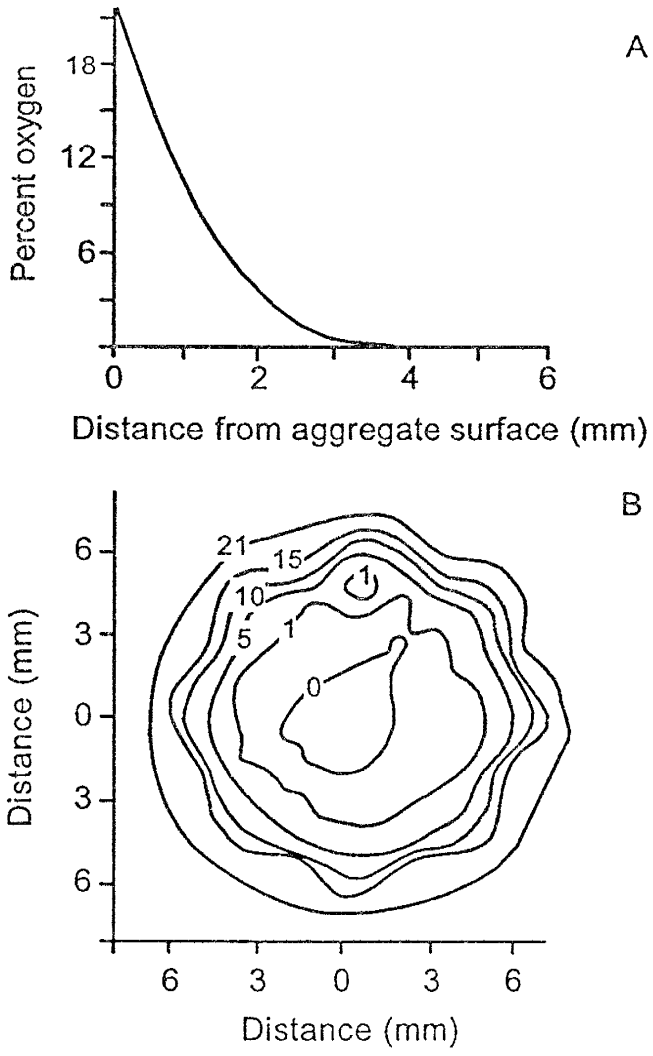

Figure 1.10. Development of anaerobic conditions in a soil ped (from Atlas and Bartha, 1993). (A) Oxygen profile from a silt-loam soil aggregate showing development of an internal anaerobic zone. (B) Oxygen contour map of a soil aggregate showing an internal anaerobic zone. Contour numbers indicate percent oxygen.

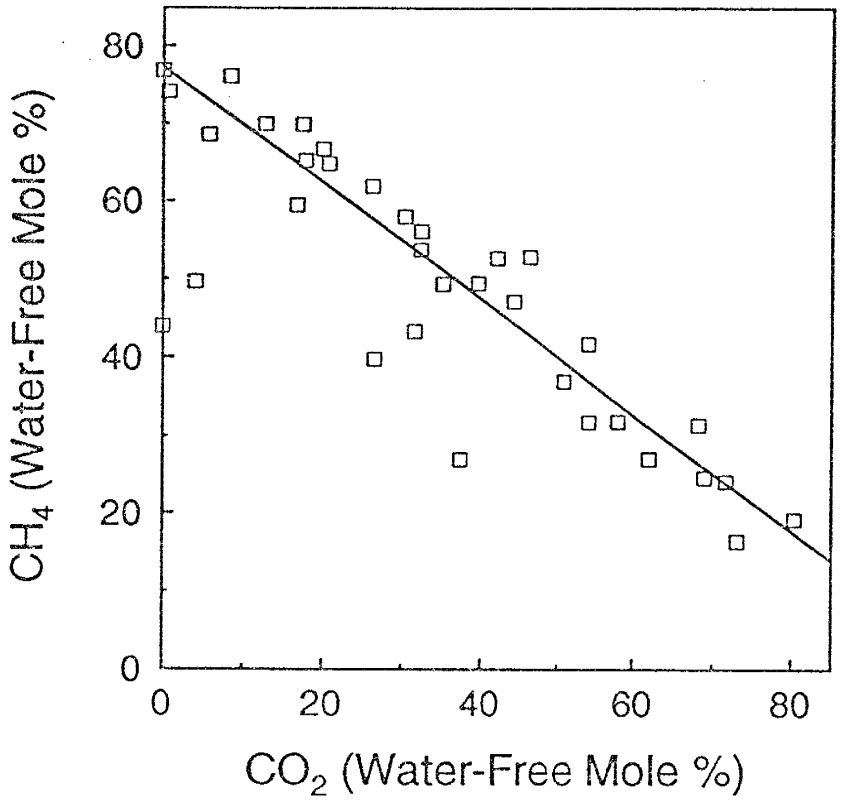

Figure 1.11. Plot showing the inverse correlation between CO_2 and CH_4 in fluid inclusion gases (R^2 = 0.90).

CHAPTER 2: INTERFLOW PATHWAYS IN A SUBHUMID PONDEROSA PINE HILLSLOPE

ABSTRACT

The mechanisms controlling interflow in semiarid and subhumid environments have received relatively little attention despite that fact that interflow can be an important runoff process in these environments. A recent study in a subhumid ponderosa pine hillslope demonstrated that interflow can be volumetrically as important as overland flow. However, the factors controlling interflow in this system were still poorly understood. The objective of the current study, carried out on the same ponderosa pine hillslope at Los Alamos, New Mexico, is to better understand the interflow process in subhumid environments and to develop a conceptual model of interflow that will aid in evaluating the potential for contaminant transport in such environments. Natural chloride and stable isotope (δD and $\delta^{18}O$) tracers were used to investigate the interflow process and the chemical changes that occur as a result of interflow. Observed differences in chemistry between soil matrix water and interflow were large (for example, chloride concentrations in matrix soil water samples were over 200 mg/L, compared with only 2 mg/L in interflow samples obtained at the same time), indicative of a two-domain

flow system in which preferential flow paths generate interflow that is not in chemical or hydrological equilibrium with the soil matrix. In addition, there were large changes in the chemistry of interflow water with time; for example, chloride concentrations were 10 times greater under saturated conditions than under unsaturated conditions. Additional evidence for the movement of interflow through preferential flow paths is provided by observed rapid shifts in interflow isotopic composition (e.g., 6 ‰ $\delta^{18}O$ in 24 hours) which are not consistent with the very low bulk hydraulic conductivity of the soils. The chloride and stable isotope tracer results show that interflow travels mainly through preferential flow paths, which affects the chemistry, residence time, and distribution of water in the soils–and thereby probably affects contaminant distribution and mobility as well.

INTRODUCTION

Interflow or subsurface stormflow is the lateral movement of water through near-surface soils, regolith, and bedrock (Anderson and Burt, 1990; Satterlund and Adams, 1992). Most of our knowledge about interflow processes comes from studies conducted at humid sites. In contrast, interflow in subhumid/semiarid regions of the United States has been little studied, probably because it was not considered an

important hydrologic process: these regions have few perennial streams, receive relatively small amounts of precipitation, and have low soil-moisture content throughout much of the year. Humid systems receive much larger amounts of water and are characterized by less variable moisture conditions.

Interflow in humid areas can be generated under both unsaturated and saturated conditions (McDonnell, 1991). Under unsaturated conditions, the flow is usually thought to occur via macropores (Germann, 1990; McDonnell, 1991). The macropores either channel water from the surface, generating interflow directly, or they feed shallow, perched saturated zones overlying bedrock that is impermeable or of low permeability, indirectly producing interflow (Whipkey, 1965; McDonnell, 1991; Peters et al., 1995; Turton et al., 1995). Macropore flow under unsaturated conditions occurs when the flux of water (precipitation or snowmelt) is greater than the hydraulic conductivity of the matrix (Germann, 1990; Sklash, 1990; McDonnell, 1991). This process will be enhanced in areas that are characterized by large or intense rains or snowmelt events and/or where the soils have low matrix conductivities.

Stable isotope tracers have been used to ascertain how much of the interflow in humid environments is "old" water and how much is

"new" water. Old, or pre-event, water has been in storage and is forced out of the soil by a current storm or snowmelt event. New, or event, water comes directly from the current event. Many of the stable isotope studies have shown that most of the hydrograph rise in streams is caused by old water (e.g., Bottomley et al., 1984; Pearce et al., 1986; McDonnell, 1991; Anderson et al., 1994; DeWalle and Pionke, 1994). To explain this dominance of old water, Sklash and Farvolden (1979) proposed the groundwater ridging concept, in which water in the tension saturated zone near the stream channel is quickly converted to a phreatic state by a relatively small additional input of water, causing a fast release of old water to the channel. Although there is always a new-water component from in-channel precipitation, overland flow, or subsurface macropore flow, it is generally small. However, new water can be important in upslope areas away from stream channels. For example, based on rainfall experiments on a humid zone soil block, Turton et al. (1995) suggested that new water was an important component of interflow during infrequently occurring high intensity storms, while old water dominated during the frequent small storms that occur during a given year.

The need for an improved understanding of how rain and snowmelt move through the soil as interflow, and the importance of

hillslope hydrology tracer studies to gain that understanding, was pointed out by Sklash (1990). Such an understanding is vital because the processes that control the movement of water through soils affect the mobility of contaminants, the distribution of nutrients, and the acid-base chemistry of surface waters (Mulholland et al., 1990). As outlined above, great strides have been made in understanding the process of interflow generation in humid environments. This study attempts to develop a comparable understanding for dry subhumid-semiarid systems.

The current study uses natural chloride and stable isotope tracers ($\delta^{18}O$ and δD) which originate from precipitation, to investigate the processes that control interflow in a subhumid hillslope. Conducted at a ponderosa-pine hillslope site at Los Alamos, New Mexico (Figure 2.1), this study builds on the work of Wilcox et al. (1996). Overland (surface) flow had been considered to be the major mechanism of runoff generation in these environments, but Wilcox et al. found that interflow can be the major runoff mechanism under particular circumstances. They found that interflow was most active during spring snowmelt and, surprisingly, was moving mostly through a dense, clay Bt soil horizon having a very low saturated hydraulic conductivity (2.5×10^{-10} m/sec). Their observation of the dynamic nature of interflow led Wilcox et al. to

hypothesize that interflow was moving, at least in part, through macropores. The hydrometric measurements used in their study suggested that interflow rates were rapid enough to require such an explanation, but these measurements alone are not sufficient for a detailed model of interflow generation. Other methods are needed to determine the pathway of interflow (macropores vs. soil matrix), the rate of water movement, and the effects of interflow on soil water chemistry. In our study, therefore, a multiple-tracer approach was used to develop a model for subhumid-semiarid interflow processes. In addition, this approach enables the processes controlling interflow in subhumid-semiarid regions to be compared with those in humid regions, thereby increasing our understanding of interflow generation across a wider range of environmental conditions.

METHODS AND MATERIALS

Site Description

The 870-m^2 ponderosa-pine hillslope study area lies within the Los Alamos National Laboratory's Environmental Research Park on the Pajarito Plateau of north-central New Mexico; it is described in detail in Wilcox et al. (1995) (Figure 2.1). The site slopes gently (average 6%) and drains into a nearby canyon. The elevation is 2,315 m and the average

annual precipitation is 510 mm (Bowen, 1990), just above the subhumid-semiarid boundary of 500 mm. The depth to groundwater is about 250 m.

The stratigraphy of the site was described by Watt and McFadden (1993) and Davenport (1994), and consists of Bandelier tuff (R horizon) at the base; a dense, smectite clay Bt horizon; and, at the top, sandy-loam (A and AB) horizons (Figure 2.2). The Bt horizon shows well-developed soil structure and contains root channels, cracks, and voids between ped faces. The sandy-loam horizons, which are both loess, are hereafter collectively referred to as the A horizon. Measured saturated hydraulic conductivities are 5.7×10^{-9} to 7.5×10^{-7} m/sec for the A horizon, 2.5×10^{-10} m/sec for the B horizon, and 1.3×10^{-9} to 7.1×10^{-9} m/sec in for the weathered tuff (Stephens, 1993). The hydraulic conductivity of unweathered Bandelier tuff ranges from 2×10^{-7} to 2.35×10^{-6} m/sec (Abeele et al., 1981).

A trench, 16 m x 2 m x 1.5 m deep, was dug across the bottom of the hillslope, perpendicular to the slope of the hill. It is equipped with two collectors so that water can be collected separately from the A and B horizons (Figure 2.2). A French drain at the bottom of the trench (not shown in the figure) collects water from a portion of the tuff. The A- and B-horizon collectors drain into separate stilling wells, in which pressure

transducers electronically measure the interflow produced at least every 15 min. A meteorological station at the site continuously records temperature, humidity, wind speed and direction, and precipitation. Soil moisture is monitored on a weekly basis, by neutron thermalization, at 10 locations on the hillslope. Additional information on the hydrometric data collection system can be found in Wilcox et al. (1996).

Sampling and Analytical Methods

Collection of hydrometric data from the hillslope has been ongoing since November 1992. Stable isotope and chloride tracer sampling began in June 1993 and included samples of interflow, precipitation and the bulk soils.

Interflow and Precipitation Samples. To obtain interflow samples, small-volume (about 50-mL) PVC collectors were inserted into the pipes that feed the stilling wells; the collectors were designed to minimize evaporation, which would adversely affect the stable isotope results. Precipitation samples were collected with a large, polyethylene funnel that drained into a 1/4-in.-diameter tube which had an elbow bend. After a rain, the bend held a plug of water preventing evaporation from the main reservoir. Water drained from the tube into a 1-L polyethylene

bottle having an overflow spout which was also bent and held a plug of water once the bottle overflowed.

The samples were usually collected on a daily basis, and two duplicate samples were taken whenever possible; one was analyzed for stable isotopes, the other for chloride. Samples were stored in 10- or 20-mL glass vials with polyseal caps (vials were rinsed with a small amount of sample before being filled). Samples were then stored in a refrigerator, at 4 °C, pending analysis.

Stable isotope analyses were conducted at the New Mexico Tech and Southern Methodist University stable isotope laboratories. The hydrogen and oxygen isotopes are reported in delta (δ) notation, as per mil (‰) differences relative to the international standard SMOW (Craig, 1961):

$$\delta D \text{ or } \delta^{18}O = \left[\frac{R_{sample} - R_{SMOW}}{R_{SMOW}}\right] \times 1000, \qquad (1)$$

where R is the D/H or $^{18}O/^{16}O$ ratio. The $\delta^{18}O$ analyses were based on the CO_2 equilibration method (Socki et al., 1992). The δD analyses were based on the uranium method (Bigeleisen et al., 1952). Sample splits were analyzed at both laboratories to ensure consistency of the data. Variation in $\delta^{18}O$ of sample splits analyzed at both laboratories was less

than 0.2 ‰. All of the δD analyses were performed at the Southern Methodist laboratory, so no interlaboratory comparison of δD analyses was done. Analytical precision was better than 0.2‰ and 2‰ for the $\delta^{18}O$ and δD analyses, respectively.

Chloride concentrations were determined using a Dionex ion chromatograph. A 1.08-mM Na_2CO_3/1.02 mM $NaHCO_3$ eluant was used with a Dionex AS4A column and self-regenerating suppressor. Calibration curves were established on the basis of five standards prepared by serial dilution from an NIST Standard chloride solution. After every five analyses, one standard and deionized water (DI) blank were run, and after every ten samples, duplicate sample analyses were run, to ensure that adequate accuracy and precision were maintained. Accuracy was 10% or better based on the periodic analyses of standards, and precision was better than 2%.

Soil Cores. Soil water chloride concentrations were determined from cores taken through the entire soil profile, in July 1993, August 1994, and June 1995. For each core, soil stratigraphy was described; the core was then split into 10-cm lengths and stored in clean mason jars or zip-lock bags. Latex gloves were worn at all times to prevent contamination of the samples. At the Los Alamos Environmental Science Group Laboratory, the core samples were first air-dried for 48 hours, and then

100-g splits were mixed with 100 mL of 17-mΩ DI water. The solutions were stirred with a glass stirring rod and allowed to equilibrate for 48 hours. A control, consisting of a beaker filled with 100 mL of the DI water, was prepared for every six soil samples. After equilibration, the solutions (leachates) were decanted, centrifuged, and filtered using disposable 0.2-μm Gelman ion chromatography filters. Leachates were analyzed for chloride using the same ion chromatography procedure described earlier for the interflow and precipitation samples. Soil moisture contents were determined gravimetrically or by neutron probe. The soil bulk density values that are needed to calculate the soil water chloride concentrations from the leachate concentrations were measured previously and are given in Wilcox et al. (1996).

Mixing Models. A simple mass balance mixing model approach was used to estimate old/new water percentages and matrix/preferential flow percentages. Stable isotope data were used in the old/new water estimates, and chloride data were used in the matrix/preferential flow estimates. Both chemical concentrations and isotope delta values can be used in this approach because the equations are based on differences between values, thus absolute quantities are not required.

Old and new water percentages were calculated from isotope values using the two component-mixing equations of Pearce et al. (1986):

$$Q_o = \left[\frac{C_i - C_n}{C_o - C_n}\right] Q_i \qquad (2)$$

and

$$Q_n = Q_i - Q_o \qquad (3).$$

where Q is discharge, C is tracer concentration, and the subscripts i, o, and n correspond, respectively, to interflow, old water, and new water. C_o was obtained from the interflow event immediately preceding the event of interest. C_n was obtained from the precipitation sample. Note that this determination of old/new water percentages assumes that the bulk samples are reasonably representative. In other words, it has been assumed that the failure to take intrastorm variations into account in the C_n value, and assuming that the isotopic value of the preceding interflow event represents old water will not result in errors large enough to cause misleading estimates of old and new water percentages. To partially compensate for this potential source of error, estimates were made only for days when there was greater than a 0.5‰ $\delta^{18}O$ or 15‰ δD difference between the isotopic values of old and new water. Because

there is no groundwater or streamflow at the hillslope, errors cannot be attributed to those components.

To estimate the relative percentages of matrix and preferential flow, a mass balance approach similar to that of Sharma and Hughes (1985) was used. The relative proportions of preferential and matrix flow were determined as follows:

$$I = I_p + I_M \tag{4}$$

and

$$IC_I = I_P C_P + I_M C_M, \tag{5}$$

where I is the interflow rate measured at the collection point, C_I is the interflow concentration at the collection point, I_P is the preferential flow rate, C_P is the preferential flow water concentration, I_M is the matrix interflow rate, and C_M is the matrix water concentration. If I, C_I, C_P, and C_M are known, the matrix interflow rate can be determined as follows:

$$I_m = I\left(\frac{C_I \quad C_P}{C_M - C_P}\right) \tag{6}.$$

This approach assumes (1) conservation of mass and solutes in the soil horizon, for example, no vertical losses to the underlying soil; and (2) no interaction between the preferential flow paths and macropores. The C_p values were estimated from typical low chloride concentrations in A- or

B-horizon interflow during unsaturated conditions. C_M was estimated on the basis of average chloride concentrations from the cores.

RESULTS

Hydrometric Results

The hydrometric results for the hillslope are discussed in detail in Wilcox et al. (1996), so only a brief overview and update are given here. Interflow from the hillslope is episodic, the largest events generally occur in the spring as a result of saturated conditions from melting snow or spring rainfall. Most of this water (83%) flows through the B horizon, the balance through the A horizon. Interflow volumes from the A and B horizons and precipitation for the period February 1993 through June 1995 are shown in Figure 2.3. Other than in the spring and summer of 1993, periods of continuous A-horizon interflow generation were generally short, compared to that of the B-horizon. In the three years of observation, there were three periods during which combined A- and B-horizon interflow rates exceeded 200 L/day, spring 1994, fall 1994, and spring 1995 (Figure 2.3). Small quantities of interflow were measured at other times, generated by individual storms or fronts. Although it makes up only a small portion of the annual water budget (≈2%), interflow can be important for shorter periods; for example, in the 1993 water year

(defined by Wilcox et al., 1996 as November to October), interflow accounted for 19% of the winter-spring water budget.

Stable Isotope Results

A $\delta^{18}O$-δD plot (Figure 2.4) comparing A- and B-horizon interflow to the Los Alamos local meteoric waterline (LMWL) of Vuataz and Goff (1986) shows that very little evaporation of the interflow waters occurs, because all of the data fall on or near the LMWL. The close agreement between interflow water and the LMWL shows, in addition, that sample integrity was preserved during the sampling process and that the analyses are of good quality.

For the A horizon, the $\delta^{18}O$ of interflow and of precipitation from June 1993 to April 1995 are shown in Figure 2.5. The variability of A-horizon interflow $\delta^{18}O$ values is much less than that of precipitation. Percentages of old and new water, calculated from equations 2 and 3, are shown in Table 2.1a for nine days of interflow. For the small volume interflow events (<0.5 L/day) that occurred during unsaturated conditions, old water dominated; new-water contributions were large (>30%) only on July 15, 1993 and February 15, 1995 when large rain or snowmelt events occurred. Unfortunately, for the very large interflow event in March 1995, which accounted for the vast majority of A-horizon

interflow generated over the sampling period, old/new water percentages could not be determined. A new water sample was not collected because the event was initiated by a thaw and not enough snowmelt was generated produce sufficient surface runoff for sampling.

For the B horizon, the $\delta^{18}O$ of interflow and of precipitation for the period June 1993-April 1995 are given in Figure 2.6. As in the A horizon, B-horizon interflow $\delta^{18}O$ values do not show as large a seasonal variation as precipitation. Some isotopically distinct precipitation events produced fast changes in the $\delta^{18}O$ values of B-horizon interflow, (e.g., the October 15, 1994 period, Figure 2.6), while other isotopically distinct events produced little change at all (e.g. events between November 12, 1994 and March 6, 1995). This difference in the effect of various storms on interflow isotopic composition is probably related to the volume of precipitation and antecedent moisture conditions. Percentages of old and new water, determined for 15 days of interflow, are shown in Table 2.1b. As in the A horizon, old water dominates in small volume events. New water contributions were large (>30%) only on days with low antecedent soil-moisture-contents and prolonged rain events or when the soil was at or near saturation. For the large March 1995 event, the lack of a new water sample prevented calculation of old/new water percentages. However, if we assume that the isotopic composition of A-

horizon interflow is approximately representative of new water than old/new percentages can be estimated (Table 2.1). The result indicates that new water was dominant in this 1400 L/day event. Although the result has a very high uncertainty, the new water dominance seems reasonable given the fact that B-horizon interflow became 0.7% lighter than the old water value, and because chloride concentrations decreased substantially (the chloride results are discussed in the next section).

Old and new water percentages for four B-horizon interflow events, calculated on the basis of δD are shown in Table 2.1C. Comparison with the $\delta^{18}O$ results for those events in Table 2.1b shows that the percentages are similar (within 20%).

Finally, a comparison of old-water percentages for eight dates on which both A- and B-horizon interflow were measured is shown in Table 2.1d. With two minor exceptions, A-horizon interflow has a higher proportion of new water than does B-horizon interflow.

Because of the assumptions discussed in the Methods section regarding the selection of parameter values for the old/new water estimates, it needs to be noted that the results in Table 2.1 have large and unquantifiable errors. For example, some estimates show greater than 100% old water, a physical impossibility. Thus, it needs to be kept in mind that while the results probably show the general trends in

old/new water percentages, there is considerable uncertainty about the values themselves.

Chloride Results

Variations in volumetric moisture content and in chloride concentrations with time are shown for the A horizon in Figure 2.7. Prior to the very wet fall 1994-spring 1995 period, chloride concentrations usually rose with increases in moisture content (e.g., Figure 2.7, July-August 1993 peak) and then declined as moisture content decreased. The maximum chloride concentration was measured in March 1995, when the A horizon became saturated. Matrix/preferential flow estimates for the A horizon are shown in Table 2.2 and suggest that preferential flow was dominant during the relatively dry 1993-1994 period, whereas during the wet period in 1995, matrix flow was dominant. One problem with this rather simple and crude method is that dilution of matrix soil waters by infiltrating water is not considered. In other words, the concentrations from the soil cores were assumed to be representative of the matrix water. It is likely that infiltrating water in the soil matrix would dilute this concentration which makes the matrix concentration input values in the mixing model unrepresentatively high. Dilution does not affect the interflow

concentration inputs because these concentrations are determined after any dilution has occurred. In order to attempt to account for the possibility of dilution of the matrix waters, the mixing model calculations were redone assuming a 50% dilution of the estimated matrix water concentrations (Table 2.2). This results in a doubling of the matrix flow percentages. The result is that during unsaturated periods prior to 1995, matrix flow still only contributes a small percentage if any of the total flow. However, when conditions were at or near saturation, matrix flow percentages increase dramatically suggesting that if significant dilution occurs, matrix flow may be dominant.

Variations in chloride concentration and volumetric moisture content for the B horizon are shown, for June 1993 through April 1995, in Figure 2.8. Between June 1993 and mid-October 1994, chloride concentrations in interflow were relatively low (below 10 mg/L), and moisture content remained below about 33%. Starting in mid-October 1994, the soils began to approach saturation; chloride concentrations increased dramatically, reaching peak levels about 6 weeks before the soils became completely saturated (March 1995). Chloride concentrations then dropped throughout the spring of 1995. Unlike their fairly steady rise, the decline in chloride concentrations was marked by sharp dips (e.g., February 12, and March 6, 1995–see arrows

in Figure 2.8). These correspond to large-volume, multiple-day interflow events during which chloride was diluted by new precipitation or snowmelt waters; they may also reflect increases in the rate of macropore flow, which would reduce the time available for diffusion of chloride from the soil matrix into the macropores. Nevertheless, in terms of total mass, more chloride was removed during the March and February events than during the rest of the June 1993-April 1995 period, because these discharges were so large.

Soil Core Results

Soil cores were taken in the summers of 1993, 1994, and 1995 from which soil water chloride concentrations were determined. Chloride concentrations increased nonlinearly with depth, and increases were especially large in the B and deeper horizons (Figure 2.9). Comparison of chloride concentrations in the cores with interflow concentrations shows that interflow was much more dilute than water in the soil matrix (Table 2.3). Additional details of the core results and determinations of vertical flux rates through the ponderosa pine soils using the soil water chloride concentrations can be found in Newman (1996).

DISCUSSION

Before a description of the conceptual model of interflow at the hillslope can be made, some discussion of how macropore flow might occur under unsaturated conditions is in order. According to McDonnell (1991), the minimal requirement for water flow via macropores is a flux density of rain that is greater than the hydraulic conductivity of the matrix. In other words, the rate of input of water exceeds that of infiltration into the matrix, causing the excess water to flow into macropores. Such a mechanism could explain the generation of both A- and B-horizon interflow under unsaturated conditions. However, in the case of the ponderosa pine hillslope, the excess water may be accumulating at the A/B interface as well as on the soil surface. The measured saturated hydraulic conductivity of the B-horizon clays is extremely low (2.5×10^{-10} m/sec) and could readily be exceeded by the flux of water through the A horizon. The excess water could then flow into B-horizon macropores and eventually be released as interflow; or, if the excess water does not encounter any macropores, it could pond on top of the B horizon, generating interflow in a portion of the A-horizon matrix.

The ponding hypothesis is supported by evidence that some matrix flow occurs in the A horizon. Matrix flow is suggested by: (1) varying

chloride concentrations shown by the multiple peaks in Figure 2.7, which are apparently caused by chloride accumulation during periods of no flow and flushing when flow begins; (2) the decrease in soil matrix water chloride concentrations over time (Table 2.3); and (3) the large matrix flow percentages calculated for certain days (Table 2.2). The infrequency and small volumes of A-horizon interflow during unsaturated periods suggest that ponding may be a small-scale or localized occurrence. Time-domain reflectometry probes were installed at the A/B horizon interface, and would have been valuable in determining whether ponding on the B horizon really occurs. However, because they never functioned properly, the ponding hypothesis remains in question.

It does not appear however, that A-horizon interflow is entirely matrix flow. Even though Table 2.2 suggests that matrix flow is important, preferential flow is evidently dominant at times. However, the sandy loam soil of the A horizon does not seem to be conducive for the formation of macropores. Field examination showed little macropore development, especially compared to the B horizon. Allison and Hughes (1983), working at a semiarid site in Australia, found that stemflow was an important preferential flow mechanism, facilitating rapid movement of water into the soil. Stemflow occurs in the area between plant stems or

roots and the surrounding soil. This same mechanism could be operating at the study site, given the considerable grass and tree cover.

In contrast to the ambiguity of how A-horizon interflow occurs, preferential flow, probably via macropores, is apparently dominant in the B horizon. This conclusion is supported by two of this study's findings. First, comparison of the $\delta^{18}O$ of precipitation with that of B-horizon interflow shows that new water can move through the system within 24 hours (see Figure 2.6, events of October 14 and November 12, 1994); such movement would not be consistent with matrix flow, given the low bulk hydraulic conductivities of the soils. Second, comparison of chloride concentrations in matrix soil water with those in interflow (Table 2.3) shows that the two are not equilibrated, which indicates that interflow water is bypassing the salt-rich matrix and moving through macropores. This is consistent with the suggestion of Thomas and Phillips (1979) and Luxmore et al. (1990) that macropores serve mainly as physical conduits and have only minor effects on aqueous chemistry. Other evidence that macropore flow can occur in the B horizon is the presence of shrinkage cracks, root channels, voids between soil peds, and mineral accumulation on the walls of some macropores.

The importance of macropore flow in the B horizon is further supported by the results in Table 2.2. The maximum matrix interflow

contribution apparently occurred on January 12, 1995, when the highest interflow chloride concentration of the study was recorded. Assuming a 50% dilution of the matrix water chloride concentrations indicates that matrix flow may have been dominant on that day. However, the rest of the results show that even with a 50% dilution factor, macropore flow is dominant even when the soils are saturated, as on March 6, 1995 (see Table 2.2).

It needs to be emphasized that interflow generation under unsaturated conditions represents only a very small fraction of the total interflow for the sampling period. Well over 90% of the total interflow generated occurred when the soils were at or near saturation. This period was also when most of the chloride was mobilized.

Conceptual Model of Interflow

The conceptual model describes interflow generation under two volumetric soil moisture regimes: (1) moisture content below approximately ≈33%; and (2) moisture content above ≈33%, and is illustrated in Figure 2.10. The ≈33% moisture content value is based on the interflow chloride data and appears to be a threshold above which major changes in interflow chemistry and old/new water percentages occur (see Figures 2.5 and 2.8, and Table 2.2). Stated another way,

moisture contents less than ≈33% represent interflow processes under unsaturated conditions, whereas moisture contents greater than ≈33% represent soil moisture conditions that are at or near saturation. Also, the 33% threshold is probably only applicable to the local area or sites with similar soils and probably cannot be universally applied to other systems.

When volumetric moisture content is below about 33%, infiltrating water is either removed by evapotranspiration or bypasses the A horizon matrix and enters the macropore system in the B horizon, where it then moves laterally. Bypassing of the A horizon matrix (which might occur by stemflow) is suggested because interflow waters are not subject to much evaporation (Figure 2.4), which indicates that they move relatively quickly through the shallow evaporative zone in the soil. Matrix bypassing is also suggested by the low chloride concentrations of B-horizon interflow (see June 1993-October 1994 period in Figure 2.8). When B-horizon interflow is generated under unsaturated conditions small amounts (<0.5 L/day) of dominantly old water interflow typically result. Under this moisture-content regime, the B horizon acts as a two-domain system: the macropore domain generates interflow, while in the matrix domain, water that manages to infiltrate moves very slowly and is subject to transpiration, which causes the chloride concentration to

increase. Any A-horizon interflow that occurs is very small in volume and may come from localized ponding on top of the B horizon. If intense or large-volume rains occur under this soil moisture regime, moderate volumes of B-horizon interflow can be generated (on the order of 30 L/day) that will be dominated by new water, as was observed in July 1993 and October 1994 (Table 2.1).

When the high moisture-content regime is in effect (and maintained longer than a few days), the apparent independence of the macropore- and matrix-flow domains disappears and the importance of new water increases as compared to typical interflow during unsaturated periods. Interflow volumes also rise dramatically and can constitute greater than 90% of the annual interflow volume (see Figure 2.3). Solute flushing and diffusion of chloride from the matrix increase, causing chloride concentrations in interflow to rise substantially (see Figures 2.7 and 2.8). It seems counter-intuitive that chloride (and probably other solute) concentrations would rise, rather than decline because of dilution, as the soils become wetter; however, in this region, the two-domain flow regime is in effect for most of the year, causing the soil matrix to act as a solute sink. Only when the soils are at or near saturation is there a continuous fluid phase that allows solutes to be transported out of the soil matrix.

Subhumid- vs. Humid-Region Interflow

When the results from this study are compared with those from humid regions (discussed in the Introduction), more similarities than differences are found. Macropore flow generation by the excess water mechanism appears to be important in both environments, effecting rapid movement of water through the soil. In addition, aspects of new/old water relationships appear to be similar. For example, Turton et al.'s (1995) finding that new water becomes important during infrequent large storms, while old water is dominant during the frequent small storms appears to hold for subhumid-semiarid environments as well. During unsaturated periods at the ponderosa pine site, large and infrequent storms produce substantial percentages of new water, while during the majority of the year, most of the interflow is old water.

However, during saturated periods, there is an apparent difference in old/water percentages at the ponderosa pine site compared to what has been observed at most humid sites. The humid sites show a dominance of old water, while the results here indicate a possible dominance or at least a much more important contribution of new water. However, this difference is probably related to the fact that there is no stream at the ponderosa pine site. Thus, the groundwater ridging mechanism suggested by Sklash and Farvolden (1979) does not apply.

Instead, it is likely that for large events, old water is readily flushed from the system allowing a substantial new water contribution to interflow.

Another difference between subhumid and humid interflow involves changes in interflow chemistry. In humid regions, evidence of solute flushing has been observed as the soils become wetter, however, changes in interflow chemistry appear to be much greater in subhumid environments. Studies in humid environments have shown changes in chloride concentrations on the order of a few mg/L (e.g., DeWalle and Pionke, 1994; Mulholland et al., 1990), whereas the flushing that occurs at or near saturation in subhumid environments produces changes on the order of 30-40 mg/L. These larger changes are caused by the tremendous salt enrichment that occurs during extended dry periods, when interflow is isolated in the macropores. With no mechanism for their removal, soluble species build up and are released in large quantities when saturated conditions are approached.

SUMMARY AND CONCLUSIONS

Stable isotope and chloride tracer results show that interflow in a subhumid ponderosa pine hillslope in New Mexico is largely controlled by preferential flow processes, which not only influences water movement, but dramatically affects soil water chemistry. Most of the

interflow is generated in the B horizon and travels mainly via macropores, which can result in extremely rapid water movement even in soils having very low bulk hydraulic conductivities. Throughout most of the year, the flow system has two domains: a macropore domain, in which water can move relatively rapidly and in which evapotranspiration has a minor effect; and a matrix domain, in which water movement is extremely slow and evapotranspiration is high, resulting in substantial water loss and increased salt concentrations. When the soils are at or near saturation (greater than ≈33% volumetric water content), a connection between the two domains is established, and concentrations of chloride and other aqueous species in interflow can rise dramatically. Under these conditions, very large volumes of interflow can be produced.

The interflow generation processes that have been identified in humid environments are also operational in this subhumid environment, but in subhumid regions the chemistry of interflow can change to a much greater extent than has been observed at humid sites. This potential for major changes in interflow chemistry may significantly influence the mobility of some contaminants.

REFERENCES

Abeele, W. V., M. L. Wheeler, and B. W. Burton. Geohydrology of Bandelier Tuff. Los Alamos National Laboratory Report, LA-8962-MS. 51 pp.

Allison, G. B. and M. W. Hughes. 1983. The Use of Natural Tracers as Indicators of Soil-Water Movement in a Temperate Semi-Arid Region. J. of Hydrol. V. 60. pp. 157-173.

Anderson, M. G. and T. P. Burt. 1990. Process Studies in Hillslope Hydrology: an Overview. In Process Studies in Hillslope Hydrology (M. G. Anderson and T. P. Burt, eds.). John Wiley and Sons, New York. pp. 1-8.

Anderson, S. P., W. E. Dietrich, R. Torres, D. R. Montgomery, and K. Loague. 1994. Water Flowpaths in a Small Catchment During Steady, Artificial Rain and a Natural Storm. Abstracts of the Eighth International Conference on Geochronology, Cosmochronology, and Isotope Geology, USGS Circular 1107. pg. 7.

Bottomley, D. J., D. Craig, L. M. Johnson. 1984. Neutralization of Acid Runoff by Groundwater Discharge to Streams in Canadian Precambrian Shield Watersheds. J. of Hydrol. V. 75. pp. 1-26.

Bigeleisen, J., M. L. Perlman, H. C. Prosser. 1952. Conversion of Hydrogenic Materials to Hydrogen for Isotopic Analysis. Analytical Chemistry, V. 24. pp. 1356-1357.

Bowen, B. M. 1990. Los Alamos Climatology. Los Alamos National Laboratory Report, LA-11735. 254 pp.

Craig, H. 1961. Standard for Reporting Concentrations of Deuterium and Oxygen-18 in Natural Waters. Science, V. 133. pp. 1833-1834.

Davenport, D. W. 1994. Unpublished Data. Los Alamos National Laboratory, Los Alamos, NM.

DeWalle, D. R. and H. B. Pionke. 1994. Streamflow Generation on a Small Agricultural Catchment During Autumn Recharge: II. Stormflow Periods. J. of Hydrol. V. 163. pp. 23-42.

Kendall, C., and T. B. Coplen. 1985. Multisample Conversion of Water to Hydrogen by Zinc for Stable Isotope Determination. Analytical Chemistry. V. 57. pp. 1437-1446.

Germann, P. F. 1990. Macropores and Hydrologic Hillslope Processes. In Process Studies in Hillslope Hydrology. M. G. Anderson and T. P. Burt (eds.). John Wiley and Sons, NY. pp. 327-363.

Hornberger, G. M., K. J. Beven, and P. F. Germann. 1990. Inferences about Solute Transport in Macroporous Forest Soils from Time Series Models. Geoderma, V. 46. pp. 249-262.

Luxmore, R. J., P. M. Jardine, G. V. Wilson, J. R. Jones, and L. W. Zelazny. 1990. Physical and Chemical Controls of Preferred Path Flow Through a Forested Hillslope. Geoderma, V. 46. pp. 139-154.

McDonnell, J. J. 1991. Preferential Flow as a Control of Stormflow Response and Water Chemistry in a Small Forested Watershed. in Preferential Flow, T. J. Gish and A. Shirmohammadi (eds.). Amer. Soc. Agric. Engineers. St. Joseph, MI. pp. 50-58.

Mulholland, P. J., G. V. Wilson, and P. M. Jardine. 1990. Hydrogeological Response of a Forested Watershed to Storms: Effects of Preferential Flow Along Shallow and Deep Pathways. Water Resour. Res. V. 26, No. 12. pp. 3021-3036.

Newman, B. D., 1996. Investigations of Soil-Water Movement in Semiarid and Subhumid Forests Using Stable Isotope and Halogen Tracers. Chapter 3, this Dissertation.

Pearce, A. J., M. K. Stewart, and M. G. Sklash. 1986. Storm Runoff Generation in Humid Headwater Catchments 1. Where Does the Water Come From? Water Resources Res., V. 22, No. 8. pp. 1263-1272.

Peters, D. L., J. M. Buttle, C. H. Taylor, and B. D. LaZerte. 1995. Runoff Production in a Forested, Shallow Soil, Canadian Shield Basin. Water Resour. Research, V. 31, No. 5. pp. 1291-1304.

Satterlund, D. L. and P. W. Adams. 1992. Wildland Watershed Management, 2nd ed. John Wiley and Sons, New York. pp. 53-54.

Sharma, M. L., and M. W. Hughes. 1995. Groundwater Recharge Estimation Using chloride, Deuterium and Oxygen-18 Profiles in the Deep Coastal Sands of Western Australia. J. of Hydrol. V. 81. pp. 93-109.

Sklash, M. G. and R. N. Farvolden. 1979. The Role of Groundwater in Storm Runoff. J. of Hydrol., V. 43. pp. 46-65.

Sklash, M. G., M. K. Stewart, and A. J. Pearce. 1986. Storm Runoff Generation in Humid Headwater Catchments 2. A Case Study of

Hillslope and Low-Order Stream Response. Water Resour. Res., V. 22. No. 8. pp. 1273-1282.

Sklash, M. G. 1990. Environmental Isotope Studies of Storm and Snowmelt Runoff Generation. In Process Studies in Hillslope Hydrology. M. G. Anderson and T. P. Burt (eds.). John Wiley and Sons, New York. pp. 401-435.

Socki, R. A., H. R. Karlsson, and E. K. Gibson. 1992. Extraction Technique for the Determination of Oxygen-18 in Water Using Preevacuated Glass Vials. Analytical Chemistry, V. 64. pp. 829-831.

Stephens, D. B. 1993. Laboratory Analysis of Hydraulic Properties of Soil Samples, No. 2-LN3-6860J-1. Daniel B. Stephens and Assoc., Inc., Albuquerque.

Turton, D. J., D. R. Barnes, Jr., and J. de Jesus Návar. 1995. Old and New Water in Subsurface Flow from a Forest Soil Block. J. Environ. Qual. V. 24. pp. 139-146.

Thomas, G. W., R. E. Phillips. 1979. Consequences of Water Movement in Macropores. J. Environ. Qual. V. 8, No. 2. pp. 149-152.

Vuataz, F.-D., and F. Goff. 1986. Isotope Geochemistry of Thermal and Nonthermal Waters in the Valles Caldera, Jemez Mountains, Northern New Mexico. J. Geophys. Res., V. 91 (B2). pp. 1835-1853.

Watt, P. M. and L. D. McFadden. Preliminary Soil Analyses from Los Alamos County. Unpublished Report.

Whipkey, R. Z. 1965. Subsurface Stormflow from Forested Slopes. Bull. Int. Assoc. Sci. Hydrol. V. 2. pp. 74-85.

Wilcox, B. P., D. Brandes and D. W. Davenport. 1996. Runoff Generation from a Subhumid Ponderosa Pine Hillslope in New Mexico. Water Resour. Research. Submitted.

Table 2.1. Old and New Water Precentages for A- and B-Horizon Interflow

Table 2.1a. A Horizon $\delta^{18}O$

Date	Qs (L/day)	Cs ‰	Cn ‰	Co ‰	Qo (L/day)	% Old	% New
7/12/93	0.06	-12.4	-5.6	-12.6	0.06	98	2
7/13/93	0.02	-12.2	-9.3	-12.4	0.02	93	7
7/14/93	7.38	-12.0	-8.9	-12.2	6.94	94	6
7/15/93	0.24	-10.1	-9.9	-12.0	0.02	10	90
8/31/93	0.22	-8.9	-13.1	-8.8	0.21	97	3
7/12/94	0.02	-10.9	-2.2	-12.2	0.02	87	13
7/18/94	0.01	-9.7	-3.9	-10.4	0.01	90	10
11/13/94	0.35	-12.7	-6.4	-14.6	0.27	77	23
2/15/95	22.9	-13.6	-14.8	-12.9	14.45	63	37

Table 2.1b. B Horizon $\delta^{18}O$

Date	Qs (L/day)	Cs ‰	Cn ‰	Co ‰	Qo (L/day)	% Old	% New
7/13/93	0.02	-13.8	-9.3	-13.8	0.020	100	0
7/14/93	1	-13.5	-8.9	-13.8	1	93	7
7/15/93	0.02	-10.6	-9.9	-13.5	0.00	19	81
8/31/93	0.02	-8.9	-13.1	-8.6	0.02	94	6
7/12/94	0.05	-12.0	-2.2	-11.4	0.05	107	-7
7/18/94	0.02	-12.1	-3.9	-12.1	0.02	101	-1
8/18/94	0.01	-11.3	-3.4	-11.3	0.01	100	0
8/25/94	0.005	-10.3	-3.8	-10.3	0.005	100	0
10/15/94	61	-15.5	-18.3	-10.5	22	36	64
10/16/94	28	-12.1	-10.5	-16.2	8	28	72
10/17/94	18	-10.3	-10.6	-10.1	11	60	40
11/13/94	114	-12.3	-6.4	-13.6	93	81	19
2/15/95	26	-12.5	-14.8	-11.8	20	78	22
3/6/95[1]	1454	-12.6	-12.9	-11.9	484.6	33	67
4/12/95	0.25	-12.9	-16.7	-12.4	0.2	88	12

Table 2.1c. B Horizon δD

Date	Qs (L/day)	Cs ‰	Cn ‰	Co ‰	Qo (L/day)	% Old	% New
7/13/93	0.02	-99	-78	-97	0.02	110	-10
8/18/94	0.01	-82	-32	-80	0.01	103	-3
10/15/94	61	-112	-126	-75	17	28	72
10/16/94	28	-86	-64	-112	13	47	53
10/17/94	18	-75	-63	-86	9	51	49

Table 2.1d. Comparison of A- and B-horizon % old water (estimated from $\delta^{18}O$).

Date	A % Old	B % Old
7/13/93	93	100
7/14/93	94	93
7/15/93	10	19
8/31/93	97	94
7/12/94	87	107
7/18/94	90	101
11/13/94	77	81
2/15/95	63	78

[1]3/6/95 New water value was estimated from the A-horizon, because there was no precipitation to sample.

Table 2.2. Calculation of matrix flow contribution to interflow.

A-Horizon Interflow

				No Dilution			50% Dilution of C_m		
Date	I (L/day)	C_I (mg/L)	C_P (mg/L)	C_M (mg/L)	I_M (L/day)	% matrix flow	50%C_M (mg/L)	I_M (L/day)	% matrix flow
7/19/93	0.03	3.2	2	101	0.0004	1.2	50.5	0.0007	2
8/16/94	0.01	2.5	2	58	0.0001	0.9	29	0.0002	2
3/6/95	144	24	2	58	57	39	29	117	81
3/13/95	0.11	33	2	58	0.06	55	29	0.126	115
6/12/95	0.01	9.2	2	18	0.005	45	9	0.01	103

B-Horizon Interflow

				No Dilution			50% Dilution of C_m		
Date	I (L/day)	C_I (mg/L)	C_P (mg/L)	C_M (mg/L)	I_M (L/day)	% matrix flow	50%CM (mg/L)	I_M (L/day)	% matrix flow
7/19/93	0.06	2.3	2	206	0.0001	0.1	103	0.0002	0.3
8/16/94	0.02	2.8	2	206	0.0001	0.4	103	0.0002	0.8
1/12/95	0.01	63	2	206	0.003	30	103	0.006	60
3/6/95	1400	23	2	206	144	10	103	291	21
6/12/95	0.01	29	2	206	0.001	13	103	0.003	27

Table 2.3. Comparison of chloride concentrations in interflow and soil matrix water.

A Horizon		
Date	Interflow Cl^- (mg/L)	Matrix Cl^- (mg/L)[1]
7/19/93	3.2	101 (59-184)
8/16/94	2.5	58.4 (32-113)
6/12/95	9.2	20 (14-33)

B Horizon		
Date	Interflow Cl^- (mg/L)	Matrix Cl^- (mg/L)[2]
7/19/93	2.3	216 (55-455)
8/16/94	2.8	329 (161 593)
6/12/95	29	298 (106 477)

[1] Average and range of concentrations of the A horizon in the core.

[2] Average and range of concentrations of the B horizon in the core.

All cores were taken in the same part of the hillslope.

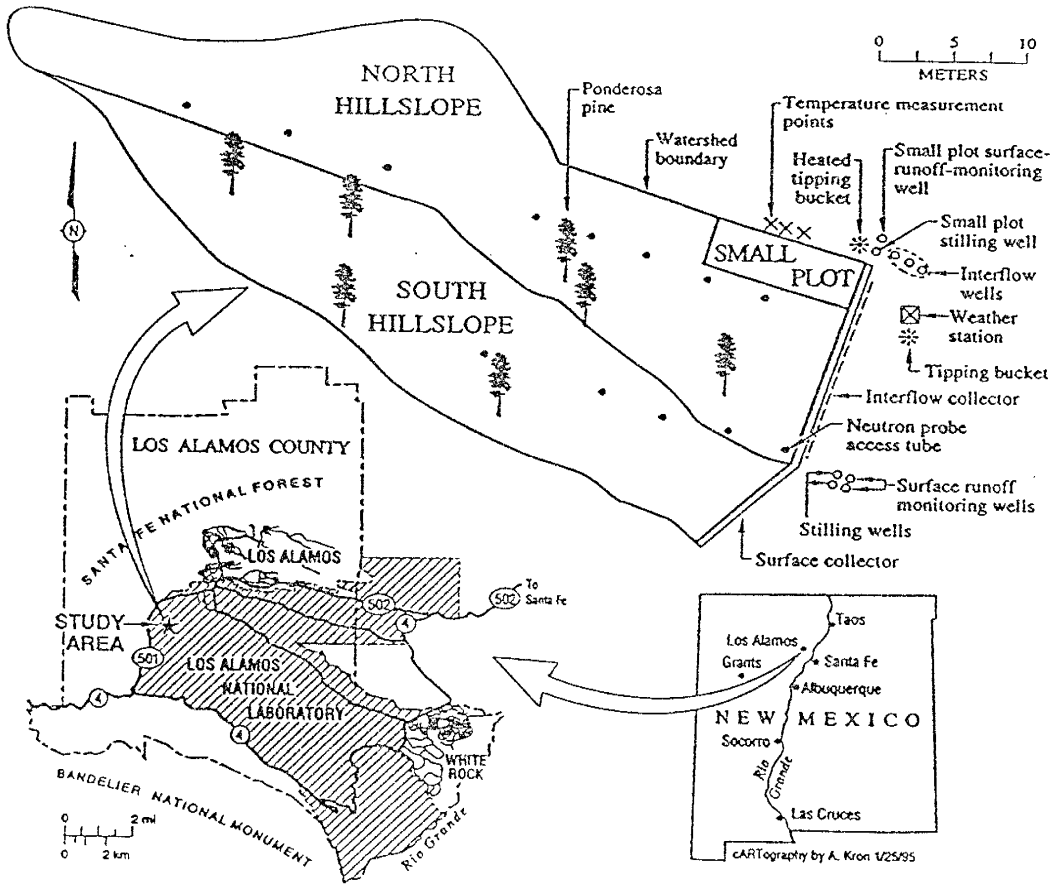

Figure 2.1. Location map and schematic of the ponderosa pine hillslope.

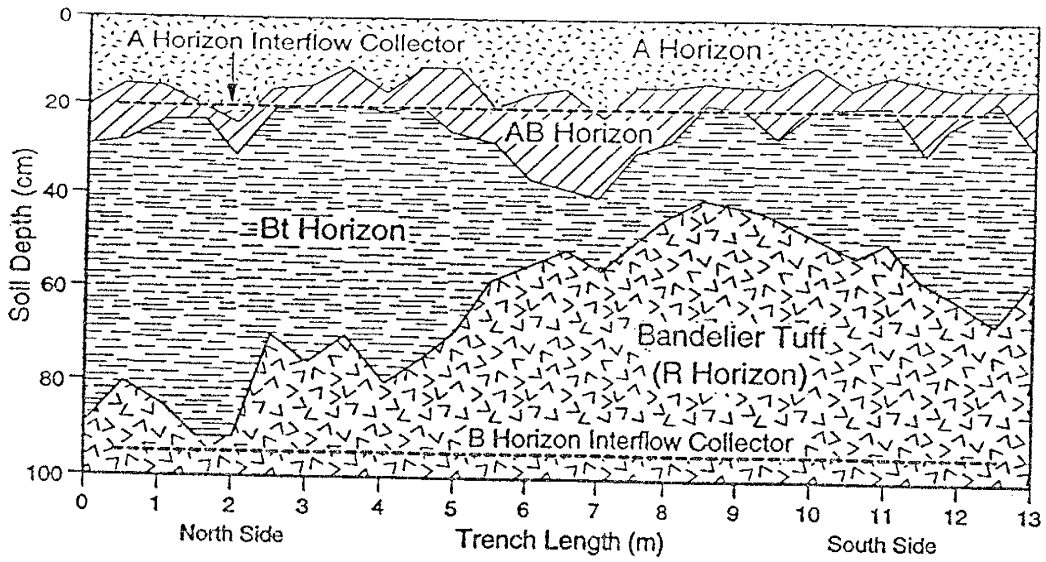

Figure 2.2. Diagram of the interflow collection trench showing soil stratigraphy and location of the interflow collectors.

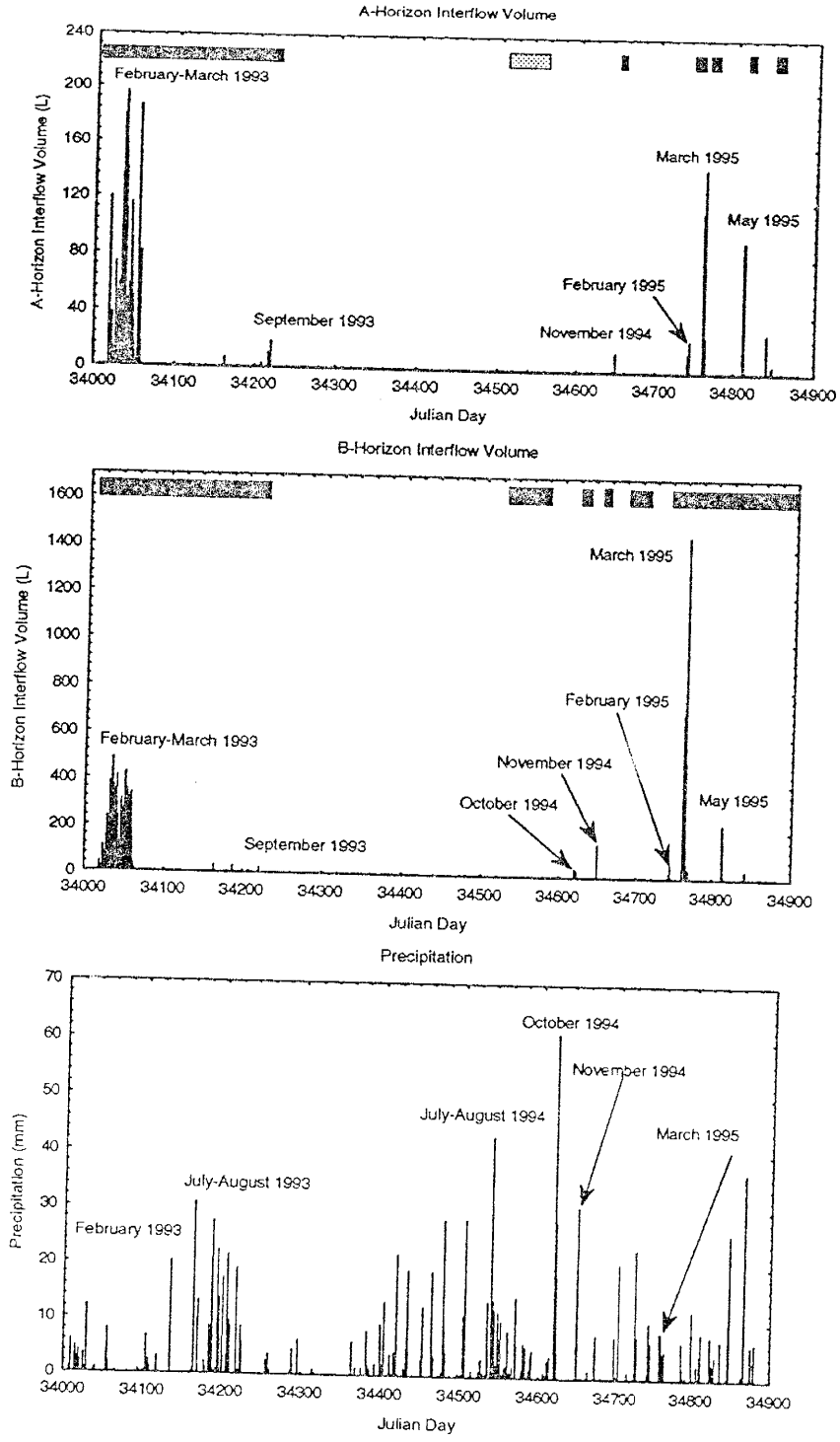

Figure 2.3. Graphs of A- and B-horizon interflow volume, and precipitation. Solid bars at the top of the interflow graphs indicate periods of continuous interflow generation. Stippled bars indicate periods of frequent, but discontinous interflow generation.

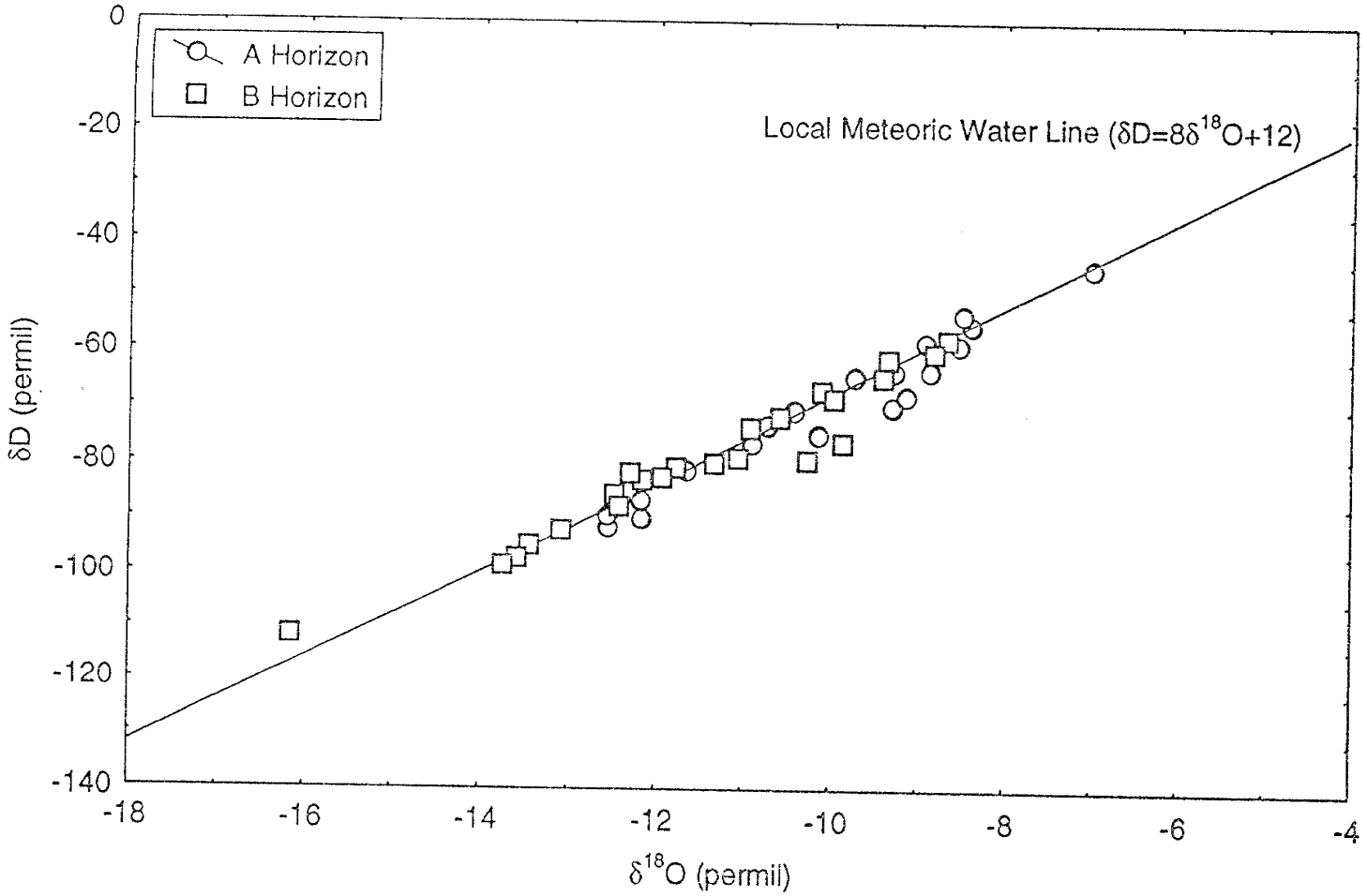

Figure 2.4. $\delta^{18}O$ versus δD for A- and B-horizon interflow plotted against the Los Alamos local meteoric water line of Vuataz and Goff (1986).

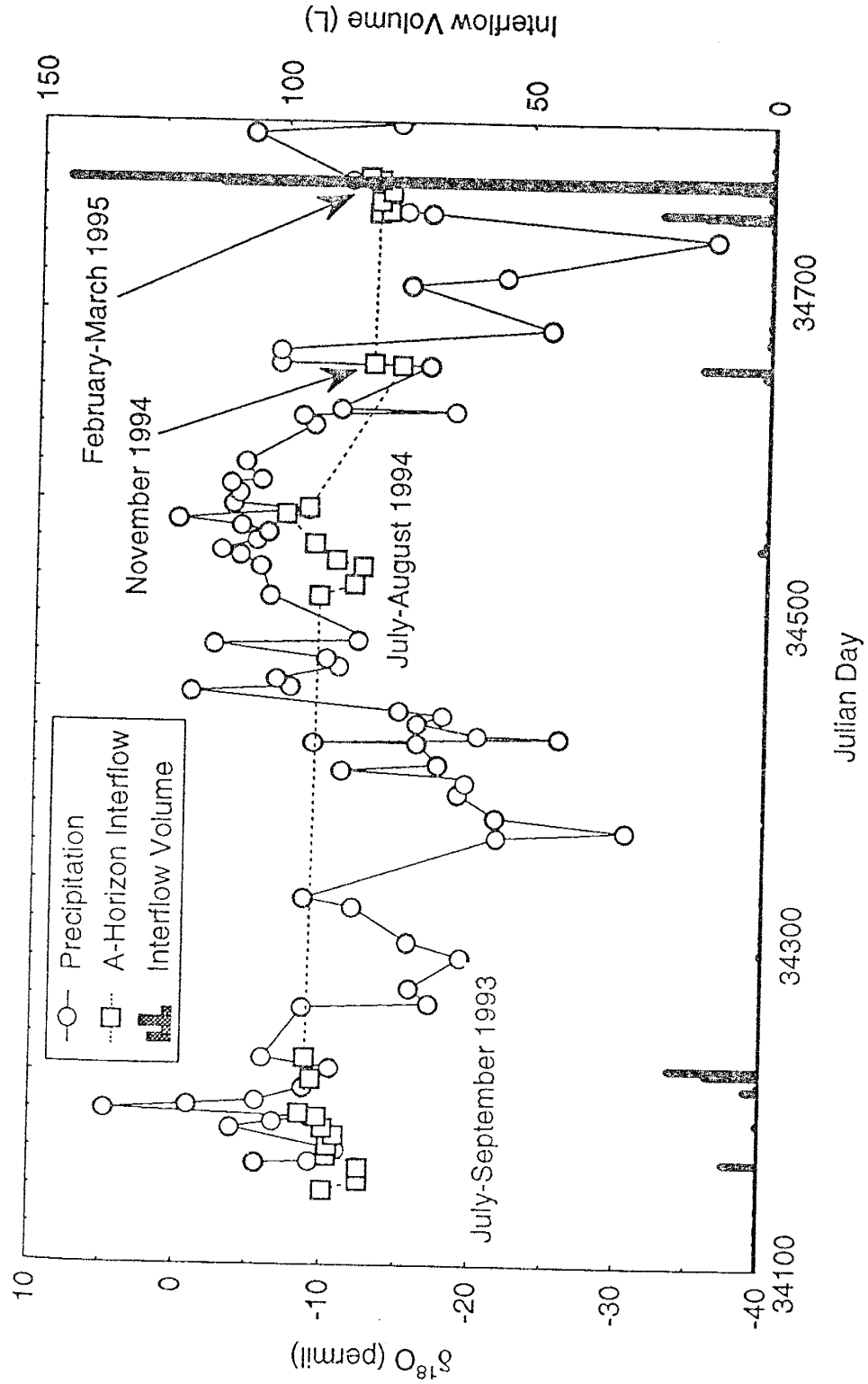

Figure 2.5. Changes in the $\delta^{18}O$ of precipitation and A-horizon interflow through time. A-horizon interflow volume is also shown.

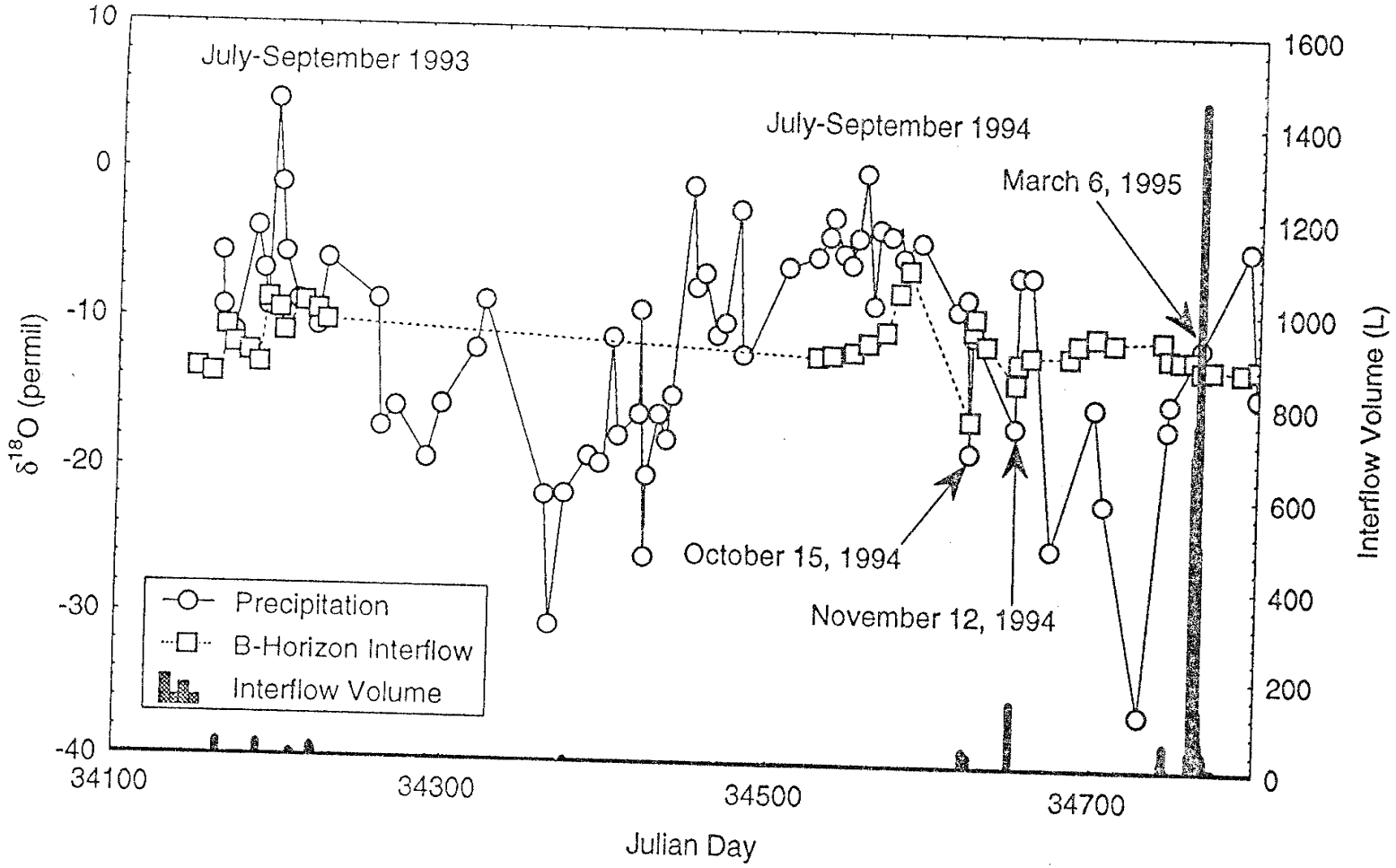

Figure 2.6. Changes in the $\delta^{18}O$ of precipitation and B-horizon interflow through time. B-horizon interflow volume is also shown.

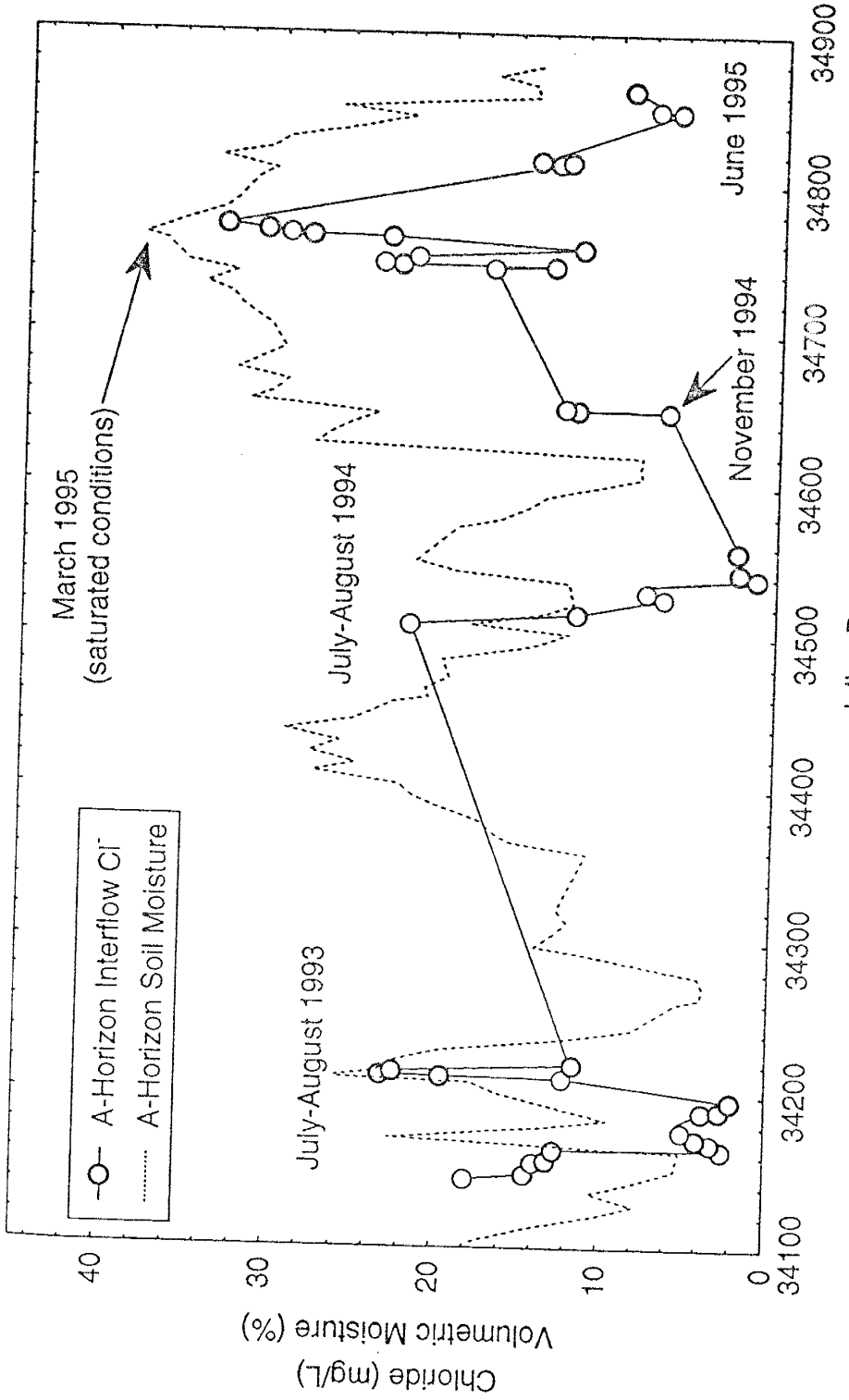

Figure 2.7. Changes in A-horizon interflow chloride concentration and volumetric moisture content through time. Volumetric moisture is the average for all neutron access tubes on the hillslope for the horizon.

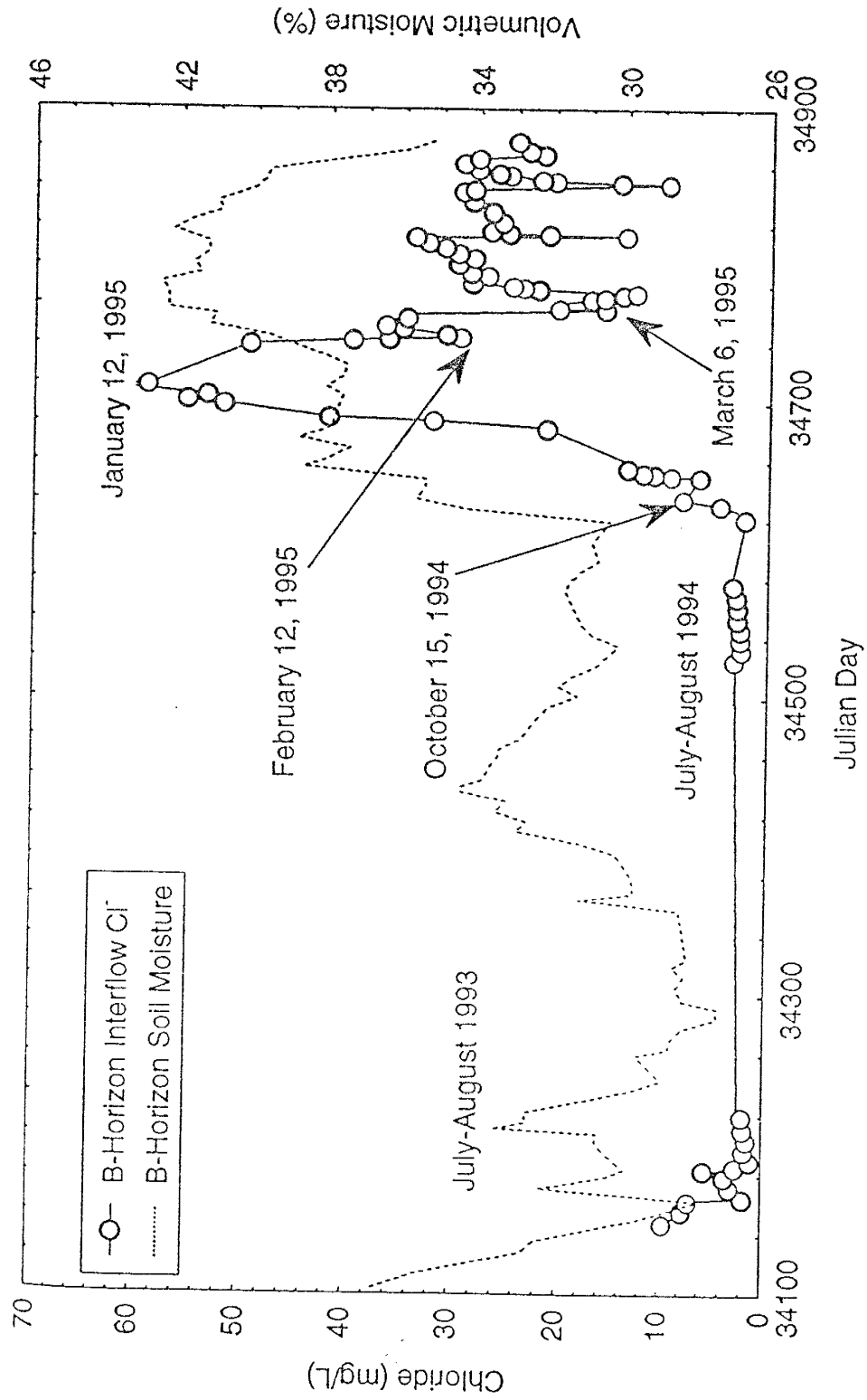

Figure 2.8. Changes in B-horizon interflow chloride concentration and volumetric moisture content through time. Volumetric moisture is the average for all neutron access tubes on the hillslope for the horizon.

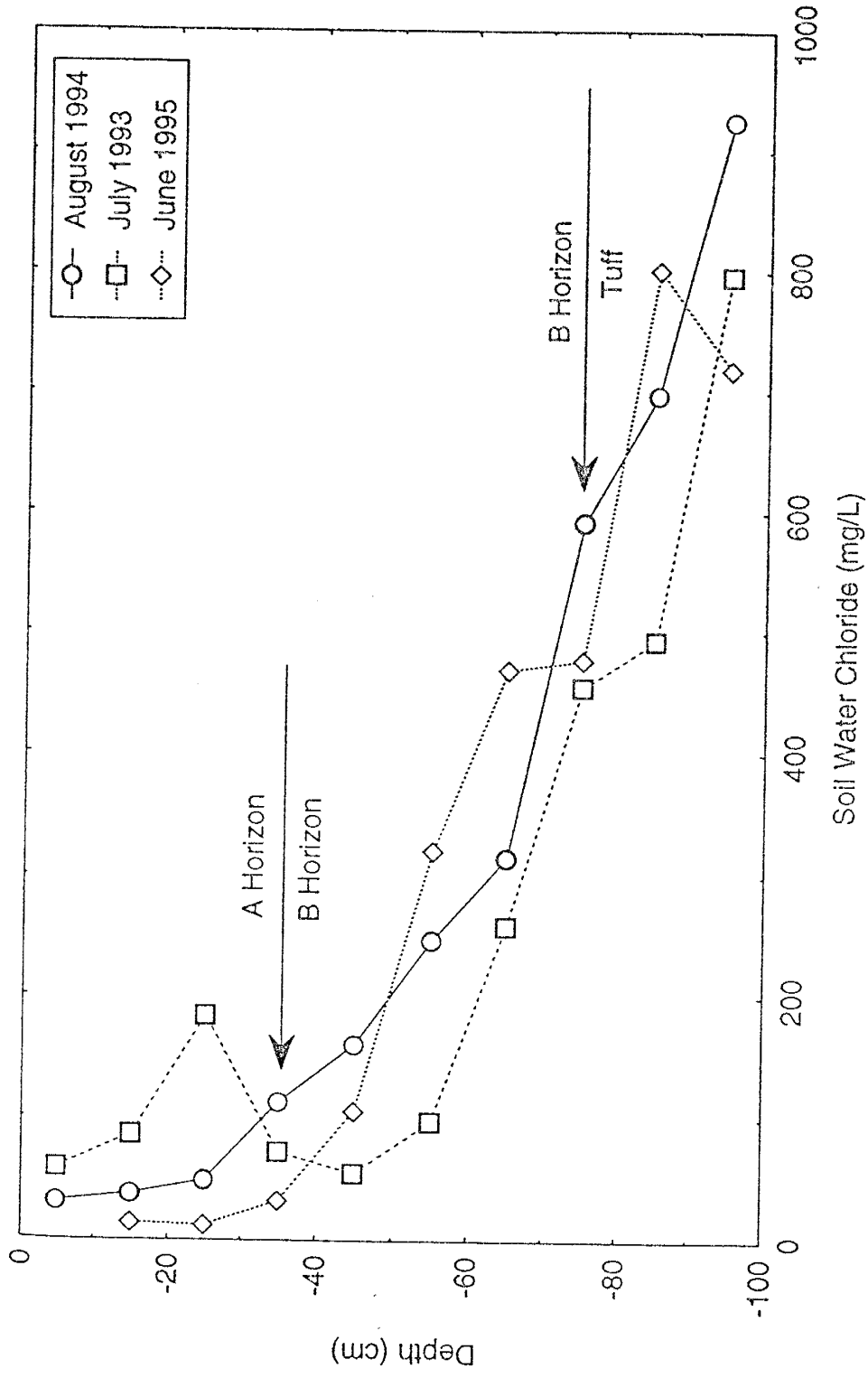

Figure 2.9. Chloride soil-water concentration profiles with depth from soil cores taken in July 1993, August 1994, and June 1995. Indicated depths of the soil horizon interfaces are approximate because of small differences in interface depths between the three cores.

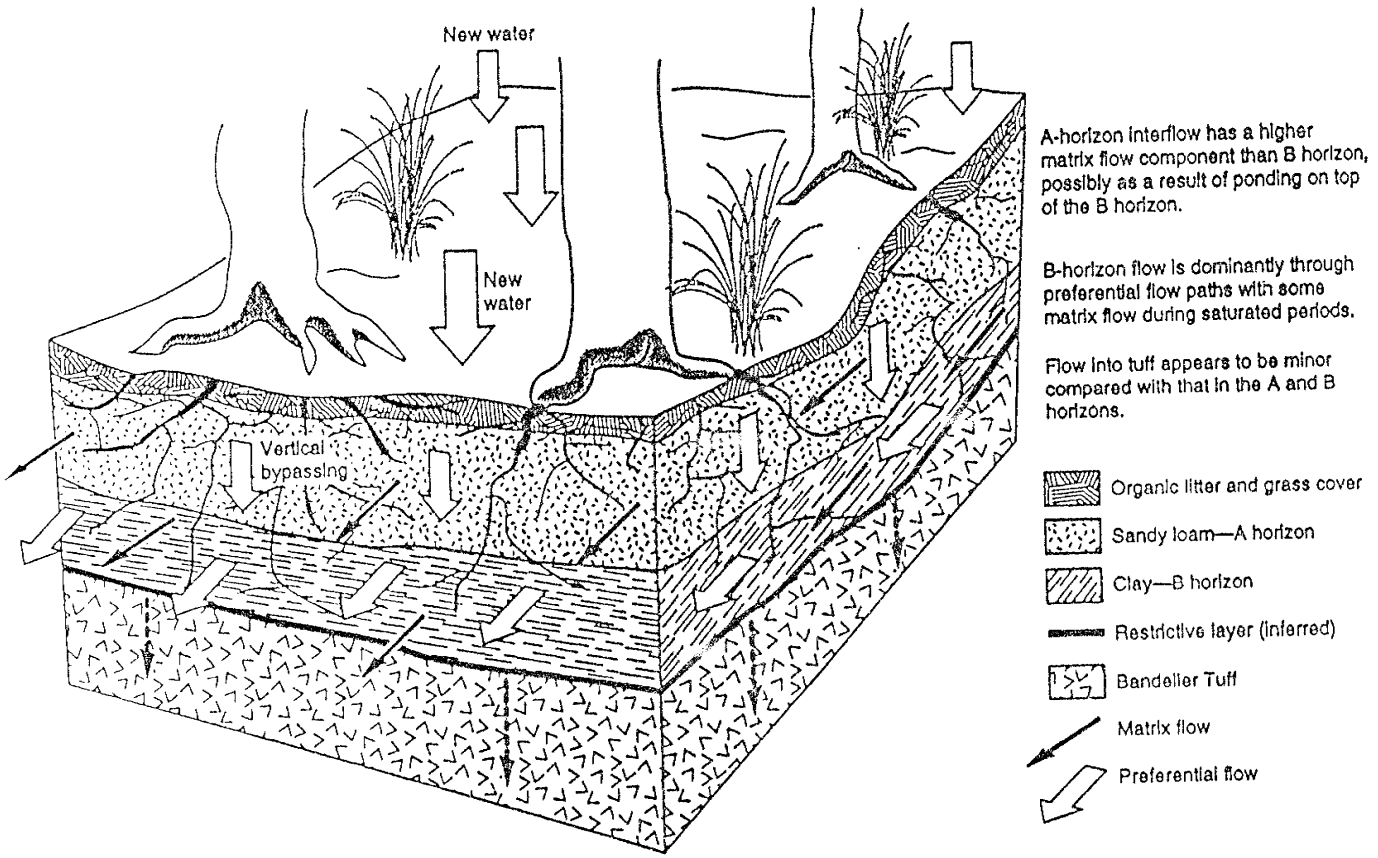

Figure 2.10. Illustration of the conceptual flow model for the hillslope.

CHAPTER 3: INVESTIGATIONS OF SOIL-WATER MOVEMENT IN SEMIARID AND SUBHUMID FORESTS USING STABLE-ISOTOPE AND HALOGEN TRACERS.

ABSTRACT

The related issues of groundwater recharge and contaminant movement in dry regions have generated considerable interest and concern in the last decade. Essential to understanding these issues is knowledge of how water moves through the near-surface vadose zone. The use of tracers, both natural and artificially introduced, is proving to be an effective method for gaining such knowledge in dry regions, where investigation by other means is difficult. In this study, stable-isotope and halogen (chloride and bromide) tracers were used to investigate water movement in the soils of a pinyon-juniper woodland and of a ponderosa pine forest in northern New Mexico. The stable-isotope data indicate that in both communities, evaporation is mainly restricted to the upper 10 cm of soil. Chloride profiles in the two communities, however, show a distinct difference: downward fluxes in the ponderosa pine forest (≈0.02 cm/yr) are an order of magnitude lower than those in the pinyon-juniper woodland (≈0.2 cm/yr), even though total precipitation is about 4 cm/yr higher in the ponderosa pine forest. A possible explanation for

this difference is that a clay-rich B horizon in the ponderosa pine woodland restricts downward movement of water through the soil matrix. An artificial bromide tracer introduced at the ponderosa pine study site indicated an order of magnitude higher flux than that found using chloride. This contrasting result is probably the result of either an artificial perturbation of the hydrologic system caused by the death of the grass cover during bromide application, and/or differences between the net advective and diffusive fluxes that controlled the distributions of the two tracers.

INTRODUCTION

Understanding the hydrology of the vadose zone is becoming increasingly important, especially in dry regions of the western United States, as growing cities and communities struggle with problems of environmental contamination, waste storage, and dwindling water supplies (Rieth, 1992; Phillips, 1994). One of the difficulties in understanding flow and transport in the vadose zone of dry regions is that physically based approaches, such as Darcy's Law and water-balance determinations, give rise to unacceptably large uncertainties because of the generally low moisture content (Scanlon, 1991; Allison et al., 1994; Phillips, 1994). One approach that circumvents this difficulty

and permits soil water movement in dry regions to be quantitatively estimated is the use of tracers. Allison et al. (1994) and Phillips (1994) review this approach and describe studies that have used tracers to investigate dry-region vadose zone processes. For the current study, stable isotopes and two halogens, chloride and bromide, were used.

The use of stable isotopes involves measuring the δD and $\delta^{18}O$ of soil water with depth. Isotopic values of soil water are affected by evaporation, which preferentially moves light isotopes into the vapor phase and leaves the remaining liquid enriched in heavy isotopes. The depth at which δD and $\delta^{18}O$ reach their maximum (heaviest) values coincides with the depth of an evaporation front (Barnes and Allison, 1983; Allison et al., 1983). In other words, the stable-isotope profile can be used to determine the depth of an evaporation front in the soil. This technique is particularly useful for comparing the effects of evaporation at different sites. In addition, the isotopic composition of the soil water can provide important clues as to the major source of that water (e.g., snowmelt vs. summer rain).

The use of chloride tracers (commonly known as the chloride mass balance method), involves measuring chloride concentrations in soil water with depth. These concentrations serve as indicators of downward flux and soil water age (Allison et al., 1983; Stone, 1984). Stated simply,

the downward flux is inversely proportional to the amount of chloride accumulation in the soil: high chloride concentrations, which represent many years of meteoric chloride accumulation coupled with evapotranspirative removal of water indicate a low downward soil water flux; relatively low chloride concentrations indicate a high downward flux, that is, water is able to move through the soil at a rate fast enough that evapotranspiration and concentration of chloride are minimized.

In the current study, in addition to the naturally occurring tracers, bromide was used as an artificial tracer to independently check the flux values obtained via the chloride mass balance method. Bromide has been shown to be useful for understanding vadose-zone water movement (e.g., Bowman and Rice, 1986; Jardine et al., 1990; Bronswijk et al., 1995); it behaves similarly to chloride (both tracers are monovalent anions when in solution) and, in addition, it generally has low background concentrations in soil water, which facilitates interpretation of tracer behavior (Bowman, 1984).

Our study focused on three sites in northern New Mexico, two of which are located within the pinyon-juniper community and the third within the ponderosa pine community. The two plant communities are found adjacent to one another throughout the southwestern United States and are important both environmentally and economically, but to

our knowledge no previous studies have attempted to estimate and compare water fluxes in these regions.

DESCRIPTION OF THE STUDY AREA

The study area is located on the Pajarito Plateau in north central New Mexico, which is characterized by a semiarid-to-subhumid, temperate mountain climate (Figure 3.1). Average annual precipitation varies from less than 360 mm/yr, at lower elevations near the Rio Grande, to over 500 mm/yr near the Jemez mountains. The plateau includes four major vegetation zones (see Figure 3.2), which are also largely governed by elevation: juniper grassland (1600-1900 m), pinyon-juniper woodland (1900-2100 m), ponderosa pine forest (2100-2300 m), and mixed conifer forest (2300-2900 m) (Allen, 1989). Topographic effects create some variations within these zones, producing the "fingered" appearance in the figure. For example, plants typical of higher elevations also grow in cooler and more moist environments at lower elevations, such as along canyon walls and bottoms. The greater part of the Los Alamos National Laboratory is within the pinyon-juniper (*Pinus edulis* and *Juniperus monosperma*) and the ponderosa pine (*Pinus ponderosa*) zones.

The study site within the ponderosa pine zone is an 870-m^2 hillslope (elevation 2315 m) where investigations of runoff processes are currently under way (Wilcox et al., 1996, Figure 3.1). The soil stratigraphy of the site, described by Davenport (1994), is illustrated in Figure 3.3. The thicknesses and depths of the horizons vary across the hillslope, but the variations in the overall stratigraphy are relatively minor. A dense, clay Bt horizon is present throughout the site.

The two study sites in the pinyon-juniper zone (elevation 2140 m) are (1) a relatively undisturbed woodland measuring approximately 2540 m^2 and (2) a treeless area (hereafter called the erosion plot site) comprising four small (3.04- x 10.64-m) plots that have been used for the development of soil erosion models (Wilcox, 1994). All vegetation, cryptogamic crust, litter, and rock cover were removed from Erosion Plots 1 and 4 in 1987 (Wilcox, 1994); currently, these plots have a sparse grass cover. Erosion Plots 2 and 3 have an undisturbed grass cover. The pinyon-juniper woodland site and the erosion plot site is approximately 180 m apart.

Cores taken from the two pinyon-juniper sites and the ponderosa pine site show the soils to be much more variable in the pinyon-juniper zone (Figure 3.3). Soil stratigraphy in this zone varies greatly over horizontal scales of only a few meters, and this variability can take the

form of differences in type and number of soil horizons or of differences in soil textural properties in a given horizon (Davenport et al., 1995). The Bt horizon is usually either absent or has a clay loam texture, which indicates a lesser degree of development than Bt horizons in the ponderosa pine zone.

METHODS AND MATERIALS

Core Collection

Details of the core sampling and analyses performed are summarized in Table 3.1. All cores were collected during the summer months (June-August) and encompassed the entire soil layer and a portion of the underlying tuff. The locations from which cores were taken at the three sites are shown in Figure 3.1. At the ponderosa pine site, twenty-two cores were taken: one in 1993, nineteen in 1994, and two in 1995. At the pinyon-juniper woodland site, six cores were taken: one in 1993, and five in 1995. At the erosion plot site, three cores were taken, all in 1993.

For the 1993 sampling, cores were collected by means of a truck-mounted drill rig. Each core, as soon as it was removed from the core barrel, was cut into 10-cm sections; each section was stored in a clean glass mason jar with a vacuum-grease-coated lid. Both stable isotope

and chloride profiles were obtained for all of the cores except cores EP2 and EP3, from the erosion plot site, for which only chloride profiles were obtained.

For the 1994 and 1995 sampling, cores were collected by hand augur, and each 10-cm portion was stored in a zip-lock bag. All of these cores were analyzed for chloride only.

Stable Isotopes

The stable isotope analyses were carried out at the New Mexico Tech stable isotope laboratory, Soil water was extracted by high-temperature vacuum distillation, following Shurbaji et al. (1995), and $\delta^{18}O$ and δD measurements were made on a Finnegan-Mat, Delta-E stable-isotope-ratio mass spectrometer using OZ-Tech gas standards. The hydrogen and oxygen isotopes are reported in delta (δ) notation as per mil (‰) differences relative to the V-SMOW international standard:

$$\delta D \text{ or } \delta^{18}O = \left[\frac{R_{sample} - R_{SMOW}}{R_{SMOW}}\right] \times 1000, \qquad (1)$$

where R is the D/H or $^{18}O/^{16}O$ ratio. The value of $\delta^{18}O$ was determined from extractions made using the carbon dioxide equilibration technique of Socki et al. (1992). For the δD analyses, hydrogen was extracted

using the zinc method of Kendall and Coplen (1985), and a linear equation ($\delta D_{actual} = 1.06\delta D_{measured} + 10.01$, R^2 of 0.99) based on regression analysis of V-SMOW and GISP standards was used to correct the analyses. The analytical precision for the $\delta^{18}O$ and δD analyses by mass spectroscopy was better than 0.2‰ and ±6‰, respectively. A few of the extractions from the pinyon-juniper woodland site gave much poorer δD precisions (up to ±11‰); these samples, from the top-20-cm, organic-rich A and AB horizons, contained an organic material that evidently caused a variable fractionation during extraction.

Chloride

Chloride concentrations in soil water were determined by leaching splits from the 10-cm-interval core samples. After the samples had been air-dried for 48 hours, 100 gm of the soil was mixed with 100 mL of deionized water. The mixture was allowed to equilibrate for 48 hours, with periodic stirring. After equilibration, the leachate was centrifuged and filtered, using disposable 0.2-μm Gelman ion-chromatography filters. Samples of the leachate were analyzed by ion chromatography, following Newman (1996). Analytical precision was ±2% or better, and accuracy was ±10% or better. Moisture content was determined

gravimetrically or by neutron probe. The chloride concentrations found in the leachate were then used to calculate the original concentrations in the soil water. The bulk density values used for these calculations were measured previously and are given in Wilcox et al. (1996).

As stated earlier, the chloride mass balance method permits the estimation of both downward moisture flux (residual flux) and soil water age. The residual flux, if determined from samples taken below the root zone, is synonymous with recharge. In the case of the Los Alamos soil profiles, all are in the root zone, and therefore the term *residual flux* will be used, as opposed to *recharge*, consistent with the usage in Phillips (1994). Residual fluxes through the soils were calculated using the cumulative chloride-cumulative water method of Stone (1984). This method is based on the following assumptions: flow occurs largely as downward piston flow; dispersive mixing of water and chloride is small; atmospheric chloride deposition has been relatively constant and is the sole source of chloride to the system; and chloride uptake by plants is negligible. Cumulative chloride-cumulative water plots are used to identify changes in flux with depth in the profile. Linear segments (segments on these plots that are formed by approximately straight lines) indicate zones of constant flux. The fluxes for these segments were estimated by

$$R = (Cl_p \cdot P)/Cl_{sw}, \quad (3)$$

where R is the residual flux (m/yr); Cl_p is the modern chloride content of precipitation (g/m^3); P is the modern average annual precipitation (m/yr); and Cl_{sw} is the average chloride content of the samples represented by the segment (g/m^3). Chloride ages at the endpoints of line segments were estimated using the relationship

$$A = Cl_{swi}/(Cl_p \cdot P), \quad (4)$$

where A is the chloride age in years, and Cl_{swi} is the cumulative chloride content (g/m^2) in the unsaturated zone at that point.

For both calculations, the value used for P were 0.51 m/yr for the ponderosa pine zone (Bowen, 1990) and 0.47 m/yr for the pinyon-juniper zone (Nyhan, 1995). For Cl_p, a value of 0.29 g/m^3 was used for all sites; the ponderosa pine and pinyon-juniper sites are close enough (6.6 km) that no significant differences in chloride input are expected. Although the long-term 0.29 g/m^3 average was measured at the Sante Fe, New Mexico, water treatment plant (Gallaher, 1995); but it is based on long-term data and appears to be reasonable for the Los Alamos area, judging from a 4-year average chloride precipitation concentration of 0.28 g/m^3 obtained for a location only a few km from the ponderosa pine

study area (Adams et al., 1995). Moreover, values used in other studies in southern New Mexico and west Texas, given in Shurbaji and Campbell (1996), are consistent with the 0.29 g/m^3 concentration.

Bromide

On November 20, 1993, a bromide solution, consisting of 1,564 gm of lithium bromide (EM Science, reagent grade) in 20 L of deionized water, was sprayed along an 8-m x 2.5-m strip situated at the top of the ponderosa pine site, perpendicular to the ground slope (Figure 3.1). The solution was applied in a criss-cross manner, using a backpack sprayer with a 5-ft boom to achieve uniform application. On August 22, 1994, 275 days after the bromide was applied, four soil cores were taken from the strip. Samples from these cores were leached and analyzed for bromide in the same manner as the samples analyzed for chloride.

RESULTS

Stable Isotope Profiles

Vertical $\delta^{18}O$ and δD profiles for the ponderosa pine site, the pinyon-juniper woodland site, and the erosion plot site are shown in Figure 3.4. The profiles for all three sites show the same general features, namely, a maximum isotopic value in the first 10 cm and,

below the maximum, a bulge extending to light values. Unfortunately, sampling was not done on a fine enough scale to locate the exact depth of the isotope maximum. The values of the maximum for the three sites range from -1.1 to 2.2 ‰ for $\delta^{18}O$ and from -73 to -65 ‰ for δD. The minimum values, which range from -13.9 to -12.1 ‰ for $\delta^{18}O$ and from -141 to -114 ‰ for δD, were found at depths between 35 and 55 cm. At the bottom of the profiles (125 cm), isotopic values range from -10.2 to -8.2 ‰ for $\delta^{18}O$ and from -98 to -86 ‰ for δD.

Chloride Profiles

Typical chloride profiles from the ponderosa pine site show that chloride concentrations increase nonlinearly with depth to at least 100 cm and that the largest increases generally coincide with the Bt and deeper soil horizons (Figure 3.5). Concentrations in the soils above the Bt horizon are consistently below 200 mg/L, while those in the Bt horizon can exceed 500 mg/L. Concentrations below the Bt horizon vary, but typically are the highest of all, exceeding 1000 mg/L in some cores.

Examples of cumulative chloride-cumulative water plots for the ponderosa pine site are shown in Figure 3.6. In most cases, two approximately linear segments can be distinguished. According to Stone

(1984), such segments indicate relatively constant rates of precipitation, chloride input, and/or flux. The upper linear segments correspond to the sandy loam horizons, and the lower linear segments correspond to the Bt, weathered tuff (CR), and tuff (R) horizons. The small slope in the shallow segment represents a higher residual flux, and the larger slope of the deeper segment represents a lower flux. The residual flux estimates and chloride ages for the ponderosa pine cores are given in Table 3.2; these typically show a decrease of about one order of magnitude between the sandy loam horizons and the deeper Bt clay and tuff horizons.

Typical chloride profiles and cumulative water-cumulative chloride plots for the pinyon-juniper woodland zone show a great deal of variability (Figures 3.7 and 3.8). Except for cores EP2 and EP4, chloride concentrations are lower than those in the ponderosa pine zone. The residual flux estimates and chloride ages for the pinyon-juniper cores are given in Table 3.3; like the stratigraphic and chloride profiles (Figures 3.3 and 3.7), the fluxes are highly variable. The large increases in chloride concentrations in the Bt and lower horizons seen in the ponderosa pine cores were not commonly observed in the pinyon-juniper cores.

Bromide Profiles

Concentrations of bromide in relation to soil depth for one of the four cores taken in the bromide application area are shown in Figure 3.9. The profile shows a band of high concentration that reaches a maximum at about 45 cm, indicating that during the 275-day period between application and core sampling, bromide had moved most of the way through the sandy loam horizons, and some had reached the Bt horizon. The profiles for the other three cores were very similar, some showing maximum concentrations in the top part of the Bt horizon. Samples of surface runoff from the area, taken after the bromide was applied, showed no bromide concentrations above natural background, indicating that nearly all of the bromide infiltrated the soil. Mass balance calculations using the core results also confirm that essentially all of the bromide had infiltrated into the soils below the application area.

DISCUSSION

Stable Isotopes: Ponderosa Pine and Pinyon-Juniper Zones

The main factors that control the isotopic composition of soil waters are (1) the isotopic composition of the precipitation entering the soil, (2) evaporation, and (3) mixing of soil waters having different

isotopic compositions. Root uptake is a nonfractionating process and thus does not affect the isotopic composition of the soil water (Dawson and Ehleringer, 1991); this is important, because transpiration effects can be disregarded when using isotope data to assess the role of evaporation.

A potentially complicating factor is that the isotopic composition of the water entering the soil varies with elevation: the isotopic composition of precipitation becomes lighter as elevation increases. At our sites, however, this difference appears to be insignificant. Isotope analyses of precipitation for locations near the pinyon-juniper and ponderosa pine sites (Adams et al., 1995) show an elevational effect that is very small, comparable in magnitude to the analytical errors. In other words, this effect is small enough that a direct comparison of the isotope results for the ponderosa pine and pinyon-juniper zones is valid.

It was initially hypothesized that because plant cover influences the amount of solar radiation reaching the soil surface (Breshears et al., 1996), the different vegetation at the three sites, by controlling the amount of evaporation, would produce different isotope profiles. However, this does not appear to be the case; vertical $\delta^{18}O$ and δD profiles for the cores from the ponderosa pine site, the pinyon-juniper woodland site, and the erosion plot site (shown in Figure 3.4) all display

similar trends. Throughout the plateau, Class A pan evaporation is much higher than annual precipitation (Bowen, 1990), which suggests that evaporative demand may be so large that it masks any plant cover effects.

The less-than-10-cm depth of maximum isotopic enrichment indicates a shallow evaporative front. This is interesting, because the time of the year when the cores were taken, at the end of the early summer (when temperatures are high, and relative humidity and precipitation rates are low), is the time when the evaporation front should be at its maximum depth.

According to the observations of Liu et al. (1995), infiltration of isotopically light, cool-weather precipitation produces a minimum bulge during wet and cool periods, and evaporation during the drier, hotter periods produces a maximum bulge. Our profiles, then, would be expected to show maximum bulges. Perhaps in the Los Alamos area, the combination of the shallow evaporative zone and the relatively cool and wet climate allows the development of a persistent minimum bulge. In other words, the evaporation front may never move deeply enough into the soil to enrich the isotopic values of the soil waters and produce a maximum bulge.

One way of determining the average isotopic composition of infiltrating water and the importance of evaporation is to determine an evaporation trend line for the data and plot this line against the meteoric water line on a $\delta^{18}O$-δD diagram (Figure 3.10). The evaporation trend line is obtained by calculating a linear regression of the soil-water isotopic compositions; linear regression is used because, as evaporation progresses, the isotopic composition of the soil water becomes increasingly heavy and follows a linear trend that is a function of the relative humidity of the atmosphere and the depth of the evaporation front. The evaporation trend lines for the soil waters at the three sites, shown in Figure 3.10, are based on data from the upper 40-50 cm only; because these data reflect isotopic compositions above the minimum bulges, they yield better constrained evaporation trend lines than does the entire data set. The point of intersection between the local meteoric water line and the evaporation trend line represents the average isotopic composition of infiltrating water.

The evaporation trend lines for all three sites have low slopes (3.6 for the erosion plot, 4.1 for the Ponderosa Pine plot, and 5.1 for the Pinyon-Juniper Woodland), indicating evaporation through a dry soil layer (Barnes and Allison, 1983, 1988). In addition, the average isotopic compositions of infiltrating water, indicated by the intersections on the

$\delta^{18}O$-δD diagrams, are light (<-21‰ $\delta^{18}O$ and <-150‰ δD) in all three cases. Light values are consistent with a snowmelt-spring rain-dominated system, but these values appear to be too light, especially for the pinyon-juniper woodland core (PJ1). All three averages are lighter than the lightest precipitation values reported in Adams et al. (1995) and Newman (1996), strongly suggesting that there is a systematic error in either the distillation or the analysis process. That the error is an analytical one is unlikely, because such errors should be random, and the δD data were corrected for hydrogen fractionation during the zinc reaction. Therefore, it is probable that the light bias was a result of the soil water distillation process. Other researchers have observed a systematic, isotopically light error when vacuum extraction was used. Walker et al. (1994) found that for dry clay soils, high-temperature vacuum distillation can produce a fractionation in which the distillate can be too light by over 19‰ in δD and over 1‰ in $\delta^{18}O$. They suggested incomplete extraction as the cause. Araguás-Araguás et al. (1995) also found a light bias in soil distillates of clay soils, but attributed the problem to isotopically light water that was weakly bound to the clay and extracted during distillation. In their study, high-temperature vacuum distillation of samples from a clay soil column resulted in values that were 10‰ too light in δD and 0.5‰ too light in $\delta^{18}O$, compared with

mobile soil water that was eluted from the column. These two studies provide good evidence that the soil distillation process produces values that are erroneously light, especially when compared with precipitation data. At the same time, even if the Los Alamos δD and $\delta^{18}O$ values had been 20‰ and 1‰ heavier, respectively, they would still indicate a light water input, consistent with a snowmelt-spring rain-dominated system.

Chloride and Bromide: Ponderosa Pine Site

There is good agreement between the calculated chloride residual fluxes for similar depth intervals of the different cores taken at the ponderosa pine site (Table 3.2), indicating that vertical movement is relatively homogeneous across the site. In addition, changes in the values of the flux estimates with depth are consistent with the soil textural properties and hydraulic conductivities of the various horizons: the residual flux estimates are typically higher in the upper sandy loam horizons than in the clay Bt horizon (Table 3.2), and the saturated hydraulic conductivity of the sandy loam is higher (7.5×10^{-5} to 5.7×10^{-7} cm/sec) than that of the Bt horizon (2.5×10^{-8} cm/sec) (Wilcox et al., 1996). These findings lead to the conclusion that the Bt horizon has a substantial effect on downward water movement at the ponderosa pine site.

The results of the bromide experiment showed peak concentrations at about the 45-cm depth after a 9-month period (Figure 3.9); during that period, bromide had traveled through the sandy-loam portion of the soil into the Bt horizon. On the basis of the depth of maximum concentration, the average linear velocity of bromide movement was 60 cm/yr. Weekly measurements of soil moisture (by neutron probe) over the 9-month period show an average moisture content of about 25% for the sandy loam soil. Multiplying that average moisture content by the bromide velocity yields a bromide flux rate of 15 cm/yr. In contrast, the chloride residual flux rate through the same soil is 0.9 cm/yr, over an order of magnitude smaller. This discrepancy is probably explained either by (1) a violation of the assumptions of the chloride method, or (2) the operation of two different flow systems.

It has been observed that lateral flow, which violates the chloride method assumptions, can result in chloride-mass-balance flux predictions that are too low. Mattick et al. (1987) found that in areas of their site where lateral flow occurred, chloride residual fluxes were lower than physically based estimates. Although their report did not discuss the precise effects of lateral flow on the chloride-based fluxes, presumably the lateral flow had brought in additional chloride from upslope areas, leading to an underestimation of flux. At our site,

however, even though strong lateral flow occurs, it does not seem to have a large impact on the flux measurements. Flux estimates based on cores taken from the same area of the site in 1994, when lateral flow was small, and again in 1995, when a period of intense lateral flow occurred, are very similar (Table 3.4). The relative insensitivity of the flux estimates to lateral flow effects is probably due to the mainly preferential (probably macropore) nature of lateral flow, which does not greatly affect the chloride distribution in the soil matrix (Newman, 1996).

A determination of the chloride budget for the hillslope tends to support the idea that lateral flow is only a minor impact on the soil chloride distribution. Based on the chloride content of the cores, there is about 61 kg of chloride in the 870 m^3 soil volume of the ponderosa pine hillslope. The cumulative loss of chloride from interflow over the sampling period was about 0.1 kg or only about 0.16% of the total chloride inventory. Interestingly, approximately 90% of the chloride loss came from one very large (>1400 L/day) interflow event in March 1994 (this event is described in Newman, 1996). It does need to be noted that the apparent loss of chloride from interflow is about 40% of the estimated chloride input over the sampling period. But, because most of the chloride was lost during one interflow event, it is difficult to determine whether this rather large loss relative to input is the long-term

norm. In addition, the loss of chloride probably represents a maximum estimate because it was assumed that interflow does not transport chloride into the hillslope. However, considering the topography and stratigraphy of the site, it is likely that some interflow does enter from outside the experimental boundaries and so the chloride loss relative to input may be less than estimated.

The discrepancy between the bromide and chloride flux estimates, then, is probably explained by differences in hydrologic conditions and processes that controlled bromide and chloride movement. There are two main factors that likely caused the difference in flux estimates. First, when the bromide was applied, the high concentration of bromide killed the grasses that covered the application area. The death of the grasses must have severely reduced transpiration in the upper part of the soil. This would almost certainly have had a large effect on the rate of water and bromide movement. Because of drastically reduced transpiration, there was little flux toward the plant roots which would normally have acted to hold water and bromide in the A horizon. In contrast, because the chloride-based flux is calculated using a chloride distribution that represents long-term conditions, it represents a system where active transpiration has occurred. In other words, the chloride-based flux would be relatively insensitive to the short term disturbance

in transpiration. Additionally, the lack of transpiration probably caused moisture contents to be locally higher in the application area than was the norm for the rest of the hillslope. Because hydraulic conductivity increases with increasing moisture content faster transport of bromide would be promoted. The wetter A horizon soils may have also resulted in a higher hydraulic gradient between the A and B horizons which would also increase the vertical flux. Ultimately, it seems likely that the difference between the bromide and chloride fluxes is related to the death of the plant roots.

There is an additional possibility that may have contributed to the difference between the chloride- and bromide-based fluxes. Because there are only ppb concentrations of bromide in the soils, the high concentrations of bromide at the soil surface would be subject not only to an advective flux, but also to a diffusive flux resulting from the high chemical gradient. This, however, is not the case for chloride. Chloride concentrations are much higher in the soil relative to the input concentrations from precipitation. This idea of advective and diffusive flux being in the same direction for bromide and in opposite directions for chloride at the soil surface may also occur near plant roots. Assuming transpiration moves water and solutes toward the deeper roots we would see both chloride and bromide being affected by this

advective flux. Because there is so little bromide in the soil, diffusion of a bromide tracer would, at least initially, be toward the plant roots. However, in the case of chloride, previous advective movement of chloride toward the roots results in higher concentrations at the root-soil interface, thus diffusion would be in the opposite direction offsetting some of the advective transport of chloride. The result of the different directions of the diffusive flux for the two tracers is that transport of bromide was potentially more rapid than chloride.

There are two main issues regarding contaminant transport that arise from the above two explanations of the bromide- and chloride-based flux rates. If plant death was the main factor that resulted in the rapid movement of bromide, then surface disturbance or contaminant toxicity that reduces transpiration can result in order of magnitude higher contaminant flux rates than those suggested by measurements under pristine conditions. If the diffusive flux direction was the main factor for the difference in the chloride and bromide results, then this implies that chloride-based flux rates may not be appropriate for estimating contaminant transport rates. This is because the input conditions of a contaminant are much more likely to be similar to that of bromide rather than chloride.

Chloride: Pinyon-Juniper Woodland and Erosion Plot Sites

The chloride profiles for the undisturbed pinyon-juniper woodland and erosion plot sites show a great deal of variability (Figure 3.7), which is consistent with the high degree of spatial variability in soil textural properties and stratigraphy described by Davenport et al. (1995). Most of the residual flux estimates for the pinyon-juniper zone (Table 3.3) are an order of magnitude larger than, and not as uniform as, those for the ponderosa pine zone (Table 3.2). These findings are consistent with those from other studies in the pinyon-juniper zone on the plateau. Breshears (1995b), using time-domain reflectrometry data, has estimated flux rates of about 0.1 cm/yr on a transect through the pinyon-juniper woodland. The absence, or poorer development, of the Bt horizon in the pinyon-juniper zone is probably the reason for the larger fluxes.

There do not appear to be any consistent differences between the fluxes calculated for the pinyon-juniper woodland site and the erosion plot site that can be attributed to the differences in plant cover. Cores EP2 and EP4 have the smallest deep fluxes estimated for the pinyon-juniper zone, but this does not seem to be a function of surface cover; the Bt horizons in these cores are the most well developed of those seen in the pinyon-juniper zone. Rather, the low flux estimates for these

cores is probably attributable to soil textural properties. Core EP3, taken from the area between EP2 and EP4 (Figure 3.1), has a weakly developed Bt horizon and a large flux estimate, consistent with the observed soil properties and flux estimates for the majority of the pinyon-juniper cores.

SUMMARY AND CONCLUSIONS

Comparison of the stable isotope results for the ponderosa and pinyon-juniper zones shows that the effect of evaporation on the soil waters is quite similar in the two zones and occurs mainly in the shallowest (upper 10 cm) soil horizon. In addition, the estimated average isotopic compositions of precipitation contributing to infiltration are quite light in both zones, suggesting that the major sources of infiltrating water are cool-weather snowmelt and spring rains.

The chloride results show that deep fluxes are typically more uniform in the ponderosa pine zone than in the pinyon-juniper zone, and are about an order of magnitude lower. These differences are probably the result of the more homogeneous soils and the more well-developed Bt horizons in the ponderosa pine zone. The pinyon-juniper zone has spatially heterogeneous soils that typically lack well-developed Bt horizons. Because such differences affect the vertical movement of water

through the soil matrix, contaminants may move quite differently in the two zones. It is interesting that no significant plant-cover effects were observed, either on the flux estimates or on the stable isotope profiles.

The discrepancy between the flux estimates based on bromide transport and those based on chloride mass balance at the ponderosa pine site were apparently the result of an artificial perturbation of the hydrologic system caused by the death of the grass cover during bromide application, and/or differences between the net advective and diffusive fluxes that controlled the distributions of the two tracers. Both of these explanations have implications for estimating potential contaminant mobility from chloride-based fluxes.

REFERENCES

Adams, A. I., F. Goff, and D. Counce. 1995. Chemical and Isotopic Variations of Precipitation in the Los Alamos Region, New Mexico. Los Alamos National Laboratory Report LA-12985-MS. Los Alamos, NM. 35 pp.

Allen, C. D., 1989. Changes in the Landscape of the Jemez Mountains, New Mexico. Ph.D. Dissertation, University of California, Berkeley. 346 pp.

Allison, G. B., and C. J. Barnes. 1983. Estimation of Evapotranspiration from Non-Vegetated Surfaces Using Natural Deuterium. Nature, 301: 143-145.

Allison, G. B., C. J. Barnes, and M. W. Hughes. 1983. The Distribution of Deuterium and ^{18}O in Dry Soils 2: Experimental. J. Hydrol., 64: 377-397.

Allison, G. B., G. W. Gee, and S. W. Tyler. 1994. Vadose-Zone Techniques for Estimating Groundwater Recharge in Arid and Semiarid Regions. Soil Sci. Soc. Am. J., 58: 6-14.

Araguás-Araguás, L., K. Rozanski, R. Gonfiantini, and D. Louvat. 1995. Isotope Effects Accompanying Vacuum Extraction of Soil Water for Stable Isotope Analyses. J. Hydrol., 168: 159-171.

Barnes, C. J., and G. B. Allison. 1983. The Distribution of Deuterium and ^{18}O in Dry Soils. 1: Theory. J. Hydrol., 60: 141-156.

Barnes, C. J., and G. B. Allison. 1988. Tracing of Water Movement in the Unsaturated Zone Using Stable Isotopes of Hydrogen and Oxygen. J. Hydrol., 100: 143-176.

Bowen, B. M. 1990. Los Alamos Climatology. Los Alamos National Laboratory Report LA-11735-MS. 254 pp.

Bowman, R. S. 1984. Evaluation of Some New Tracers for Soil Water Studies. Soil Sci. Soc. Am. J., 48: 987-993.

Bowman, R. S., and R. C. Rice. 1986. Transport of Conservative Tracers in the Field Under Intermittent Flood Irrigation. Water Resour. Res., 22(11): 1531-1536.

Breshears, D. D., P. M. Rich, and F. J. Barnes. 1996. Heterogeneity in Solar Radiation and Soil Moisture Imposed by Overstory with Intermediate Closure. Submitted to Ecological Applications.

Breshears, D. D. 1995. Unpublished Results. Los Alamos National Laboratory, Los Alamos, NM.

Bronswijk, J. J. B., W. Hamminga, and K. Oostindie. 1995. Field-Scale Solute Transport in a Heavy Clay Soil. Water Resour. Res., 31(3): 517-526.

Davenport, D. W. 1994. Unpublished Data. Los Alamos National Laboratory, Los Alamos, NM.

Davenport, D. W., B. P. Wilcox, and D. D. Breshears. 1995. Soil Morphology as Influenced by a Piñon-Juniper Woodland. Soil Sci. Soc. Am. J., in press.

Dawson, T. E., and J. R. Ehleringer. 1991. Streamside Trees That Do Not Use Stream Water. Nature, 350: 335-337.

Gallaher, B. M. 1995. Personal Communication. Los Alamos National Laboratory, Los Alamos, NM.

Jardine, P. M., G. V. Wilson, and R. J. Luxmoore. 1990. Unsaturated Solute Transport Through a Forest Soil During Rain Storm Events. Geoderma, 46: 103-118.

Kendall, C., and T. B. Coplen. 1985. Multisample Conversion of Water to Hydrogen by Zinc for Stable Isotope Determination. Analytical Chemistry, 57: 1437-1446.

Liu, B., F. Phillips, S. Hoines, A. R. Campbell, and P. Sharma. 1995. Water Movement in Desert Soil Traced by Hydrogen and Oxygen Isotopes, Chloride, and Chlorine-36, Southern Arizona. J. Hydrol. 168: 91-110.

Los Alamos Environmental Research Park. 1976. The Los Alamos National Environmental Research Park. Los Alamos National Laboratory Report, Los Alamos, NM. 37 pp.

Mattick, J. L., T. A. Duval, and F. M. Phillips. 1987. Quantification of Groundwater Recharge Rates in New Mexico using Bomb ^{36}Cl, Bomb-^{3}H, and Chloride as Soil-Water Tracers. New Mexico Water Resour. Res. Inst. Rpt. No. 220. 184 pp.

Newman, B. D., 1996. Interflow Pathways in a Subhumid Ponderosa Pine Hillslope. Chapter 2, this dissertation.

Nyhan, J. W. 1995. Unpublished Data. Los Alamos National Laboratory, Los Alamos, NM.

Phillips, F. M. 1994. Environmental Tracers for Water Movement in Desert Soils of the American Southwest. Soil Sci. Soc. Am. J., 58: 15-24.

Reith, C. C. 1992. Waste Management and the Arid-Land Disposal Concept. In: C. C. Reith and B. M. Thomson (eds), Deserts as Dumps? The Disposal of Hazardous Materials in Arid Ecosystems. University of New Mexico Press, Albuquerque. pp. 3-19.

Scanlon, B. R. 1991. Evaluation of Moisture Flux from Chloride Data in Desert Soils. J. Hydrol., 128: 137-156.

Shurbaji, A.-R.M., and A. R. Campbell. 1996. A Study of Evaporation and Recharge in Desert Soil using Environmental Tracers, New Mexico. Environ. Geol., in press.

Shurbaji, A.-R.M., F. M. Phillips, A. R. Campbell, and R. G. Knowlton. 1995. Application of a Numerical Model for Simulating Water Flow,

Isotope Transport, and Heat Transfer in the Unsaturated Zone. J. Hydrol., 171: 143-163.

Socki, R. A., H. R. Karlsson, and E. K. Gibson. 1992. Extraction Technique for the Determination of Oxygen-18 in Water Using Preevacuated Glass Vials. Anal. Chem., 64: 829-831.

Stephens, D. B. 1993. Laboratory Analysis of Hydraulic Properties of Soil Samples, Report No. 2-LN3-6860J-1. Daniel B. Stephens and Assoc. Inc., Albuquerque.

Stone, W. J. 1984. Recharge in the Salt Lake Coal Field Based on Chloride in the Unsaturated Zone. New Mexico Bureau of Mines and Mineral Resources, Open-File Report 214. 64 pp.

van Genuchten, M. Th., F. J. Leij, and S. R. Yates. 1991. The RETC code for Quantifying the Hydraulic Functions of Unsaturated Soils. U.S. Environmental Protection Agency Report No. EPA/600.2-91/065.

Vuataz, F.-D., and F. Goff. 1986. Isotope Geochemistry of Thermal and Nonthermal Waters in the Valles Caldera, Jemez Mountains, Northern New Mexico. J. Geophys. Res., 91(B2): 1835-1853.

Walker, G. R., P. H. Woods, and G. B. Allison. 1994. Interlaboratory Comparison of Methods to Determine the Stable Isotope Composition of Soil Water. Chem. Geol., 111: 297-306.

Wilcox, B. P., 1994. Runoff and Erosion in Intercanopy Zones of Pinyon-Juniper Woodlands. J. Range. Manage., 47: 285-295.

Wilcox, B. P., D. Brandes, and D. W. Davenport. 1996. Runoff generation from a Subhumid Ponderosa Pine Hillslope in New Mexico. Water Resour. Res. Submitted.

Table 3.1. Core sampling and analysis information

Ponderosa Pine Site

Core	Date Sampled	Isotope Analysis	Chloride Analysis	Bromide Analysis
LJ	1993	Yes	Yes	No
BR1	1994	No	Yes	Yes
BR2	1994	No	Yes	Yes
BR3	1994	No	Yes	Yes
BR4	1994	No	Yes	Yes
BR5	1995	No	Yes	Yes
PO2	1994	No	Yes	No
PO3	1994	No	Yes	No
PO4	1994	No	Yes	No
PO5	1994	No	Yes	No
PO7	1994	No	Yes	No
PO8	1994	No	Yes	No
PO8.5	1995	No	Yes	No
PO9	1994	No	Yes	No
PO10	1994	No	Yes	No
PO12	1994	No	Yes	No
PO13	1994	No	Yes	No
PO14	1994	No	Yes	No
PO15	1994	No	Yes	No
PO16	1994	No	Yes	No
PO18	1994	No	Yes	No
PO19	1994	No	Yes	No

Pinyon-Juniper Woodland Site

Core	Date Sampled	Isotope Analysis	Chloride Analysis	Bromide Analysis
PJ1	1993	Yes	Yes	No
PJ2	1995	No	Yes	No
PJ160	1995	No	Yes	No
PJ182	1995	No	Yes	No
PJ704	1995	No	Yes	No
PJ1216	1995	No	Yes	No

Erosion Plot Site

Core	Date Sampled	Isotope Analysis	Chloride Analysis	Bromide Analysis
EP2	1993	No	Yes	No
EP3	1993	No	Yes	No
EP4	1993	Yes	Yes	No

Table 3.2. Ponderosa pine zone: residual flux estimates and soil water ages

Core	Date Collected	Depth interval (cm)	Residual flux (cm/yr)	Age at bottom of segment (yr)	Depth interval (cm)	Residual flux (cm/yr)	Age at bottom of segment (yr)	Depth interval (cm)	Residual flux (cm/yr)	Age at bottom of segment (yr)
LJ	1993	0-40	0.15	27	85-255	0.01	2147			
BR1	1994	0-40	0.9	9	40-110	0.03	796			
BR2	1994	0-30	0.9	11	50-90	0.04	329			
BR3	1994	0-30	1.4	8	30-85	0.06	247			
BR4	1994	0-30	1.4	11	30-110	0.05	518			
BR5	1995	0-40	0.7	8	40-110	0.03	807			
PO2	1994	0-40	0.7	16	40-75	0.09	126	75-123	0.02	550
PO3	1994	0-47	0.6	21	47-110	0.03	596			
PO4	1994	0-50	0.5	29	60-130	0.04	491			
PO5	1994	0-40	0.7	14	80-130	0.05	334			
PO7	1994	0-30	0.6	13	30-70	0.1	116			
PO8	1994	0-50	0.8	19	50-90	0.03	458			
PO8.5	1995	0-30	0.9	6	30-50	0.2	36	50-80	0.06	204
PO9	1994	0-30	0.7	9	30-90	0.08	237			
PO10	1994	0-40	0.8	10	40-70	0.1	84	70-100	0.03	390
PO12	1994	0-30	1.5	6	30-60	0.2	68			
PO13	1994	0-30	1.1	7	30-130	0.02	1076			
PO14	1994	0-30	0.7	7	30-60	0.07	163	60-100	0.02	910
PO15	1994	0-40	0.3	19	40-70	0.06	174	70-100	0.02	635
PO16	1994	0-40	0.4	15	40-90	0.02	541			
PO18	1994	0-50	0.5	20	50-100	0.05	393	100-125	0.01	961
PO19	1994	0-30	1.6	4	30-60	0.3	56	60-110	0.04	586

Table 3.3. Pinyon juniper zone: residual flux estimates and soil water ages

Pinyon-Juniper Woodland Site

Core	Date Sampled	Depth interval (cm)	Residual flux (cm/yr)	Age at bottom of segment (yr)	Depth interval (cm)	Residual flux (cm/yr)	Age at bottom of segment (yr)	Depth interval (cm)	Residual flux (cm/yr)	Age at bottom of segment (yr)
PJ1	1993	0-60	0.6	13	60-90	0.2	37	100-130	0.05	92
PJ2	1995	0-100	1.1	12						
PJ160	1995	0-30	0.65	5.8						
PJ182	1995	0-30	0.18	21	30-60	0.8	18			
PJ704	1995	0-20	0.08	17	20-80	0.68	32	80-110	0.11	49
PJ1216	1995	0-40	0.15	36	40-70	0.34	44			

Erosion Plot Site

Core	Date Sampled	Depth interval (cm)	Residual flux (cm/yr)	Age at bottom of segment (yr)	Depth interval (cm)	Residual flux (cm/yr)	Age at bottom of segment (yr)	Depth interval (cm)	Residual flux (cm/yr)	Age at bottom of segment (yr)
EP2	1993	0-40	0.4	17	40-140	0.02	318			
EP3	1993	0-20	0.2	12	20-130	0.7	30			
EP4	1993	0-40	0.5	10	40-100	0.03	258	100-130	0.1	271

Table 3.4. Ponderosa pine site: comparison of residual flux estimates for adjacent cores taken in 1994 and 1995.

Core	Date Sampled	Depth interval (cm)	Residual flux (cm/yr)
BR1	1994	0-40	0.9
		40-110	0.03
BR5	1995	0-40	0.7
		40-110	0.03
BR2	1994	0-30	0.9
		50-90	0.04
PO8	1994	0-50	0.8
		50-90	0.03
PO8.5	1995	0-30	0.9
		50-80	0.06
PO9	1994	0-30	0.7
		30-90	0.08

Estimates for 1995 cores are shown between those for the two spatially closest 1994 cores.

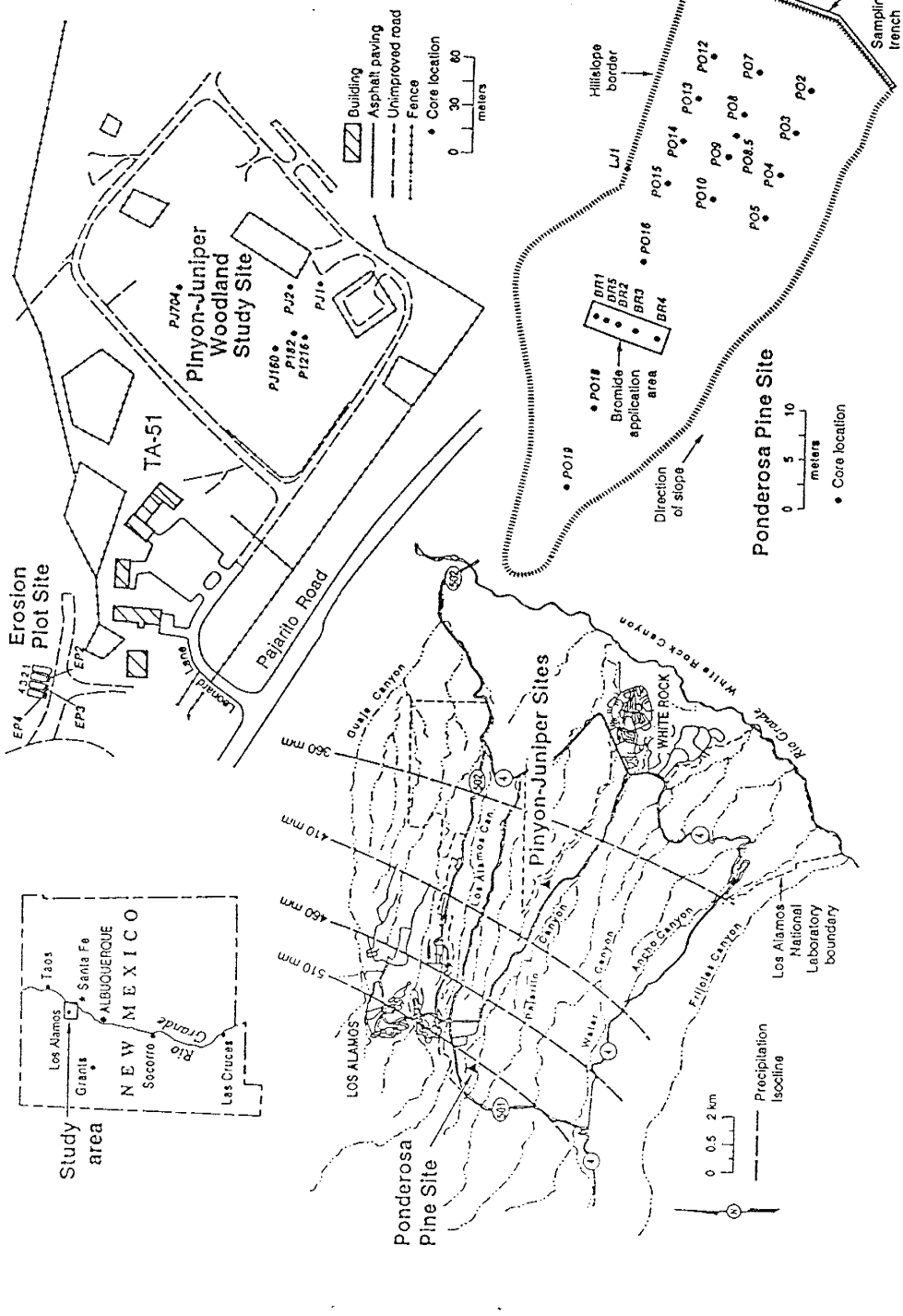

Figure 3.1. Location map of the ponderosa pine, pinyon-juniper woodland, and erosion plot study areas, showing core sampling locations and annual precipitation isoclines, the latter from Bowen, (1990).

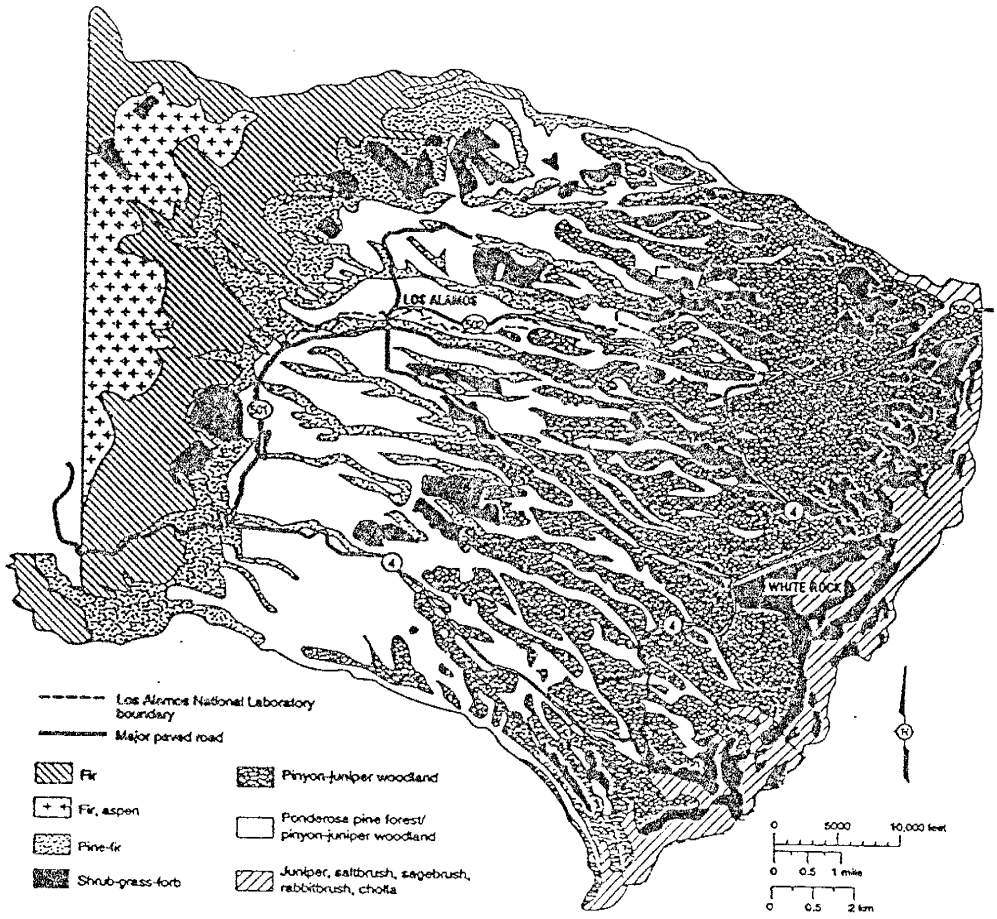

Figure 3.2. Major vegetation types on the Pajarito Plateau (from Los Alamos Environmental Research Park documentation, 1976).

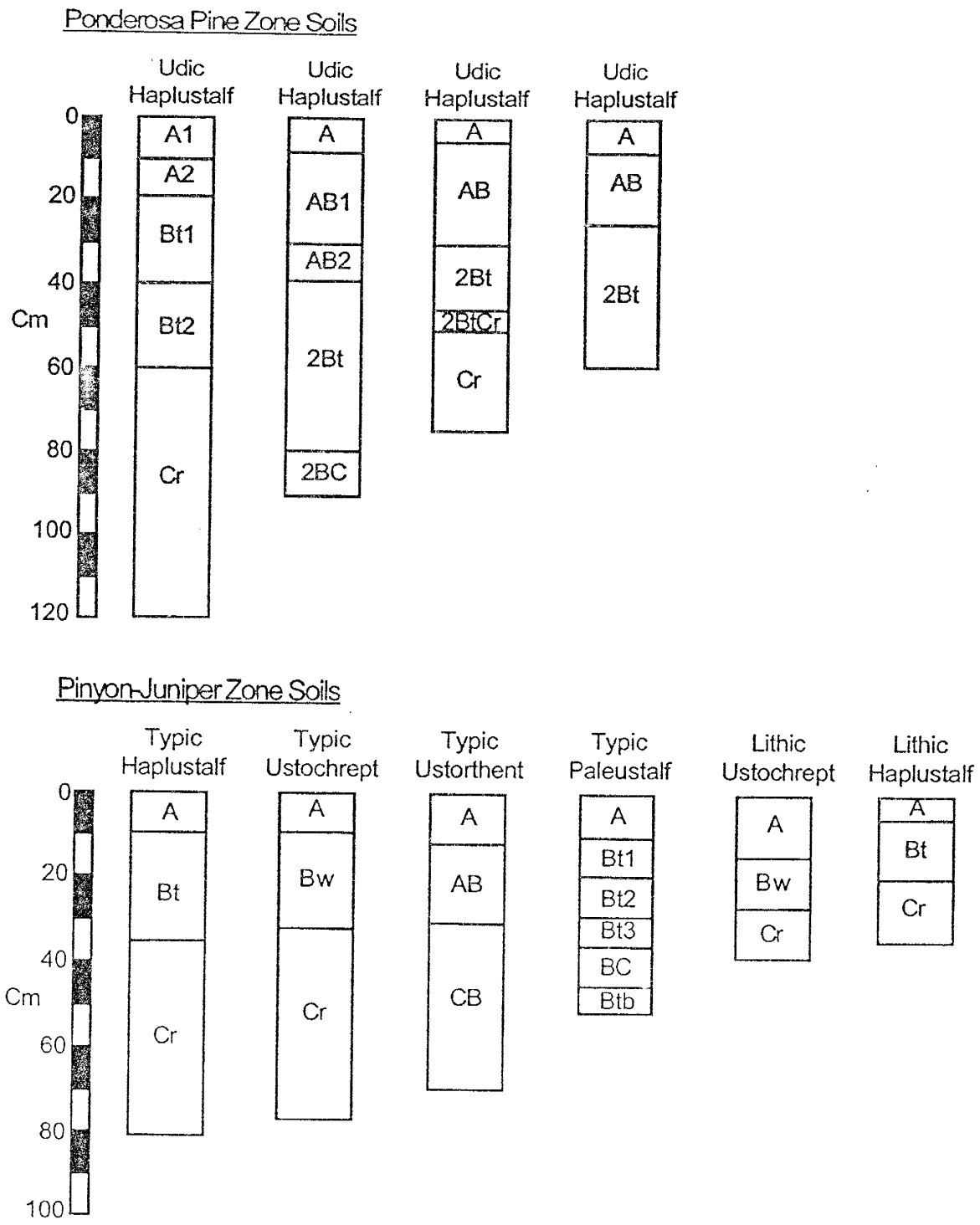

Figure 3.3. Examples of soil profiles for the ponderosa pine and pinyon-juniper zones (Davenport, 1994, 1995).

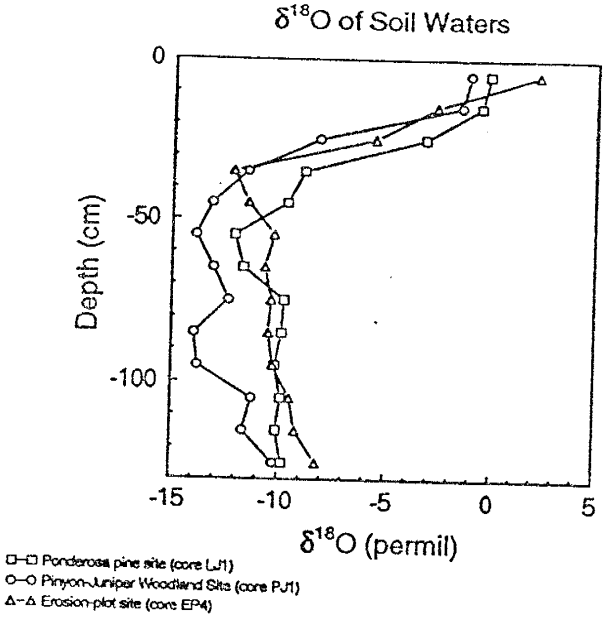

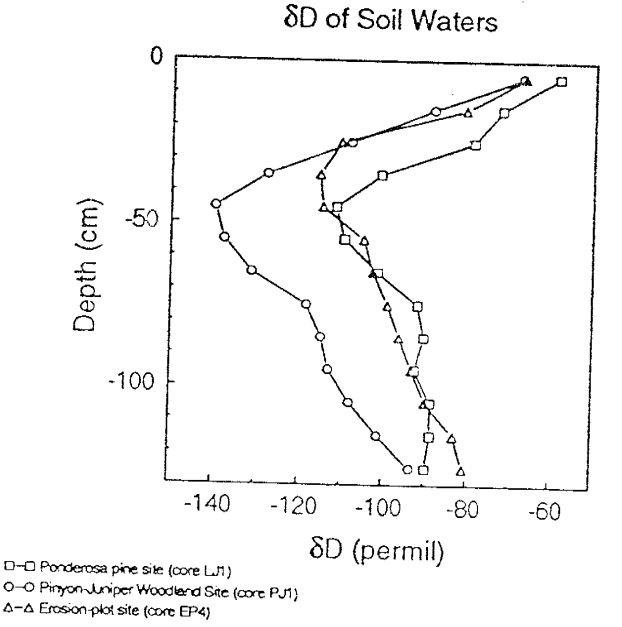

Figure 3.4. (A) Vertical $\delta^{18}O$ profiles for cores from the ponderosa pine, pinyon-juniper woodland, and erosion plot sites. (B) Vertical δD profiles for cores from the ponderosa pine, pinyon-juniper woodland, and erosion plot sites.

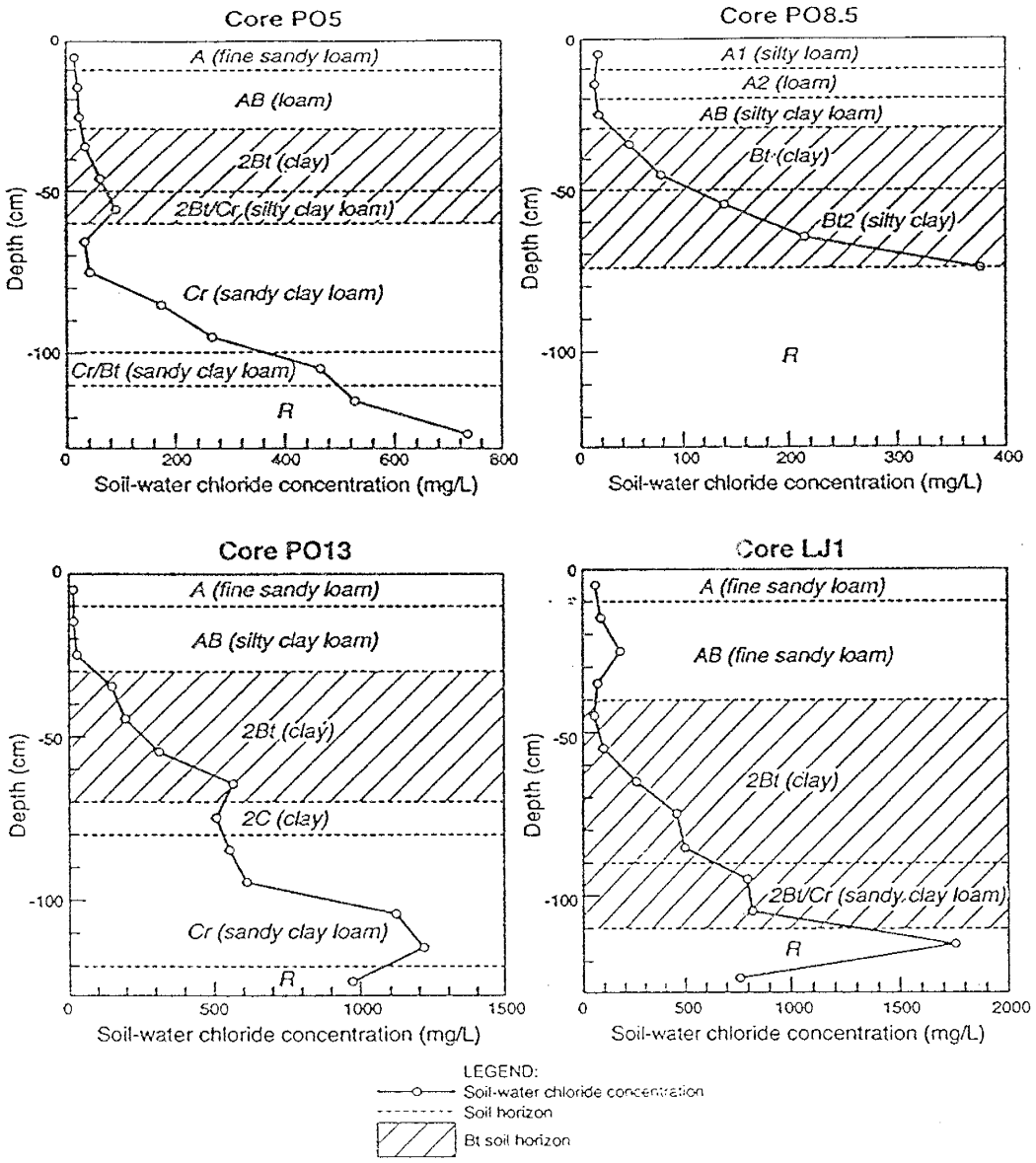

Figure 3.5. Ponderosa pine site: examples of vertical chloride profiles.

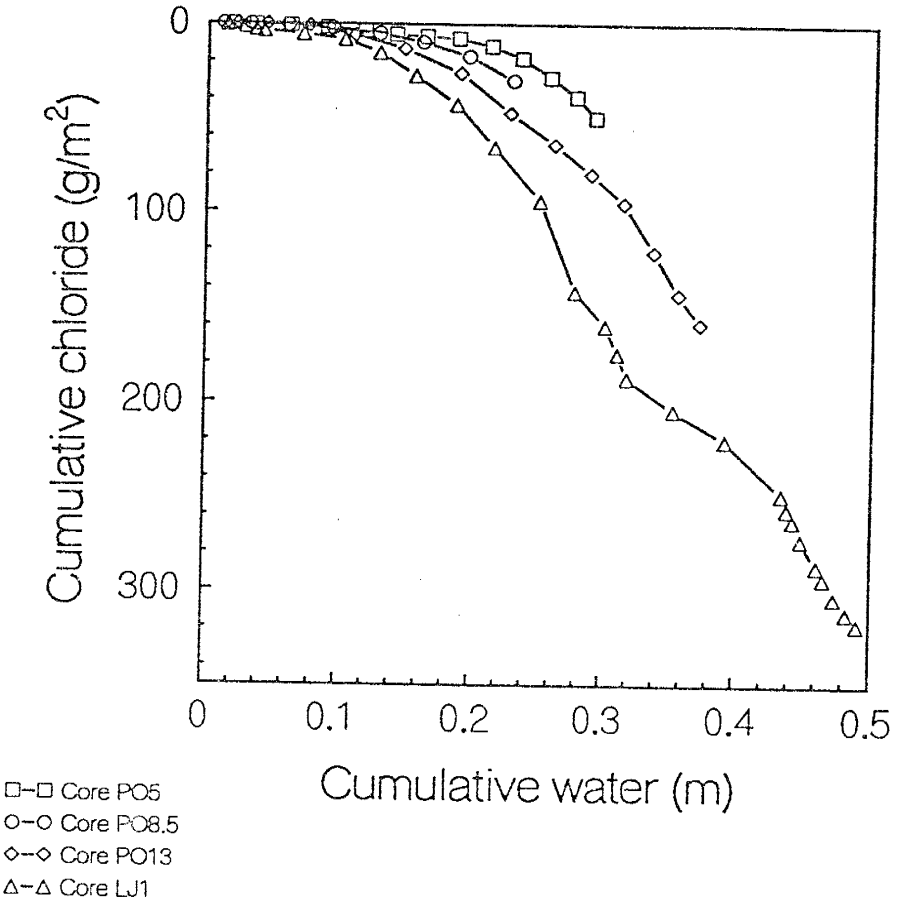

Figure 3.6. Ponderosa pine site: examples of cumulative chloride-cumulative water plots.

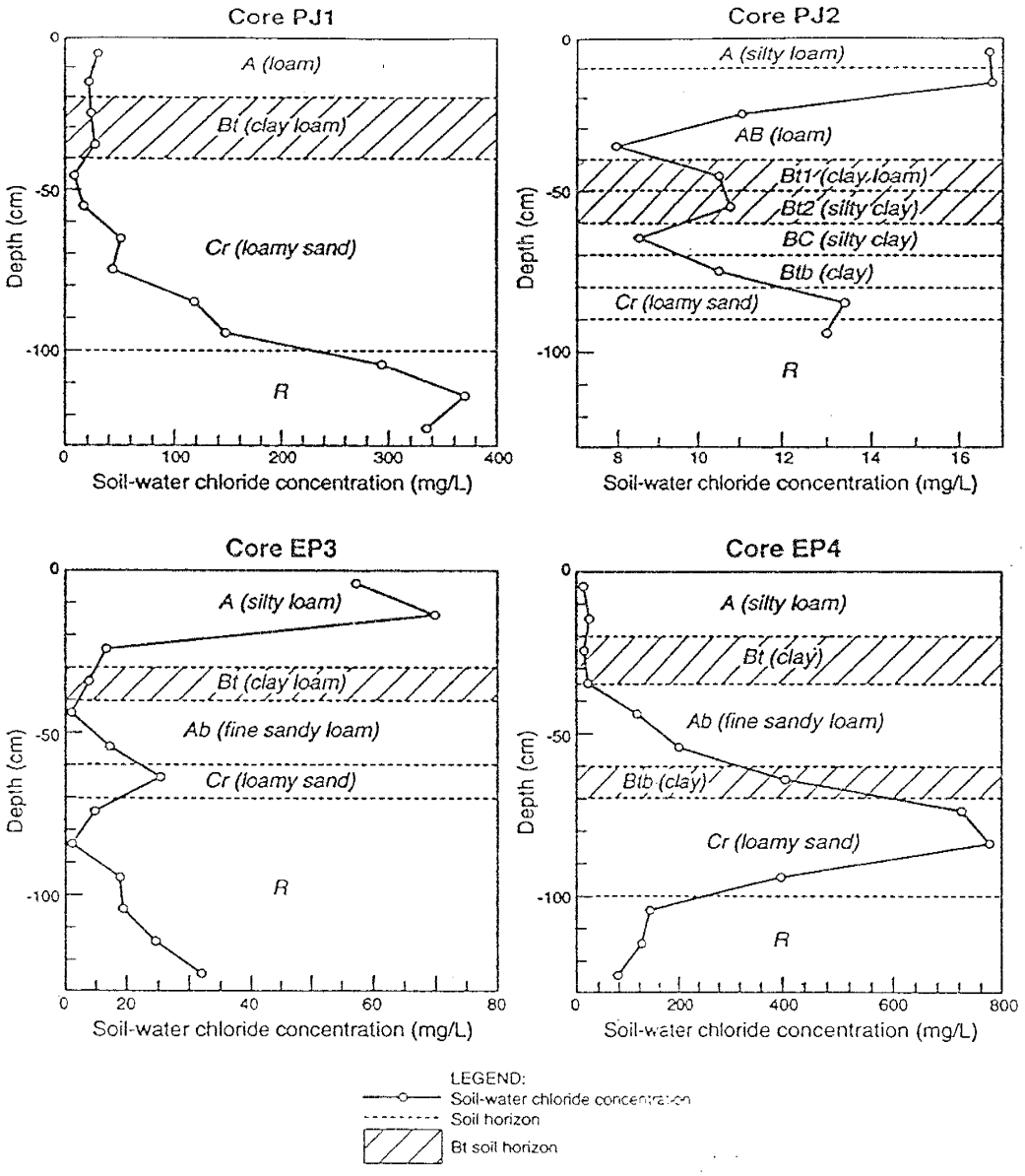

Figure 3.7. Pinyon-juniper woodland and erosion plot sites: examples of vertical chloride profiles.

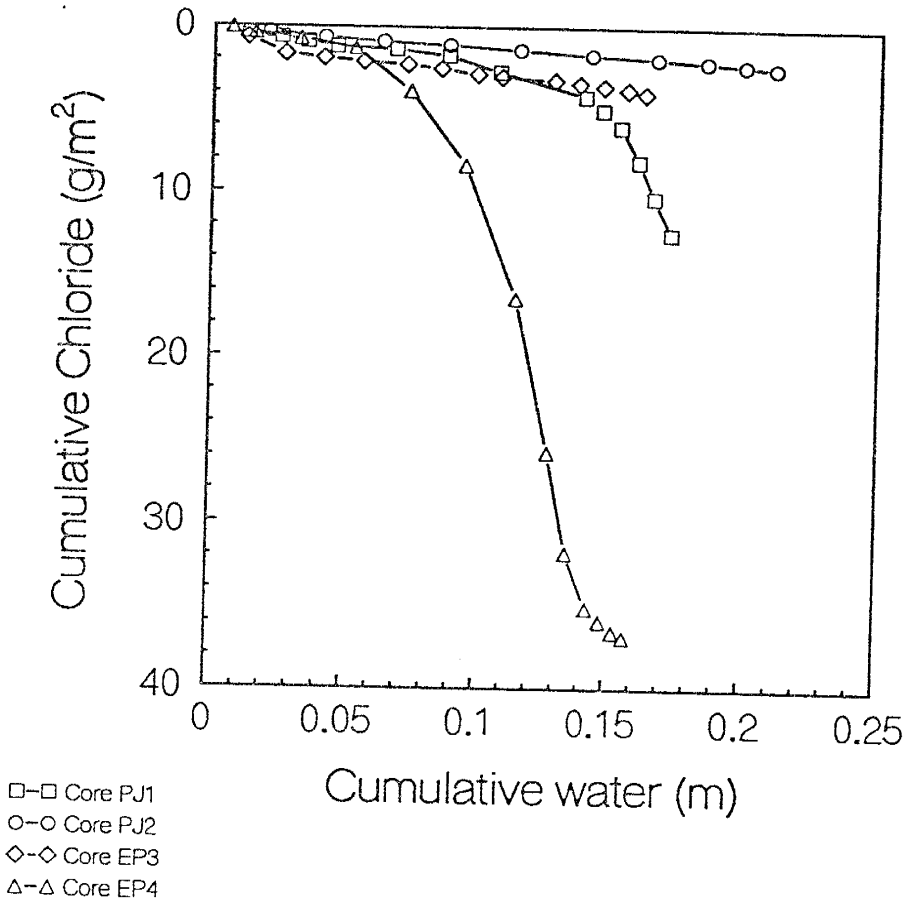

Figure 3.8. Pinyon-juniper woodland and erosion plot sites: examples of cumulative chloride-cumulative water plots.

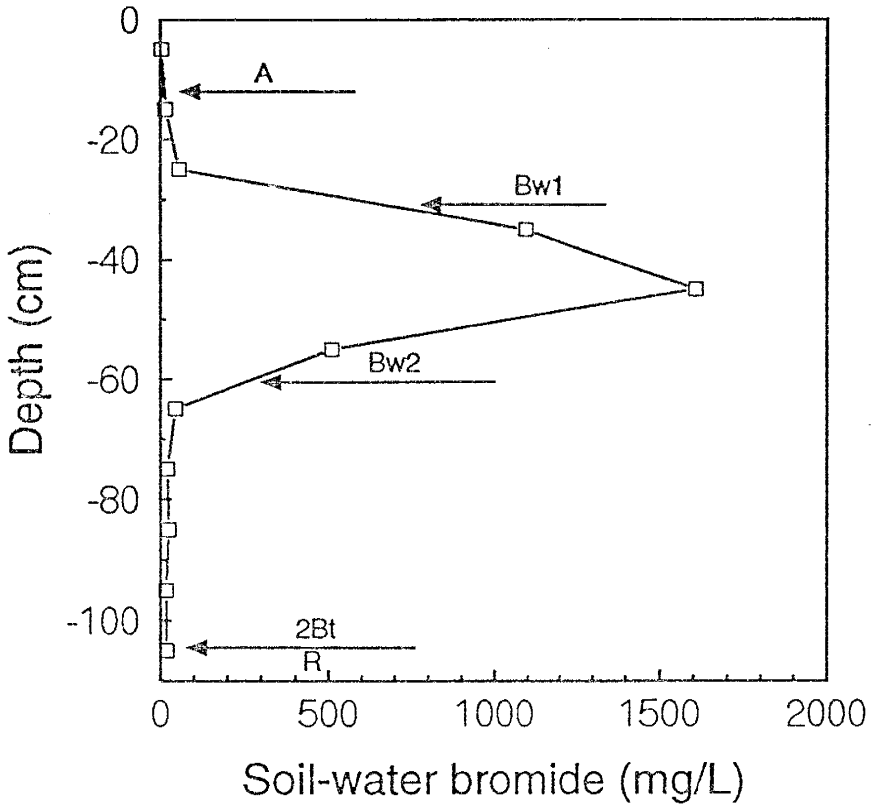

Figure 3.9. Ponderosa pine site: vertical bromide profile for core BR1.

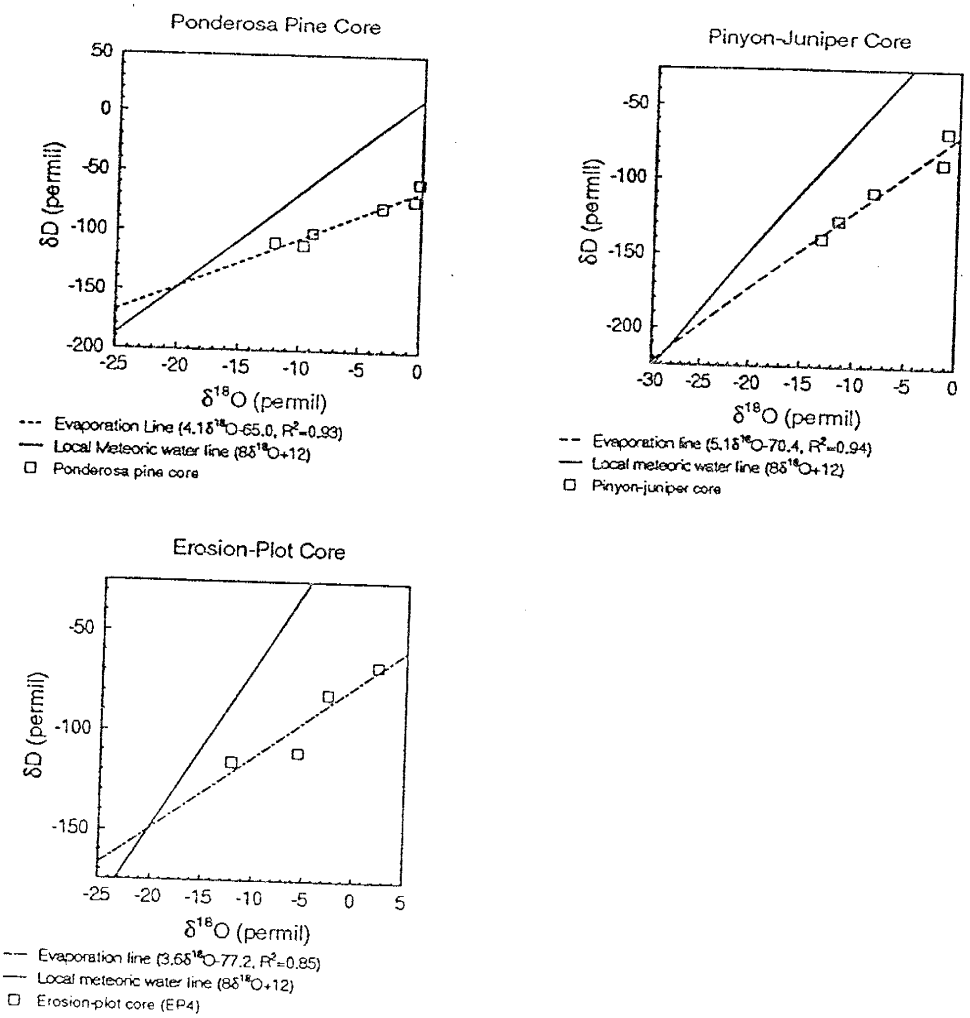

Figure 3.10. $\delta^{18}O$-δD plots of the soil water distillates in relation to the Los Alamos local meteoric water line of Vuataz and Goff (1986).

CHAPTER 4: THE IMPORTANCE OF MESA TOP AND FRACTURE HYDROGEOLOGIC PROCESSES ON THE PAJARITO PLATEAU

ABSTRACT

The development of a detailed understanding of the hydrogeology of the Pajarito Plateau in north-central New Mexico is a priority at Los Alamos National Laboratory because of the need to protect the groundwater system from potential contamination resulting from past and present research activities. This is a difficult task because of the complexity of the hydrogeologic system and a previous lack of focused study. Currently, there is no model of the plateau hydrologic system that is fully supportable by the existing data. Specifically, five different recharge pathways to the main aquifer have been proposed by various investigators, but, the evidence supporting each pathway is either speculative, equivocal, or incomplete. This study reexamines the plateau hydrogeologic system based on research conducted in the last few years and describes new insights on the plateau system, especially the importance of mesa top processes and fracture flow. Field-based and modeled flux rates suggest that matrix flow in the mesas is probably not an important recharge pathway. However, it has been demonstrated that the mesa tops host a very active hydrogeologic system and that

lateral and vertical flow in the mesa top soils may be very important in some contaminant clean up scenarios. The role of fracture flow as a recharge mechanism is still an open question. The presence of fracture fills and roots clearly indicates that near-surface fracture flow does occur. There is some evidence that deep fracture flow may occur in canyon bottoms, but there is a lack of field evidence on whether deep fracture flow occurs through the mesas. Modeling studies suggest that deep fracture flow in the mesas does not occur. It has also been found that fracture chemistry can be very complex and is controlled by unique biological and geochemical processes which would almost certainly affect contaminant mobility. Lastly, the presence of anomalously light stable isotope values from waters from the confined aquifer on the eastern edge of plateau has lead previous researchers to suggest that recharge may be from the high elevation Sangre de Cristo Mountains to the east, rather than from the west by which of most of the plateau groundwater is apparently recharged. However, an alternative hypothesis based on paleoclimate considerations is proposed. Because the confined aquifer water is Pleistocene in age it probably was recharged under cooler climatic conditions than the present which would result in isotopically light water. Thus, the confined aquifer could have been recharged via

the westward pathways, but under cooler Pleistocene climatic conditions.

INTRODUCTION

The hydrogeologic processes that control recharge and contaminant transport on the Pajarito Plateau in north central New Mexico are poorly understood, but are important because they influence the distribution and chemical state of contaminants produced from research activities at Los Alamos National Laboratory (Figure 4.1). The Laboratory is currently heavily involved with assessing the fate of contaminants on the plateau and in determining appropriate remediation strategies at contaminated sites. Unfortunately, because of the complex nature of the plateau hydrogeology and insufficient study of the hydrogeologic system, there are conflicting models that describe how the plateau hydrogeologic system works, and this makes it difficult to determine the potential for contaminant transport. Models have been described by Spiegel and Baldwin (1964), Griggs, (1964), Cushman (1965), Abelee (1981), and Purtymun, (1984). The models, which are discussed later, differ mainly in how they describe recharge to the main aquifer. In their hydrogeologic review of the Los Alamos Environmental Restoration Program, Stephens et al. (1993) concluded that there is

insufficient information to determine which, if any, of the hydrologic models for the plateau are correct and that more research is needed to understand the hydrogeologic system and evaluate the potential for contaminant migration. In part one of this paper, a summary of the current understanding of the plateau hydrogeologic system is presented. In addition, some of the more important unknown factors that may influence the plateau system are described. Stephens et al. (1993) have identified that a lack of knowledge of mesa top hydrogeologic processes is one of the main unknowns, and recent research relating to the mesas will be discussed in part two of this paper. In part three, the potential for and importance of fracture flow, another significant unknown, is discussed. Finally, in part four, interpretations of the plateau paleohydrology and paleoclimate are discussed.

I. DESCRIPTION OF THE PAJARITO PLATEAU HYDROGEOLOGIC SYSTEM

The Pajarito Plateau is composed of volcanic ash flow and ash fall deposits and gently dips from the Jemez mountains on the west to the Rio Grande on the east (Figure 4.1). The plateau is semiarid to subhumid and precipitation and plant cover varies with elevation.

Erosion has caused the development of deep, east-southeast trending canyons separated by long, narrow mesas.

A generalized cross section of the Pajarito Plateau is shown in Figure 4.2. The stratigraphic units of importance in terms of the plateau hydrologic system include the Tschicoma Formation, Sante Fe Group, Totavi Formation, Puye Formation, Cerros del Rio Basalts, Bandelier Tuff, and the soils and alluvium in canyon bottoms and on mesa tops. Starting from the bottom of the profile, the Sante Fe Group (18-4.5 Ma, Los Alamos National Laboratory, 1993a) is composed of a thick series of clastic sedimentary rocks derived from Jemez Mountain volcanics with minor amounts of limestones, evaporites, tuffs, and intercalated basalts. The Totavi Formation, also known as the Totavi Lentil, contains gravels and lacustrine deposits. The Puye Formation (4-1.7 Ma, Waresback and Turbeville, 1990), is a fanglomerate which is interstratified with the Cerros del Rio basalts. The Bandelier Tuff is composed of the 1.5 Ma Otowi Member and the 1.13 Ma Tshirege Member (Spell et al., 1990). The Otowi Member includes the Guaje pumice bed, thin surge beds, and massive nonwelded pyroclastic flow units. The Otowi and Tshirege Members are separated by the 1.5-1.2 Ma Cerro Toledo rhyolite which has also been called the Tsankawi Member. The Tshirege Member has a basal pumice fall deposit which is overlain by thin surge beds and

variably welded pyroclastic flow units. The Tschicoma Formation (7-3 Ma, Gardner et al., 1986) is a sequence of dacitic domes and lavas and occurs along the western edge of the plateau at the Pajarito fault (Figure 4.2). A thin veneer of soils is usually present on the mesa tops and in parts of the canyon bottoms. Beneath the soils, the canyon bottoms are mainly filled with alluvium. The complexity of the geology translates to a complex hydrologic system because hydrologic properties vary between stratigraphic units, and even within units. Additional information about the plateau geology can be found in Bailey et al. (1969), Bailey and Smith (1978), Burton (1982), and Broxton and Reneau (1995).

The main aquifer is located in the Sante Fe Group and part of the Puye Formation (in the western part of the plateau) (Figure 4.2). The general groundwater flow direction is from the Jemez Mountains to the Rio Grande, and the main discharge area is along the eastern edge of the plateau at the Rio Grande. Perched aquifers occur in the Puye Formation and alluvial aquifers occur in the canyon bottoms. Studies by Purtymun (1973, 1975) indicate that the alluvial aquifers can recharge the deeper perched aquifers. The main aquifer is suggested to be isolated from the perched aquifers by thick sequences of unsaturated tuff and sediment (Environmental Surveillance Group, 1991), however, there has been only limited study of recharge from the perched aquifers

(Stephens et al, 1993). The Bandelier Tuff and upper Puye Formation form a thick vadose zone up to 335 m thick under the mesa tops (Stephens et al, 1993). Surface water occurs primarily as ephemeral streams in the canyons (Purtymun, 1975). Springs on the flanks of the Jemez Mountains supply perennial flow to the upper reaches of the major canyons, but the perennial flow is not maintained across the plateau. Overland flow and lateral subsurface flow (interflow) can occur on the mesa tops (Wilcox et al., 1996).

What Needs to be Determined?

There are still many questions about how the Pajarito Plateau hydrogeologic system works that need to be answered, both in terms of the plateau hydrogeologic processes and in how contaminants might migrate through the system. Some of the more important questions are addressed below.

One of the major problems in understanding the hydrology of the plateau is that the sources of recharge to the main aquifer are not known. Cushman (1965) suggested that recharge could occur via infiltration of runoff in canyon bottoms, underflow from the Valles caldera through the Tschichoma Formation, and by infiltration on the

mesas. Others have suggested that the Pajarito fault zone and possibly other faults may be important recharge pathways (Stephens et al., 1993).

Evidence which supports caldera recharge is the westward-rising water table in the main aquifer, ^{14}C and ^{3}H dating that shows the groundwaters become progressively older to the east (Environmental Surveillance Group, 1995), and the large groundwater storage capacity of the caldera. However, no subsurface data between the caldera and the Pajarito fault zone exists, and the westward steepening gradient could also be explained by recharge at the Pajarito fault zone or along perennial streams in the canyon heads. Studies by Conover et al. (1963) and Griggs (1964) do not support the caldera recharge model because groundwater from the caldera is known to discharge to the southwest, not the east, and the Tschicoma Formation, in which groundwater would need to pass through to reach the plateau, is of low permeability.

Alternatively, downward percolation at the Pajarito fault zone has been suggested as a possible recharge pathway (Figure 4.2) (Stephens et al. 1993). Evidence for fault zone recharge is, as in the caldera model, that the water table rises toward the fault zone and groundwater ages become older away from the fault. Otherwise, there is little information on Pajarito fault zone recharge and how it might occur. In addition,

other fault zones such as the Guaje and Rendija Canyon faults, could possibly contribute recharge (Stephens et al., 1993), although again, there is a lack of data to support or reject this pathway.

Griggs (1964), Spiegel and Baldwin (1964), and Cushman (1965) proposed that canyon bottom infiltration may be an important recharge mechanism on the plateau. It has been established that the canyons recharge the alluvial and perched aquifers, but a pump test by Stoker et al. (1991) shows that the perched aquifer at Mortandad Canyon does not recharge the main aquifer. However, the possibility that other perched aquifers may be recharging the main aquifer has not been investigated.

Another possible recharge pathway is infiltration through the mesa tops. Although Cushman (1965) considered mesa top infiltration as a possible source of recharge, Abrahams et al. (1961), Purtymun and Kennedy (1971), and Purtymun (1984) suggest that mesa top recharge is insignificant. Evidence against mesa recharge is that the mesas constitute a thick vadose zone (up to 335 m) which typically has very low volumetric moisture contents, on the order of 2-4%, and that annual evapotranspiration potential is greater than annual precipitation (Stephens et al., 1993). However, until recently, there have been no definitive field tests that attempted to quantify mesa top recharge or downward flux rates.

Finally, Goff and Sayer (1980) and Blake et al. (1995) have suggested that some recharge may occur from the Sangre de Cristo mountains to the east (Figure 4.3), based on chemical and stable isotope analyses. This has been suggested as a possible reason for artesian conditions near the Rio Grande (Stephens et al., 1993).

After review of the existing models, it is clear that at present, there is no consensus as to which are the important recharge mechanisms on the plateau. There is also a severe lack of data by which an assessment of the important recharge mechanisms can be made.

Understanding whether fracture flow occurs is very important in determining how the plateau aquifers are recharged and in evaluating the mobility of contaminants. However, the importance of fracture flow is difficult to ascertain because there is no widely accepted methodology for determining fracture hydrogeologic properties in the field (Stephens et al., 1993). In their review of the plateau hydrogeologic system, the authors of Stephens et al. (1993) were somewhat divided on the importance of fracture flow. Fractures in the Bandelier tuff lack connectivity over great depths (fracture density is very low in the nonwelded Otowi Member that lies beneath the more fractured Tshirege Member, Figure 4.2) and may act as capillary barriers to unsaturated flow. However, the presence of roots, and mineral fillings indicate that at

a minimum, shallow fracture flow occurs. Roots have been observed at depths of 12 m (Abeele et al., 1981) which indicates flow can occur at least to that depth. Davenport et al. (1995) and Newman (1996a) have examined clay and calcite fracture fills respectively, that show near-surface fracture flow has occurred in the past. A field study described by Rogers (1977) also showed that fracture flow occurs in the near surface after some rainfall events.

In apparent contradiction to the field evidence, Birdsell et al. (1995) described fracture modeling results using the FEHM (Zyvoloski, 1995) code which indicated that in all but the most extreme infiltration conditions, fractures in the Bandelier Tuff on Mesita del Buey do not act as fast flow paths for liquids. When water enters a clean fracture with no coatings on the fracture edges, the simulations show that the water is imbibed into the matrix after only a short distance (<10 m), whereupon it is subject to matrix flow conditions. Simulations with fracture coatings having hydraulic conductivities four orders of magnitude less than the tuff suggest that deeper movement can occur. However, simulations with a discontinuity in the low-conductivity coating interrupted fast flow in the fracture which suggests that coatings must be continuous for long distances in order to effectively enhance water movement down the fractures. Simulations of filled fractures show that these are barriers to

flow because they are of lower conductivity than the tuff matrix. Though their simulations do not suggest that mesa top fractures play a significant role in moving water from the surface to the water table, Birdsell et al. (1995) do state that high influx conditions such as large snowmelt or runoff events might be sufficient to produce flow over longer distances. Rogers and Gallaher (1995) used the RETC code of van Guenuchten et al. (1991) to obtain moisture content-hydraulic conductivity relationships and calculated average linear velocities for various stratigraphic units and locations on the plateau. Their estimated velocities were 10 to 5000 times slower than the observed movement of tritium, chloride, and nitrate contamination at some canyon bottom locations, which suggests that fast paths such as fracture flow may be important under wetter conditions.

The above summary has described of some of the more important problems in understanding the hydrogeologic system of the Pajarito Plateau. The next two sections of this paper (Sections II and III) focus on the problems of mesa top hydrogeology and fracture flow, and how these two problems fit into an overall understanding of the processes occurring on the plateau. The last section of the paper (Section IV) describes new information about the paleohydrology and paleoclimate of the plateau

and how this may also be important in understanding the hydrogeologic system.

II. MESA TOP PROCESSES

Mesa Top Flow and Recharge

One of the least understood aspects of Pajarito Plateau hydrogeology is what happens to water on the mesas. Nearly all of the existing models consider mesa top recharge as insignificant. However, the information used to support the no mesa top recharge hypothesis is largely observational and is not based on actual determinations of recharge or mesa flux rates. In addition, the models disregard the possibility of fracture flow which may result in deep movement of water in dry environments (Stephens, 1994). The mesa top recharge issue is a concern because potential sources of contamination from Los Alamos National Laboratory are concentrated on the mesas. Rogers and Gallaher (1995) estimated linear velocities for various Bandelier tuff units based on pressure potential-moisture content data obtained from cores taken on mesa tops and found average linear velocities that ranged from 10^{-8} to 10^{-7} cm/sec. They also state that though their predictions for some of the wetter canyon bottoms severely underestimated observed

tracer velocities, predictions for the mesas may be representative because of the drier conditions which would favor matrix flow.

Newman (1996b) used chloride mass balance to estimate fluxes of 0.01 to 1.5 cm/year through mesa top soils and near-surface Bandelier tuff, which when converted to average linear velocities, yield similar values to those in Rogers and Gallaher (1995). The fluxes indicate that matrix recharge is probably negligible. This can be shown by a simple water balance calculation for the plateau. First, the annual mesa recharge is estimated assuming a $2x10^{-3}$ m/yr mesa flux. This flux value seems reasonable for the mesas based on the results in Birdsell et al. (1995); Rogers and Gallaher, (1995); and Newman (1996b). The area of the main aquifer is about $1.3x10^{8}$ m^2 (Stoker and Purtymun, 1993), assuming the mesas cover half of the aquifer area, the mesa area contributing to recharge would be about $6.5x10^{7}$ m^2. Multiplying the flux by the mesa recharge area gives an estimated mesa recharge rate of $1.3x10^{5}$ m^3/yr. Next, the mesa recharge rate is compared to the estimated aquifer discharge. Main aquifer discharge at the Rio Grande, between Otowi Bridge and the mouth of Rito De Frijoles is estimated to be between 5.3 to $6.8x10^{6}$ m^3/yr (Environmental Surveillance Group, 1993). Assuming a discharge of $5.3x10^{6}$ m^3/yr, the estimated mesa top recharge ($1.3x10^{5}$ m^3/yr) only contributes about 2.5% of the annual

discharge. Thus, recharge of the main aquifer via matrix flow in the mesas is apparently not important. However, a few cautionary notes need to be made regarding the calculation. Some of the values used have large uncertainties which could dramatically affect the result. For example, if either the flux or the mesa area that contributes recharge is actually an order of magnitude larger than the value used above, then 25% of the annual discharge may come from the mesas. Another important assumption is that the hydrologic system is in equilibrium. In other words, it is assumed that annual recharge is equal to annual discharge. This, however, has not been demonstrated.

Comparing mesa and main aquifer chloride concentrations also indicates that matrix recharge through the mesas is minor. Chloride concentrations in the main aquifer are about 3 mg/L (Blake et al., 1995), while chloride concentrations from a 1500 m deep core taken from a mesa top site are 50 mg/L and higher (Gallaher, 1996). This difference in concentrations supports the idea that the mesas are not the major contributor of recharge because it would take a substantial dilution to lower the chloride concentration from 50 to 3 mg/L.

It appears that matrix flow through the mesas is not important as a recharge process, but is it important in terms of contaminant movement? If a no remediation scenario (also known as the no further

action response) is acceptable, then the slow rate of water movement indicates that contaminants will probably move slowly as well, and thus the mesas are not going to contribute any contamination to the main aquifer for a very long time. However, the no further action response may not be acceptable to some regulatory organizations or stakeholders who may require clean closure. In this case, consideration of the matrix flux is important because it aids in determining the potential amount of soil and tuff that will need to be excavated, which is a major factor in controlling the cost of cleanup. The flux and velocity estimates in Newman (1996b) and Rogers and Gallaher (1995) are valuable in estimating the depth of contaminant transport in the case of a clean closure remediation, in which all of the contaminated soil and tuff is excavated and removed for treatment or transport to a landfill. One other consideration is that Newman (1996b) has shown that near-surface matrix fluxes vary depending on the textural characteristics of the mesa top soils. Fluxes are generally higher in the soils which do not contain clay-rich Bt horizons, such as those typical of the pinyon-juniper zone on the plateau. If transport occurs by matrix flow, soil texture is an important consideration because contaminants may move at different rates depending on the soils. In addition, the soils and the near surface fluxes in the pinyon-juniper zone are highly spatially variable and the

development of a nonuniform contaminant front would need to be considered.

Mesa Top Runoff Processes

One component of the Pajarito Plateau hydrologic system that has until recently, been neglected is surface flow, in particular, the importance of runoff processes on the mesa tops has not been addressed. Wilcox (1994) and Wilcox et al. (1996) examined water balances at different mesa top experimental sites and found that except for some short term periods, mesa top runoff processes are generally of minor importance when compared to the evapotranspirative component of the water balance. However, in terms of contaminant transport and clean up of mesa top areas, runoff processes may be very important. Newman (1996c) and Wilcox et al. (1996) show that tremendous volumes of water can move laterally on the mesa tops as overland flow and interflow (e.g., interflow rates of over 1000 L/day were measured through a 16 m^2 trench face). The rapid movement of these relatively large volumes of water suggests that runoff processes could cause a redistribution of particulate and soluble contaminants in the soil zone over a much larger area than would be predicted otherwise.

Another important point is the very episodic nature of runoff processes (Wilcox et al., 1996; Newman, 1996c). Very large runoff events may occur only once every year, or even once every few years. This suggests that hydrologic modeling should focus on rare, large volume precipitation or snowmelt events rather than using yearly precipitation averages, because it is the rare large events that drive the mesa top hydrologic system.

Preferential Flow In The Mesa Soils

Preferential flow, especially macropore flow, appears to be very important in controlling both the vertical and horizontal flow of water in the mesa top soils, especially in the ponderosa pine zone. Newman (1996c) found that much of the interflow generated in the ponderosa pine zone apparently occurs by macropore flow. It was determined that matrix flow was of minimal importance except perhaps during saturated conditions. Recognition of the existence of a two domain flow (matrix and preferential) system in the ponderosa zone soils is important because this type of flow system can have interesting consequences with regard to contaminant mobility. For example, contaminants that enter the macropore system may move relatively rapidly, whereas contaminants in the matrix will probably move quite slowly. There is an

additional complication because there is exchange between the matrix and macropores, especially under saturated conditions. Large changes in interflow chemistry can occur when the soils become saturated (Newman, 1996c). The mechanism for this change is diffusion or flushing of soluble species from the soil matrix into the macropores. Thus, if a contaminant is in the matrix, it is not sequestered there permanently and may become mobilized if moisture contents rise. The result is that the matrix may act as a periodic source of contaminants to the macropore flow system. In other words, the macropore flow system may rapidly flush contaminants resulting in low concentration or contaminant-free interflow, but saturated conditions may later resupply the macropores with additional contaminants that were stored in the matrix and contaminant concentrations in interflow would rise again.

III. FRACTURE FLOW

Fracture Hydrology

There are two questions that need to be answered with regard to fracture flow on the Pajarito Plateau. Does fracture flow occur, and what is its importance? The first question can be answered easily. Fracture flow does occur; the presence of roots, clay fillings, and calcite fillings throughout the plateau provide ample evidence of this. The second

question is far more difficult to answer. The modeling by Birdsell et al. (1995) indicates that long distance fracture flow in the mesa environment is unlikely. Also, roots and fracture fillings have not been found much deeper than 10 m which suggests that fracture flow may only occur at the near-surface. These two pieces of evidence suggest that mesa fracture flow may not be an important recharge pathway. However, the available evidence does not seem adequate to rule out the possibility of deep fracture flow. The previously mentioned study by Rogers and Gallaher (1995) suggests that deep fracture flow may be important in the canyon bottoms, but more research is needed to verify this.

Fracture Chemical Environment

One question regarding fracture flow has received little attention, and that is, if fracture flow occurs, what effect will fracture chemistry have on contaminant transport? Stephens et al. (1993) noted that there is little information regarding the chemical influences on contaminant mobility for the plateau. There have been a few studies of sorption of radionuclides on Bandelier Tuff (e.g., Christenson and Thomas, 1962; Polzer and Essington, 1984; and Purtymun and Stoker, 1987) but there is no information on the interaction of tuff minerals with other metals or

organics, nor have there been any studies specific to fracture conditions. Fracture chemistry may involve the interaction of water, contaminants, and tuff minerals and this is what was explored in the above mentioned radionuclide studies. However, if plant roots are indicative of the fractures that conduct water, then a different and more complicated chemical environment may be representative of the fractures. Recent studies by Reneau and Vaniman (1994), and Newman (1996a) describe fracture chemistries that may strongly influence contaminant mobility. Both of these studies showed that plant root growth and microbial processes are very important in some of the fractures. The biological processes produce a wide variety of compounds, some of which could potentially increase contaminant solubilities and enhance mobility, while others could potentially inhibit mobility.

There are two main kinds of contaminants at Los Alamos, metals and organics, and general examples of how these two types of contaminants might be affected by fracture chemistry are given below. This is not an exhaustive or detailed accounting of the impact fracture chemistry may have on contaminant transport, but is meant to demonstrate how complex the contaminant-fracture chemistry might be, and to provide a discussion of some of the chemical processes that may be important in the fractures.

There are a large number of metal contaminants on the plateau. For example, barium, beryllium, cadmium, chromium, copper, lead, mercury, plutonium, silver, and uranium are all contaminants of concern (Los Alamos National Laboratory, 1993b; Stephens et al, 1993). These metal contaminants can occur in different chemical forms which strongly influences mobility. Metals can occur as free metal ions, inorganic ion pairs and complexes, organic complexes and chelates, colloids, and as precipitates and adsorbed species on immobile substrates such as fracture walls. Possible implications of fracture chemistry on each of these forms are discussed below.

Bacteria, fungi, and other microorganisms can exert a powerful influence on the mobility of metals because they can affect or control environmental EH and pH conditions (Rose et al., 1991). The EH and pH of a system has a large affect on the valence of free metal ions and the types of inorganic ion pairs and complexes that are formed. For example, uranium is a redox sensitive species and under oxidizing conditions aqueous uranium can be mobile, while under reducing conditions, uranium is generally immobile (Rose et al., 1991). What is special about the fractures that host plant roots is that anaerobic conditions can apparently form within an otherwise oxidizing system (Newman, 1996a). Thus, the EH conditions in the fractures may not be

what is normally expected, and would influence the mobility of redox sensitive species.

Growth of plant roots and decomposition of the plant roots by microbes can provide many different types of organics that would be available for complexation and chelation. Organic complexes and chelates are chemical compounds that result from the association of an metal and an organic molecule (ligand). A complex has one bonding site between the metal and the organic ligand, while a chelate can have multiple bonds between the metal and organic ligand. The consequence of the formation of complexes and chelates is that the solubility of a metal can increase dramatically, resulting in more metal in solution, and thus, more of the metal is available for transport. One important chelator that is present in the fractures as a result of fungal growth is oxalate (Reneau and Vaniman, 1994). Oxalate grows on the outside of fungal hyphae and is a very effective chelator of metals. For example, Graustein et al. (1977) indicate that oxalate can increase the solubility of iron and aluminum by several orders of magnitude. Presumably, oxalate chelation would also affect other metal species as well.

Colloids can be important mobile forms of metals, both as metal precipitates and as adsorbed species on other inorganic or organic materials. Colloids are organic or inorganic particles between about 10

Å and 1 mm in diameter (Hiemenz, 1986). Because of their small size, colloids can be very mobile, in addition, their small size per unit volume results in a high surface area where soluble species can adsorb. The adsorption of a metal to a colloid is a function of the type and chemical form of the metal and the surface properties of the organic or mineral colloid, and these factors can all be influenced by fracture biogeochemical processes. Colloidal transport of adsorbed metals may be quite important in the fracture environment because organic and inorganic colloidal material is surely present, and Penrose et al. (1990) have shown that colloidal transport of adsorbed plutonium does occur on the plateau. With regard to colloids formed from metal-precipitates, the precipitation is a function of the chemical activity of the metal, and EH and pH conditions, which as discussed earlier, will be affected by the fracture chemical environment.

Metal-precipitates and metals adsorbed to stationary organic and mineral substrates represent immobile metal forms. The factors controlling precipitation and adsorption on immobile substrates are basically the same as discussed above for colloids. Mineral surfaces on the edges of fractures and immobile organic material such as roots may act as substrates for precipitation and adsorption and, the biogeological

processes in the fracture will dictate if precipitation or adsorption occurs.

A variety of organic contaminants are also present on the plateau, including organic solvents and organics derived from explosives testing. Organic contaminants have an affinity for adsorption onto other organic materials, and can adsorb onto immobile organic substrates which would decrease mobility. However, if the organic contaminants adsorb onto organic colloids, mobility may be enhanced.

Another process that may affect the mobility of organic contaminants is microbial degradation. The active microbiota in the fractures may utilize organic contaminants as a carbon source, transforming the organic contaminants into other kinds of chemical species. So, like the metals, the mobility of organic contaminants will probably be affected by the complex biogeochemical processes occurring in the fractures.

IV. PLATEAU PALEOCLIMATE AND PALEOHYDROLOGY

Calcite Paleoclimate Interpretations

As mentioned earlier, calcites found in fractures on the Pajarito Plateau provide evidence of past fracture flow. Using ^{14}C dating, Newman (1996a) found that some of the calcites were formed during the

Pleistocene and are 20,000-24,800 years old. Newman (1996a) also measured calcite $\delta^{18}O$ values, which if the temperature during precipitation is known, can be used to estimate the $\delta^{18}O$ values of water in the fractures at the time of precipitation. This, then, permits a comparison of the isotopic values of water from over 20,000 years ago to that of the present. The comparison is useful because it may indicate the climatic conditions that prevailed in a much earlier stage in the evolution of the plateau hydrologic system.

The comparison of the $\delta^{18}O$ values of ancient waters (estimated from calcite $\delta^{18}O$ values) to modern precipitation is given in Table 4.1. Predicted water $\delta^{18}O$ values were determined based on modern and late-Pleistocene (20,000-24,800 ^{14}C yr. B.P.) temperatures. The modern temperature (9°C) is the average annual temperature for the plateau (Bowen, 1990). The late-Pleistocene temperatures of 2-6.5 °C are from reconstructions made by Phillips et al. (1986) and Stute et al. (1992).

Calculation of ancient water $\delta^{18}O$ values using the modern average annual temperature yields values that are indistinguishable from modern precipitation (Table 4.1). This might lead one to conclude that the late-Pleistocene climate was similar to the present. However, the paleoclimate interpretation of Stute et al. (1992), based on noble gas and ^{14}C analyses of waters from the Carrizo aquifer (Texas), was that average

annual temperatures were 2.5 °C cooler during the period when the Los Alamos calcites apparently precipitated. Assuming a temperature of 6.5 °C (2.5 °C lower than the modern average) yields predicted $\delta^{18}O$ water values that are also indistinguishable from modern precipitation (Table 4.1). Phillips et al. (1986) used groundwater stable isotope values, noble gases and ^{14}C dating to determine Pleistocene and Holocene recharge temperatures for the Ojo Alamo aquifer in north-western New Mexico. Their results suggest a greater degree of cooling than Stute et al. (1992) for the period of calcite precipitation with temperatures on the order of 5-7 °C cooler than modern. Predicted water $\delta^{18}O$ values from the Los Alamos calcites using 2 and 4 °C temperatures based on the Phillips et al. results are again not discernible from average modern precipitation (Table 4.1). Thus, it appears that for the Los Alamos calcites, the $\delta^{18}O$ record is not sensitive enough for the predicted Pleistocene climate change to be resolved. This is an interesting result in light of the research by Gardner (1984) and Liu et al. (1996) . Both of these studies observed relatively constant $\delta^{18}O$ values for pedogenic calcites precipitated during the Pleistocene and Holocene. Gardner and Liu et al. suggested that the constant values might reflect an insensitivity of calcite $\delta^{18}O$ values to climate change because the isotopic fractionation factor changes with temperature. In other words, the temperature

control on fractionation could offset any differences resulting from changes in the isotopic composition of precipitation. Garder also suggested that "batching" or the sequential precipitation of small aliquots of calcite with differing isotopic composition may also serve to obscure a climatic signal. The fact that the Los Alamos water $\delta^{18}O$ predictions in Table 4.1 are not resolvable from modern precipitation supports the suggestion of Gardner (1984) and Liu et al. (1996) that counter-acting effects might mask the calcite $\delta^{18}O$ climate record.

Paleohydrologic Interpretations

Both the results of Phillips et al. (1986) and Stute et al. (1992) indicate that there was a cooler climate during the Pleistocene. Assuming that these cooler temperatures prevailed at Los Alamos suggests that a substantial portion of the main Los Alamos aquifer was recharged under conditions different than the present. Carbon-14 ages for waters in the main aquifer range from modern to Pleistocene (0-40,000 yrs.), with the oldest waters being on the eastern edge of the plateau near the Rio Grande (Environmental Surveillance Group, 1995). Thus, the isotopic composition of the oldest water in the eastern portion of the aquifer should reflect Pleistocene climatic conditions. Based on the results of Phillips et al. (1986) for the Ojo Alamo aquifer, Pleistocene

water should be on the order of 3‰ lighter in $\delta^{18}O$ and 25‰ lighter in δD than Holocene water. Examination of the stable isotope data for plateau groundwater (Blake et al., 1995) did not reveal any discernible differences in isotopic composition across the main aquifer. Based on chemical data, Blake et al. suggested that the aquifer is well mixed, which could account for the homogeneity of the isotope values. However, the water analyzed from wells and springs that are supplied by the confined portion of the main aquifer do yield anomalously light values. The confined aquifer water is of Pleistocene age and ranges from about 2 to 4‰ lighter in $\delta^{18}O$ and 10 to 28‰ lighter in δD than the water under unconfined conditions. These differences are similar to those between Holocene and Pleistocene waters in the Ojo Alamo aquifer mentioned above, which suggests that a Pleistocene climatic signal may be preserved in the confined aquifer water. Alternatively, the light isotope values are one of the main pieces of evidence that lead Goff and Sayer (1980), and Blake et al. (1995) to suggest that the confined aquifer was being recharged from the Sangre de Cristos to the east (Figure 4.3). They evaluated the isotopic values of the plateau waters based on an elevational gradient which involved using a linear model that predicts the recharge elevation given the isotopic composition of a groundwater sample. The light isotopic values from the confined aquifer water

indicated a recharge source that was higher than the Jemez Mountains, and the taller Sangre de Cristo Mountains were suggested as a possible recharge area. However, the relation between elevation and isotopic composition was developed from modern precipitation trends and may not apply to conditions when temperatures were cooler than the present. Therefore, it appears that the isotopically light waters of the confined aquifer might reflect the cooler temperatures of the Pleistocene rather than a high elevation recharge source. Thus, an alternative hypothesis to the Sangre de Cristo recharge pathway is that the light confined aquifer water may have been recharged in the same manner as the rest of the main aquifer and the isotopic composition reflects past cooler climatic conditions.

IV. SUMMARY AND CONCLUSIONS

At the present time, many of the questions about the hydrogeologic system of the Pajarito Plateau remain unanswered. However, some new conclusions regarding mesa top and fracture processes can be made based on studies completed in the last few years. First, matrix flow through the mesas is probably not a significant recharge process. Field based and modeled soil water fluxes are very low and estimated annual recharge from the mesas is only a small fraction of

the annual aquifer discharge. But, in terms of contaminant clean up, vertical and lateral flow on the mesas may be very important. Vertical flow though slow, can redistribute contaminants in the soil zone and the vertical distributions may be spatially variable because of the different textural properties of the soils across the plateau. In addition to vertical flow, interflow and overland flow can potentially distribute contaminants laterally over a relatively large area. Some of the mesa top soils also behave as a two domain flow system. The distribution of contaminants between matrix and macropore flow domains, and the chemical exchange between these domains, will affect how quickly contaminants are transported in the soil environment.

The possibility of fracture recharge to the main aquifer is still unanswerable at this time. Research by Rogers and Gallaher (1995) suggest that fracture flow may be important in some of the canyon bottoms. On the mesas, fracture flow does occur, but evidence suggests that this is a near surface phenomena. The difficulty in understanding fracture flow is that it is a very localized, episodic process, and the planar nature of fractures make them hard to observe at depth. If contaminants do enter fractures, their mobility will more than likely be drastically affected by the biogeochemisty of the fracture system.

Finally, assessment of paleoclimate data suggests an alternative explanation for the isotopically-light waters in the confined aquifer on the eastern edge of the plateau. The light waters may be the result of recharge during a cooler Pleistocene climate and could have been recharged along the same pathways as the rest of the plateau waters instead of a high-elevation recharge pathway from the Sangre de Cristo Mountains as has been suggested by others.

REFERENCES

Abeele, W. V., M. L. Wheeler, and B. W. Burton. 1981. Geohydrology of Bandelier Tuff. Los Alamos National Laboratory Report LAMS-8962.

Adams, A. I., F. Goff, and D. Counce. 1995. Chemical and Isotopic Variations of Precipitation in the Los Alamos Region, New Mexico. Los Alamos National Laboratory Report, LA-12985-MS, Los Alamos, NM. 35 pp.

Bailey, R. A., R. L. Smith, and C. S. Ross. 1969. Stratigraphic Nomenclature of Volcanic Rocks in the Jemez Mountains, New Mexico. US Geol. Survey Bull. 1274-P. 19 pp.

Bailey, R. A. and R. L. Smith. 1978. Volcanic Geology of the Jemez Mountains, New Mexico. in Guidebook to the Rio Grande Rift in New Mexico and Colorado, Circular 163, New Mexico Bureau of Mines and Mineral Resources, Socorro, New Mexico. pp. 184-196.

Birdsell, K. H., W. E. Soll, N. D. Rosenberg, and B. A. Robinson. 1995. Numerical Modeling of Unsaturated Groundwater Flow and Radionuclide Transport at MDA G. Los Alamos National Laboratory Report, LA-UR-95-2735, Los Alamos, NM. 49 pp.

Blake, W. D., F. Goff, A. I. Adams, and D. Counce. 1995. Environmental Geochemistry for Surface and Subsurface Waters in the Pajarito Plateau and Outlying areas, New Mexico. Los Alamos National Laboratory Report, LA-12912-MS, Los Alamos, NM. 43 pp.

Bowen, B. M. 1990. Los Alamos Climatology. Los Alamos National Laboratory Report, LA-11735-MS, Los Alamos, NM. 254 pp.

Broxton, D. E., S. L. Reneau. 1995. Stratigraphic Nomenclature of the Bandelier Tuff for the Environmental Restoration Project at Los Alamos

National Laboratory. Los Alamos National Laboratory Report, LA-13010-MS. 19 pp.

Burton, B. W. 1982. Geologic Evolution of the Jemez Mountains and Their Potential for Future Volcanic Activity. Los Alamos National Laboratory Report, LA-8795-GEOL. 31 pp.

Christenson, C. W. and R. G. Thomas. 1962. Movement of Plutonium Through Los Alamos Tuff. in Ground Disposal of Radioactive Wastes, Second Conference Proceedings, No. TID-7628. Johns Hopkins University, Baltimore. pp. 248-281.

Cushman, R. L. 1965. An Evaluation of Aquifer and Well Characteristics of Municipal Well Fields in Los Alamos and Guaje Canyons near Los Alamos New Mexico. USGS Water Supply Paper 1809-D.

Davenport, D. W., B. P. Wilcox, and B. L. Allen. 1995. Micromorphology of Pedogenically Derived Fracture Fills in Bandelier Tuff, New Mexico. Soil Sci. Soc. Am. J. V. 59. pp. 1672-1683.

Environmental Surveillance Group. 1993. Environmental Surveillance at Los Alamos During 1991. Los Alamos National Laboratory Report LA-12572-ENV.

Environmental Surveillance Group. 1995. Environmental Surveillance at Los Alamos During 1993. Los Alamos National Laboratory Report LA-12973-ENV.

Friedman, I., and J. R. O'Niel. 1977. Compilation of Stable Isotope Fractionation Factors of Geochemical Interest. In M. Fleischer (ed.) Data of Geochemistry, sixth ed., Chapter KK, USGS Prof. Paper 440-KK. 12 pp.

Gallaher, B. M. 1996. Personal communication. Los Alamos National Laboratory, Los Alamos, NM.

Gardner, J. N., F. Goff, S. Garcia, and R. C. Hagan. 1986. Stratigraphic Relations and Lithologic Variations in the Jemez Volcanic Field, New Mexico. J. of Geophys. Res., V. 91. pp. 1763-1778.

Gardner, L. R. 1984. Carbon and Oxygen Isotope Composition of Pedogenic $CaCO_3$ from Soil Profiles in Nevada and New Mexico, U.S.A. Isotope Geos. V. 2. pp. 55-73.

Goff, F. E. and S. Sayer. 1980. A Geothermal Investigation of Spring and Well Waters of the Los Alamos Region, New Mexico. Los Alamos National Laboratory Report, LA-8326-MS, Los Alamos, NM. 21 pp.

Graustein, W. C., K. Cromack Jr., and P. Sollins. 1977. Calcium Oxalate: Occurrence in Soils and Effects on Nutrient and Geochemical Cycles. Science, V. 198. pp. 1252-1254.

Griggs, R. L. 1964. Geology and Ground-Water Resources of the Los Alamos Area, New Mexico. USGS Water Supply Paper 1753. 107 pp.

Hiemenz, P. C. 1986. Principles of Colloid and Surface Chemistry, 2nd ed. Marcel Dekker, Inc. New York. 815 pp.

Liu, B., F. M. Phillips, and A. R. Campbell. 1996. Stable Carbon and Oxygen Isotopes of Pedogenic Carbonates, Ajo Mountains, Southern

Arizona: Implications for Paleoenvironmental Change. PALAEO, In Review.

Los Alamos National Laboratory. 1993a. Installation Work Plan for Environmental Restoration, V. 1, Rev. 3. November, 1993. Los Alamos National Laboratory Report LA-UR-93-3987.

Los Alamos National Laboratory. 1993b. RFI Work Plan for Operable Unit 1132, June, 1993. Los Alamos National Laboratory Report LA-UR-93-768.

Newman, B. D., 1996a. A Model for Microbially Induced Precipitation of Vadose-Zone Calcites in Fractures at Los Alamos, New Mexico. Chapter 1, this Dissertation.

Newman, B. D., 1996b. Investigations of Soil-Water Movement in Semiarid and Subhumid Forests Using Stable Isotope and Halogen Tracers. Chapter 3, this Dissertation.

Newman, B. D., 1996c. Interflow Pathways in a Subhumid Ponderosa Pine Hillslope. Chapter 2, this Dissertation.

Penrose, W. R., W. L. Polzer, E. H. Essington, D. M. Nelson, and K. A Orlandini. 1990. Mobility of Plutonium and Americium Through a Shallow Aquifer in a Semiarid Region. Environ. Sci. and Tech., V. 24. pp. 228-234.

Phillips, F. M., L. A. Peters, M. K. Tansey, and S. N. Davis. 1986. Paleoclimatic Inferences from an Isotopic Investigation of Groundwater in the Central San Juan Basin, New Mexico. Quat. Res. V. 26. pp. 179-193.

Polzer, W. L. and E. H. Essington. 1984. Modified Freundlich Adsorption Equation for Modeling of Ion Exchange Reactions in Soils. Los Alamos National Laboratory Report LA-UR-84-2512.

Purtymun, W. D. 1973. Regional Survey of Tritium in Surface and Groundwater in the Los Alamos Area, New Mexico, August 1966 through May, 1969. Los Alamos National Laboratory Report LA-5234-MS.

Purtymun, W. D. 1975. Geohydrology of the Pajarito Plateau with Reference to Quality of Water, 1949-1972. Los Alamos National Laboratory Report LA-5744.

Purtymun, W. D. 1984. Hydrologic Characteristics of the Main Aquifer in the Los Alamos Area: Development of Ground Water Supplies. Los Alamos National Laboratory Report LA-9957-MS.

Purtymun, W. D. and W. R. Kennedy. 1971. Geology and Hydrology of Mesita del Buey. Los Alamos National Laboratory Report LA-4660. 12 pp.

Purtymun, W. D. and A. K. Stoker. 1987. Environmental Status of Technical Area 49, Los Alamos, New Mexico. Los Alamos National Laboratory Report LA-11135-MS.

Reneau, S. L. and D. T. Vaniman. 1994. Fracture Characteristics in a Disposal Pit on Mesita del Buey, Los Alamos National Laboratory. Unpublished Los Alamos Report. 17 pp.

Rogers, D. B., B. M. Gallaher. 1995. The Unsaturated Hydraulic Characteristics of the Bandelier Tuff. Los Alamos National Laboratory Report, LA-12968-MS.

Rogers, M. A. 1977. History and Environmental Setting of LASL Near-Surface Land Disposal Facilities for Radioactive Wastes (Areas A, B, C, D, E, F, G, and T). Los Alamos National Laboratory Report LA-6848-MS, V. 1 and 2.

Rose, A. W., H. E. Hawkes, and J. S. Webb. Geochemistry in Mineral Exploration, 2nd edition. Academic Press, NY. p. 238.

Spell, T., T. M. Harrison, J. A. Wolff. 1990. $^{40}Ar/^{39}Ar$ Dating of the Bandelier Tuff and San Diego Canyon Ignimbrites, Jemez Mountains, New Mexico: Temporal Constraints on Magmatic Evolution. J. of Vol. and Geotherm. Res. V. 43. pp. 175-193.

Spiegel, Z. and B. Baldwin. 1964. Geology and Water Resources of the Santa Fe Area, New Mexico. USGS Water Supply Paper 1525.

Stephens, D. B., P. M. Kearl, and R. W. Lee. 1993. Hydrogeologic Review for the Environmental Restoration Program at Los Alamos National Laboratory. D. B. Stephens and Assoc., Inc. Albuquerque, NM 68 pp.

Stephens, D. B. 1994 A Perspective on Diffuse Natural Recharge Mechanisms in Areas of Low Precipitation. Soil Sci. Soc. Am. J., V. 58. pp. 40-48.

Stoker, A. K., and W. D. Purtymun. 1993. Long Term Piezometric Surface Trends in the Los Alamos Main Aquifer. Abstract, Rocky Mountain Groundwater Conference, Albuquerque, October 27-29, 1993. New Mexico Section, American Water Resources Association.

Stute, M., P. Schlosser, J. F. Clark, and W. S. Broecker. 1992. Paleotemperatures in the Southwestern United States Derived from Noble Gases in Ground Water. Science, V. 256. pp. 1000-1002.

van Genuchten, M. Th., F. F. Leij, and S. R. Yates. 1991. The RETC Code for Quantifying the Hydraulic Functions of Unsaturated Soils. U.S. Environmental Protection Agency Report No. EPA/600.2-91/065.

Waresback, D. B., and B. N. Turbeville. 1990. Evolution of a Plio-Pleistocene Volcanogenic-Alluvial Fan: The Puye Formation, Jemez Mountains, New Mexico. Geol. Soc. of Am. Bulletin, V. 102. pp. 298-314.

Wilcox, B. P., 1994. Runoff and Erosion in Intercanopy Zones of Pinyon-Juniper Woodlands. J. Range. Manage., 47: 285-295.

Wilcox, B. P., D. Brandes and D. W. Davenport. 1996. Runoff Generation from a Subhumid Ponderosa Pine Hillslope in New Mexico. Water Resour. Research. Submitted.

Zyvoloski, G. A., B. A. Robinson, Z. V. Dash, and L. L. Trease. 1995. Users Manual for the FEHMN Application. Los Alamos National Laboratory Report LA-UR-94-3788, Rev. 1.

Table 4.1. Comparison of $\delta^{18}O$ values of modern and ancient plateau waters.

Modern ave. annual precipitation is -11.0‰[1]

	Equilibration Temperature[3]			
	9°C	6.5°C	4°C	2°C
Calcite $\delta^{18}O$[2]	Water $\delta^{18}O$ (‰)	Water $\delta^{18}O$ (‰)	Water $\delta^{18}O$ (‰)	Water $\delta^{18}O$ (‰)
Lightest calcite, 20‰	-12.2	-12.8	-13.4	-13.9
Average calcite, 21.8‰	-10.4	-11.0	-11.7	-12.2
Heaviest calcite, 23.5‰	-8.7	-9.4	-10.0	-10.5

[1]average for TA-51, near calcite sampling location (Adams et al., 1994).
[2]calcite values represent the range of $\delta^{18}O$ values in Newman (1996a).
[3]water $\delta^{18}O$ values were calculated using the given calcite $\delta^{18}O$, equilibration temperature, and the calcite-water equation of Friedman and O'Niel (1977). 9°C is the modern average annual plateau temperature (Bowen, 1990). 2, 4, and 6.5°C are paleoclimate reconstruction temperatures for the period of calcite precipitation based on Phillips et al. (1986) and Stute et al. (1992).

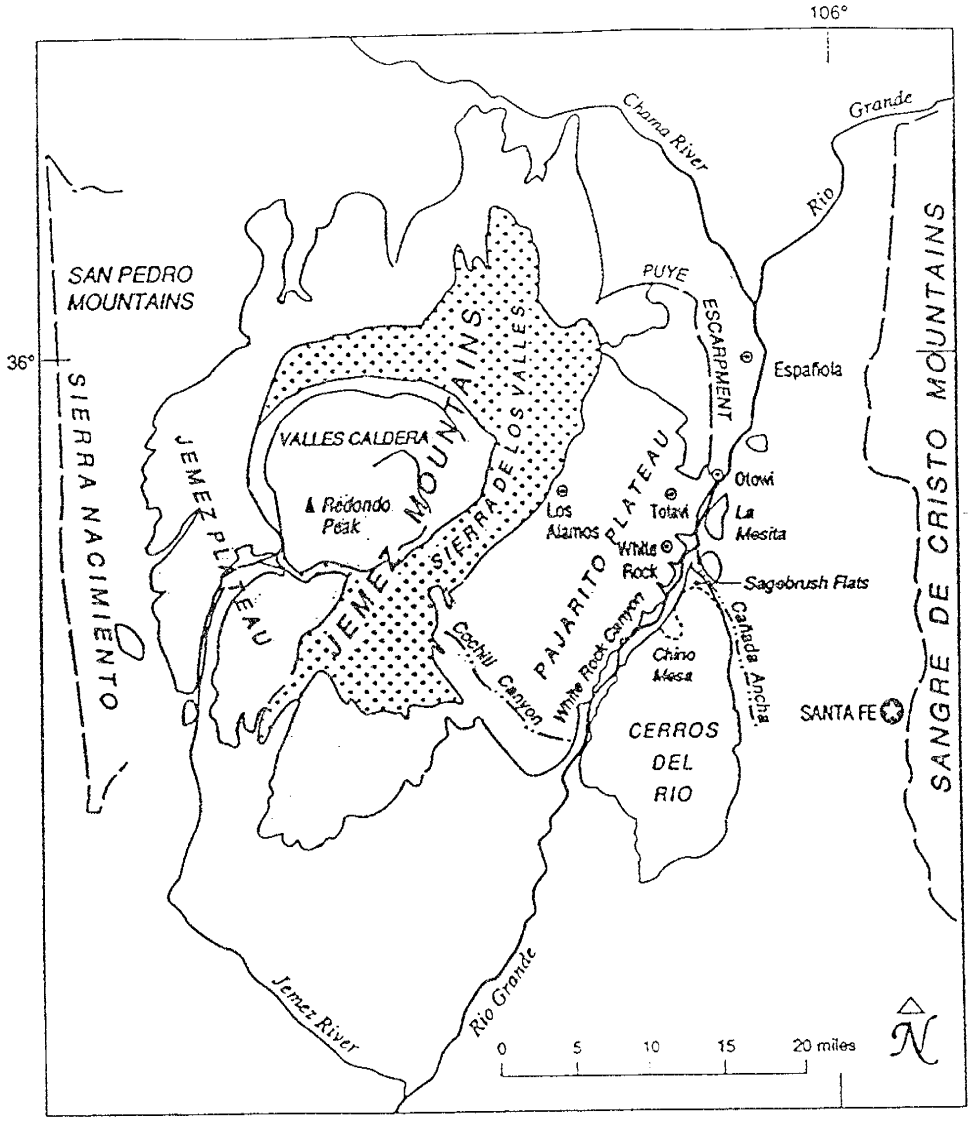

Figure 4.1. Location map of the Pajarito Plateau (From Los Alamos National Laboratory, 1993a).

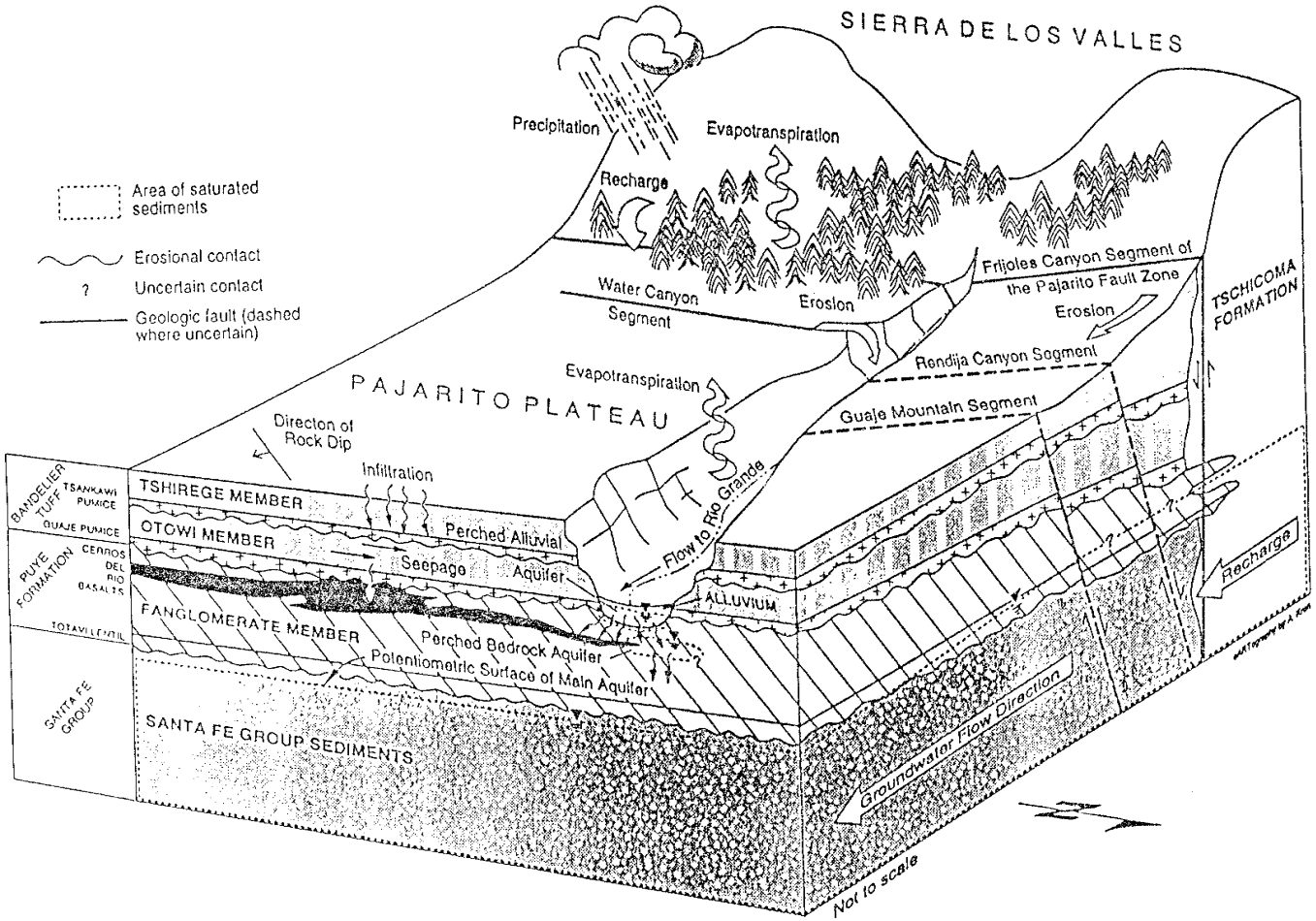

Figure 4.2. Generalized cross section of the Pajarito Plateau showing topography, geology, and hydrology (Unpublished Los Alamos Environmental Restoration Program Figure).

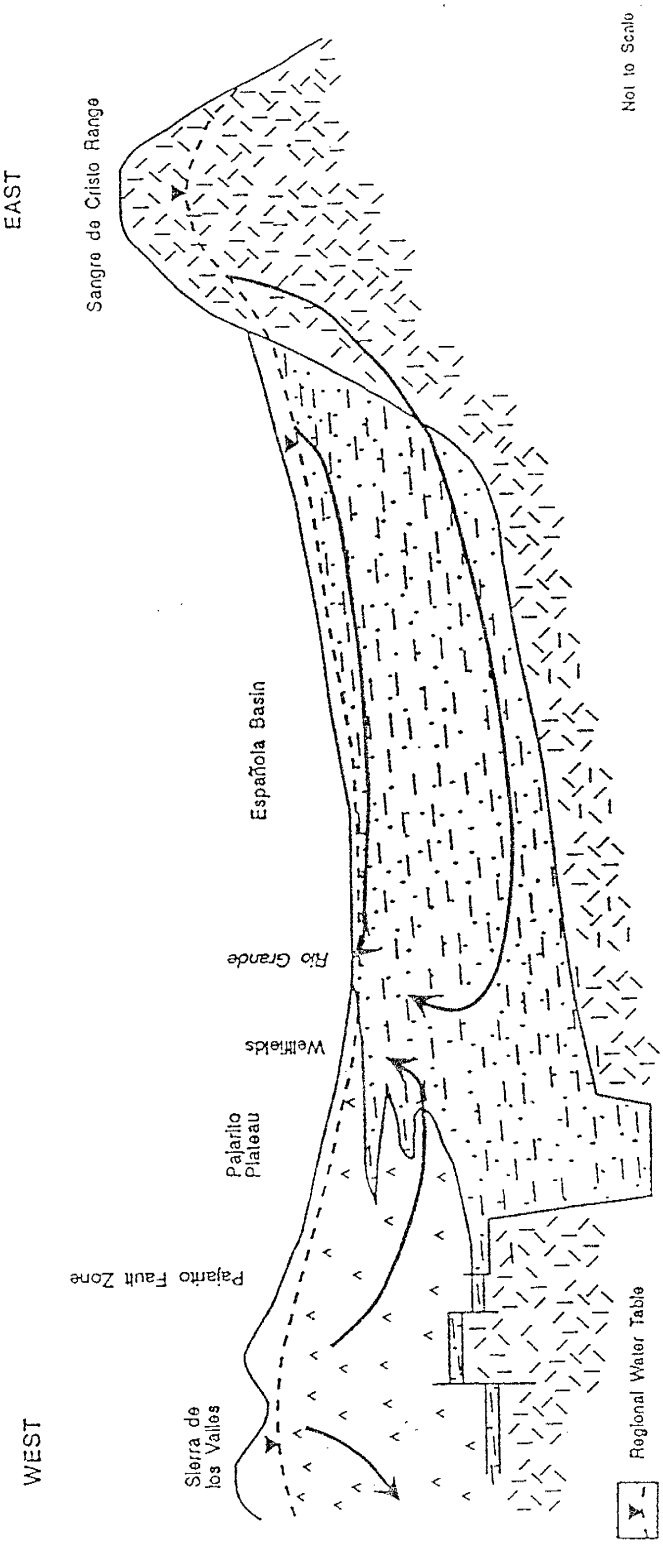

Figure 4.3. Alternative model of recharge to the plateau main aquifer (from Stephens et al., 1993).

APPENDIX A: Lipid Biomarker Analyses for the Calcite Fracture Fills

Appendix A. Calcite Lipid Analyses

	PLFA pmol/g			PLFA mole%			Total Lipid pmol/g	mol%
Fatty Acid	R3	R2	R1	R3	R2	R1	R3	R3
14:0	0.0	0.0	0.0	0.0	0.0	0.0	0.0	0.0
i15:0	0.1	0.0	0.0	0.6	0.0	0.0	3.0	0.4
a15:0	0.1	0.0	0.0	0.7	0.0	0.0	3.7	0.5
15:0	0.0	0.0	0.0	0.3	0.0	0.0	1.0	0.1
br16:1	0.0	0.0	0.0	0.0	0.0	0.0	1.5	0.2
i16:0	0.2	0.1	0.3	1.9	0.9	0.4	8.4	1.0
16:1w9c	0.0	0.0	0.0	0.0	0.0	0.0	0.0	0.0
16:1w7c	0.0	0.0	0.0	0.1	0.0	0.0	8.2	1.0
16:1w7t	0.0	0.0	0.0	0.0	0.0	0.0	0.0	0.0
16:1w5c	0.0	0.0	0.0	0.0	0.0	0.0	4.2	0.5
16:0	0.5	0.5	0.5	3.8	3.1	0.9	50.7	6.3
br16:0a	0.2	0.2	0.3	1.3	1.3	0.5	10.3	1.3
br16:0b	0.0	0.0	0.1	0.2	0.3	0.1	0.0	0.0
i17:1	0.0	0.0	0.1	0.0	0.1	0.1	0.0	0.0
9me16:0	0.0	0.1	0.2	0.4	0.8	0.3	0.0	0.0
10me16:0	0.5	1.1	1.4	4.4	7.1	2.3	24.1	3.0
i17 :0	0.1	0.2	0.4	1.2	1.4	0.7	5.5	0.7
a17:0	0.1	0.2	0.4	1.1	1.4	0.7	7.9	1.0
cy17:0	0.1	0.4	0.5	1.1	2.8	0.8	5.7	0.7
17:0	0.0	0.0	0.1	0.1	0.2	0.1	3.2	0.4
br17:0a	1.1	1.6	2.4	9.5	9.9	4.0	14.7	1.8
br17:0b	0.0	0.1	0.2	0.3	0.6	0.3	2.4	0.3
br17:0c	0.1	0.3	0.7	1.2	2.0	1.2	4.2	0.5
18:2w6	0.0	0.0	0.0	0.0	0.0	0.0	52.5	6.6
i18:0	0.0	0.0	0.0	0.0	0.0	0.0	0.0	0.0
18:1w9c	0.8	1.5	2.2	7.1	9.8	3.6	66.7	8.3
18:1w7c	0.5	0.9	1.4	4.6	5.5	2.3	13.4	1.7
18:1w7t	0.0	0.0	0.2	0.0	0.1	0.3	0.0	0.0
18:0	0.7	1.0	1.5	5.7	6.5	2.5	53.9	6.7
br18:0	0.0	0.1	0.1	0.1	0.3	0.2	0.0	0.0
br19:1	0.0	0.1	0.2	0.2	0.4	0.4	0.0	0.0
10me18	2.3	3.6	6.2	20.0	22.9	10.2	15.7	2.0
12me18	0.2	0.0	0.0	1.6	0.0	0.0	0.0	0.0
i19:0	0.0	0.0	0.1	0.0	0.0	0.1	5.2	0.6
a19:0/19:1	0.0	0.0	0.0	0.0	0.2	0.1	9.9	1.2
19:1w6c	0.3	0.7	1.6	2.7	4.6	2.6	0.0	0.0
cy19:0	1.2	1.5	31.3	10.3	9.6	51.7	0.0	0.0
br19:0a	0.1	0.2	0.4	1.1	1.6	0.7	3.6	0.4
20:1w9c	0.2	0.3	0.8	1.7	2.2	1.3	11.2	1.4
20:1w7c	0.0	0.1	0.2	0.3	0.9	0.4	0.0	0.0

Appendix A. Calcite Lipid Analyses

	PLFA pmol/g			PLFA mole%			Total Lipid pmol/g	mol%
Fatty Acid	R3	R2	R1	R3	R2	R1	R3	R3
20:0	0.0	0.1	0.5	0.4	0.4	0.9	12.2	1.5
br20:0a	0.1	0.2	0.0	1.0	1.2	0.0	5.7	0.7
br20:0b	0.0	0.0	0.1	0.0	0.1	0.2	0.0	0.0
2-oxo-20:0	0.1	0.1	0.6	0.7	0.7	1.0	24.2	3.0
dimeth21:0	1.5	0.0	4.6	12.9	0.0	7.6	8.2	1.0
dimeth22:0	0.1	0.2	0.8	1.3	1.2	1.4	216.7	27.0
22:0	0.0	0.0	0.0	0.0	0.0	0.0	28.2	3.5
23:0	0.0	0.0	0.0	0.0	0.0	0.0	8.8	1.1
24:1	0.0	0.0	0.0	0.0	0.0	0.0	6.7	0.8
24:0	0.0	0.0	0.0	0.2	0.0	0.0	57.6	7.2
25:0	0.0	0.0	0.0	0.0	0.0	0.0	4.0	0.5
26:0	0.0	0.0	0.0	0.0	0.0	0.0	10.0	1.2
27:0	0.0	0.0	0.0	0.0	0.0	0.0	2.3	0.3
28:0	0.0	0.0	0.0	0.0	0.0	0.0	12.2	1.5
29:0	0.0	0.0	0.0	0.0	0.0	0.0	2.2	0.3
30:0	0.0	0.0	0.0	0.0	0.0	0.0	11.6	1.5
Tot.	11.7	15.8	60.4	100.0	100.0	100.0	801.4	100.0

	LPS-OHFA pmol/g			LPS-OHFA mole%		
Fatty Acid	R3	R2	R1	R3	R2	R1
2-OH16:0	22.5	16.8	15.6	28.4	39.4	34.6
2-OH18:0	13.2	11.7	12.7	16.7	27.4	28.0
2-OH23:0	5.1	2.9	3.4	6.5	6.8	7.6
2-OH22:0	4.6	2.5	3.1	5.8	5.9	7.0
2-OH24:1	6.8	2.5	3.3	8.6	6.0	7.3
2-OH24:0	20.4	4.5	5.6	25.8	10.5	12.4
2-OH25:0	3.5	1.7	1.4	4.5	4.0	3.2
2-OH26:0	3.1	0.0	0.0	3.9	0.0	0.0
Tot.	79.2	42.5	45.2	100.0	100.0	100.0

	sterol pmol/g			sterol mole%		
Sterol	R3	R2	R1	R3	R2	R1
campesterol	8.6	2.7	2.3	4.9	8.3	7.4
stigmasterol	26.0	5.6	6.8	14.7	17.5	21.7
sterol A	12.1	3.0	1.8	6.8	9.4	5.7
sitosterol	124.1	18.2	17.9	70.2	56.6	57.5
sterol B	6.0	2.7	2.4	3.4	8.2	7.8
Tot.	176.8	32.2	31.2	100.0	100.0	100.0

Appendix A. Calcite Lipid Analyses

	PLFA pmol/g			PLFA mole%			Total Lipid pmol/g	Total Lipid mol%
Fatty Acid	R3	R2	R1	R3	R2	R1	R3	R3
	di-ether pmol/g			di-ether mole%				
Di-Ether	R3	R2	R1	R3	R2	R1		
eto16:0a	16.4	2.6	4.1	7.3	21.1	35.6		
eto16:0b	81.2	7.5	4.7	36.2	60.9	41.0		
eto16:0c	115.7	2.2	2.7	51.5	18.1	23.4		
eto16:0d	11.1	0.0	0.0	4.9	0.0	0.0		
Tot.	224.4	12.3	11.6	100.0	100.0	100.0		

APPENDIX B: Stable Isotopes, Chloride, and Bromide in Interflow and Precipitation for the Ponderosa Pine Hillslope

Appendix B. Ponderosa Pine Interflow Stable Isotope, Chloride and Bromide Data

DATE	Julian Day	Isotope Sample	Anion Sample	$\delta^{18}O$ (permil)	δD (permil)	Cl (mg/L)	Br (mg/L)
6/25/93	176	A1	-	-10.18	-90.2	18.019	0.083
6/28/93	179	A2	-			14.409	0.065
6/28/93	179	B1	-	-13.44	-95.1	9.503	0.089
6/29/93	180	A3	A1			14.191	0
6/29/93	180	B2	-			8.881	0.142
7/1/93	182	A4	A2	-12.54	-91.9	14.165	0
7/1/93	182	B3	B1	-13.58	-97.4	8.64	0
7/6/93	187	A5	A3			13.882	0
7/6/93	187	B4	B2			7.602	0
7/7/93	188	A6	A4			13.117	0
7/7/93	188	B5	B3	-13.74	-98.7	7.908	0
7/9/93	190	A7	A5	-12.55	-89.6	13.16	0
7/9/93	190	B6	B4			7.381	0
7/12/93	193	P1	P1	-5.61	-43.2	1.721	0
7/12/93	193	A8	A6	-12.38		12.578	0
7/12/93	193	B7	B5	-13.83	-97	6.73	0
7/13/93	194	P2	-	-9.25	-78.4	0.843	0.073
7/13/93	194	A9	A7	-12.16	-90.2	12.956	0
7/13/93	194	B8	B6	-13.82	-98.8	6.948	0
7/14/93	195	P3	P2	-8.86	-67.2	2.228	0
7/14/93	195	A10	A8	-11.97		12.675	0
7/14/93	195	B9	B7			6.481	0
7/15/93	196	P4	P3	-9.89	-63.8	0.145	0
7/15/93	196	R1	R1	-10.45	-54.8	0.683	0
7/15/93	196	A11	A9	-10.10		2.483	0
7/15/93	196	B10	B8	-10.58	-71.9	1.693	0
7/16/93	197	A12	A10	-10.41	-70.8	1.925	0
7/16/93	197	B11	B9			2.646	0
7/19/93	200	A13	A11			3.151	0
7/19/93	200	B12	B10			2.284	0
7/20/93	201	P5	P4	-10.99	-96.1	0.21	0
7/20/93	201	R2	R2			0.527	0
7/20/93	201	A14	-	-10.72	-73.3	3.533	0
7/20/93	201	B13	B11	-11.77	-80.9	2.277	0
7/21/93	202	R3	R3	-13.63	-92.3	0.266	0
7/21/93	202	A15	-			3.64	0
7/21/93	202	B14	B12			2.319	0
7/22/93	203	A16	-	-10.47	-71.8	4.027	0
7/22/93	203	B15	B13	-11.93	-82.6	2.978	0
7/23/93	204	A17	-			4.462	0
7/23/93	204	B16	B14	-12.16	-83.1	2.578	0
7/26/93	207	A18	A12	-10.71	-75	4.467	0
7/26/93	207	B17	B15			2.913	0
7/27/93	208	A19	-			4.907	0
7/27/93	208	B18	-			3.12	0.066

Appendix B. Ponderosa Pine Interflow Stable Isotope, Chloride and Bromide Data

DATE	Julian Day	Isotope Sample	Anion Sample	$\delta^{18}O$ (permil)	δD (permil)	Cl (mg/L)	Br (mg/L)
7/28/93	209	A20	-			4.791	0
7/28/93	209	B19	B16			3.21	0
7/29/93	210	P6	-			0.999	0.075
7/29/93	210	R4	R4	-10.96	-76	2.139	0
7/29/93	210	A21	-	-10.89	-76.5	4.657	0
7/29/93	210	B20	-	-12.3	-81.9	3.466	0
7/30/93	211	B21	-			2.887	0
8/2/93	214	P7	P5	-3.9	-40.3	1.726	0
8/2/93	214	A23	-	-10.13	-75	5.204	0
8/2/93	214	B22	B17			3.074	0
8/3/93	215	B23	B18	-12.48	-85.7	5.461	0
8/4/93	216	P8	P6			0.693	0
8/4/93	216	R5	R5			0.757	0
8/4/93	216	B24	B19	-13.08	-92.3	2.581	0
8/5/93	217	P9	-			5.939	0.104
8/5/93	217	B25	B20			2.461	0
8/6/93	218	P10	P7	-6.76	-46.5	7.269	0
8/6/93	218	R6	R6			0.446	0
8/6/93	218	B26	B21			2.647	0
8/9/93	221	P11	P8	-9.24	-64.3	1.278	0
8/9/93	221	R7	R7	-7.89	-48.2	0.174	0
8/9/93	221	A28	A13	-9.72	-64.8	3.691	0
8/9/93	221	B27	B22	-8.67	-57.9	1.09	0
8/10/93	222	A29	A14			2.654	0
8/10/93	222	B28	B23			1.282	0
8/11/93	223	P13	-			2.159	0.074
8/11/93	223	A30	A15	-8.53	-59	2.723	0
8/11/93	223	B29	B23.5			1.282	0
8/12/93	224	B30	B24	-8.82	-60.3	1.6	0
8/13/93	225	P14	P9	4.7	18.5	2.779	0
8/13/93	225	B31	B25			1.664	0
8/16/93	228	P15	P10	-0.94	-1.2	1.457	0
8/16/93	228	R8	R8	-3.25	-11.7	0.504	0
8/16/93	228	A33	-	-8.39	-55.4	2.007	0
8/16/93	228	B32	B26	-9.35	-61.6	1.6	0
8/17/93	229	P16	P11			0.544	0
8/17/93	229	R9	-			0.764	0.076
8/17/93	229	B33	B27			1.701	0
8/18/93	230	B34	B28			1.482	0
8/19/93	231	P17	P12	-5.59	-26.2	1.1	0
8/19/93	231	B35	B29	-10.92	-73.8	1.608	0
8/20/93	232	B36	-			1.387	0
8/23/93	235	B37	B30			1.42	0
8/24/93	236	B38	-			1.458	0.062
8/27/93	239	P19	P13	-8.77	-56.1	0	0

Appendix B. Ponderosa Pine Interflow Stable Isotope, Chloride and Bromide Data

DATE	Julian Day	Isotope Sample	Anion Sample	$\delta^{18}O$ (permil)	δD (permil)	Cl (mg/L)	Br (mg/L)
8/27/93	239	R10	R9			0.862	0
8/27/93	239	B39	B31			2.14	0
8/30/93	242	P20	P14	-9.2	-56.3	0.126	0
8/30/93	242	R11	R10	-10.53	-60.3	0.308	0
8/30/93	242	A37	A16	-8.82		12.216	0
8/30/93	242	B40	B32	-8.59		1.738	0
8/31/93	243	P21	P15	-13.1		0.22	0
8/31/93	243	R12	R11			0.778	0
8/31/93	243	A38	A17	-8.94		19.56	0
8/31/93	243	B41	B33	-8.88	-60.2	1.777	0
9/1/93	244	A39	A18	-9.29	-70	23.13	0
9/1/93	244	B42	B34			1.724	0
9/2/93	245	B43	-			1.815	0.064
9/3/93	246	A41	-	-9.13	-68.1	22.407	0.179
9/3/93	246	B44	-			2.362	0.067
9/8/93	251	P22	P16	-10.5	-70.4	0	0
9/8/93	251	R13	R12	-12.53	-85.1	0.664	0
9/8/93	251	A42	A19			11.601	0
9/8/93	251	B45	B35	-9.4	-64.8	1.861	0
9/9/93	252	A43	A20	-8.42		11.759	0
9/9/93	252	B46	-	-9.612		1.754	0
9/14/93	257	P23	P17	-5.97	-39.6	0.188	0
9/14/93	257	R14	R13			0.299	0
9/14/93	257	A44	A21	-8.86	-63.7	11.962	0
9/14/93	257	B47	-	-10.1	-67.2	2.376	0
10/15/93	288	P26	P18	-8.62	-68.5	0.233	0
10/18/93	291	P27	P19	-17.15	-129.9	0.236	0
10/18/93	291	R15	R14	-18.95	-134.5	5.475	0
10/27/93	300	S1	S1	-15.79	-109.1	0.575	0
10/29/93	302	S2	S2			9.237	0
11/12/93	316	P28	P20			0.483	0
11/12/93	316	R16	R15	-13.9	-102.3	0.495	0
11/15/93	319	S3	S3	-19.21	-138.3	0.495	0
11/24/93	328	P29	P21	-15.61	-118.3	0.189	0.359
11/24/93	328	R17	R16	-14.66	-104.5	0.245	0
12/13/93	347	S4	S4			80.388	0
12/15/93	349	S5	S5	-11.84	-68	45.173	0
12/20/93	354	S6	S6	-8.57	-73.9	45.024	0
12/22/93	356	S7	S7			17.923	0
1/26/93	26	S8	-			0.447	0
1/27/93	27	S9	S9	-21.56	-153.1	4.921	0
1/28/93	28	S10	S10			1.167	0
1/31/94	31	S11	S11	-30.45	-225.1	0.296	0
2/8/94	39	S12	S12	-21.44	-166.4	2.13	0
2/11/94	42	B48	-	-9.96	-68.6	9.006	0

Appendix B. Ponderosa Pine Interflow Stable Isotope, Chloride and Bromide Data

DATE	Julian Day	Isotope Sample	Anion Sample	$\delta^{18}O$ (permil)	δD (permil)	Cl (mg/L)	Br (mg/L)
2/14/94	45	S13	S13			0.93	0
2/17/94	48	S14	S14			9.487	0
2/18/94	49	S15	S15			2.485	0
2/18/94	49	R18	R17	-17.9	-134	0.958	0
2/22/94	53	S16	S16	-18.89	-137	9.329	0
2/22/94	53	R19	R18			0.921	0
2/25/94	56	R20	R19			1.082	0
3/1/94	60	S17	S17	-19.35	-138.6	2.104	0
3/1/94	60	S18	S18			0.851	0
3/1/94	60	R21	R20	-15.46	-132.8	0.783	0
3/4/94	63	S19	S19	-19.01	-150.1	1.289	0
3/4/94	63	R22	R21			0.998	0
3/8/94	67	P30	P22	-10.94	-73.4	0.268	0
3/8/94	67	R23	R22			0.421	0
3/9/94	68	S20	S20			3.661	0
3/9/94	68	R24	R23			0.467	0
3/9/94	68	R25	R24	-13.34	-107.6	0.587	0
3/12/94	71	S21	S21	-17.49	-125.5	0.532	0
3/12/94	71	R26	R25			0.373	0
3/15/94	74	R27	R26			0.262	0
3/16/94	75	R28	R27			0.261	0
3/18/94	77	R29	R28	-14.88	-114.2	0.298	0
3/25/94	84	P31	P23	-16.04	-124.9	0.381	0
3/25/94	84	S22	S22	-9.04	-57.5	1.818	0
3/28/94	87	S23	S23			1.093	0
3/29/94	88	S24	S24	-25.74	-192.9	0.322	0
3/30/94	89	S25	S25	-20.14	-148.6	0.329	0
4/6/94	96	S26	S26	-16.04	-114.9	5.534	0
4/11/94	101	P32	P24	-17.76	-132.5	0.459	0
4/11/94	101	S27	S27			0.92	0
4/12/94	102	R30	R29	-15.63	-112.4	1.327	0
4/14/94	104	P33	P25	-14.76	-106.1	0.266	0
4/14/94	104	R31	-	-15.48	-111.2	1.605	0
4/21/94	111	P34	-			20.531	0
4/25/94	115	P35	-	-0.72	-16.5	6.208	0.086
4/28/94	118	P36	-	-7.46	-43.1	3.239	0.075
5/3/94	125	P37	P26	-6.51	-32.7	0.711	0.088
5/11/94	131	P38	P27	-10.66	-72.2	0.419	0.171
5/12/94	132	P39	P28			0.413	0.069
5/12/94	132	R32	R30	-10.5	-67.7	7.219	0.144
5/13/94	133	P40	P29			0.435	0
5/16/94	136	P41	P30	-9.84	-70.6	0.395	0.072
5/16/94	136	R33	R31			1.339	0.086
5/24/94	144	P42	P31	-2.25	-18.9	1.982	0.249
5/27/94	147	P44	P33	-11.96	-81.9	0.549	0.092

Appendix B. Ponderosa Pine Interflow Stable Isotope, Chloride and Bromide Data

DATE	Julian Day	Isotope Sample	Anion Sample	$\delta^{18}O$ (permil)	δD (permil)	Cl (mg/L)	Br (mg/L)
5/31/94	151	P45	P34	-11.92	-90	0.292	0
6/20/94	171	P46	P35			1.072	0.085
6/20/94	171	R34	R32	-4.97	-36.4	3.404	0.07
6/23/94	174	P47	P36	-6	-41.1	0.296	0
6/23/94	174	R35	R33			0.496	0.073
6/23/94	174	A45	-	-9.27	-63.8	21.966	0.066
6/30/94	181	P48	P37			2.561	0.035
6/30/94	181	A46	A22	-11.64	-81.4	11.967	0.061
7/11/94	192	P49	P38	-5.29	-40.4	1.725	0.144
7/11/94	192	A47	A23	-12.17	-86.8	6.703	0.069
7/11/94	192	B48.5	B36	-11.38		3.093	0.062
7/12/94	193	P50	P39	-2.24		0.826	0.071
7/12/94	193	A48	-	-10.88		6.969	0
7/12/94	193	B49	B37	-12.03	-81.9	2.62	0.189
7/15/94	196	-	P40			6.467	0.097
7/15/94	196	A49	-	-10.41	-72.3	7.775	0
7/15/94	196	B50	B38	-12.08		2.502	0
7/18/94	199	P51	P41	-3.92	-30.4	2.499	0.079
7/18/94	199	B51	B39	-12.12	-83.6	2.427	0.079
7/20/94	201	P52	P42			0.401	0.074
7/20/94	201	R35.5	R33.5	-9.03	-57.5	3.387	0.075
7/20/94	201	A51	-	-10.62		7.943	0
7/20/94	201	B52	B40			2.508	0.068
7/21/94	202	P53	P43	-2.63	-20.2	0.406	0.08
7/21/94	202	B53	-	-11.92	-82.1	2.525	0.061
7/22/94	203	B54	B41	-12.41	-85.4	2.657	0.064
7/25/94	206	P54	P44			0.262	0.073
7/25/94	206	R36	R34			0.498	0.073
7/25/94	206	A52	A24	-8.92	-58.5	1.103	0
7/25/94	206	B55	B42	-12.42	-87.8	2.494	0.059
7/26/94	207	A53	-			1.42	0
7/26/94	207	B56	-			2.647	0.063
7/27/94	208	P55	P45	-5.04	-29.9	0.66	0.223
7/28/94	209	P56	P46			0.389	0.163
7/28/94	209	A54	-	-8.42	-54.1	1.73	0
7/28/94	209	B57	B43			2.713	0.159
7/29/94	210	P57	P47			0.325	0.078
7/29/94	210	A54.5	-	-		2.141	0
7/29/94	210	B58	-			2.442	0
8/1/94	213	P58	P48	-5.78	-43.5	0.357	0.092
8/1/94	213	B59	B44			2.513	0.063
8/2/94	214	P59	P49			0.263	0
8/2/94	214	R37	R35	-7.04	-51.4	0.831	0
8/3/94	215	P60	P50			0.378	0.085
8/3/94	215	B60	-	-11.7	-81.2	2.548	0

Appendix B. Ponderosa Pine Interflow Stable Isotope, Chloride and Bromide Data

DATE	Julian Day	Isotope Sample	Anion Sample	$\delta^{18}O$ (permil)	δD (permil)	Cl (mg/L)	Br (mg/L)
8/4/94	216	B61	-			3.115	0
8/5/94	217	P61	P51	-3.97	-29.1	0.391	0.074
8/5/94	217	B62	-			2.941	0
8/8/94	220	P62	P52			0.222	0
8/8/94	220	R38	R36	-1.96	-27.2	0.681	0
8/8/94	220	B63	-			2.775	0
8/9/94	221	P63	P53	0.36	-4.6	0.589	0.132
8/11/94	223	P64	P54			0.515	0
8/12/94	224	A55	-	-6.99	-44.8	2.285	0
8/12/94	224	B64	B45	-11.06	-79.1	2.852	0.074
8/15/94	227	P65	P55	-8.48	-57.8	0.252	0.07
8/16/94	228	P66	-			0.713	0
8/16/94	228	A56	-	-8.49	-53.5	2.458	0
8/16/94	228	B65	-	-11.33	-80.1	2.784	0
8/18/94	230	P67	P56	-3.4	-31.5	0.486	0.078
8/18/94	230	B66	-	-11.33	-81.5	2.989	0
8/19/94	231	B67	-			3.477	0.061
8/22/94	234	P68	P57			0.282	0.103
8/22/94	234	R39	R37	-7.41	-50.7	1.226	0.072
8/22/94	234	B68	-			3.037	0
8/23/94	235	B69	-	-10.26	-79.4	2.929	0
8/25/94	237	P69	P58	-3.81	-20.3	0.225	0.086
8/25/94	237	R40	R38			0.592	0.064
8/26/94	238	P70	P59			0.365	0.105
8/26/94	238	R41	R39			1.099	0.059
8/31/94	243	P71	-	-3.19	-18.7	0.949	0
8/31/94	243	B71	-	-7.63	-73	3.253	0
9/1/94	244	P72	P60			0.368	0.114
9/2/94	245	P73	P61	-5.28	-30	0.35	0
9/6/94	249	P74	P62			0.237	0
9/6/94	249	B73	-	-6.08	-75.3	3.306	0
9/7/94	250	P75	P63	-4.6	-30.4	0.308	0
9/12/94	255	P76	P64			0.447	0
9/13/94	256	P77	P65	-4.21	-20.1	0.296	0
9/14/94	257	P78	P66			0.267	0
9/14/94	257	R42	R40	-8.97	-65	1.391	0
10/4/94	277	P79	P67			0.565	0
10/6/94	279	P80	P68	-8.76	-70.2	0.808	0
10/12/94	285	P81	P69	-7.96	-59	0.458	0
10/14/94	287	P82	P70	-9.32		0.221	0
10/14/94	287	R43	R41	-9.47		3.528	0.073
10/15/94	288	P83	P71	-18.31	-125.7	0.197	0
10/15/94	288	S29	S29			0.757	0.08
10/15/94	288	R44	R42	-17.71		0.57	0
10/15/94	288	B74	B46	-16.15	-111.8	2.154	0.074

Appendix B. Ponderosa Pine Interflow Stable Isotope, Chloride and Bromide Data

DATE	Julian Day	Isotope Sample	Anion Sample	$\delta^{18}O$ (permil)	δD (permil)	Cl (mg/L)	Br (mg/L)
10/16/94	289	P84	P72	-10.52	-64.1	0.423	0
10/16/94	289	S30	S30	-10.75	-68.6	1.181	0
10/16/94	289	R45	R43	-9.98	-74	0.709	0
10/16/94	289	B75	B47	-10.13	-86.3	1.94	0
10/17/94	290	P85	P73	-10.56	-62.5	0.356	0
10/17/94	290	S31	S31			0.614	0
10/17/94	290	R46	R44			0.379	0
10/17/94	290	B76	B48	-9.23	-74.6	1.461	0
10/18/94	291	B77	B49	-9.86	-76.3	1.757	0
10/24/94	297	B78	B50	-11.08		4.59	0.093
10/28/94	301	B79	-			7.979	0.19
11/3/94	307	P86	P74			2.311	0
11/5/94	309	P87	P75			0.83	0.031
11/8/94	312	P88	P76	-14.76		0.41	0
11/12/94	316	P89	P77	-16.54		0.275	0.023
11/12/94	316	R47	R45	-17.43		0.405	0
11/12/94	316	B80	B51	-13.62		6.558	0.097
11/12/94	316	A57	A25	-14.59		6.617	0.049
11/13/94	317	P90	P78	-6.38		0.298	0
11/13/94	317	B81	B52	-12.27		9.433	0.04
11/13/94	317	A58	A26	-12.68		12.177	0.062
11/14/94	318	B82	B53			11.094	0.015
11/14/94	318	A59	-			12.889	0.049
11/15/94	319	B83	B54			12.204	0.023
11/16/94	320	B84	B55	-12.33		12.198	0.025
11/18/94	322	B85	B56			13.736	0.028
11/21/94	325	P91	-	-6.38		0.997	0
11/21/94	325	B86	B57	-11.80		13.182	0
11/28/94	332	P92	-	-9.99		1.222	0.022
11/28/94	332	S32	S32			1.091	0
12/5/94	339	P93I	P79A	-24.80		0.705	0
12/5/94	339	S33I	S33A			3.432	0
12/6/94	340	P94I	P80A	-29.66		1.48	0
12/8/94	342	P95I	-	-20.58		6.575	0.075
12/15/94	349	B87I	B58A	-11.81		21.558	0
12/16/94	350	B88I	-			22.451	0
12/20/94	354	B89I	B59A	-10.93		32.12	0
12/22/94	356	B90I	-			41.989	0
12/31/94	365	B91I	B60A	-10.42		51.889	0
12/31/94	365	S34I	S34A	-15.16		0.445	
1/3/95	3	B92I	B61A			55.313	0
1/6/95	6	B93I	B62A	-10.60		53.488	
1/6/95	6	S35I	S35A	-21.65		0.496	0
1/11/95	11	B94I	-	-10.84		61.193	0
1/11/95	11	R48I	R46A			1.216	0

Appendix B. Ponderosa Pine Interflow Stable Isotope, Chloride and Bromide Data

DATE	Julian Day	Isotope Sample	Anion Sample	$\delta^{18}O$ (permil)	δD (permil)	Cl (mg/L)	Br (mg/L)
1/12/95	12	B95I	-			62.468	0
1/12/95	12	R49I	R47A			1.077	0
1/13/95	13	B96I	-	-10.73		59.05	1.727
1/13/95	13	R50I	R48A			1.434	0
1/17/95	17	R51I	R49A			1.152	0
1/23/95	23	R52I	R50A			0.655	0.159
1/27/95	27	S36I	S36A			0.173	0
1/30/95	30	S37I	S37A	-36.15		0.165	0
1/30/95	30	R53I	R51A			0.53	0.146
2/3/95	34	R55I	R52A			1.087	0.185
2/10/95	41	B97I	B63A	-10.60		49.526	
2/13/95	44	B98I	B64A	-12.03		39.851	
2/14/95	45	P95.5I	P81A	-16.50		0.193	0.783
2/14/95	45	A61I	A27A	-12.89		17.364	
2/14/95	45	B99I	B65A	-11.79		36.424	
2/15/95	46	P96I	P82A	-14.81		0.218	0
2/15/95	46	S38I	S38A	-21.99		0.175	0
2/15/95	46	C1I	-			39.553	0.914
2/15/95	46	A62I	A28A	-13.60		13.722	
2/15/95	46	B100I	B66A	-12.45		29.69	0.15
2/16/95	47	A63I	A29A	-12.87		22.874	0.128
2/16/95	47	B101I	B67A	-12.32		27.563	0.072
2/17/95	48	A64I	A30A			23.951	0.166
2/17/95	48	B102I	B68A			32.295	0.059
2/21/95	52	A65I	A31A	-12.94		21.962	0.129
2/21/95	52	B103I	B69A	-11.90		37.742	
2/22/95	53	B104I	B70A			38.535	
2/23/95	54	B105I	B71A	-11.95		39.054	
2/24/95	55	B106I	B72A			39.374	
2/27/95	58	A66I	A32A	-13.71		12.036	0.14
2/27/95	58	B107I	B73A	-12.13		38.698	
2/28/95	59	B108I	B74A			37.069	0.172
3/1/95	60	S39I	S39A	-12.15		0.291	0
3/1/95	60	B109I	B75A	-11.86		36.492	
3/2/95	61	S40I	S40A	-9.98		0.258	0
3/2/95	61	B110I	B76A	-12.06		33.832	
3/3/95	62	B111I	B77A	-11.82		3.366	
3/6/95	65	R56I	R53A	-10.07		1.022	0
3/6/95	65	A67I	A33A	-12.92		23.527	0.172
3/6/95	65	B112I	B78A	-12.58		16.073	0.701
3/6/95	65	P97I	-	-11.01		-	-
3/7/95	66	A68I	A34A	-12.72		27.251	0.294
3/7/95	66	B113I	B79A			20.577	0.933
3/8/95	67	A69I	A35A	-13.00		29.207	0.265
3/8/95	67	B114I	B80A	-12.30		21.39	0.895

Appendix B. Ponderosa Pine Interflow Stable Isotope, Chloride and Bromide Data

DATE	Julian Day	Isotope Sample	Anion Sample	$\delta^{18}O$ (permil)	δD (permil)	Cl (mg/L)	Br (mg/L)
3/8/95	67	A7OI	AIC	-12.20		-	-
3/8/95	67	B115I	B2C	-12.57		-	-
3/9/95	68	A71I	A36A			28.825	0.228
3/9/95	68	B116I	B81A	-13.08		20.932	0.867
3/9/95	68	-	Z1A			57.946	0.487
3/9/95	68	-	Z2A	-13.95		29.076	0.194
3/9/95	68	-	Z3A			327.171	1.159
3/10/95	69	A72I	A37A	-12.812		30.594	0.204
3/10/95	69	B117I	B82A	-12.249		21.04	0.837
3/13/95	72	A73I	A38A	-12.454		33.332	0.178
3/13/95	72	B118I	B83A	-12.483		17.508	0.435
3/14/95	73	B119I	B84A			16.143	0.369
3/16/95	75	B120I	B85A			14.357	0.278
3/17/95	76	B121I	B86A	-12.494		13.077	0.244
3/20/95	79	B122I	B87A			22.493	0.093
3/21/95	80	B123I	B88A			23.922	0.116
3/22/95	81	B124I	B89A			24.901	0.069
3/24/95	83	B125	B90			28.672	0.064
3/27/95	86	B126	B91			28.256	0
3/28/95	87	B127	B92			28.004	0
3/28/95	87	S40.5	S40.5	-8.29		0.566	0.132
3/29/95	88	B128	B93			27.268	0
3/29/95	88	S41	S41	-11.2		0.468	0
3/30/95	89	B129	B94			29.119	0.002
3/31/95	90	B130	B95	-12.659		28.816	0.006
3/31/95	90	P97.5	P83			0.979	0
4/3/95	93	B131	B96			29.378	0
4/4/95	94	B132	B97			29.159	0
4/4/95	94	P98		-4.418		1.122	0
4/5/95	95	B133	B98	-12.27		28.702	0
4/6/95	96	B134	B99			29.98	0
4/7/95	97	B135	B100			29.338	0
4/10/95	100	B136	B101	-12.417		28.542	0
4/10/95	100	P98.5	P84	-14.26		1.093	0
4/10/95	100	S42	S42	-16.66		0.412	0
4/11/95	101	B137	B102			28.211	0
4/11/95	101	S43	S43			0.336	0
4/12/95	102	B138	B103	-12.92		29.053	0
4/13/95	103	B139	B104			29.954	0
4/14/95	104	B140	B105			29.572	0.012
4/17/95	107	B141	B106	-12.81		31.195	0.008
4/18/95	108	B142	B107	-12.71		31.783	0
4/18/95	108	P99	P85			0.83	0
4/20/95	110	B143	B108	-12.176		32.754	0
4/20/95	110	P100	P86	-13.057		0.565	0

Appendix B. Ponderosa Pine Interflow Stable Isotope, Chloride and Bromide Data

DATE	Julian Day	Isotope Sample	Anion Sample	$\delta^{18}O$ (permil)	δD (permil)	Cl (mg/L)	Br (mg/L)
4/24/95	114	B144	B109			33.981	0.124
4/24/95	114	P101	P87			0.531	0
4/24/95	114	S44	S44			0.37	0
4/25/95	115	A74	A39			13.55	0.155
4/25/95	115	B145	B110			14.098	0.172
4/25/95	115	S45	S45			0.391	0
4/26/95	116	A75	A40			12.848	0.141
4/26/95	116	B146	B111			21.543	0.068
4/26/95	116	R56	R53			1.504	0
4/27/95	117	A76	A41			14.724	0.15
4/27/95	117	B147	B113			25.319	0.173
4/28/95	118	B148	B113			26.976	0.159
5/2/95	122	P102	-			2.343	0.13
5/2/95	122	B149	B114			25.931	
5/4/95	124	B150	B114.5			25.91	
5/5/95	125	B151	B115			25.248	
5/8/95	128	B152	B116			26.572	
5/8/95	128	S46	S46			0.392	0
5/9/95	129	B153	B117			26.053	
5/10/95	130	B154	B118			26.316	
5/11/95	131	P103	P88			0.521	0
5/11/95	131	B155	B119			26.834	
5/12/95	132	B156	B120			26.71	
5/15/95	135	B157	B121			26.854	
5/16/95	136	B158	B122			27.394	
5/17/95	137	B159	B123			27.341	0
5/18/95	138	B160	B124			28.709	0
5/23/95	143	P104	P89			0.6	0
5/23/95	143	B161	B125			28.876	0
5/24/95	144	P105	P90			0.531	0
5/24/95	144	B162	B126			29.13	
5/25/95	145	B163	B127			29.555	
5/26/95	146	B164	B128			28.574	0
5/30/95	150	P106	P91			0.407	0
5/30/95	150	A78	A42			6.254	0.151
5/30/95	150	B165	B129			9.976	0
5/31/95	151	P107	-			0.764	0.138
5/31/95	151	A79	A43			7.632	0
5/31/95	151	B166	B130			14.675	0
6/1/95	152	A80	-			7.161	0.151
6/1/95	152	B167	B131			21.01	0
6/2/95	153	B168	B132			22.296	0
6/5/95	156	P108	-			1.543	0
6/5/95	156	B169	B133			25.214	0
6/6/95	157	B170	B134			26.295	

Appendix B. Ponderosa Pine Interflow Stable Isotope, Chloride and Bromide Data

DATE	Julian Day	Isotope Sample	Anion Sample	$\delta^{18}O$ (permil)	δD (permil)	Cl (mg/L)	Br (mg/L)
6/7/95	158	B171	B135			25.808	
6/8/95	159	B172	B136			27.155	
6/9/95	160	B173	B137			28.264	
6/12/95	163	B174	B138			28.993	
6/13/95	164	A81	A44			9.18	0.16
6/13/95	164	B175	B139			29.532	
6/14/95	165	B176	B140			29.455	
6/15/95	166	P109	P92			1.912	0.13
6/15/95	166	B177	B141			28.505	
6/16/95	167	P110	P93			1.125	0.132
6/16/95	167	B178	B142			28.21	
6/19/95	170	P111	P94			0.542	0
6/19/95	170	R57	R54			0.978	0
6/19/95	170	B179	B143			22.077	0
6/20/95	171	P112	-			1.786	0
6/20/95	171	B180	B144			22.674	0
6/21/95	172	B181	B145			23.474	0
6/22/95	173	B182	B146			22.404	0
6/23/95	174	B183	B147			21.939	0
6/26/95	177	P113	P95			0.792	0
6/26/95	177	R58	-			3.397	0.144
6/26/95	177	B184	B148			22.947	0
6/26/95	177	B185	-			23.258	0
6/27/95	178	P114	P96			0.376	0
6/27/95	178	R59	R55			2.246	0.073
6/27/95	178	B186	B149			23.944	0
6/28/95	179	P115	P97			0.484	0
6/28/95	179	B187	B150			24.524	0
6/29/95	180	P116	-			0.685	0
6/29/95	180	B188	B151			25.058	0
6/30/95	181	P117	P98			0.502	0
6/30/95	181	B189	B152			24.698	0
7/5/95	186	P118	P99			0.416	0
7/5/95	186	B190	B153			25.165	
7/6/95	187	B191	B154			25.797	
7/7/95	188	B192	-			25.062	
7/10/95	191	B193	B155			26.073	
7/11/95	192	B194	B156			27.048	0
7/12/95	193	B195	B157			26.605	0
7/13/95	194	B196	B158			24.811	0
7/14/95	195	B197	B159			25.059	0
7/17/95	198	P119	P100			0.663	0
7/17/95	198	B198	B160			24.625	0
7/18/95	199	P120	P101			0.434	0
7/18/95	199	R60	R56			0.939	0

Appendix B. Ponderosa Pine Interflow Stable Isotope, Chloride and Bromide Data

DATE	Julian Day	Isotope Sample	Anion Sample	$\delta^{18}O$ (permil)	δD (permil)	Cl (mg/L)	Br (mg/L)
7/18/95	199	B199	B161			21.977	0
7/19/95	200	P121	P102			0.476	0
7/19/95	200	B200	B162			21.129	0
7/20/95	201	B201	B163			21.035	0
7/21/95	202	B202	B164			19.795	0
7/24/95	205	P122	-			1.036	3.668
7/24/95	205	B203	B165			19.574	0.177
7/25/95	206	B204	B166			19.219	0
7/26/95	207	B205	-			20.231	0
7/27/95	208	B206	-			1.036	3.618
7/28/95	209	B207	-			18.997	0

APPENDIX C: Stable Isotopes in Soil Waters From the Ponderosa Pine and Pinyon-Juniper Zone Cores

Appendix C. Core Water Stable Isotopes

Ponderosa Pine Core LJ1			Pinyon-Juniper Core PJ1			Erosion Plot Core EP4		
Depth	$\delta^{18}O$	δD	Depth	$\delta^{18}O$	δD	Depth	$\delta^{18}O$	δD
-5	-0.2	-59	-5	-1.1	-68	-5	2.2	-67
-15	-0.6	-73	-15	-1.5	-89	-15	-2.7	-81
-25	-3.2	-79	-25	-8.2	-108	-25	-5.6	-111
-35	-8.9	-101	-35	-11.5	-128	-35	-12.2	-116
-45	-9.7	-112	-45	-13.2	-140	-45	-11.5	-115
-55	-12.1	-110	-55	-13.9	-138	-55	-10.3	-105
-65	-11.7	-102	-65	-13.1	-131	-65	-10.7	-103
-75	-9.8	-92	-75	-12.4	-118	-75	-10.4	-99
-85	-9.9	-90	-85	-13.9	-115	-85	-10.5	-96
-95	-10.2	-92	-95	-13.8	-113	-95	-10.3	-93
-105	-9.9	-89	-105	-11.2	-108	-105	-9.5	-90
-115	-10.1	-89	-115	-11.6	-101	-115	-9.2	-83
-125	-9.8	-90	-125	-10.2	-93	-125	-8.2	-81
-135	-8.4	-83						
-145	-5.1	-85						
-155	-10.3	-81						
-165	-10.4	-90						
-175	-8.6	-96						
-185	-9.1	-82						
-195	-7.9	-86						
-205	-9.0	-84						
-215	-8.6	-93						
-225	-7.4	-77						
-235	-8.3	-93						
-245	-7.49	-89						
-255	-8.1	-85						

APPENDIX D: Chloride and Bromide in Soil Waters from Ponderosa Pine Zone Cores

Appendix D. Ponderosa Pine Zone Chloride and Bromide Soil Water Concentrations, and Chloride Residual Flux Data

Core	Depth Range (cm)	Soil Horizon	Weight Leached (g)	H2O Leach (L)	Cl (mg/L)	Br (mg/L)	Vol. Water (%)	Bulk Density (g/cm3)	Soil H2O (L)	Soil Cl (mg)	Soil Br (mg)	Clsw (mg/L)	Brsw (mg/L)	Clswi (g/m3)	Cum Clswi (g/m3)
PO 18	80-90	2BC	200	0.2	103.6	0.684	35.34	1.34	0.0527	20.7192	0.1368	392.809	2.59	138.819	430.589
PO 18	90-100	2BC	200	0.2	112.81	0.685	69.92	1.34	0.1044	22.5610	0.1370	216.188	1.31	151.159	581.747
PO 18	100-110	R	200	0.2	228.37	1.425	34.58	1.36	0.0508	45.6748	0.2850	898.240	5.60	310.589	892.336
PO 18	110-120	R	200	0.2	264.8	1.443	24.81	1.36	0.0365	52.9598	0.2886	1451.54	7.91	360.127	1252.462
PO 18	120-125	R	200.01	0.2	247.78	1.459	21.65	1.36	0.0318	49.5554	0.2918	1556.40	9.16	336.960	1589.422
PO 19	0-10	A	200	0.2	0.931	0.098	16.16	1.37	0.0236	0.1862	0.0196	7.893	0.83	1.275	1.275
PO 19	10-20	A/B	200	0.2	0.909	0.125	16.16	1.56	0.0207	0.1818	0.0250	8.775	1.21	1.418	2.693
PO 19	20-30	A/B	200	0.2	1.82	0.176	25.14	1.56	0.0322	0.3640	0.0352	11.294	1.09	2.839	5.532
PO 19	30-40	2Bt	200	0.2	3.933	0.241	28.18	1.59	0.0354	0.7866	0.0482	22.191	1.36	6.253	11.786
PO 19	40-50	2Bt	200	0.2	12.872	0.166	31.22	1.59	0.0393	2.5744	0.0332	65.556	0.85	20.466	32.252
PO 19	50-60	2Bt	200	0.2	31.491	0.263	38.14	1.59	0.0480	6.2982	0.0526	131.281	1.10	50.071	82.323
PO 19	60-70	2Bt	200	0.2	76.81	0.627	39.69	1.59	0.0499	15.3620	0.1254	307.704	2.51	122.128	204.451
PO 19	70-80	2Bt	200.01	0.2	110.1	0.789	41.24	1.59	0.0519	22.0192	0.1578	424.452	3.04	175.044	379.495
PO 19	80-90	2BC	200.01	0.2	115.46	0.944	38.08	1.34	0.0568	23.0928	0.1888	406.287	3.32	154.714	534.209
PO 19	90-100	2BC	200	0.2	106.45	0.78	38.08	1.34	0.0568	21.2900	0.1560	374.588	2.74	142.643	676.852
PO 19	100-110	2BC	200.01	0.2	141.7	0.967	38.14	1.34	0.0569	28.3392	0.1934	497.829	3.40	189.863	866.715
PO 8.5	0-10	A1	200	0.2	1.514	0.065	11.64	1.37	0.0170	0.3028	0.0130	17.823	0.77	2.074	2.074
PO 8.5	10-20	A2	200	0.2	1.811	0.078	20.04	1.37	0.0293	0.3622	0.0156	12.379	0.53	2.481	4.555
PO 8.5	20-30	A/B	200	0.2	3.323	0.072	28.45	1.52	0.0374	0.6646	0.0144	17.755	0.38	5.051	9.606
PO 8.5	30-40	Bt	200.01	0.2	10.029	0.173	33.62	1.59	0.0423	2.0058	0.0346	47.424	0.82	15.945	25.551
PO 8.5	40-50	Bt	200	0.2	17.128	0.322	35.01	1.59	0.0440	3.4256	0.0644	77.799	1.46	27.234	52.785
PO 8.5	50-60	Bt2	200.01	0.2	28.874	0.559	32.60	1.59	0.0410	5.7748	0.1118	140.842	2.73	45.907	98.692
PO 8.5	60-70	Bt2	200	0.2	47.258	0.727	34.76	1.59	0.0437	9.4516	0.1454	216.200	3.33	75.140	173.832
PO 8.5	70-80	Bt2	200	0.2	91.647	1.006	33.84	1.39	0.0487	18.3294	0.2012	376.501	4.13	127.389	301.222

Appendix D. Ponderosa Pine Zone Chloride and Bromide Soil Water Concentrations, and Chloride Residual Flux Data

Core	Depth Range (cm)	Soil Horizon	Weight Leached (g)	H2O Leach (L)	Cl (mg/L)	Br (mg/L)	Vol. Water (%)	Bulk Density (g/cm3)	Soil H2O (L)	Soil Cl (mg)	Soil Br (mg)	Clsw (mg/L)	Brsw (mg/L)	Clswi (g/m3)	Cum Clswi (g/m3)
PO 14	90-100	2BC-R	200	0.2	170.66	1.166	29.38	1.365	0.0431	34.1324	0.2332	792.808	5.42	232.954	1346.341
PO 15	0-10	A	200.01	0.2	2.524	0.076	10.83	1.37	0.0158	0.5048	0.0152	31.942	0.96	3.458	3.458
PO 15	10-20	A/B1	200	0.2	2.75	0.098	10.83	1.52	0.0142	0.5500	0.0196	38.614	1.38	4.180	7.638
PO 15	20-30	A/B1	200.01	0.2	3.868	0.103	11.86	1.52	0.0156	0.7736	0.0206	49.565	1.32	5.879	13.517
PO 15	30-40	A/B2	200.01	0.2	9.622	0.106	12.90	1.52	0.0170	1.9244	0.0212	113.392	1.25	14.625	28.142
PO 15	40-50	2Bt	200.01	0.2	25.923	0.266	25.64	1.59	0.0323	5.1846	0.0532	160.747	1.65	41.216	69.357
PO 15	50-60	2Bt	200.01	0.2	47.68	0.346	30.69	1.59	0.0386	9.5360	0.0692	247.030	1.79	75.807	145.165
PO 15	60-70	2Bt	200.01	0.2	70.845	0.595	35.74	1.59	0.0450	14.1690	0.1190	315.203	2.65	112.638	257.803
PO 15	70-80	2Bt	200.01	0.2	137.35	1.184	36.86	1.59	0.0464	27.4692	0.2368	592.509	5.11	218.369	476.172
PO 15	80-90	2BC	200.01	0.2	164.44	1.253	31.56	1.34	0.0471	32.8882	0.2506	698.079	5.32	220.340	696.512
PO 15	90-100	R	200.01	0.2	174.99	1.43	26.27	1.39	0.0378	34.9982	0.2860	925.779	7.57	243.225	939.737
PO 16	0-10	A	200	0.2	5.975	0.093	12.29	1.37	0.0179	1.1950	0.0186	66.605	1.04	8.186	8.186
PO 16	10-20	A/B	200	0.2	1.947	0.078	12.29	1.52	0.0162	0.3894	0.0156	24.080	0.96	2.959	11.145
PO 16	20-30	A/B	200	0.2	1.507	0.075	13.42	1.52	0.0177	0.3014	0.0150	17.075	0.85	2.291	13.436
PO 16	30-40	A/B	200.01	0.2	6.149	0.119	16.33	1.52	0.0215	1.2298	0.0238	57.250	1.11	9.346	22.782
PO 16	40-50	A/B-2Bt	200.01	0.2	29.93	0.309	19.24	1.54	0.0250	5.9860	0.0618	239.615	2.47	46.090	68.872
PO 16	50-60	2Bt	200.01	0.2	82.783	0.689	26.82	1.59	0.0337	16.5566	0.1378	490.839	4.09	131.618	200.490
PO 16	60-70	2Bt	200.01	0.2	113.9	0.892	26.36	1.59	0.0332	22.7800	0.1784	686.995	5.38	181.092	381.582
PO 16	70-80	2Bt-2BC	200	0.2	119.83	0.956	25.91	1.46	0.0355	23.9658	0.1912	675.354	5.39	174.950	556.533
PO 16	80-90	3Btb	200.01	0.2	153.53	1.245	25.96	1.59	0.0327	30.7056	0.2490	940.282	7.63	244.097	800.630
PO 18	0-10	A	200.01	0.2	1.61	0.05	18.87	1.37	0.0275	0.3220	0.0100	11.691	0.36	2.206	2.206
PO 18	10-20	A/B1	200.01	0.2	2.057	0.049	18.87	1.52	0.0248	0.4114	0.0098	16.573	0.39	3.126	5.332
PO 18	20-30	A/B1	200	0.2	2.188	0.082	19.60	1.52	0.0258	0.4376	0.0164	16.970	0.64	3.326	8.658
PO 18	30-40	A/B1	200.01	0.2	5.145	0.198	21.57	1.52	0.0284	1.0290	0.0396	36.263	1.40	7.820	16.478
PO 18	40-50	A/B2	200.01	0.2	8.432	0.189	23.53	1.52	0.0310	1.6864	0.0378	54.472	1.22	12.816	29.294
PO 18	50-60	2Bt	200	0.2	32.995	0.318	33.29	1.59	0.0419	6.5990	0.0636	157.579	1.52	52.462	81.756
PO 18	60-70	2Bt	200	0.2	57.949	0.434	34.21	1.59	0.0430	11.5898	0.0868	269.333	2.02	92.139	173.895
PO 18	70-80	2Bt	200	0.2	74.135	0.511	35.13	1.59	0.0442	14.8270	0.1022	335.515	2.31	117.875	291.770

Appendix D. Ponderosa Pine Zone Chloride and Bromide Soil Water Concentrations, and Chloride Residual Flux Data

Core	Depth Range (cm)	Soil Horizon	Weight Leached (g)	H2O Leach (L)	Cl (mg/L)	Br (mg/L)	Vol. Water (%)	Bulk Density (g/cm3)	Soil H2O (L)	Soil Cl (mg)	Soil Br (mg)	Clsw (mg/L)	Brsw (mg/L)	Clswi (g/m3)	Cum Clswi (g/m3)
PO 12	0-10	A	200	0.2	1.527	0.094	27.80	1.37	0.0406	0.3054	0.0188	7.525	0.46	2.092	2.092
PO 12	10-20	A/B	200	0.2	1.346	0.085	27.80	1.52	0.0366	0.2692	0.0170	7.359	0.46	2.046	4.138
PO 12	20-30	A/B	200.01	0.2	3.154	0.11	32.60	1.52	0.0429	0.6308	0.0220	14.705	0.51	4.794	8.932
PO 12	30-40	2Bt	200	0.2	10.859	0.225	33.50	1.59	0.0421	2.1718	0.0450	51.540	1.07	17.266	26.198
PO 12	40-50	2Bt	200	0.2	20.96	0.183	34.40	1.59	0.0433	4.1920	0.0366	96.879	0.85	33.326	59.524
PO 12	50-60	2Bt	200.01	0.2	26.057	0.253	36.22	1.59	0.0456	5.2114	0.0506	114.380	1.11	41.429	100.953
PO 13	0-10	A	200.01	0.2	1.404	0.032	22.18	1.37	0.0324	0.2808	0.0064	8.671	0.20	1.923	1.923
PO 13	10-20	E	200	0.2	1.095	0.062	22.18	1.52	0.0292	0.2190	0.0124	7.503	0.42	1.664	3.587
PO 13	20-30	E	200.01	0.2	4.701	0.107	31.84	1.52	0.0419	0.9402	0.0214	22.444	0.51	7.145	10.733
PO 13	30-40	2Bt	200	0.2	31.915	0.269	34.45	1.59	0.0433	6.3830	0.0538	147.304	1.24	50.745	61.477
PO 13	40-50	2Bt	200.01	0.2	45.364	0.291	37.06	1.59	0.0466	9.0728	0.0582	194.604	1.25	72.125	133.603
PO 13	50-60	2Bt	200.01	0.2	81.231	0.428	42.11	1.59	0.0530	16.2462	0.0856	306.735	1.62	129.151	262.753
PO 13	60-70	2Bt	200	0.2	133.66	0.8	37.96	1.59	0.0477	26.7322	0.1600	559.929	3.35	212.521	475.274
PO 13	70-80	2BC	200.01	0.2	126.44	0.694	33.81	1.34	0.0505	25.2884	0.1388	501.180	2.75	169.424	644.698
PO 13	80-90	Cr	200	0.2	110.87	0.682	28.16	1.39	0.0405	22.1736	0.1364	547.253	3.37	154.107	798.805
PO 13	90-100	Cr	200	0.2	111.14	0.738	25.51	1.39	0.0367	22.2280	0.1476	605.584	4.02	154.485	953.289
PO 13	100-110	Cr	200.01	0.2	184.24	1.124	22.93	1.39	0.0330	36.8486	0.2248	1116.86	6.81	256.085	1209.374
PO 13	110-120	Cr	200	0.2	162.25	1.044	18.66	1.39	0.0268	32.4504	0.2088	1208.63	7.78	225.530	1434.905
PO 13	120-130	R	200.01	0.2	112.04	0.721	16.12	1.39	0.0232	22.4074	0.1442	966.177	6.22	155.724	1590.628
PO 14	0-10	A-A/B1	200.01	0.2	3.722	0.057	14.25	1.445	0.0197	0.7444	0.0114	37.740	0.58	5.378	5.378
PO 14	10-20	A/B1	200.01	0.2	1.733	0.149	14.25	1.52	0.0188	0.3466	0.0298	18.484	1.59	2.634	8.012
PO 14	20-30	A/B2	200.01	0.2	1.459	0.143	22.15	1.52	0.0291	0.2918	0.0286	10.012	0.98	2.218	10.230
PO 14	30-40	2Bt	200	0.2	16.856	0.308	27.36	1.59	0.0344	3.3712	0.0616	97.948	1.79	26.801	37.031
PO 14	40-50	2Bt	200.01	0.2	50.665	0.425	32.58	1.59	0.0410	10.1330	0.0850	247.286	2.07	80.553	117.584
PO 14	50-60	2Bt	200.01	0.2	77.63	0.529	38.19	1.59	0.0480	15.5260	0.1058	323.174	2.20	123.426	241.009
PO 14	60-70	2Bt	200	0.2	121.68	0.769	40.08	1.59	0.0504	24.3362	0.1538	482.676	3.05	193.473	434.482
PO 14	70-80	2Bt-2BC	200	0.2	213.56	1.346	38.25	1.465	0.0522	42.7118	0.2692	817.945	5.16	312.864	747.346
PO 14	80-90	2BC	200	0.2	273.17	1.783	34.02	1.34	0.0508	54.6330	0.3566	1076.06	7.02	366.041	1113.387

Appendix D. Ponderosa Pine Zone Chloride and Bromide Soil Water Concentrations, and Chloride Residual Flux Data

Core	Depth Range (cm)	Soil Horizon	Weight Leached (g)	H2O Leach (L)	Cl (mg/L)	Br (mg/L)	Vol. Water (%)	Bulk Density (g/cm3)	Soil H2O (L)	Soil Cl (mg)	Soil Br (mg)	Clsw (mg/L)	Brsw (mg/L)	Clswi (g/m3)	Cum Clswi (g/m3)
PO 8	0-10	A	200.01	0.2	2.275	0.1	23.96	1.37	0.0350	0.4550	0.0200	13.006	0.57	3.117	3.117
PO 8	10-20	A/B	200.01	0.2	1.338	0.094	23.96	1.52	0.0315	0.2676	0.0188	8.487	0.60	2.034	5.151
PO 8	20-30	A/B	200.01	0.2	2.104	0.162	30.31	1.52	0.0399	0.4208	0.0324	10.550	0.81	3.198	8.349
PO 8	30-40	2Bt	200	0.2	4.019	0.266	30.81	1.59	0.0388	0.8038	0.0532	20.743	1.37	6.390	14.739
PO 8	40-50	2BC	200.01	0.2	10.378	0.275	31.30	1.34	0.0467	2.0756	0.0550	44.428	1.18	13.906	28.645
PO 8	50-60	3Btb	200.01	0.2	37.376	0.401	33.16	1.34	0.0495	7.4752	0.0802	151.037	1.62	50.081	78.726
PO 8	60-70	Btb-3BC	200.01	0.2	75.062	0.621	33.61	1.34	0.0502	15.0124	0.1242	299.265	2.48	100.578	179.304
PO 8	70-80	3BCb	200	0.2	192.36	1.253	32.65	1.39	0.0470	38.4716	0.2506	818.921	5.33	267.378	446.682
PO 8	80-90	R	200	0.2	166.29	1.221	28.20	1.39	0.0406	33.2574	0.2442	819.642	6.02	231.139	677.821
PO 8.5	0-10	A1	200	0.2	1.514	0.065	11.64	1.37	0.0170	0.3028	0.0130	17.823	0.77	2.074	2.074
PO 8.5	10-20	A2	200	0.2	1.811	0.078	20.04	1.37	0.0293	0.3622	0.0156	12.379	0.53	2.481	4.555
PO 8.5	20-30	A/B	200	0.2	3.323	0.072	28.45	1.52	0.0374	0.6646	0.0144	17.755	0.38	5.051	9.606
PO 8.5	30-40	Bt	200.01	0.2	10.029	0.173	33.62	1.59	0.0423	2.0058	0.0346	47.424	0.82	15.945	25.551
PO 8.5	40-50	Bt	200	0.2	17.128	0.322	35.01	1.59	0.0440	3.4256	0.0644	77.799	1.46	27.234	52.785
PO 8.5	50-60	Bt2	200.01	0.2	28.874	0.559	32.60	1.59	0.0410	5.7748	0.1118	140.842	2.73	45.907	98.692
PO 8.5	60-70	Bt2	200	0.2	47.258	0.727	34.76	1.59	0.0437	9.4516	0.1454	216.200	3.33	75.140	173.832
PO 8.5	70-80	Bt2	200	0.2	91.647	1.006	33.84	1.39	0.0487	18.3294	0.2012	376.501	4.13	127.389	301.222
PO 9	80-90	2BC-R	200.01	0.2	87.1	0.93	30.25	1.365	0.0443	17.4200	0.1860	393.065	4.20	118.886	420.107
PO 10	0-10	A	200.01	0.2	2.092	0.069	14.36	1.37	0.0210	0.4184	0.0138	19.963	0.66	2.866	2.866
PO 10	10-20	A/B	200.01	0.2	1.316	0.096	14.36	1.52	0.0189	0.2632	0.0192	13.933	1.02	2.000	4.866
PO 10	20-30	A/B	200	0.2	1.907	0.103	19.45	1.52	0.0256	0.3814	0.0206	14.902	0.80	2.899	7.765
PO 10	30-40	A/B	200.01	0.2	4.536	0.127	23.41	1.52	0.0308	0.9072	0.0254	29.451	0.82	6.894	14.659
PO 10	40-50	2Bt	200	0.2	9.488	0.132	27.37	1.59	0.0344	1.8976	0.0264	55.118	0.77	15.086	29.745
PO 10	50-60	2Bt	200	0.2	17.908	0.174	29.16	1.59	0.0367	3.5816	0.0348	97.642	0.95	28.474	58.219
PO 10	60-70	2Bt	200.01	0.2	41.098	0.388	29.75	1.59	0.0374	8.2196	0.0776	219.639	2.07	65.343	123.561
PO 10	70-80	2BC	200.01	0.2	74.912	0.708	30.34	1.34	0.0453	14.9824	0.1416	330.868	3.13	100.377	223.938
PO 10	80-90	2BC	200	0.2	146.09	1.362	25.61	1.34	0.0382	29.2170	0.2724	764.290	7.13	195.754	419.692
PO 10	90-100	R	200	0.2	113.02	0.956	23.33	1.39	0.0336	22.6032	0.1912	673.493	5.70	157.092	576.785

Appendix D. Ponderosa Pine Zone Chloride and Bromide Soil Water Concentrations, and Chloride Residual Flux Data

Core	Depth Range (cm)	Soil Horizon	Weight Leached (g)	H2O Leach (L)	Cl (mg/L)	Br (mg/L)	Vol. Water (%)	Bulk Density (g/cm3)	Soil H2O (L)	Soil Cl (mg)	Soil Br (mg)	Clsw (mg/L)	Brsw (mg/L)	Clswi (g/m3)	Cum Clswi (g/m3)
PO 4	50-60	2Bt/Cr1	200.01	0.2	12.592	0.221	25.70	1.49	0.0345	2.5184	0.0442	73.001	1.28	18.761	61.494
PO 4	60-70	Cr1	200.01	0.2	18.022	0.273	26.56	1.39	0.0382	3.6044	0.0546	94.318	1.43	25.049	86.543
PO 4	70-80	Cr1	200.01	0.2	24.497	0.347	30.28	1.39	0.0436	4.8994	0.0694	112.466	1.59	34.049	120.593
PO 4	80-90	Cr1	200.01	0.2	68.552	0.788	26.48	1.39	0.0381	13.7104	0.1576	359.896	4.14	95.283	215.875
PO 4	90-100	Cr2	200.01	0.2	83.23	0.991	23.31	1.39	0.0335	16.6460	0.1982	496.320	5.91	115.684	331.559
PO 4	100-110	Cr/Bt	200.01	0.2	117.86	1.262	20.78	1.49	0.0279	23.5724	0.2524	845.274	9.05	175.606	507.165
PO 4	110-120	Cr/Bt	200.01	0.2	75.745	0.759	22.01	1.49	0.0295	15.1490	0.1518	512.780	5.14	112.854	620.019
PO 4	120-130	R	200.01	0.2	76.103	0.684	19.93	1.39	0.0287	15.2206	0.1368	530.658	4.77	105.778	725.797
PO 5	0-10	A	200.01	0.2	1.801	0.087	17.89	1.37	0.0261	0.3602	0.0174	13.793	0.67	2.467	2.467
PO 5	10-20	A/B	200.01	0.2	2.04	0.097	17.89	1.52	0.0235	0.4080	0.0194	17.334	0.82	3.101	5.568
PO 5	20-30	A/B	200	0.2	3.8	0.112	26.01	1.52	0.0342	0.7600	0.0224	22.211	0.65	5.776	11.344
PO 5	30-40	2Bt	200	0.2	5.786	0.179	27.55	1.59	0.0347	1.1572	0.0358	33.390	1.03	9.200	20.543
PO 5	40-50	2Bt	200	0.2	11.025	0.22	29.1	1.59	0.0366	2.2050	0.0440	60.240	1.20	17.530	38.073
PO 5	50-60	2Bt/Cr	200.01	0.2	14.061	0.248	22.59	1.46	0.0309	2.8122	0.0496	90.882	1.60	20.528	58.601
PO 5	60-70	Cr1	200	0.2	5.646	0.13	23.04	1.34	0.0344	1.1292	0.0260	32.840	0.76	7.566	66.167
PO 5	70-80	Cr1	200	0.2	7.556	0.116	23.82	1.34	0.0356	1.5112	0.0232	42.506	0.65	10.125	76.292
PO 5	80-90	Cr1	200.01	0.2	32.507	0.358	24.95	1.34	0.0372	6.5014	0.0716	174.560	1.92	43.557	119.849
PO 5	90-100	Cr2	200	0.2	46.207	0.424	23.5	1.34	0.0351	9.2414	0.0848	263.501	2.42	61.917	181.766
PO 5	100-110	Cr/Bt	200.01	0.2	70.139	0.591	22.04	1.46	0.0302	14.0278	0.1182	464.542	3.91	102.398	284.164
PO 5	110-120	R	200.01	0.2	74.172	0.649	19.59	1.39	0.0282	14.8344	0.1298	526.191	4.60	103.094	387.258
PO 5	120-130	R	200.01	0.2	80.734	0.676	15.29	1.39	0.0220	16.1468	0.1352	734.029	6.15	112.215	499.473
PO 7	0-10	A/A/B	200	0.2	7.562	0.044	24.48	1.445	0.0339	1.5124	0.0088	44.646	0.26	10.927	10.927
PO 7	10-20	A/B	200.01	0.2	2.999	0.048	24.48	1.52	0.0322	0.5998	0.0096	18.624	0.30	4.558	15.485
PO 7	20-30	A/B	200	0.2	2.211	0.069	30.28	1.52	0.0398	0.4422	0.0138	11.101	0.35	3.361	18.846
PO 7	30-40	2Bt	200	0.2	6.404	0.188	29.71	1.59	0.0374	1.2808	0.0376	34.277	1.01	10.182	29.028
PO 7	40-50	2Bt/2BtC	200.01	0.2	10.446	0.26	29.14	1.49	0.0391	2.0892	0.0520	53.415	1.33	15.564	44.592
PO 7	50-60	2BtCr	200.01	0.2	20.676	0.278	31.38	1.39	0.0452	4.1352	0.0556	91.583	1.23	28.738	73.330
PO 7	60-70	Cr	200	0.2	70.327	0.545	32.50	1.39	0.0468	14.0654	0.1090	300.745	2.33	97.755	171.085

Appendix D. Ponderosa Pine Zone Chloride and Bromide Soil Water Concentrations, and Chloride Residual Flux Data

Core	Depth Range (cm)	Soil Horizon	Weight Leached (g)	H2O Leach (L)	Cl (mg/L)	Br (mg/L)	Vol. Water (%)	Bulk Density (g/cm3)	Soil H2O (L)	Soil Cl (mg)	Soil Br (mg)	Clsw (mg/L)	Brsw (mg/L)	Clswi (g/m3)	Cum Clswi (g/m3)
PO 2	30-40	Bt1	200	0.2	6.511	0.254	26.11	1.59	0.0328	1.3022	0.0508	39.646	1.55	10.352	23.172
PO 2	40-50	Bt2	200.01	0.2	15.481	0.345	24.37	1.59	0.0306	3.0962	0.0690	101.020	2.25	24.614	47.785
PO 2	50-56	Bt2	200.01	0.2	34.634	0.465	24.11	1.59	0.0303	6.9268	0.0930	228.392	3.07	55.065	102.851
PO 2	56-66	Bt2-2Cr1	200	0.2	29.959	0.249	23.86	1.46	0.0327	5.9918	0.0498	183.358	1.52	43.740	146.591
PO 2	66-75	2Cr1	200	0.2	50.965	0.468	24.27	1.34	0.0362	10.1930	0.0936	281.447	2.58	68.293	214.884
PO 2	75-85	2Cr2	200.01	0.2	91.086	0.752	22.18	1.34	0.0331	18.2172	0.1504	550.267	4.54	122.049	336.933
PO 2	85-93	2Cr2	200	0.2	106.49	0.82	20.18	1.34	0.0301	21.2978	0.1640	707.112	5.44	142.695	479.628
PO 2	93-101	2Cr2	200.01	0.2	90.043	0.559	17.83	1.34	0.0266	18.0086	0.1118	676.602	4.20	120.652	600.280
PO 2	101-110	2Cr2	200	0.2	131.9	0.884	15.49	1.34	0.0231	26.3804	0.1768	1141.42	7.65	176.749	777.029
PO 2	110-120	2Cr3	200.01	0.2	75.142	0.508	13.84	1.34	0.0207	15.0284	0.1016	727.757	4.92	100.685	877.714
PO 2	120-123	R	200	0.2	82.998	0.457	13.31	1.39	0.0191	16.5996	0.0914	867.097	4.77	115.367	993.081
PO 3	0-10	A1	200	0.2	2.547	0.126	26.20	1.37	0.0382	0.5094	0.0252	13.318	0.66	3.489	3.489
PO 3	10-20	A2	200.01	0.2	2.271	0.131	26.20	1.37	0.0383	0.4542	0.0262	11.874	0.68	3.111	6.600
PO 3	20-30	A2-Bt	200.01	0.2	4.119	0.176	28.55	1.48	0.0386	0.8238	0.0352	21.351	0.91	6.096	12.696
PO 3	30-40	Bt	200.01	0.2	4.74	0.221	27.85	1.59	0.0350	0.9480	0.0442	27.060	1.26	7.536	20.232
PO 3	40-47	Bt	200.01	0.2	9.136	0.239	27.15	1.59	0.0342	1.8272	0.0478	53.501	1.40	14.526	34.758
PO 3	47-52	Cr1	200	0.2	22.475	0.255	25.93	1.39	0.0373	4.4950	0.0510	120.502	1.37	31.240	65.998
PO 3	52-61	Cr1	200.01	0.2	32.893	0.351	24.70	1.39	0.0355	6.5786	0.0702	185.097	1.98	45.719	111.717
PO 3	61-70	Cr2	200	0.2	36.738	0.327	25.88	1.39	0.0372	7.3476	0.0654	197.356	1.76	51.066	162.783
PO 3	70-80	Cr2	200	0.2	84.782	0.605	27.05	1.39	0.0389	16.9564	0.1210	435.664	3.11	117.847	280.630
PO 3	80-90	Cr2	200.01	0.2	132.84	1.007	22.58	1.39	0.0325	26.5680	0.2014	817.587	6.20	184.638	465.268
PO 3	90-98	Cr2	200.01	0.2	177.99	1.234	19.91	1.39	0.0286	35.5980	0.2468	1242.56	8.61	247.394	712.662
PO 3	98-110	Cr2	200	0.2	148.99	1.053	18.70	1.39	0.0269	29.7984	0.2106	1107.48	7.83	207.099	919.761
PO 4	0-10	A	200.01	0.2	1.68	0.078	24.00	1.37	0.0350	0.3360	0.0156	9.590	0.45	2.301	2.301
PO 4	10-20	A/B	200.01	0.2	4.702	0.1	24.00	1.52	0.0316	0.9404	0.0200	29.778	0.63	7.147	9.448
PO 4	20-30	A/B	200.01	0.2	8.499	0.189	27.63	1.52	0.0364	1.6998	0.0378	46.761	1.04	12.918	22.366
PO 4	30-40	2Bt	200.01	0.2	5.78	0.183	27.66	1.59	0.0348	1.1560	0.0366	33.221	1.05	9.190	31.555
PO 4	40-50	2Bt	200	0.2	7.03	0.18	27.70	1.59	0.0348	1.4060	0.0360	40.353	1.03	11.178	42.733

Appendix D. Ponderosa Pine Zone Chloride and Bromide Soil Water Concentrations, and Chloride Residual Flux Data

Core	Depth Range (cm)	Soil Horizon	Weight Leached (g)	H2O Leach (L)	Cl (mg/L)	Br (mg/L)	Vol. Water (%)	Bulk Density (g/cm3)	Soil H2O (L)	Soil Cl (mg)	Soil Br (mg)	Clsw (mg/L)	Brsw (mg/L)	Clswi (g/m3)	Cum Clswi (g/m3)
LJ1	55	2Bt	100	0.1	19.252	1.749	31.38	1.590	0.0197	1.9252	0.1749	97.554	8.86	30.611	86.482
LJ1	65	2Bt	200	0.2	42.776	1.786	26.33	1.590	0.0331	8.5552	0.3572	258.318	10.79	68.014	154.496
LJ1	75	2Bt	200	0.2	77.169	0.991	26.99	1.590	0.0339	15.4338	0.1982	454.622	5.84	122.699	277.194
LJ1	85	2BC	200	0.2	113.77	1.458	30.91	1.340	0.0461	22.7536	0.2916	493.170	6.32	152.449	429.643
LJ1	95	2BC-R	200	0.2	168.78	1.334	28.82	1.360	0.0424	33.7554	0.2668	796.399	6.29	229.537	659.180
LJ1	105	R	100	0.1	204.53	1.222	34.77	1.390	0.025	20.4527	0.1222	817.723	4.89	284.293	943.473
LJ1	115	R	100	0.1	344.21	2.175	27.41	1.390	0.0197	34.4210	0.2175	1745.70	11.03	478.452	1421.924
LJ1	125	R	100	0.1	129.45	0.893	23.66	1.390	0.017	12.9454	0.0893	760.394	5.25	179.941	1601.866
LJ1	135	R	50	0.05	106.33	0.619	9.446	1.390	0.0034	5.3165	0.0310	1564.66	9.11	147.799	1749.664
LJ1	145	R	100	0.1	91.189	0.534	7.424	1.390	0.0053	9.1189	0.0534	1707.22	10.00	126.753	1876.417
LJ1	155	R	100	0.1	123.47	0.724	35.36	1.390	0.0254	12.3465	0.0724	485.389	2.85	171.616	2048.033
LJ1	165	R	50	0.05	113.99	0.755	38.57	1.390	0.0139	5.6995	0.0378	410.763	2.72	158.446	2206.479
LJ1	175	R	50	0.05	205.57	1.426	42.32	1.390	0.0152	10.2786	0.0713	675.230	4.68	285.744	2492.223
LJ1	185	R	100	0.1	54.956	0.428	4.048	1.390	0.0029	5.4956	0.0428	1887.17	14.70	76.389	2568.612
LJ1	195	R	100	0.1	43.176	0.321	4.51	1.390	0.0032	4.3176	0.0321	1330.58	9.89	60.015	2628.627
LJ1	205	R	100	0.1	72.26	0.463	5.989	1.390	0.0043	7.2260	0.0463	1677.12	10.75	100.441	2729.068
LJ1	215	R	100	0.1	98.992	0.610	11.66	1.390	0.0084	9.8992	0.0610	1179.88	7.27	137.599	2866.667
LJ1	225	R	100	0.1	47.017	0.335	4.796	1.390	0.0035	4.7017	0.0335	1362.54	9.71	65.354	2932.020
LJ1	235	R	100	0.1	72.964	0.507	7.998	1.390	0.0058	7.2964	0.0507	1268.13	8.81	101.420	3033.440
LJ1	245	R	100	0.1	58.855	0.370	9.096	1.390	0.0065	5.8855	0.0370	899.410	5.65	81.808	3115.249
LJ1	255	R	100	0.1	43.339	0.296	8.076	1.390	0.0058	4.3339	0.0296	745.913	5.09	60.241	3175.490
PO 2	0-10	A1	200.01	0.2	1.595	0.051	22.06	1.37	0.0322	0.3190	0.0102	9.905	0.32	2.185	2.185
PO 2	10-20	A2	200	0.2	2.123	0.075	24.96	1.37	0.0364	0.4246	0.0150	11.653	0.41	2.909	5.094
PO 2	20-30	Bt1	200	0.2	4.859	0.079	27.86	1.59	0.0350	0.9718	0.0158	27.731	0.45	7.726	12.819

Appendix D. Ponderosa Pine Zone Chloride and Bromide Soil Water Concentrations, and Chloride Residual Flux Data

Core	Depth Range (cm)	Soil Horizon	Weight Leached (g)	H2O Leach (L)	Cl (mg/L)	Br (mg/L)	Vol. Water (%)	Bulk Density (g/cm3)	Soil H2O (L)	Soil Cl (mg)	Soil Br (mg)	Clsw (mg/L)	Brsw (mg/L)	Clswi (g/m3)	Cum Clswi (g/m3)
Br 3	80-85	2BC	200.01	0.2	65.181	4.791	31.68	1.34	0.0473	13.0362	0.9582	275.659	20.26	87.338	408.905
Br 4	0-10	A	200.01	0.2	0.727	1.222	16.70	1.37	0.0244	0.1454	0.2444	5.964	10.02	0.996	0.996
Br 4	10-20	A/B	200	0.2	0.953	2.408	16.70	1.52	0.0220	0.1906	0.4816	8.674	21.92	1.449	2.445
Br 4	20-30	A/B	200	0.2	1.557	46.945	14.40	1.52	0.0189	0.3114	9.3890	16.435	495.53	2.367	4.811
Br 4	30-40	2Bt	200	0.2	7.186	229.24	16.25	1.59	0.0204	1.4372	45.8480	70.312	2243.03	11.426	16.237
Br 4	40-50	2Bt	200	0.2	16.584	114.49	18.10	1.59	0.0228	3.3168	22.8986	145.683	1005.77	26.369	42.606
Br 4	50-60	2Bt-2BC	200	0.2	23.513	12.908	24.67	1.465	0.0337	4.7026	2.5816	139.648	76.66	34.447	77.052
Br 4	60-70	2BC	200	0.2	38.805	1.08	27.82	1.59	0.0350	7.7610	0.2160	221.809	6.17	61.700	138.752
Br 4	70-80	2BC	200.01	0.2	49.964	1.303	27.55	1.34	0.0411	9.9928	0.2606	243.007	6.34	66.948	205.700
Br 4	80-90	2BC	200.01	0.2	68.135	0.9	31.68	1.34	0.0473	13.6270	0.1800	288.152	3.81	91.296	296.997
Br 4	90-100	2BC	200	0.2	117.83	1.284	32.73	1.34	0.0489	23.5658	0.2568	482.355	5.26	157.891	454.888
Br 4	100-110	R	200.01	0.2	223.96	1.546	30.70	1.39	0.0442	44.7914	0.3092	1013.96	7.00	311.285	766.172
Br 5	0-20	A	200	0.2	1.081	7.231	10.32	1.37	0.0151	0.2162	1.4462	14.347	95.97	1.481	1.481
Br 5	20-30	A	200	0.2	1.842	32.465	19.91	1.37	0.0291	0.3684	6.4930	12.676	223.42	2.524	4.005
Br 5	30-40	A/B	200	0.2	5.231	93.018	24.38	1.52	0.0321	1.0462	18.6036	32.612	579.91	7.951	11.956
Br 5	40-50	Bt1	200.01	0.2	16.228	134.21	24.38	1.59	0.0307	3.2456	26.8426	105.826	875.23	25.801	37.757
Br 5	50-60	Bt2	200	0.2	40.107	132.82	19.91	1.59	0.0250	8.0214	26.5630	320.332	1060.79	63.770	101.527
Br 5	60-70	Bt3	200	0.2	88.819	79.911	30.13	1.59	0.0379	17.7638	15.9822	468.670	421.67	141.222	242.749
Br 5	70-80	Bt/Cr	200	0.2	108.52	17.774	33.92	1.49	0.0455	21.7042	3.5548	476.699	78.08	161.696	404.446
Br 5	80-90	Cr	200.01	0.2	180.25	4.453	31.27	1.39	0.0450	36.0500	0.8906	801.199	19.79	250.535	654.980
Br 5	90-100	Cr	200.01	0.2	170.5	6.219	32.99	1.39	0.0475	34.1000	1.2438	718.312	26.20	236.983	891.964
Br 5	100-110	Cr	200.01	0.2	216.96	3.839	31.74	1.39	0.0457	43.3920	0.7678	950.167	16.81	301.559	1193.523
LJ1	5	A	100	0.1	6.103	0.318	14.08	1.370	0.0103	0.6103	0.0318	59.379	3.09	8.361	8.361
LJ1	15	Bw	100	0.1	7.567	0.444	13.61	1.560	0.0087	0.7567	0.0444	86.715	5.09	11.805	20.166
LJ1	25	Bw	100	0.1	9.546	0.360	8.081	1.560	0.0052	0.9546	0.0360	184.292	6.95	14.892	35.057
LJ1	35	Bw	200	0.2	2.842	0.403	6.121	1.560	0.0078	0.5684	0.0806	72.436	10.27	4.434	39.491
LJ1	45	2Bt	100	0.1	10.302	3.328	29.69	1.590	0.0187	1.0302	0.3328	55.172	17.82	16.380	55.871

Appendix D. Ponderosa Pine Zone Chloride and Bromide Soil Water Concentrations, and Chloride Residual Flux Data

Core	Depth Range (cm)	Soil Horizon	Weight Leached (g)	H2O Leach (L)	Cl (mg/L)	Br (mg/L)	Vol. Water (%)	Bulk Density (g/cm3)	Soil H2O (L)	Soil Cl (mg)	Soil Br (mg)	Clsw (mg/L)	Brsw (mg/L)	Clswi (g/m3)	Cum Clswi (g/m3)
Br 1	0-10	A	200.01	0.2	1.307	0.406	16.70	1.37	0.0244	0.2614	0.0812	10.722	3.33	1.791	1.791
Br 1	10-20	A/B1	200	0.2	2.295	1.76	16.70	1.52	0.0220	0.4590	0.3520	20.889	16.02	3.488	5.279
Br 1	20-30	A/B1	200.01	0.2	1.855	5.268	14.40	1.52	0.0189	0.3710	1.0536	19.580	55.60	2.819	8.099
Br 1	30-40	A/B2	200	0.2	3.354	117.07	16.25	1.52	0.0214	0.6708	23.4148	31.373	1095.09	5.098	13.197
Br 1	40-50	A/B2	200	0.2	16.372	191.51	18.10	1.52	0.0238	3.2744	38.3020	137.489	1608.26	24.885	38.082
Br 1	50-60	A/B2	200.01	0.2	46.032	82.755	24.67	1.52	0.0325	9.2064	16.5510	283.642	509.92	69.965	108.048
Br 1	60-70	2Bt	200.01	0.2	83.131	7.869	27.82	1.59	0.0350	16.6262	1.5738	475.153	44.98	132.172	240.219
Br 1	70-8	2Bt	200.01	0.2	85.804	3.796	27.55	1.59	0.0347	17.1608	0.7592	495.178	21.91	136.422	376.641
Br 1	80-90	2Bt	200.01	0.2	101.17	4.964	31.68	1.59	0.0399	20.2342	0.9928	507.692	24.91	160.854	537.495
Br 1	90-100	2Bt	200	0.2	169.31	3.659	32.73	1.59	0.0412	33.8618	0.7318	822.407	17.77	269.201	806.696
Br 1	100-110	2Bt-R	200.01	0.2	248.21	3.945	30.70	1.49	0.0412	49.6424	0.7890	1204.62	19.15	369.817	1176.51
Br 2	0-10	A	200.01	0.2	0.5	0.355	16.70	1.37	0.0244	0.1000	0.0710	4.102	2.91	0.685	0.685
Br 2	10-20	A/B	200.01	0.2	1.627	2.268	16.70	1.52	0.0220	0.3254	0.4536	14.808	20.64	2.473	3.158
Br 2	20-30	A/B	200.01	0.2	2.46	71.285	14.40	1.52	0.0189	0.4920	14.2570	25.965	752.42	3.739	6.897
Br 2	30-40	2Bt1	200.01	0.2	5.177	245.81	16.25	1.59	0.0204	1.0354	49.1620	50.652	2405.04	8.231	15.128
Br 2	40-50	2Bt1	200.01	0.2	11.737	181.69	18.10	1.59	0.0228	2.3474	36.3380	103.099	1595.98	18.661	33.789
Br 2	50-60	2Bt2	200.01	0.2	33.494	55.134	24.67	1.59	0.0310	6.6988	11.0268	215.889	355.37	53.253	87.042
Br 2	60-70	2Bt2	200.01	0.2	72.221	6.307	27.82	1.59	0.0350	14.4442	1.2614	412.794	36.05	114.826	201.867
Br 2	70-80	2BC	200.01	0.2	84.588	3.907	27.55	1.34	0.0411	16.9176	0.7814	411.406	19.00	113.342	315.210
Br 2	80-90	2BC	200.01	0.2	106.38	1.814	31.68	1.34	0.0473	21.2758	0.3628	449.892	7.67	142.541	457.750
Br 3	0-10	A	200	0.2	0.518	0.347	16.70	1.37	0.0244	0.1036	0.0694	4.249	2.85	0.710	0.710
Br 3	10-20	A/B1	200.01	0.2	0.976	1.673	16.70	1.52	0.0220	0.1952	0.3346	8.883	15.23	1.483	2.193
Br 3	20-30	A/B1	200.01	0.2	1.855	31.53	14.40	1.52	0.0189	0.3710	6.3060	19.580	332.80	2.819	5.013
Br 3	30-40	A/B1-B2	200	0.2	4.527	250.22	16.25	1.52	0.0214	0.9054	50.0440	42.345	2340.52	6.881	11.894
Br 3	40-50	A/B2	200.01	0.2	35.722	52.895	18.10	1.52	0.0238	7.1444	10.5790	299.971	444.18	54.295	66.189
Br 3	50-60	2Bt	200.01	0.2	44.692	7.087	24.67	1.59	0.0310	8.9384	1.4174	288.067	45.68	71.057	137.245
Br 3	60-70	2Bt	200.01	0.2	51.92	2.369	27.82	1.59	0.0350	10.3840	0.4738	296.760	13.54	82.549	219.794
Br 3	70-80	2Bt-2BC	200.01	0.2	69.473	1.496	27.55	1.465	0.0376	13.8946	0.2992	369.411	7.95	101.773	321.567

APPENDIX E: Graphs of Soil-Water Chloride Concentrations with depth for the Ponderosa Pine Zone Cores

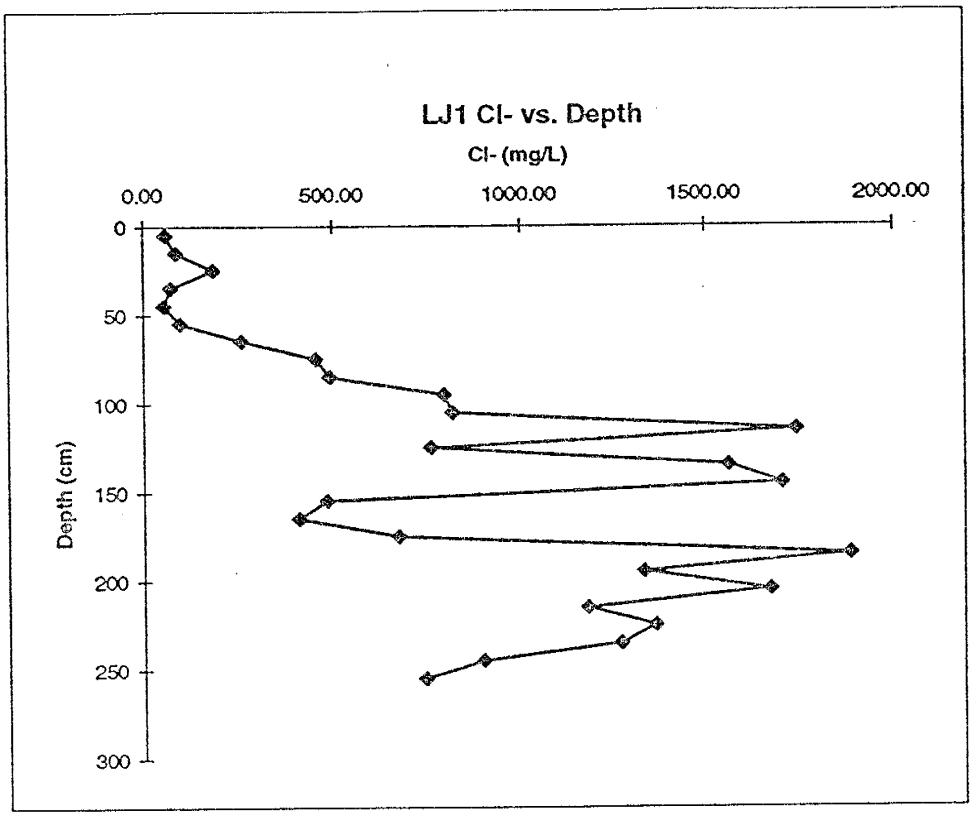
LJ1 Cl- vs. Depth
Cl- (mg/L)
0.00
500.00
1000.00
1500.00
2000.00
Depth (cm)
0
50
100
150
200
250
300

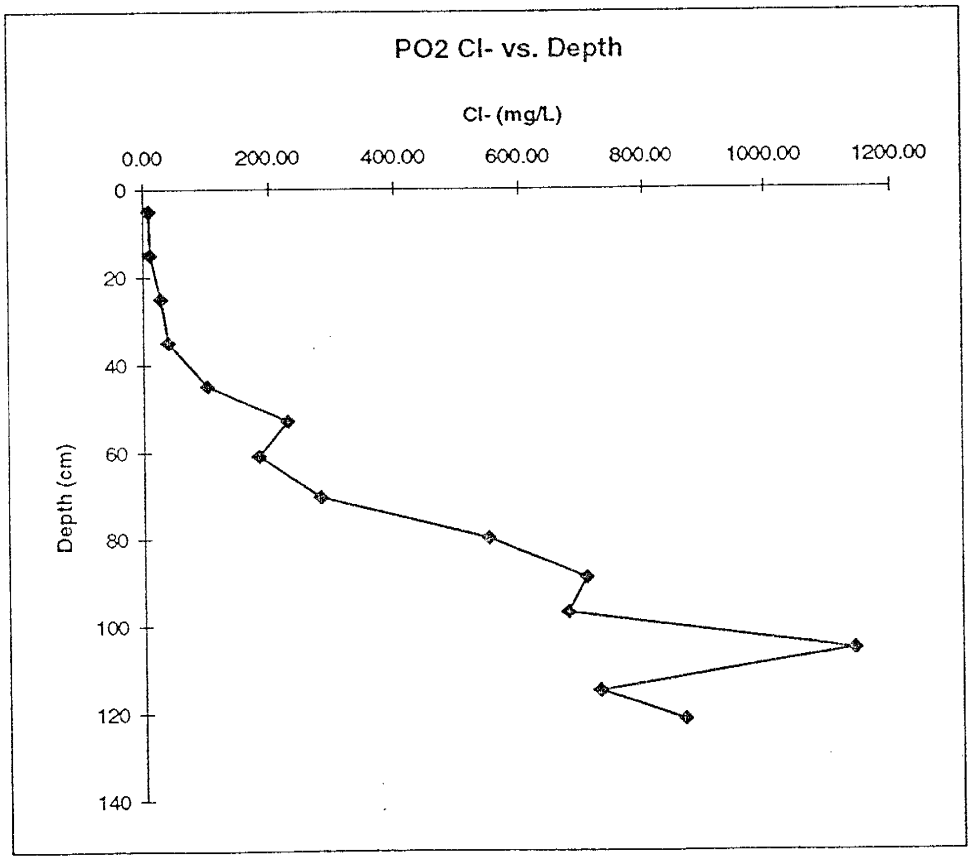
PO2 Cl- vs. Depth
Cl- (mg/L)
0.00
200.00
400.00
600.00
800.00
1000.00
1200.00
Depth (cm)
0
20
40
60
80
100
120
140

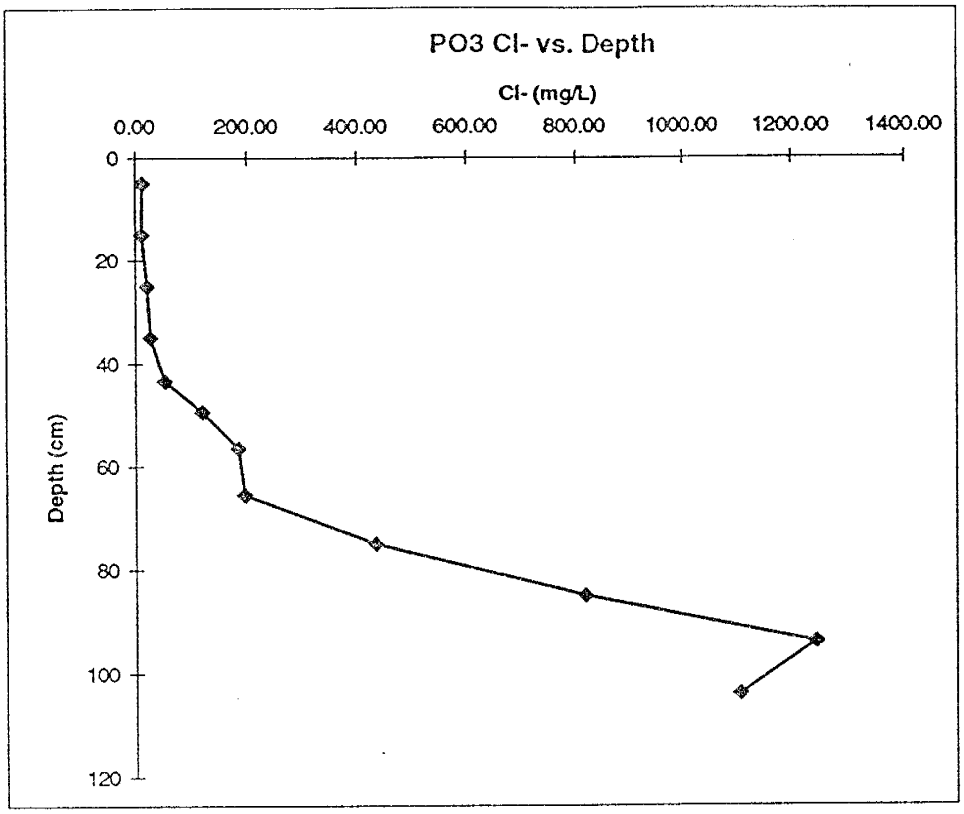
PO3 Cl- vs. Depth
Cl- (mg/L)
0.00
200.00
400.00
600.00
800.00
1000.00
1200.00
1400.00
Depth (cm)
0
20
40
60
80
100
120

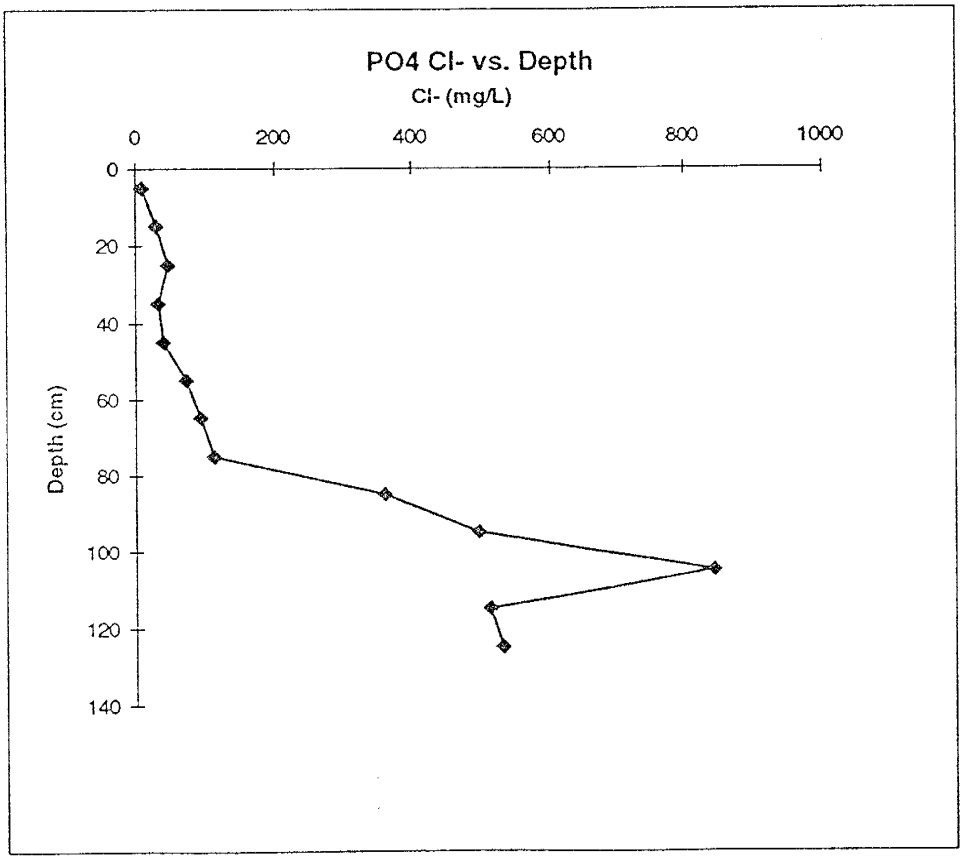
PO4 Cl- vs. Depth
Cl- (mg/L)
0
200
400
600
800
1000
Depth (cm)
0
20
40
60
80
100
120
140

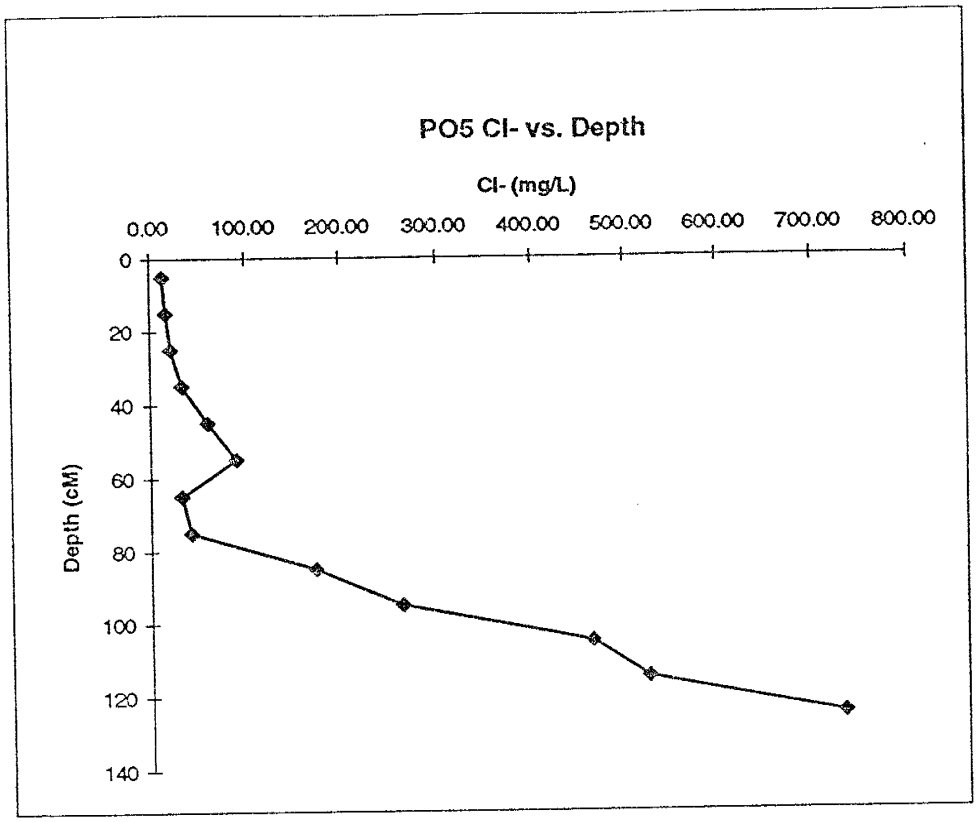
PO5 Cl- vs. Depth
Cl- (mg/L)
0.00
100.00
200.00
300.00
400.00
500.00
600.00
700.00
800.00
0
20
40
60
80
100
120
140
Depth (cM)

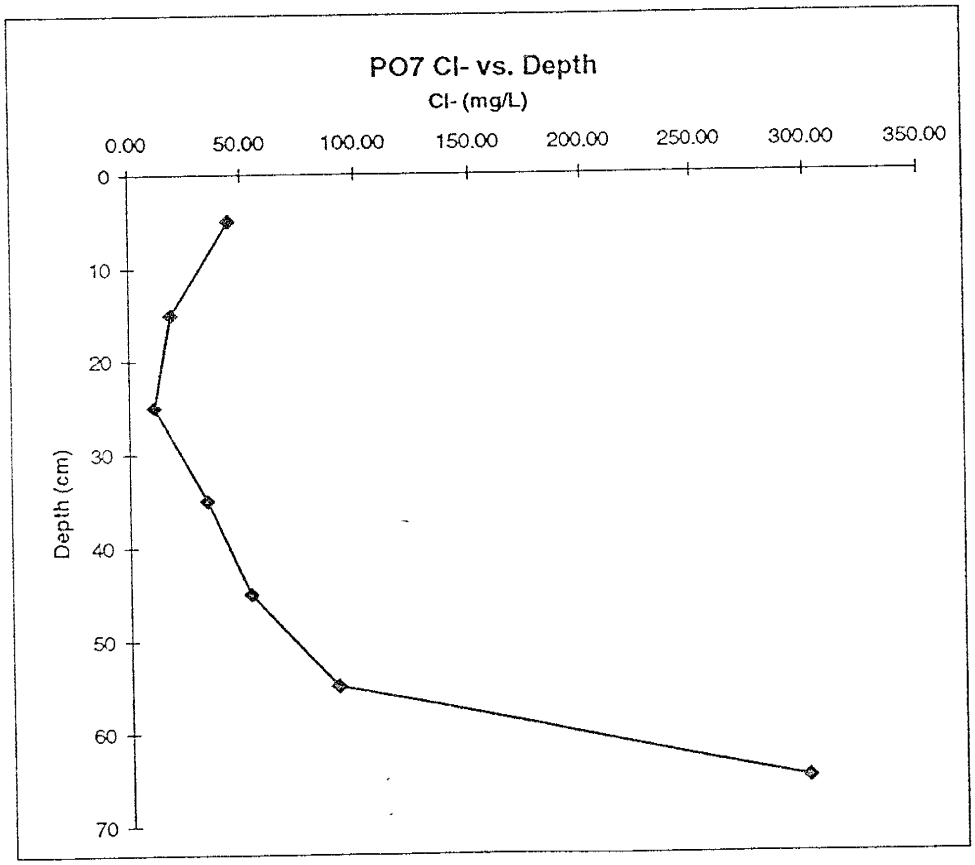
PO7 Cl- vs. Depth
Cl- (mg/L)
0.00
50.00
100.00
150.00
200.00
250.00
300.00
350.00
0
10
20
30
40
50
60
70
Depth (cm)

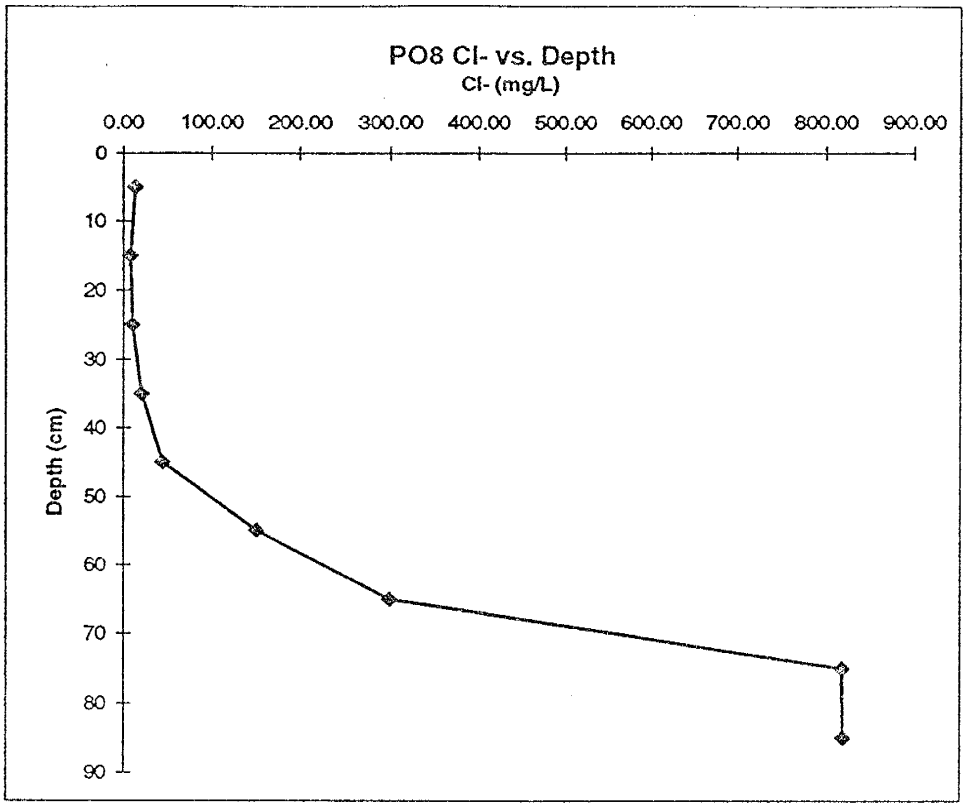
PO8 Cl- vs. Depth
Cl- (mg/L)
0.00
100.00
200.00
300.00
400.00
500.00
600.00
700.00
800.00
900.00
Depth (cm)
0
10
20
30
40
50
60
70
80
90

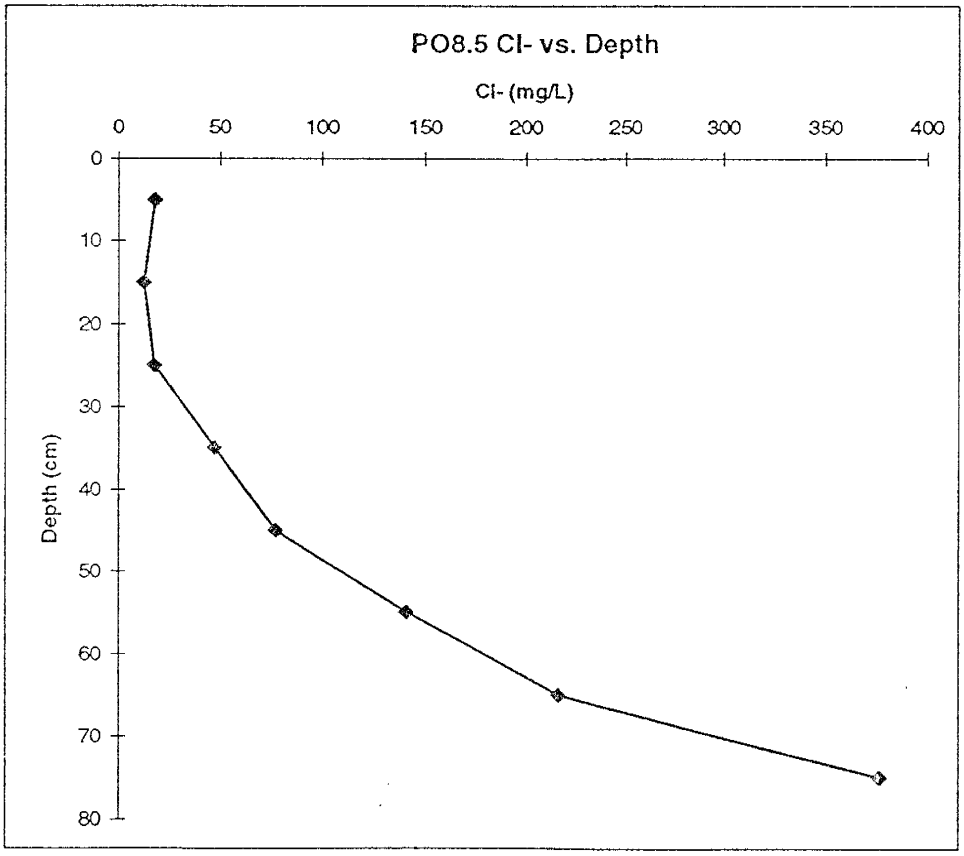
PO8.5 Cl- vs. Depth
Cl- (mg/L)
0
50
100
150
200
250
300
350
400
Depth (cm)
0
10
20
30
40
50
60
70
80

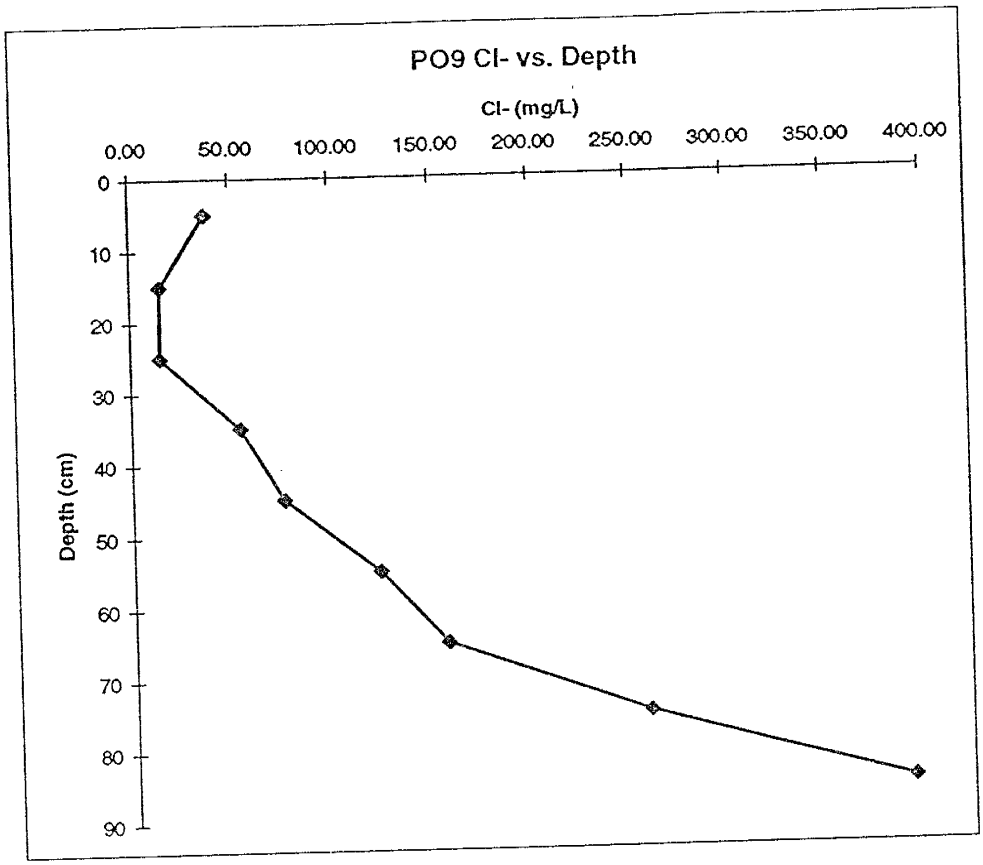
PO9 Cl- vs. Depth
Cl- (mg/L)
0.00
50.00
100.00
150.00
200.00
250.00
300.00
350.00
400.00
Depth (cm)
0
10
20
30
40
50
60
70
80
90

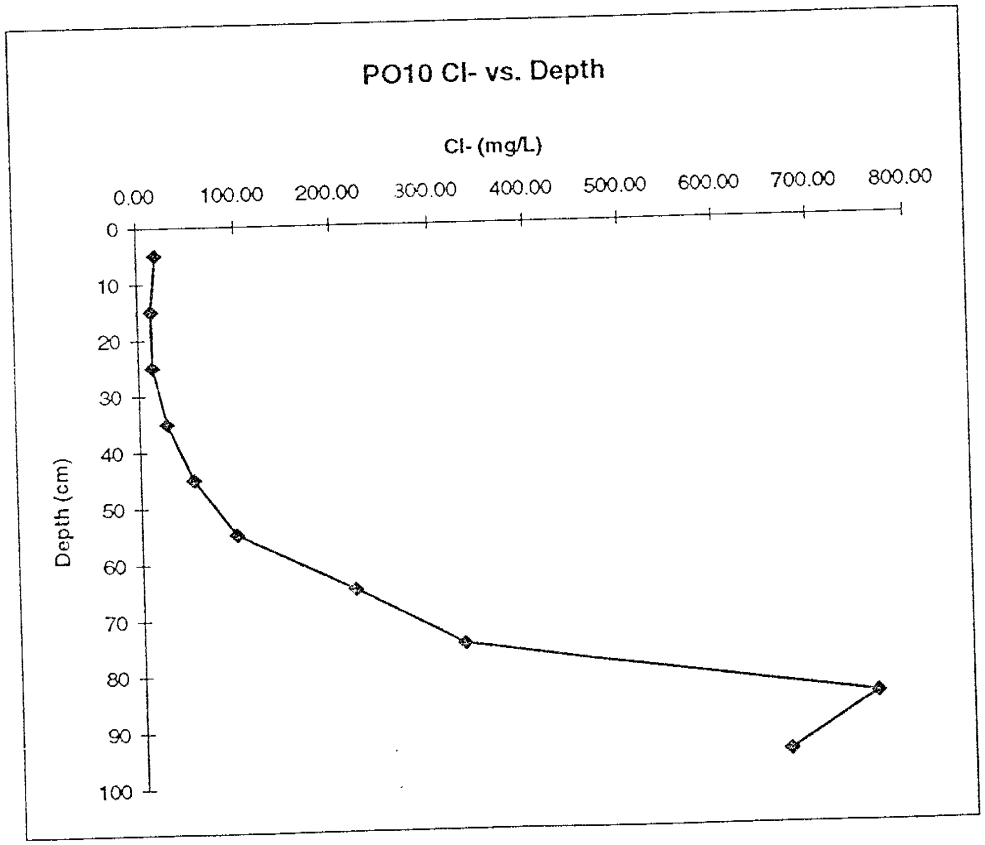
PO10 Cl- vs. Depth
Cl- (mg/L)
0.00
100.00
200.00
300.00
400.00
500.00
600.00
700.00
800.00
Depth (cm)
0
10
20
30
40
50
60
70
80
90
100

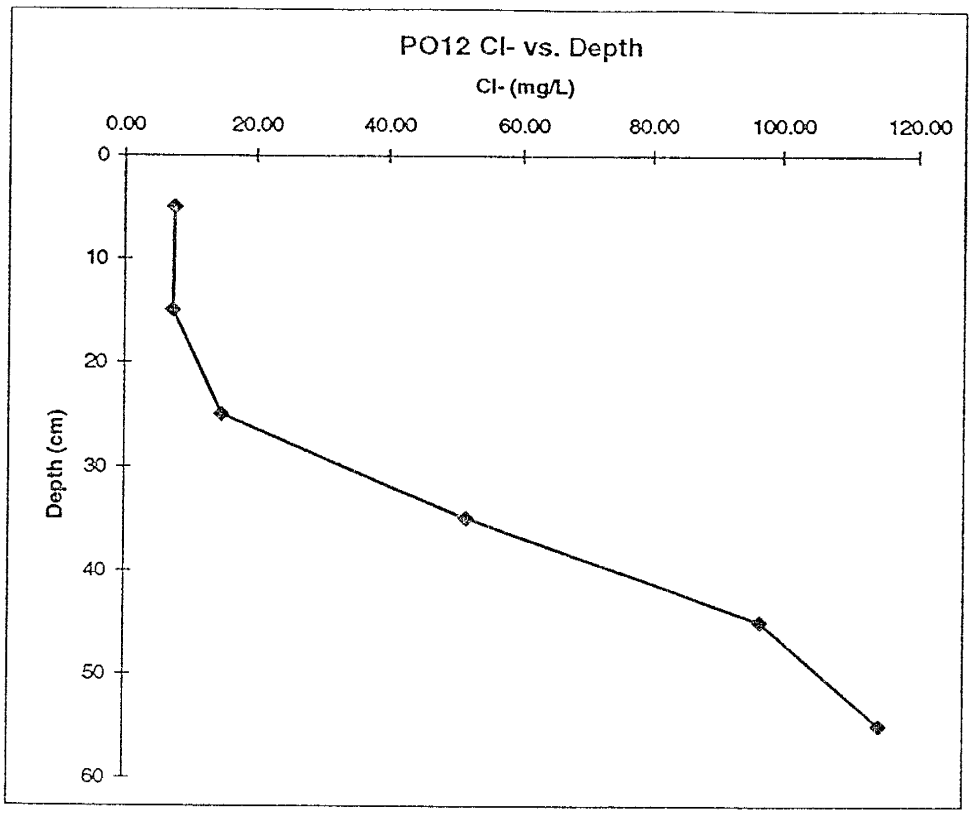
PO12 Cl- vs. Depth
Cl- (mg/L)
0.00
20.00
40.00
60.00
80.00
100.00
120.00
0
10
20
30
40
50
60
Depth (cm)

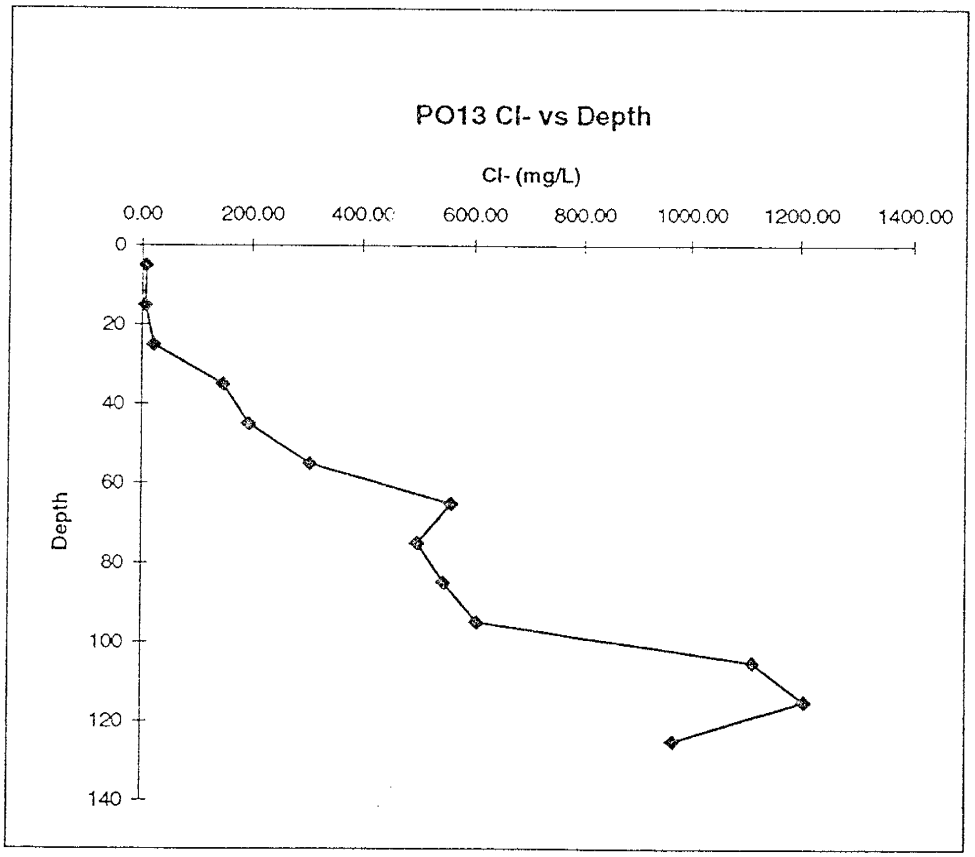
PO13 Cl- vs Depth
Cl- (mg/L)
0.00
200.00
400.00
600.00
800.00
1000.00
1200.00
1400.00
0
20
40
60
80
100
120
140
Depth

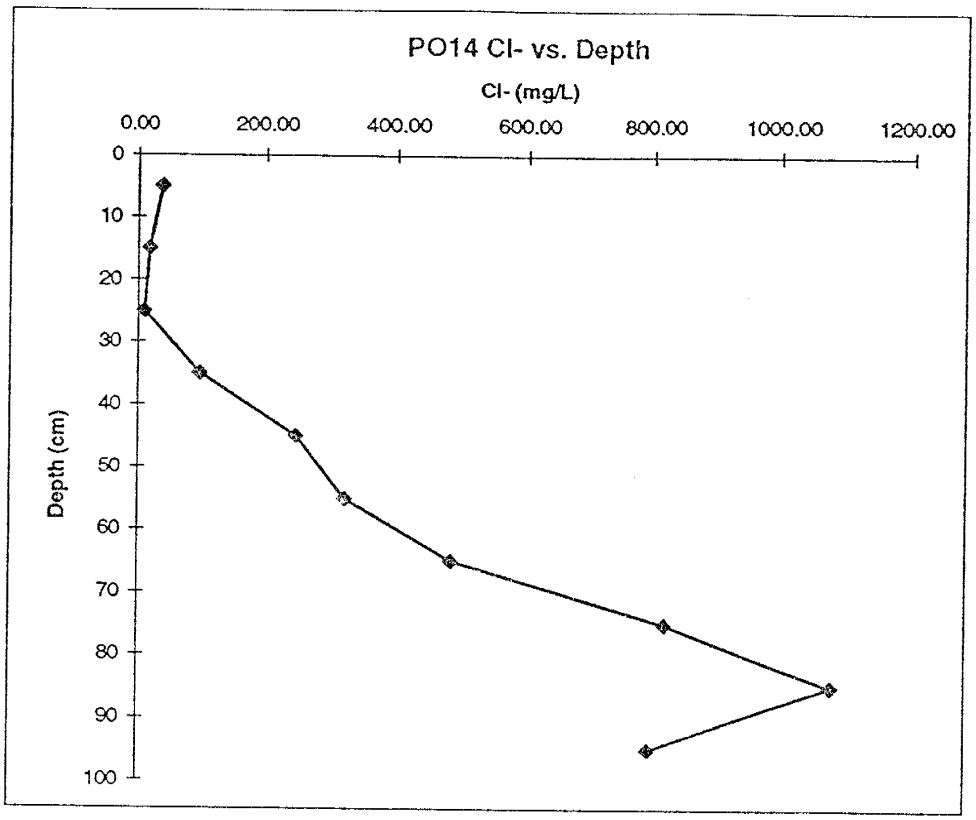
PO14 Cl- vs. Depth
Cl- (mg/L)
0.00
200.00
400.00
600.00
800.00
1000.00
1200.00
Depth (cm)
0
10
20
30
40
50
60
70
80
90
100

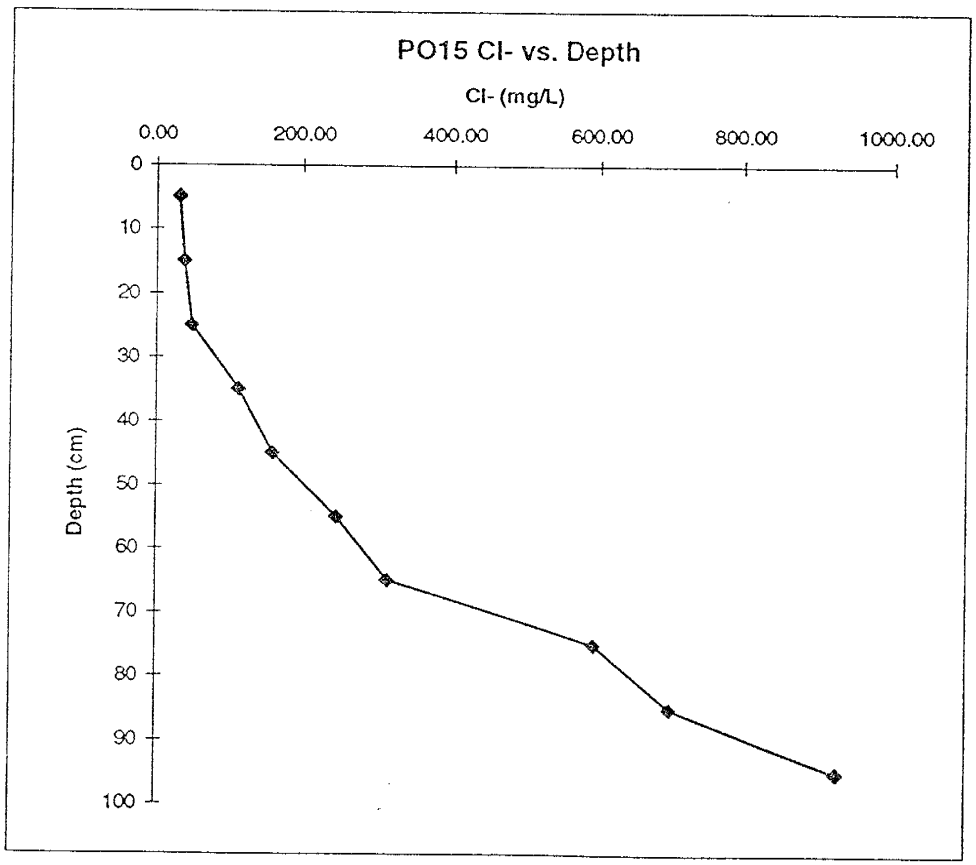
PO15 Cl- vs. Depth
Cl- (mg/L)
0.00
200.00
400.00
600.00
800.00
1000.00
Depth (cm)
0
10
20
30
40
50
60
70
80
90
100

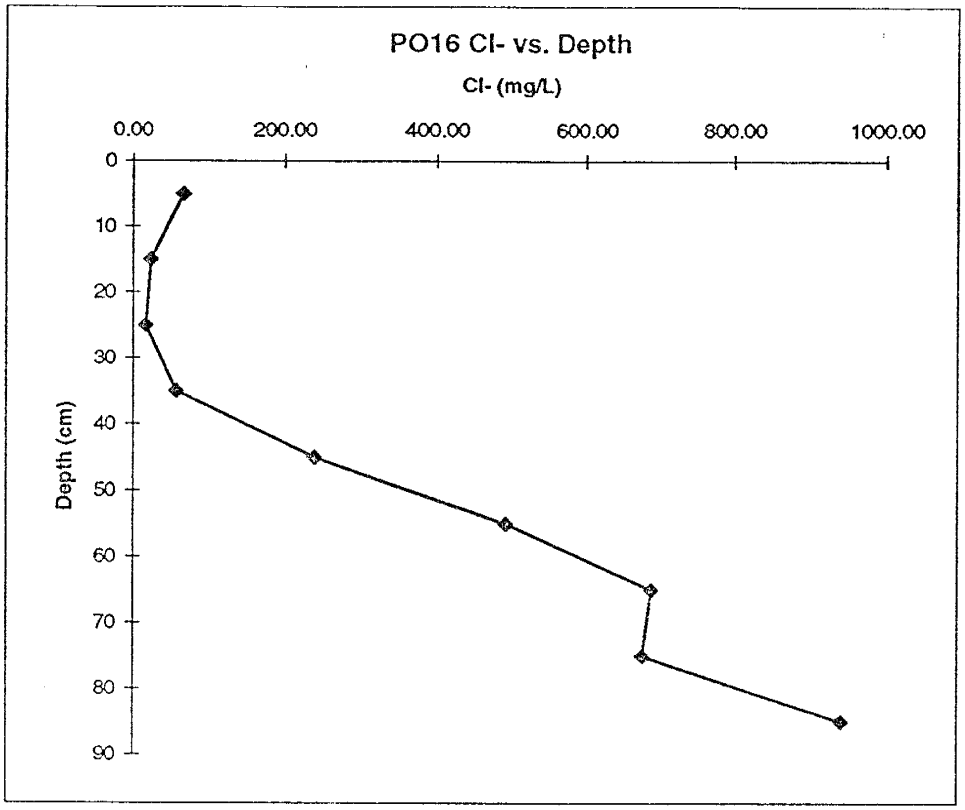
PO16 Cl- vs. Depth
Cl- (mg/L)
0.00
200.00
400.00
600.00
800.00
1000.00
Depth (cm)
0
10
20
30
40
50
60
70
80
90

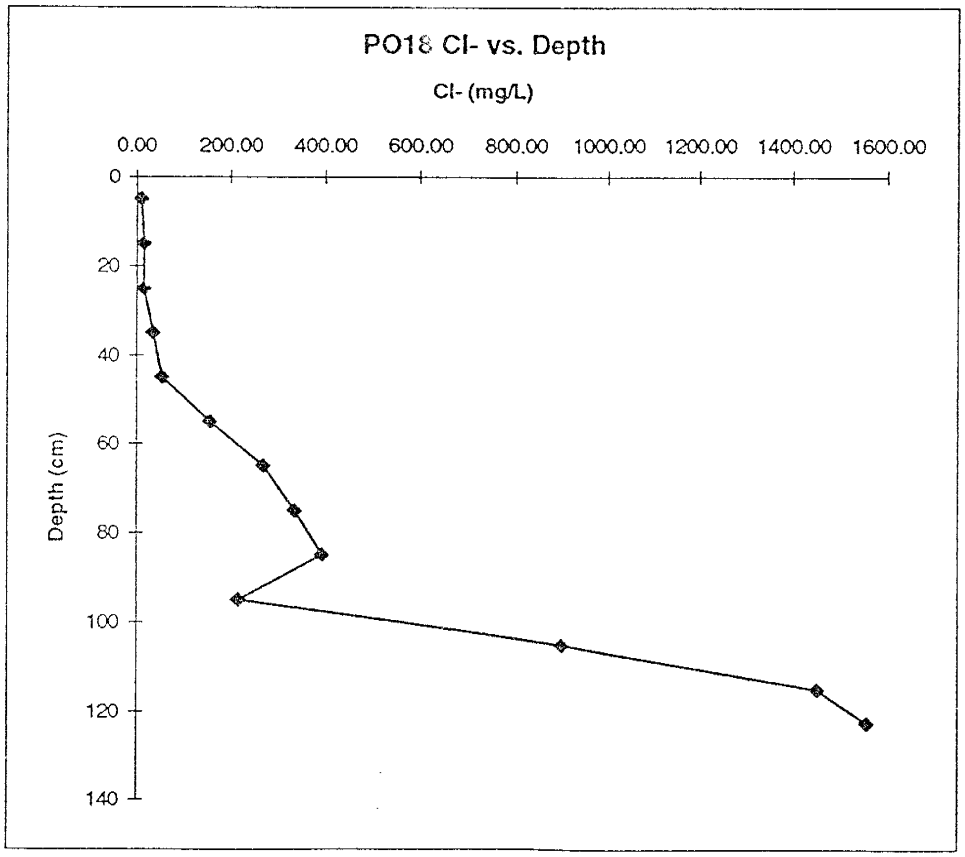
PO18 Cl- vs. Depth
Cl- (mg/L)
0.00
200.00
400.00
600.00
800.00
1000.00
1200.00
1400.00
1600.00
Depth (cm)
0
20
40
60
80
100
120
140

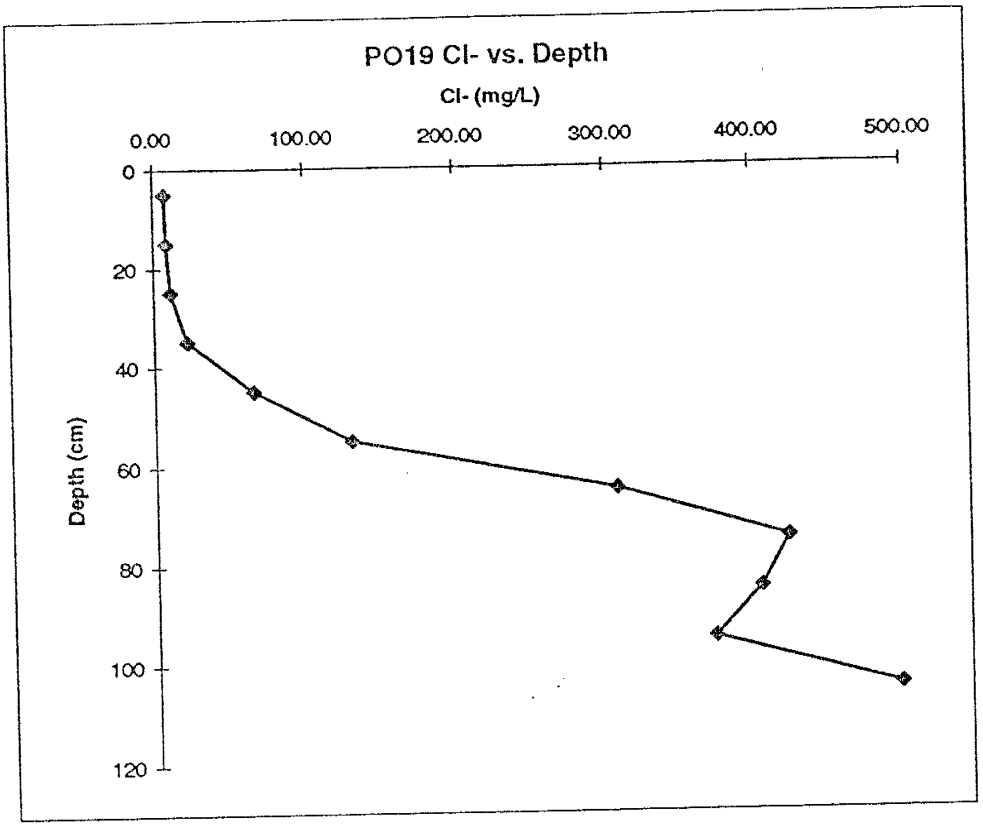
PO19 Cl- vs. Depth
Cl- (mg/L)
0.00
100.00
200.00
300.00
400.00
500.00
Depth (cm)
0
20
40
60
80
100
120

APPENDIX F: Chloride and Bromide in Soil Waters From the Pinyon-Juniper Zone Cores

Appendix F. Pinyon-Juniper Zone Chloride and Bromide Soil Water Concentrations, and Chloride Residual Flux Data

Core	Depth Range (cm)	Soil Horizon	Bulk density (g/cm3)	Gravim. Water Content %	Volum. water Content (%)	Cl (mg/L)	Br (mg/L)	H2O leach (L)	Soil (g)	Soil H20 (L)	Soil Cl (mg)	Soil Br (mg)	Clsw (mg/L)	Brsw (mg/L)	Clswi (g/m3)	Cum Clswi (g/m3)
PJ1	0-10	Ap	1.49	8.673	12.923	2.719	0.496	0.1	100	0.0087	0.2719	0.0496	31.35	5.72	4.05	4.05
PJ1	10-20	Ap	1.49	8.008	11.932	1.761	0.484	0.2	200	0.0160	0.3522	0.0968	21.99	6.04	2.62	6.68
PJ1	20-30	Bt	1.49	6.518	9.711	1.632	0.681	0.2	200	0.0130	0.3264	0.1362	25.04	10.45	2.43	9.11
PJ1	30-40	Bt	1.49	7.330	10.922	2.118	0.978	0.2	200	0.0147	0.4236	0.1956	28.89	13.34	3.16	12.26
PJ1	40-50	C-Cr	1.59	14.058	22.352	1.077	1.059	0.2	200	0.0281	0.2154	0.2118	7.66	7.53	1.71	13.98
PJ1	50-60	Cr	1.59	12.477	19.839	2.317	0.705	0.2	200	0.0250	0.4634	0.1410	18.57	5.65	3.68	17.66
PJ1	60-70	Cr	1.59	12.214	19.420	6.287	0.625	0.1	100	0.0122	0.6287	0.0625	51.47	5.12	10.00	27.66
PJ1	70-80	Cr	1.59	20.732	32.963	9.14	1.138	0.1	100	0.0207	0.9140	0.1138	44.09	5.49	14.53	42.19
PJ1	80-90	Cr	1.39	4.854	6.748	5.789	0.124	0.1	100	0.0049	0.5789	0.0124	119.25	2.55	8.05	50.23
PJ1	90-100	Cr	1.39	5.023	6.981	7.38	0.15	0.2	200	0.0100	1.4760	0.0300	146.94	2.99	10.26	60.49
PJ1	100-11	Cr	1.39	5.059	7.032	14.792	0.399	0.2	200	0.0101	2.9584	0.0798	292.40	7.89	20.56	81.05
PJ1	110-12	Cr	1.39	4.250	5.908	15.709	0.229	0.2	200	0.0085	3.1418	0.0458	369.59	5.39	21.84	102.89
PJ1	120-13	Cr	1.39	4.739	6.587	15.902	0.239	0.2	200	0.0095	3.1804	0.0478	335.57	5.04	22.10	124.99
PJ 2	0-10	A1	1.45	20.537	20.537	2.363	0	0.2	200	0.0283	0.4726	0.0000	16.68	0.00	3.43	3.43
PJ 2	10-20	A/B	1.52	20.537	20.537	2.267	0	0.2	200	0.0270	0.4534	0.0000	16.78	0.00	3.45	6.87
PJ 2	20-30	A/B	1.52	21.972	21.972	1.603	0.09	0.2	200	0.0289	0.3206	0.0180	11.09	0.62	2.44	9.31
PJ 2	30-40	A/B	1.52	24.844	24.844	1.304	0.108	0.2	200	0.0327	0.2608	0.0216	7.98	0.66	1.98	11.29
PJ 2	40-50	Bt1	1.59	26.738	26.738	1.767	0.114	0.2	200	0.0336	0.3534	0.0228	10.51	0.68	2.81	14.10
PJ 2	50-60	Bt2	1.59	27.654	27.654	1.875	0.067	0.2	200	0.0348	0.3750	0.0134	10.78	0.39	2.98	17.08
PJ 2	60-70	BC	1.34	24.879	24.879	1.58	0.071	0.2	200	0.0371	0.3160	0.0142	8.51	0.38	2.12	19.20
PJ 2	70-80	Btb	1.34	18.414	18.414	1.444	0.071	0.2	200	0.0275	0.2888	0.0142	10.51	0.52	1.93	21.13
PJ 2	80-90	Cr	1.39	13.896	13.896	1.342	0.071	0.2	200	0.0200	0.2684	0.0142	13.42	0.71	1.87	23.00
PJ 2	90-100	R	1.39	11.325	11.325	1.058	0.151	0.2	200	0.0163	0.2116	0.0302	12.99	1.85	1.47	24.47
PJ 12	0-10	A	1.45	4.252	6.166	4.979	0.15	0.2	200	0.0085	0.9958	0.0300	117.09	3.53	7.22	7.22
PJ 12	10-20	A	1.45	7.431	10.775	6.927	0.235	0.2	200	0.0149	1.3854	0.0470	93.21	3.16	10.04	17.26
PJ 12	20-30	B/A	1.52	10.043	15.266	7.392	0.697	0.2	200	0.0201	1.4784	0.1394	73.60	6.94	11.24	28.50
PJ 12	30-40	Bt	1.59	15.156	24.097	12.777	1.534	0.2	200	0.0303	2.5554	0.3068	84.31	10.12	20.32	48.82

Appendix F. Pinyon-Juniper Zone Chloride and Bromide Soil Water Concentrations, and Chloride Residual Flux Data

Core	Depth Range (cm)	Soil Horizon	Bulk density (g/cm3)	Gravim. Water Content %	Volum. water Content (%)	Cl (mg/L)	Br (mg/L)	H2O leach (L)	Soil (g)	Soil H20 (L)	Soil Cl (mg)	Soil Br (mg)	Clsw (mg/L)	Brsw (mg/L)	Clswi (g/m3)	Cum Clswi (g/m3)
PJ 12	40-50	Bt-R	1.49	6.220	9.268	5.178	0.181	0.2	200	0.0124	1.0356	0.0362	83.24	2.91	7.72	56.53
PJ 12	50-60	R	1.39	6.385	8.875	1.112	0.118	0.2	200	0.0128	0.2224	0.0236	17.42	1.85	1.55	58.08
PJ 12	60-70	R	1.39	6.519	9.061	1.314	0.133	0.2	200	0.0130	0.2628	0.0266	20.16	2.04	1.83	59.90
PJ 18	0-10	A	1.45	6.469	9.380	8.089	0.28	0.2	200	0.0129	1.6178	0.0560	125.04	4.33	11.73	11.73
PJ 18	10-20	A/B	1.52	9.840	14.957	7.247	0.782	0.2	200	0.0197	1.4494	0.1564	73.65	7.95	11.02	22.74
PJ 18	20-30	A/B	1.52	11.176	16.988	3.479	0.692	0.2	200	0.0224	0.6958	0.1384	31.13	6.19	5.29	28.03
PJ 18	30-40	Bt	1.59	9.400	14.945	2.122	0.64	0.2	200	0.0188	0.4244	0.1280	22.58	6.81	3.37	31.41
PJ 18	40-50	Bt	1.59	15.342	24.394	2.208	0.786	0.2	200	0.0307	0.4416	0.1572	14.39	5.12	3.51	34.92
PJ 18	50-60	Cr	1.39	11.074	15.393	1.607	0.746	0.2	200	0.0221	0.3214	0.1492	14.51	6.74	2.23	37.15
PJ 16	0-10	A-Bt	1.52	4.454	6.770			0.2	200	0.0089	0.0000	0.0000	0.00	0.00	0.00	-
PJ 16	10-20	Bt	1.59	13.335	21.203	2.057	0.807	0.2	200	0.0267	0.4114	0.1614	15.43	6.05	3.27	3.27
PJ 16	20-30	Bt/Cr	1.49	10.212	15.215	1.651	0.822	0.2	200	0.0204	0.3302	0.1644	16.17	8.05	2.46	5.73
PJ 72	0-10	A	1.45	5.099	7.394	8.335	0.234	0.2	200	0.0102	1.6670	0.0468	163.45	4.59	12.09	12.09
PJ 72	10-20	B/A	1.52	7.217	10.970	5.797	0.721	0.2	200	0.0144	1.1594	0.1442	80.32	9.99	8.81	20.90
PJ 72	20-30	B/A	1.52	6.757	10.270	5.109	0.593	0.2	200	0.0135	1.0218	0.1186	75.61	8.78	7.77	28.66
PJ 72	30-40	B/A	1.52	9.163	13.928	4.057	0.829	0.2	200	0.0183	0.8114	0.1658	44.27	9.05	6.17	34.83
PJ 72	40-50	Bt1	1.59	7.916	12.586	4.019	0.697	0.2	200	0.0158	0.8038	0.1394	50.77	8.81	6.39	41.22
PJ 70	0-10	A	1.45	4.062	5.890	8.64	0.429	0.2	200	0.0081	1.7280	0.0858	212.71	10.56	12.53	12.53
PJ 70	10-20	B/A	1.52	6.353	9.657	7.239	0.735	0.2	200	0.0127	1.4478	0.1470	113.94	11.57	11.00	23.53
PJ 70	20-30	B/A	1.52	7.794	11.847	2.584	0.548	0.2	200	0.0156	0.5168	0.1096	33.15	7.03	3.93	27.46
PJ 70	30-40	B/A	1.52	10.226	15.543	1.835	0.591	0.2	200	0.0205	0.3670	0.1182	17.94	5.78	2.79	30.25
PJ 70	40-50	Bt1	1.59	11.577	18.408	1.969	0.787	0.2	200	0.0232	0.3938	0.1574	17.01	6.80	3.13	33.38
PJ 70	50-60	Bt1	1.59	12.449	19.794	1.769	0.516	0.2	200	0.0249	0.3538	0.1032	14.21	4.14	2.81	36.19
PJ 70	60-70	Bt2	1.59	16.084	25.574	2.938	1.51	0.2	200	0.0322	0.5876	0.3020	18.27	9.39	4.67	40.86
PJ 70	70-80	Cr	1.39	7.417	10.310	1.487	0.436	0.2	200	0.0148	0.2974	0.0872	20.05	5.88	2.07	42.93
PJ 70	80-90	R	1.39	4.628	6.433	1.105	0.149	0.2	200	0.0093	0.2210	0.0298	23.87	3.22	1.54	44.47
PJ 70	90-100	R	1.39	5.168	7.184	12.102	0.91	0.2	200	0.0103	2.4204	0.1820	234.17	17.61	16.82	61.29

Appendix F. Pinyon-Juniper Zone Chloride and Bromide Soil Water Concentrations, and Chloride Residual Flux Data

Core	Depth Range (cm)	Soil Horizon	Bulk density (g/cm3)	Gravim. Water Content %	Volum. water Content (%)	Cl (mg/L)	Br (mg/L)	H2O leach (L)	Soil (g)	Soil H20 (L)	Soil Cl (mg)	Soil Br (mg)	Clsw (mg/L)	Brsw (mg/L)	Clswi (g/m3)	Cum Clswi (g/m3)
PJ 70	100-11	R	1.39	2.945	4.093	3.85	0.192	0.2	200	0.0059	0.7700	0.0384	130.74	6.52	5.35	66.64
EP2	0-10	A	1.49	10.3	15.347	8.24	0.601	0.1	100	0.0103	0.824	0.06	80.00	5.83	12.28	12.278
EP2	10-20	A	1.49	12.65	18.8485	3.211	1.686	0.1	100	0.0127	0.3211	0.17	25.38	13.33	4.78	17.062
EP2	20-30	A	1.49	10.74	16.0026	1.74	1.706	0.1	100	0.0107	0.174	0.17	16.20	15.88	2.59	19.655
EP2	30-40	A	1.49	10.46	15.5854	2.754	2.191	0.1	100	0.0105	0.2754	0.22	26.33	20.95	4.10	23.758
EP2	40-50	Bt	1.59	9.16	14.5644	16.029	1.332	0.1	100	0.0092	1.6029	0.13	174.99	14.54	25.49	49.245
EP2	50-60	Bt	1.59	6.74	10.7166	28.019	0.707	0.1	100	0.0067	2.8019	0.07	415.71	10.49	44.55	93.795
EP2	60-70	Bt	1.59	9.11	14.4849	52.919	0.997	0.1	100	0.0091	5.2919	0.10	580.89	10.94	84.14	177.94
EP2	70-80	Cr	1.39	9.15	12.7185	37.468	0.586	0.1	100	0.0092	3.7468	0.06	409.49	6.40	52.08	230.02
EP2	80-90	Cr	1.39	9.41	13.0799	51.49	0.716	0.1	100	0.0094	5.149	0.07	547.18	7.61	71.57	301.59
EP2	90-100	Cr	1.39	2.63	3.6557	38.852	0.637	0.1	100	0.0026	3.8852	0.06	1477.3	24.22	54.00	355.59
EP2	100-11	Cr	1.39	2.6	3.614	17.503	0.306	0.1	100	0.0026	1.7503	0.03	673.19	11.77	24.33	379.92
EP2	110-12	Cr	1.39	2.28	3.1692	12.265	0.28	0.1	100	0.0023	1.2265	0.03	537.94	12.28	17.05	396.97
EP2	120-13	R	1.39	2.64	3.6696	12.698	0.255	0.1	100	0.0026	1.2698	0.03	480.98	9.66	17.65	414.62
EP2	130-14	R	1.39	2.79	3.8781	13.462	0.28	0.1	100	0.0028	1.3462	0.03	482.51	10.04	18.71	433.33
EP3	0-10	A	1.45	8.6	12.47	4.927	0.491	0.1	100	0.0086	0.4927	0.05	57.29	5.71	7.14	7.144
EP3	10-20	A	1.45	9.75	14.1375	6.831	1.369	0.1	100	0.0098	0.6831	0.14	70.06	14.04	9.90	17.049
EP3	20-30	A	1.45	9.79	14.1955	1.651	1.159	0.1	100	0.0098	0.1651	0.12	16.86	11.84	2.39	19.443
EP3	30-40	A	1.45	10.26	14.877	1.432	1.055	0.1	100	0.0103	0.1432	0.11	13.96	10.28	2.08	21.519
EP3	40-50	Bt	1.59	10.39	16.5201	1.131	0.921	0.1	100	0.0104	0.1131	0.09	10.89	8.86	1.80	23.318
EP3	50-60	Bt	1.59	8.01	12.7359	1.381	0.569	0.1	100	0.008	0.1381	0.06	17.24	7.10	2.20	25.513
EP3	60-70	Bt	1.59	8.64	13.7376	2.179	1.01	0.1	100	0.0086	0.2179	0.10	25.22	11.69	3.46	28.978
EP3	70-80	Cr	1.39	6.61	9.1879	0.969	0.143	0.1	100	0.0066	0.0969	0.01	14.66	2.16	1.35	30.325
EP3	80-90	Cr	1.39	14.65	20.3635	1.574	0.683	0.1	100	0.0147	0.1574	0.07	10.74	4.66	2.19	32.513
EP3	90-100	Cr	1.39	6.81	9.4659	1.268	0.156	0.1	100	0.0068	0.1268	0.02	18.62	2.29	1.76	34.275
EP3	100-11	Cr	1.39	6.71	9.3269	1.295	0.138	0.1	100	0.0067	0.1295	0.01	19.30	2.06	1.80	36.075
EP3	110-12	Cr	1.39	6.53	9.0767	1.589	0.353	0.1	100	0.0065	0.1589	0.04	24.33	5.41	2.21	38.284

Appendix F. Pinyon-Juniper Zone Chloride and Bromide Soil Water Concentrations, and Chloride Residual Flux Data

Core	Depth Range (cm)	Soil Horizon	Bulk density (g/cm3)	Gravim. Water Content %	Volum. water Content (%)	Cl (mg/L)	Br (mg/L)	H2O leach (L)	Soil (g)	Soil H20 (L)	Soil Cl (mg)	Soil Br (mg)	Clsw (mg/L)	Brsw (mg/L)	Clswi (g/m3)	Cum Clswi (g/m3)
EP3	120-13	R	1.39	4.8	6.672	1.511	0.139	0.1	100	0.0048	0.1511	0.01	31.48	2.90	2.10	40.384
EP4	0-10	A	1.45	4.6786632	6.78406	0.887	0.173	0.1	100	0.0047	0.0887	0.02	18.96	3.70	1.29	1.286
EP4	10-20	A	1.45	5.8172303	8.43498	1.922	0.86	0.1	100	0.0058	0.1922	0.09	33.04	14.78	2.79	4.0729
EP4	20-30	A	1.45	11.536024	16.7272	2.452	1.19	0.1	100	0.0115	0.2452	0.12	21.26	10.32	3.56	7.6283
EP4	30-40	A	1.45	14.138993	20.5015	3.941	1.737	0.1	100	0.0141	0.3941	0.17	27.87	12.29	5.71	13.343
EP4	40-50	Bt	1.59	13.363179	21.2475	16.457	1.691	0.1	100	0.0134	1.6457	0.17	123.15	12.65	26.17	39.509
EP4	50-60	Bt	1.59	13.228312	21.033	27.701		0.1	100	0.0132	2.7701		209.41		44.04	83.554
EP4	60-70	Bt	1.59	12.399089	19.7146	51.001		0.1	100	0.0124	5.1001		411.33		81.09	164.65
EP4	70-80	Bt	1.34	9.5541974	12.8026	69.598		0.1	100	0.0096	6.9598		728.45		93.26	257.91
EP4	80-90	Cr	1.39	5.5634582	7.73321	43.439		0.1	100	0.0056	4.3439		780.79		60.38	318.29
EP4	90-100	Cr	1.39	5.9514816	8.27256	23.907	0.347	0.1	100	0.006	2.3907	0.03	401.70	5.83	33.23	351.52
EP4	100-11	Cr	1.39	3.7296217	5.18417	5.544	0.113	0.1	100	0.0037	0.5544	0.01	148.65	3.03	7.71	359.22
EP4	110-12	Cr	1.39	3.5868482	4.98572	4.656	0.106	0.1	100	0.0036	0.4656	0.01	129.81	2.96	6.47	365.7
EP4	120-13	R	1.39	2.9601803	4.11465	2.399	0.074	0.1	100	0.003	0.2399	0.01	81.04	2.50	3.33	369.03

APPENDIX G: Graphs of Soil-Water Chloride Concentrations with Depth for the Pinyon-Juniper Zone Cores

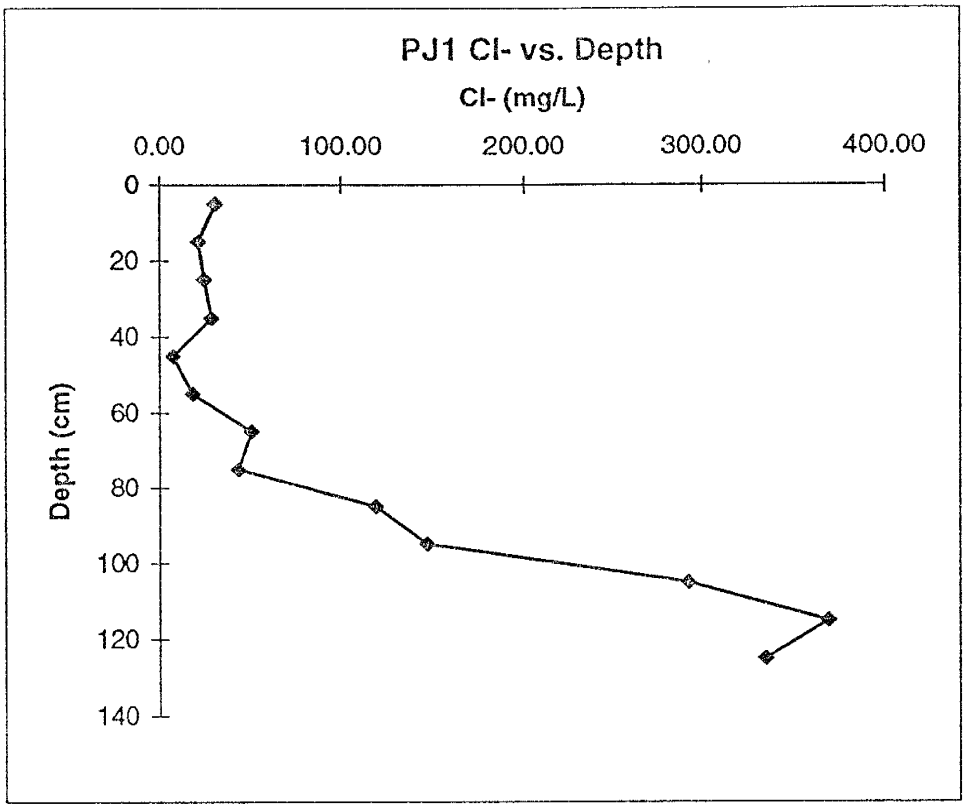
PJ1 Cl- vs. Depth
Cl- (mg/L)
0.00
100.00
200.00
300.00
400.00
Depth (cm)
0
20
40
60
80
100
120
140

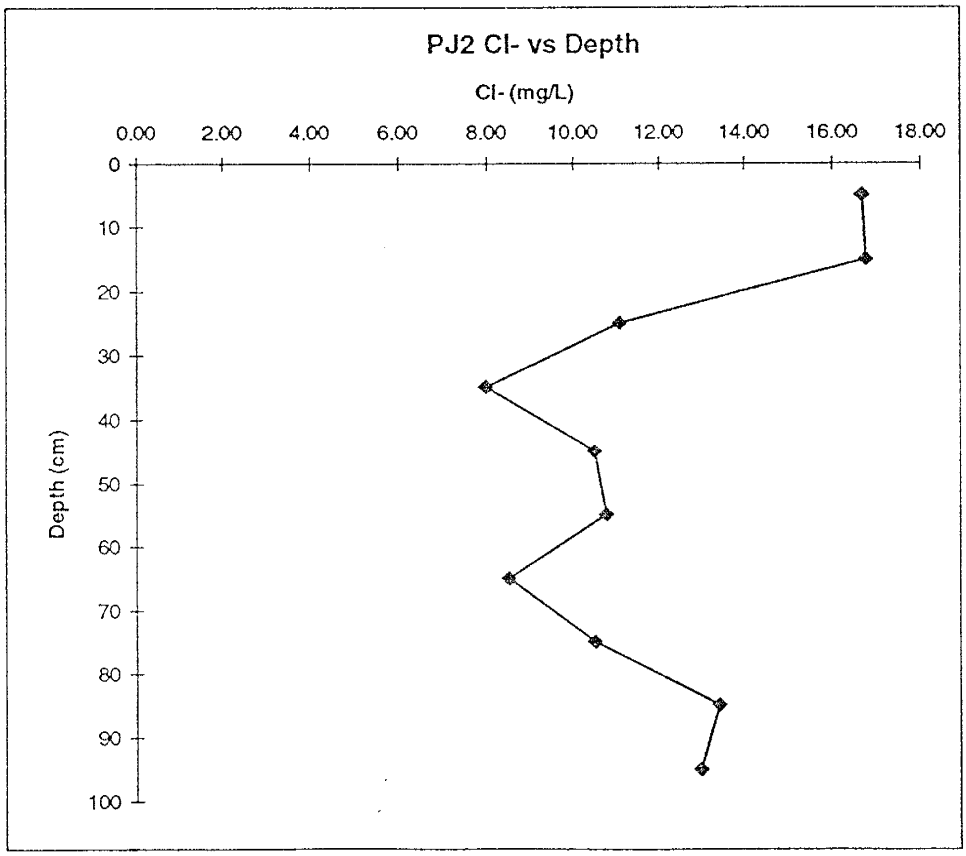
PJ2 Cl- vs Depth
Cl- (mg/L)
0.00
2.00
4.00
6.00
8.00
10.00
12.00
14.00
16.00
18.00
Depth (cm)
0
10
20
30
40
50
60
70
80
90
100

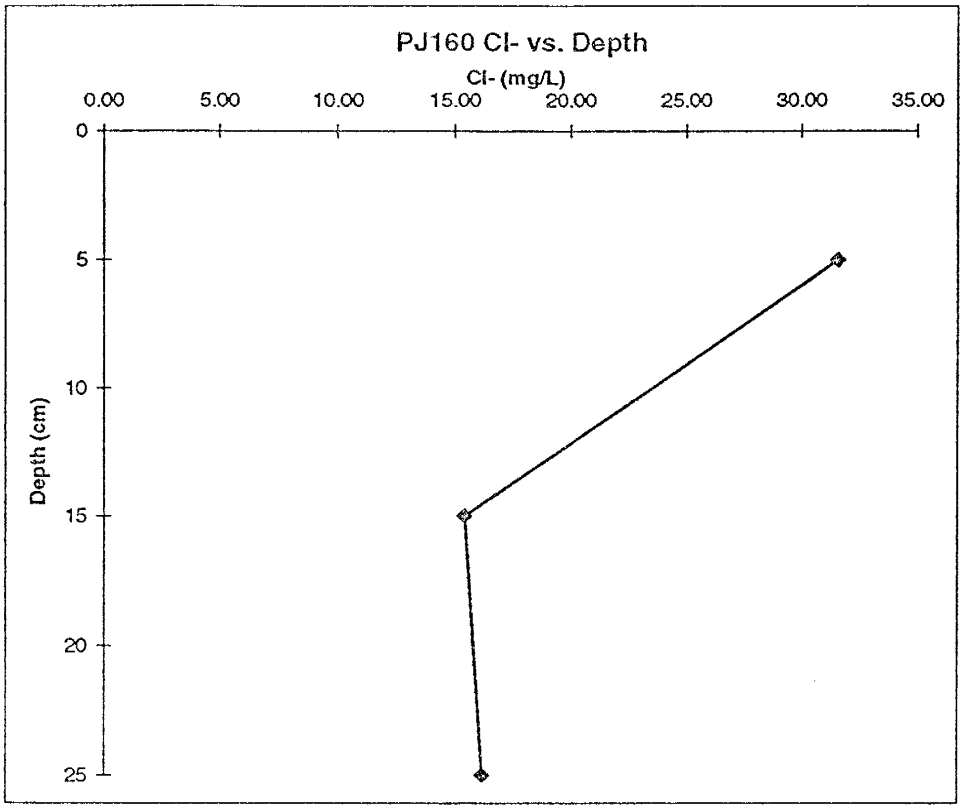
PJ160 Cl- vs. Depth
Cl- (mg/L)
0.00
5.00
10.00
15.00
20.00
25.00
30.00
35.00
Depth (cm)
0
5
10
15
20
25

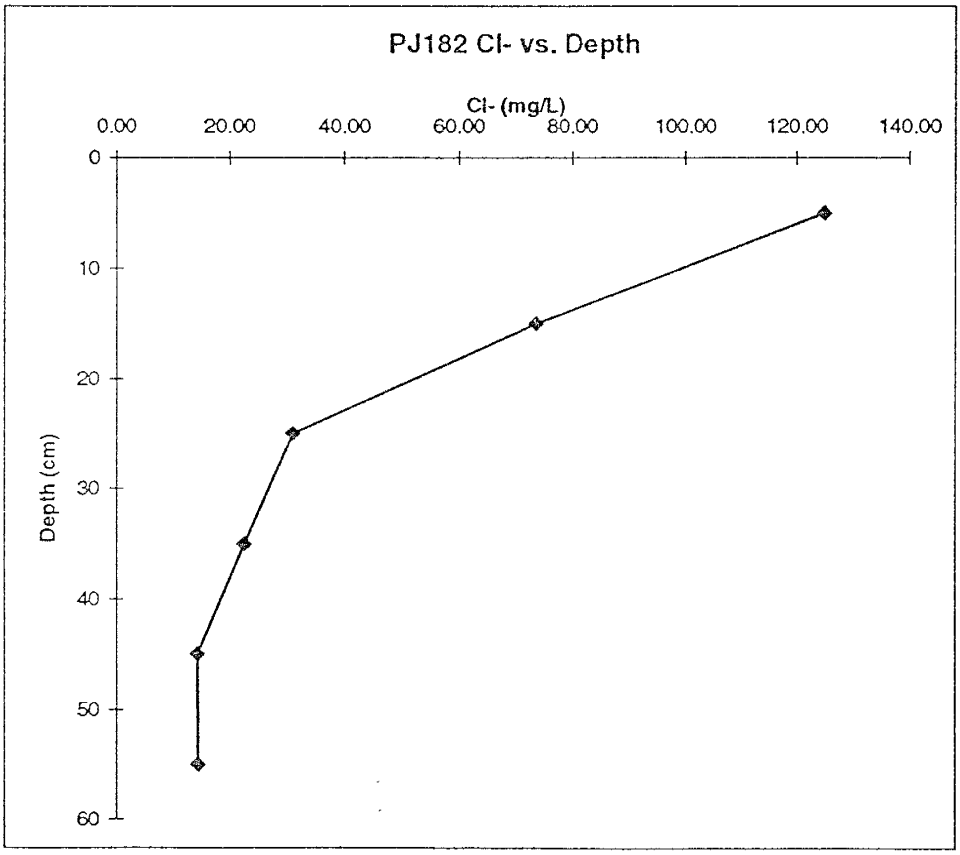
PJ182 Cl- vs. Depth
Cl- (mg/L)
0.00
20.00
40.00
60.00
80.00
100.00
120.00
140.00
Depth (cm)
0
10
20
30
40
50
60

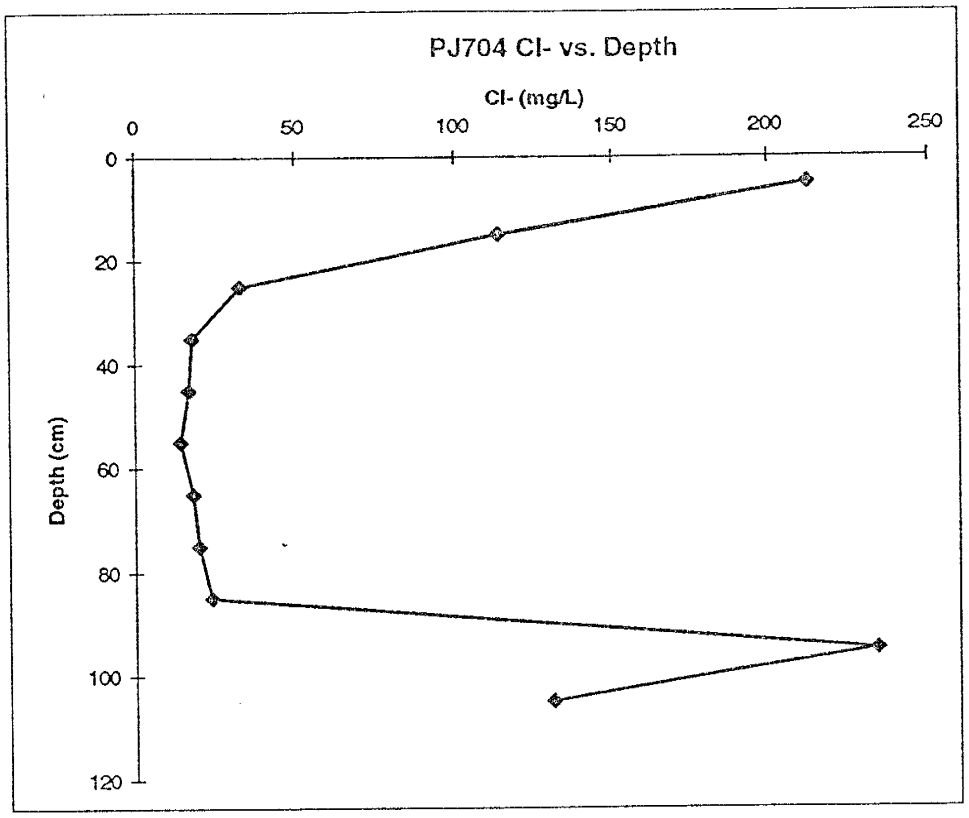
PJ704 Cl- vs. Depth
Cl- (mg/L)
0
50
100
150
200
250
Depth (cm)
0
20
40
60
80
100
120

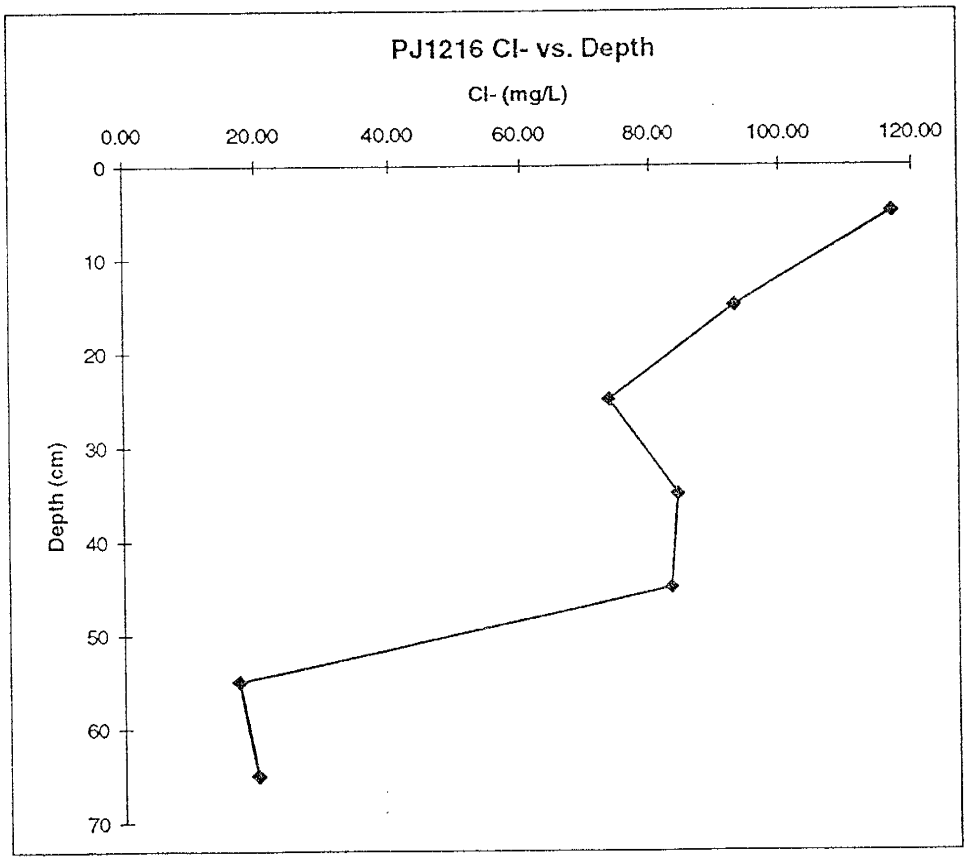
PJ1216 Cl- vs. Depth
Cl- (mg/L)
0.00
20.00
40.00
60.00
80.00
100.00
120.00
Depth (cm)
0
10
20
30
40
50
60
70

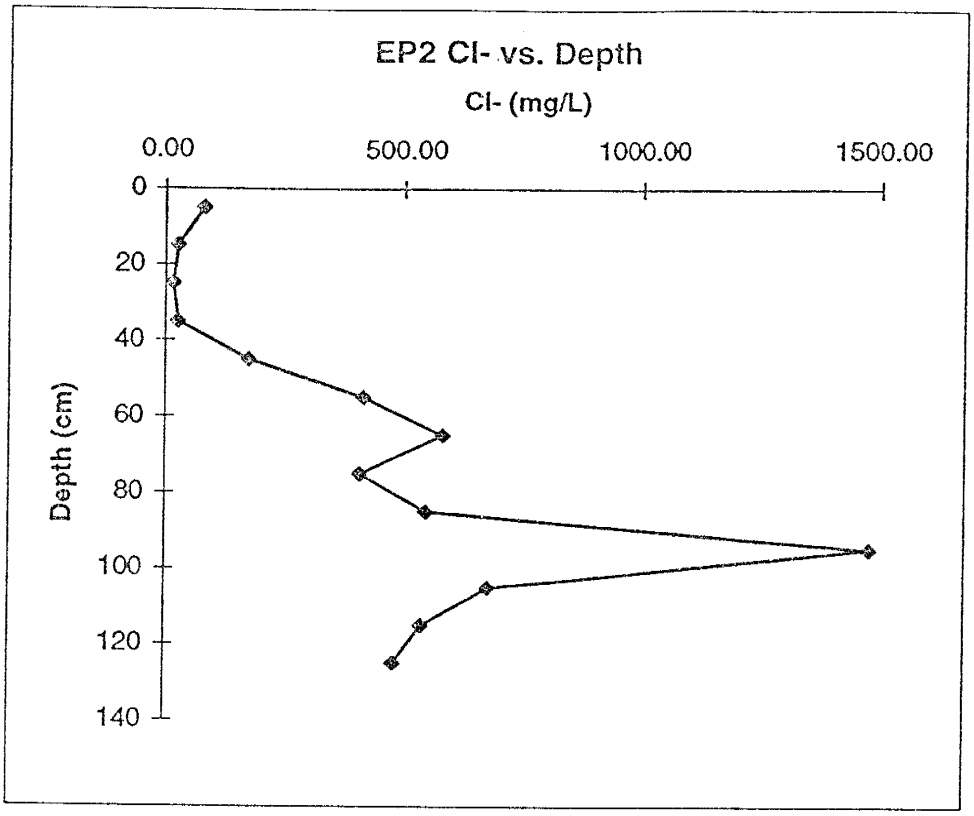
EP2 Cl- vs. Depth
Cl- (mg/L)
0.00
500.00
1000.00
1500.00
0
20
40
60
80
100
120
140
Depth (cm)

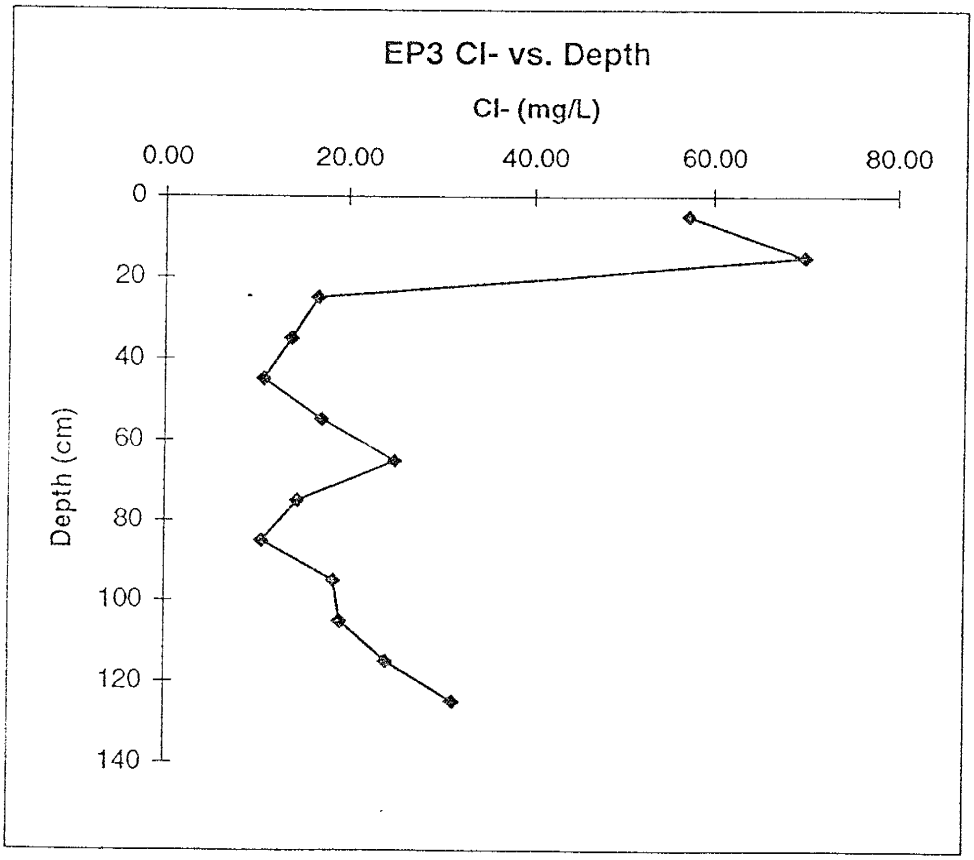
EP3 Cl- vs. Depth
Cl- (mg/L)
0.00
20.00
40.00
60.00
80.00
0
20
40
60
80
100
120
140
Depth (cm)

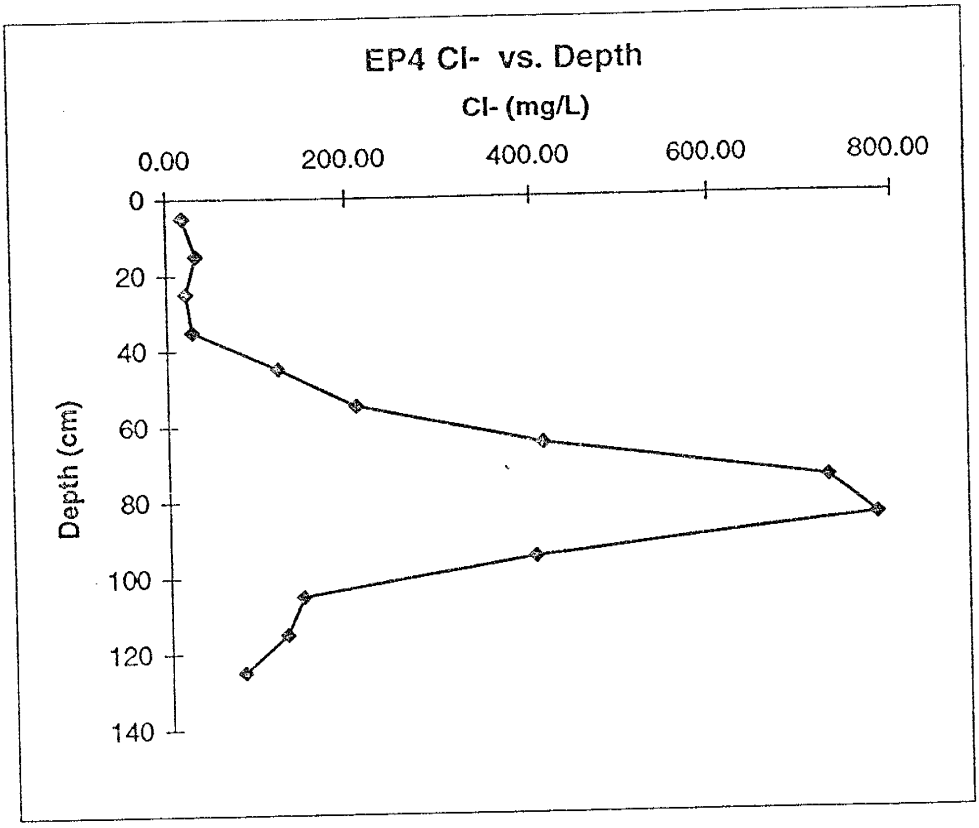
EP4 Cl- vs. Depth
Cl- (mg/L)
0.00
200.00
400.00
600.00
800.00
Depth (cm)
0
20
40
60
80
100
120
140

This dissertation is accepted on behalf of the faculty of the Institute by the following committee:

Andrew Campbell

Adviser

April 18 1996

Date

I release this document to New Mexico Institute of Mining and Technology.

Brett D. Newman april 18, 1996

Students Signature Date